Probability of occurrence of parametric roll on a predefined sea state

Vivien Luthy

ÉCOLE DOCTORALE SCIENCES DES MÉTIERS DE L'INGÉNIEUR

Laboratoire IRENav, Institut de Recherche de l'Ecole navale

THÈSE

Présentée par : **Vivien LUTHY**

Soutenue le : **16 février 2023**

Pour obtenir le grade de : **Docteur**

Spécialité : **Hydrodynamique Navale**

Préparée à : **L'Ecole Nationale Supérieure d'Arts et Métiers**

Lieu de thèse : **Institut de Recherche de l'Ecole Navale**

En partenariat avec : **CMA CGM, IRENav, ENSM**

Probability of occurrence of parametric roll on a predefined sea state

THÈSE dirigée par :

M. BILLARD Jean-Yves

et co-encadrée par :

M. GRINNAERT François

Jury

M. David LE TOUZÉ	Professeur, Ecole Centrale de Nantes	Président
M. Yves-Marie SCOLAN	Professeur, ENSTA-Bretagne HDR, IRDL, Brest	Rapporteur
M. Gabriele BULIAN	Professeur, Université de Trieste, Italie	Rapporteur
M. Vadim BELENKY	Ingénieur docteur, DTRC, USA	Examinateur
M. Pepijn DE JONG	Ingénieur docteur, MARIN, Pays bas	Examinateur
M. Jean-Yves BILLARD	Professeur, ENSAM, IRENAV, Brest	Examinateur
M. François GRINNAERT	Docteur, ENSM, IRENAV, Le Havre	Examinateur
M. Jocelyn RAPP	Commandant, CMA CGM, Marseille	Invité
M. Jean-François LEGUEN	Ingénieur expert, DGATH, Val-de-Reuil	Invité

THÈSE

PROBABILITY OF OCCURRENCE OF PARAMETRIC ROLL ON A PREDEFINED SEA STATE

Vivien Luthy

PhD Thesis

Supervised by Jean-Yves Billard and François Grinnaert

16th of February 2023

Ecole Navale

BCRM Brest – CC 600

F-29240 BREST Cedex 09

ACKNOWLEDGMENTS

First and foremost, I would like to express my sincere gratitude to my supervisors Professor Jean-Yves Billard and Doctor François Grinnaert for their continuous supports and advice during my PhD. As well, I would like to express my sincere gratitude to Jocelyn Rapp from CMA CGM for his operational and technical advice along this project.

I express my sincere gratitude to CMA CGM for their technical and financial supports. I also would like to thank the Ecole Nationale Supérieure Maritime (ENSM) for hosting this project along the 3 years, the French Naval Academy Research Institute IRENav for their scientific support and the Ecole Nationale Supérieure d'Arts et Métiers (ENSAM).

I would like to thank all the people who helped me at some point and who throughout their advice, exchange, support, and encouragement made this project possible:

Vadim Belenky, Guillaume Bonfils, Thomas Bruneau, Gabriele Bulian, Aude Charbonnel, Maxime Crochemore, Guillaume De Hauteclocque, Pepijn De Jong, Cyrille Dufresnes, Capucine Edou, Guillaume Édouard, Martin Eliander, Caroline Fonti, Phillipe Gagnaire, Florent Gansinhounde, Pascale Hauret, Stephanie Hertenshtein, Bernard Lattif, Jean-Francois Leguen, Olivier Lemattre, Mylene Lempereur, Charlotte Leroux, Gersendre Le Dimna, David Le Touzé, Hervé Martin, Remi Menard, Thomas Roy, Yves-Marie Scolan, Jaap-Jan Strocker, Yann Vachias, Clève Wangdi, Dacheng Zhu. All CMA CGM seafarers who answered my survey.

And of course, Jean-Claude, Cathy and Clémentine.

OUTLINE

INTRODUCTION

Context

In 2011, 4849 container ships were sailing around the world, representing a total capacity of 14,277,000 Twenty-foot Equivalent Unit (TEU), (BRS, 2011). On the 31st of December 2021, 5515 container ships were sailing around the world representing a total capacity of 24,970,022 TEU (BRS, 2022). The world container ship capacity almost doubled in 10 years, while the number of ships only increased by about 14 %. This capacity increase significantly reflects the World's growing demand and the tendency to build larger ships. As the number of container ships increases, the associated risks of incidents increase as well. Thus, incidents occur, which may be due to technical failures, fire, or stability issues among others (AGCS, 2022). The stability failures can be consecutive to an inadequate loading plan, human error, or to unforcasted heavy weather. The consequences of a stability failure are multiple. One of the most publicised consequences is the loss of containers at sea. The container loss may be accentuated by an insufficient or deteriorated lashing of the containers or by a misestimation of the risk. Stack weights and heavy loaded container on high tiers are serious issues which lead to increase the risk of containers to fall overboard. To reduce the incident rate and face the new challenges of the shipping industry, the regulation permanently evolves. Especially, the declaration of the container weight is important to reduce the number of containers lost at sea. Therefore, the International Maritime Organisation (IMO) amended the Safety Of Life At Sea (SOLAS) Convention in 2014 (IMO, 2014) in order to mandate the shipper to precisely declare the container gross tonnage loaded onboard (IMO, 2020b, Chapter 6 Reg.2). The amendment entered in force on the first of July 2016. Thus, the shipper shall provide the weight of his container, otherwise, the container shall not be loaded onboard. This new regulation has risen questions from the shippers on how to estimate the weight. Two methods are proposed in the SOLAS Convention (IMO, 2020b, Chapter 6 Reg.2). To provide help on its application, the TT Club (International Insurance Club) and the World Shipping Council (WSC) provided some answers to the most common questions raised from the shippers (TT Club, 2015). However, some errors remain on the declared loading weight since it can be determined by the sum of all elements loaded in the container (and the container itself) which is sometime not properly realised. Based on the declared mass repartition, the ship's loading condition and the ship's stability are established. It then permits to verify that the ship complies with the regulations. However, the ship's stability evolves along the voyage due to fuel consumption, ballast management and with encountered waves. The routing of the vessel is realised based on this estimated loading condition to reduce fuel consumption and to avoid the high-risk areas where the forecasted weather is judged unacceptable for the vessel. However, the vessel may encounter unforecasted unfavourable weather conditions leading to unexpected large motions. Those large roll motions may be due to several stability failures in waves which may lead to the loss of containers at sea. IMO recognized the loss of containers at sea as a source of plastic pollution during its Assembly on the 6th of December 2017 (CEREMA, 2021). The related cost directly imputable to the shipowner linked to container loss can be very important. The Nairobi International Convention on the Removal of Wrecks (WRC convention) applies if the container is lost within the area under the jurisdiction of the States which ratified the Convention (IMO, 2007b). As the definition of wreck is provided by the Convention, it includes any object lost from a ship which is adrift, sunken, or stranded. Thus, the shipowner shall remove the container considered as a wreck to avoid further danger and pollution (International Chamber of Shipping et al., 2021). In consequence, IMO and shipowners together desire to reduce as much as possible the number of containers lost at sea. However, accidents continue to occur. In some cases,

stability failures are in cause. Parametric roll is one of them. This specific stability failure which occurs in longitudinal waves is responsible of several accidents in the past decades.

Series of Unexpected Accidents in waves

Unexpected accidents due to stability failures have occurred on ships while the stability rules into force were complied. Most of those accidents occurred in heavy weather. It is not possible here to presents an exhaustive list of the accidents due to stability failures in waves. Thus, only a few accidents having robust analysis are presented here under. Those accidents are assessed in their respective reports to be or may be consecutive to the phenomenon of parametric roll.

- The Post Panamax C11-class container ship *APL China* (4800 TEU), built in 1995, was sailing Eastwards North Pacific Ocean from Kaohsiung (Taiwan) to Seattle (USA) in October 1998. The vessel encountered typhoon-type weather conditions. The master reduced speed at the approach of heavy weather attempting to steer more easily the vessel. However, the vessel became uncontrollable in heavy weather due to extensive yaw motions up to 20 degrees from the desired course. The vessel suffered unexpected extreme large roll motions up to 40 degrees. Of the 1300 containers on deck, almost a third were lost overboard, and another third damaged. This accident was analysed in detail by France et al. (2003). They conclude that the accident was due to the phenomenon of parametric roll. This accident has led to a total cost estimated over 50 million dollars, which was greater than the value of the vessel herself (Ginsberg, 1998).
- The Panama G-class container ship *Maersk Carolina* (4306 TEU), built in 1998, was sailing Westward North Atlantic from Algeciras (Spain) to Halifax (Nova Scotia, Canada) in January 2003. The vessel encountered heavy weather. The master followed the procedure in such conditions and reduced speed. However, unexpected heavy roll motions appeared in few roll cycles leading to roll amplitudes up to 47 degrees (Carmel, 2006). Of the 3685 TEU onboard at the time, 133 containers were lost overboard and 50 were damaged. Carmel (2006) concludes that the accident was due to the phenomenon of parametric roll. The cargo claims exceeded 4 million dollars.
- The A. Lincoln-Class container ship *CMA CGM G. Washington* (14400 TEU), built in 2017, was sailing Eastwards North Pacific Ocean from Xiamen (China) to Los Angeles (USA) in January 2018. Extreme bad weather was forecasted on the vessel route with swell up to 6 metres. The master was advised by the routing department to modify the route and head more southerly to avoid the worse condition of the storm. The master followed the instruction, and the lashing was verified periodically by the crew. The swell raised up to 4.5 metres. During a fire drill, the vessel suffered sudden roll motions up to 15 degrees without consequences. During the night unexpected slow roll motions appeared and the vessel rolled up to 20 degrees. No damages were visible from the bridge at this time. However, at the morning the officers reported that 137 containers were lost overboard, and 85 containers were damaged. “It is almost certain that CMA CGM G. Washington experienced parametric roll prior to and at the time of the container collapses” (MAIB, 2020).
- The *APL England* (5780 TEU), built in 2001, was sailing Southerly East of Australia from Ningbo (China) to Sydney (Australia) in May 2020. The vessel left Ningbo heading to Sydney in calm weather. Two days after the departure, the master was ordered to change destination for Melbourne due to COVID-19 regulation at that time. While heading South in the East of Australia the master was informed of a low-pressure system developing, leading to wave height of 5 to 6 metres. The master monitored the weather forecast. He decided to reduce speed from 14 to 7 knots when the weather deteriorated (4.5m sweel). An unexpected large roll motion appeared during the night. The master altered course

southerly and maintained speed. A second large roll motion appeared later. The master altered course again to reduce roll motions. Two hours later the vessel experimented unexpected very large roll motions up to 25 degrees. Consequently, an alarm raised shutting down the main engine (piston cooling oil low pressure). The vessel continues to roll heavily and without power altered course to beam seas while the crew react and restart the main engine. At the end, of the 3161 containers loaded onboard, 50 containers were lost overboard and 63 were damaged. The preliminary report of the Australian Transport Safety Bureau (ATSB) states that the vessel encountered conditions which may have led to parametric roll (ATSB, 2020a).

- The Maersk Edinburgh-class container ship *Maersk Essen* (13100 TEU), built in 2010, was sailing Eastwards Pacific Ocean from Xiamen (China) to Los Angeles (USA) in January 2021. Heavy weather was forecasted for the voyage. Thus, prior departure, the 2nd officer requested weather routing advice from the Company. The master was advised by the routing department to increase speed and to alter course to a southern route to avoid low-pressure system. The master followed the recommendation on the route modification. However, to avoid arriving too early, he did not increase speed as recommended. The vessel suffered from unexpected roll motions up to 15 degrees several times. The crew was on deck when finally she suffered from unexpected roll motions up to 30 degrees. Following this event, the master decided to alter course of more than 90 degrees and increase speed to avoid further undesired roll motions. During this large roll episode, 689 containers were lost at sea and 258 were damaged. The report of the Danish Maritime Accident Investigation Board (DMAIB, 2022) concludes that this accident is consecutive to the phenomenon of parametric roll. At the time of the container loss, the crew was on deck. This could have result in fatalities.

Each accident has been highly mediatized leading to client concerns on their cargo. The ship owner suffers a reputation loss which may be more financially damageable than the cargo loss itself. However, parametric roll is not the only cause of cargo loss. As an example, *MSC ZOE* lost 342 containers overboard while sailing in beam seas. *MSC ZOE* experienced synchronous roll motions up to 30 degrees (Panama Maritime Authority et al., 2020; DSB, 2020). This type of accidents leads to the extensive study which demonstrated the risk of synchronous roll in beam seas. It has to be noticed that during some accidents, heavy roll motions lead to engine failure, leaving the ship without propulsion for several minutes. In those cases, the vessel in dead ship condition may continue to roll heavily until the crew reaction permits to resume the voyage. Thus, several stability failures may be the cause of container loss during a single accident.

Table 1 presents recent accidents which led to the loss of containers at sea. It shows that in the past years, old-build and new-build ships have suffered from stability failures in waves. Thus, the hull form evolutions realised in the past years to fit the new owners' requirements such as average speed design did not modify the problem. As well, all sizes of ships are concerned, even ships which length is larger than 360 metres *(ONE Apus, ONE Aquila, MSC Aries, CMA CGM G. Washington).*

Name	Accident date	Vessel age [year]	Container lost	Capacity [TEU]	References
Pacific Adventurer	11/03/2009	19	31	1123	ATSB, 2009
Svendborg Maersk	14/02/2014	16	517	8160	DMAIB, 2014
MSC Zoe	02/01/2018	3	342	19224	Panama Maritime Authority et al., 2020; DSB, 2020
CMA CGM G. Washington	20/01/2018	1	137	13460	MAIB, 2020
YM Efficiency	01/06/2018	9	81	4250	ATSB, 2020b
Munich Maersk	02/12/2020	2	200	19630	TATA AIG, 2021
BG Jade	10/02/2020	2	Missing data	1004	W E Cox Claims Group, 2022
OOCL Rauma	11/02/2020	11	7	1425	WMN, 2020
APL England	24/05/2020	19	50	5510	ATSB, 2020a
ONE Acquila	03/11/2020	2	100	14000	TATA AIG, 2021
Maersk Seroja Lima	27/11/2020	9	27	8540	TATA AIG, 2021; W K Webster, 2022
ONE Apus	30/11/2020	1	1816	14000	IIMS, 2020
Evergreen Liberal	30/12/2020	6	36	9466	TATA AIG, 2021; W K Webster, 2022
Maersk Essen	16/01/2021	11	689	13100	DMAIB, 2022
MSC Aries	29/01/2021	1	41	14300	TATA AIG, 2021; W K Webster, 2022
Maersk Eindhoven	17/02/2021	11	260	13100	TATA AIG, 2021; W K Webster, 2022
Dyros	21/03/2022	14	90	4578	TATA AIG, 2022; W K Webster, 2022
APL Vanda	03/07/2022	9	55	17300	W E Cox Claims Group, 2022

Table 1 - Recent stability failures in waves

Figure 1 represents a timeline of some accidents which have led to container loss or damage. The vessel names followed by a star are either identified as consecutive to parametric roll or under investigations where parametric roll is suspected. The other accidents are displayed here since they are considered as major accidents leading to container loss.

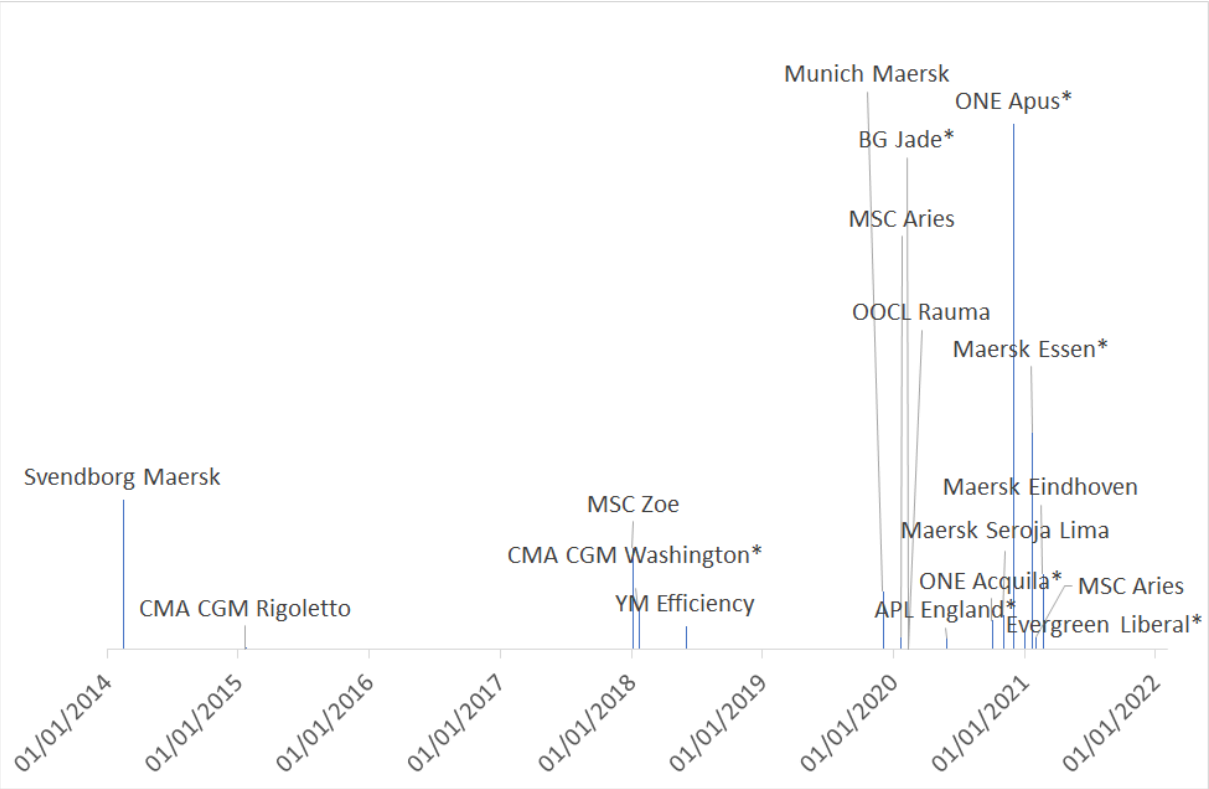

Figure 1 - Timeline: Some accidents leading to container loss from 2014

Figure 1 shows that in the last few years the accidents rate due to parametric roll is much higher than during the previous decades. However, this may be due to the fact that parametric roll was not a well-known phenomenon at that time and therefore not fully assessed when accidents investigations were conducted. As well, during the last decades, all accidents leading to container loss may not have been reported as accurately as they are nowadays. At the time of the writing of this PhD thesis, there is no mandatory reporting of containers lost at sea.

Figure 2 presents the geographical repartition of accidents which have led to loss of container at sea. Those accidents are the one listed in Table 1 and others for which the position of the accident was known based on the declaration found from insurance companies (TATA AIG, 2021; TATA AIG, 2022; W K Webster, 2022). The accidents pointed in red are identified as consecutive to parametric roll, or for which parametric roll is suspected. It shows that container loss mostly occurs in the North Pacific Ocean and in the North Atlantic Ocean, where there is the highest containership traffic density. It can be noticed that the accidents occurred evenly near the coast as in deep seas.

Figure 2 - Recorded accidents which lead to container loss

Focus on the container loss

As observed, many accidents leading to container loss appeared in heavy weather in the last decades leading to heavy financial loss. The average number of containers lost at sea per year depends widely on the source of information. According to the centre of documentation, Monterey Bay Aquarium Research Institute (MBARI) about 10 000 containers are lost at sea every year (Barry, 2011). The report of the World Shipping Council (WSC) state that in average from 2008 to 2019 about 1382 containers are lost at sea every year (WSC, 2020) and 1629 containers from 2009 to 2021 (IMO, 2022). Figure 3 presents the number of containers lost at sea every year since 2008 (IMO, 2022). In 2013 a peak of the average number of containers lost at sea appears, it is due to the accident of the Mol Comfort where 4293 containers were lost during a single event (vessel sunk), Committee on Large Container Ship Safety (2013). Nowadays, important loss during a single event have occurred with a higher frequency due to the increasing size of container ships. As an example, the modern ultra large container ships One Apus suffered from heavy roll motions leading to the loss of 1816 containers during a single event in 2020 (Table 1). This single event may reach 200 million dollars (IIMS, 2020).

Even if those numbers are impressive, it should be compared to the number of containers transported by sea each year. In 2019, the shipping industry transported approximately 226 million of containers (40 foots containers count as 1 single container, it is not TEU). Thus, the average of 1629 containers loss represents only a thousand of percent of the number of containers shipped each year (IMO, 2022). Thus, maritime transport is reliable with a very small percentage of accidents. However, each time such accidents occurs, the ship owner must deal with shipping delays due to the investigation or detention, pollution concerns, reputation concerns, containers value, and mediatization. There is a real challenge to avoid container loss, especially when due to stability failures such as parametric roll.

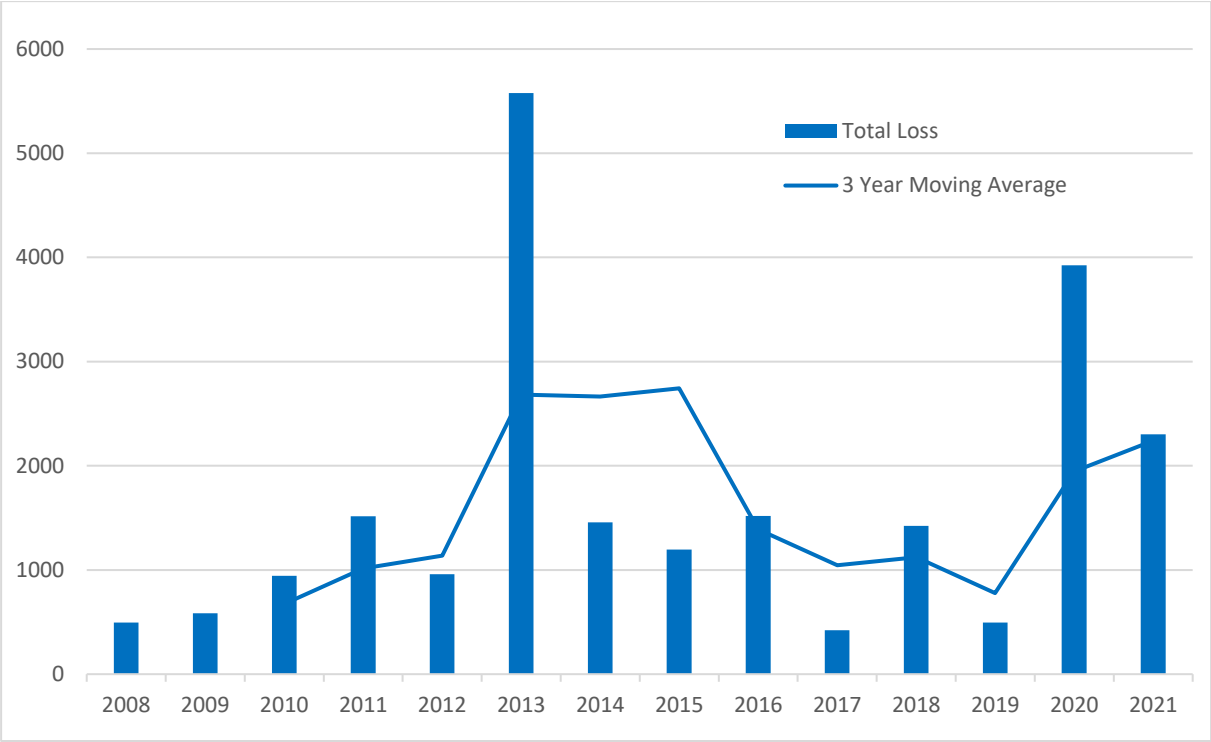

Figure 3 - Number of containers lost at sea (IMO, 2022)

Avoiding parametric roll

Parametric roll stability failure occurs in head and following seas where the masters feel safe. Therefore, it is counterintuitive for the master to avoid these headings relative to the waves. Thus, methods to evaluate the sensibility of the vessel to this phenomenon and to warn the master of the risk are required. Several types of assessments exist to evaluate the risk of appearance of parametric roll.

A global assessment of the ship regarding parametric roll can be conducted. This type of assessment provides an estimation of the vulnerability of the vessel towards parametric roll throughout her life. It can be based on empiric formula considering the main ships characteristics or on simulations considering simplified descriptions of the sea states (regular waves). This assessment does not permit to avoid the appearance of the phenomenon; however, it permits to qualify the vulnerability of the vessel and therefore this type of assessment is chosen as regulatory process (IMO, 2020a).

A real-time assessment of the ship's motions permits to detect the appearance of the phenomenon of parametric roll. The associated methods do not require to be fitted to each vessel and thus it only requires access to the real-time information provided by the inertial unit fitted onboard. Such assessment permits to qualify the roll motion and therefore to initiate countermeasures. However, this detection may occur during a large roll motion episode, and thus, if no signs of smaller roll motions due to this phenomenon were previously observed, the countermeasure may not be engaged sufficiently in advance.

Finally, 6-degree-of-freedom (DoF) time-domain assessment of the ship's motions in waves can be conducted. Such assessment permits to realise operational roll polar plots presenting the maximum roll amplitudes calculated for selected loading and environmental conditions. The ship motions are computed with a time-domain solver. Thus, this requires a full description of the hull geometry, an estimation of the roll damping and to select the loading and environmental cases to be assessed. This type of assessment is computationally heavy since it requires to realise a roll

polar plot for each pre-defined loading and environmental conditions. This assessment does not evaluate the vessel motions on the actual encountered conditions and therefore it should be considered to avoid the worse combination of course and speed.

Thus, several types of assessment to avoid parametric roll exist. Each type of assessment considers its own set of assumptions and therefore all assessments should be considered as complementary.

Objective

Parametric roll stability failure leads to remarkable accidents, especially on container ships. The financial consequence as well as the impact on the reputation of the Owner Company are tremendous. This rare stability failure is counterintuitive for the masters and Officer Of the Watch since it appears in head or following seas where roll motions are expected to be the least.

The aim of this PhD is to improve the operational avoidance of parametric roll throughout a deep study the phenomenon. Parametric roll avoidance requires several complementary assessments methods. Thus, the study of the real-time ship's motions permit to qualify the roll motions as due to parametric roll. When the ship suffers parametric roll, the most adequate manoeuvre should be engaged immediately. Thus, the strategy is to develop a new detection method and to statistically assess several manoeuvres to avoid the worse roll motions due to parametric roll.

In addition, the ship roll motions can be estimated based on the vessel geometry, loading condition, and forecasted weather. A non-linear phenomenon such as parametric roll requires specific tools to compute the vessel roll motions. Time-domain simulations in 6 degrees of freedom permit to reproduce numerically the ship's motions. Hundreds of computations hours permit to realise roll polar plots which can then operationally be used to select the most appropriate combination of course and speed. Here, an assessment of the currently available methods to compute operational roll polar plots is realised. Detailed sensibility studies of several time-domain input parameters to increase the reliability of the roll polar plots are conducted.

Finally, even if those decision support tools are accurate, they do not replace the immediate response actions engaged by the Officer Of the Watch. Thus, operational guidance provided through an operational reaction guide are expected by the Officer Of the Watch, to help understanding the physics of the phenomenon and to provide an effective advice on general immediate actions (Annex 2).

Outline

The first chapter presents the physics of the phenomenon of parametric roll and the different methods used to evaluate the vulnerability of the vessel. The regulation towards parametric roll and both existing lifetime and real-time assessments are described. The time-domain solvers used to assess the vessel's vulnerability within this PhD thesis are also presented in this chapter.

The second chapter presents an innovative energy method to calculate the amplitude of parametric roll in longitudinal seas at any speed, considering non-linear transverse stability. The results are validated by comparison with the one obtained from a 1-DoF time-domain solver.

The third chapter presents the results of additional works conducted with the aim to validate and increase the relevance of the inputs of time-domain simulations, with the aim to improve them. A method to calculate the roll damping coefficients to be set in the solver to reproduce roll decay time series obtained from other sources is presented. An evaluation of the value of the spreading

angle leading to the most conservative roll amplitudes is also presented in this chapter. Finally, other studies and validations of 6-DoF simulation inputs are presented.

The fourth chapter describes an innovative method to evaluate the risk of parametric roll in real time based on the vessel motions. The method is validated on regular waves. Then a statical study is conducted considering results from simulations in 5-DoF on real sea state. Finally, a real case validation is conducted.

The fifth chapter presents a study realised in 6-DoF on a container ship conducted to assess the effect of several manoeuvres to undertake after parametric roll is detected. Statistically, the most relevant manoeuvre to execute in case of unexpected heavy roll motions in head or following seas is defined.

The symbols used in this thesis are defined once inline when encountered for the first time and reported in the glossary in page 176. Most of them are in accordance with the latest recommendations on symbols and terminology provided by the International Towing Tank Conference (ITTC, 2021b).

CHAPTER 1. STATE OF THE ART: ASSESSMENT OF THE VESSEL VULNERABILITY TO PARAMETRIC ROLL

This chapter presents the phenomenon of parametric roll, the numerical tools used within the scope of this PhD thesis to simulate it, and the existing methods to assess the vulnerability of the vessel towards the phenomenon. First, the physical background of the phenomenon is introduced. Then, a presentation of the time-domain solvers used to compute the vessel's roll motions is provided, with their respective assumptions. Then, existing methods of parametric roll global assessment are detailed. Among them, the new regulatory assessment provided by the IMO is presented, in addition to the assessment procedures provided by Bureau Veritas and American Bureau of Shipping. Finally, existing real-time methods to detect and/or avoid the parametric roll are presented.

1.1. PHYSICS OF PARAMETRIC ROLL

Parametric resonance was known and studied by mathematicians (Mathieu, 1868), mechanical engineers (Sanmartín Losada, 1984), optical engineers (Giordmaine, 1965), and naval architects (Froude, 1861; Kerwin, 1955). This phenomenon has been extensively studied in the maritime field in the past decades since several container vessels suffered from unexpected large roll motions leading to container losses and imputed to this phenomenon (see introduction).

In the Cathedral of Santiago de Compostela, eight men used a large swinging censer (a thurible, named "Botafumeiro") to spread incense inside the cathedral. The men understood that the phenomenon of parametric resonance could be profitable to their task. The large censer is attached to a rope suspended on a cylinder under the cathedral roof. The rope is coiled on the cylinder, permitting to avoid the rope to drop down in the axis of the censer. After an initial push, to facilitate its oscillations a cyclic variation of the rope length is realised by pulling on the rope. The men pulled twice on the rope in one swinging cycle to increase the amplitude of the motion, thus providing a parametric excitation. The censer can reach its maximum angle of about 82 degrees in usually 17 cycles. Thus, the phenomenon of parametric oscillation permits the Botafumeiro to swing largely in few oscillations (Sanmartín Losada, 1984).

Parametric resonance phenomenon applies as well to ships when encountering waves in some specific conditions and may lead to unexpected large roll amplitudes. Contrary to the Botafumeiro, the large roll motion of the ship is undesired. The stiffness of the system, which is materialised by the length of the rope, is the ship transverse stability, represented by the metacentric height (GM) and the righting arm (GZ). Thanks to Bouguer (1746), for a given height of the centre of gravity, the metacentric height is directly linked to the ship's waterplane. Moreover, the largest variations of the waterplane geometry appears when the ship's sails in longitudinal seas. Thus, in regular waves, it is in longitudinal and following seas that the waterplane area varies the most. On a wave which length is equal to the one of the ships, usually, maximum and minimum waterplane areas (and transversal stability) appear respectively for the wave centred on the perpendiculars and amidship (Figure 4).

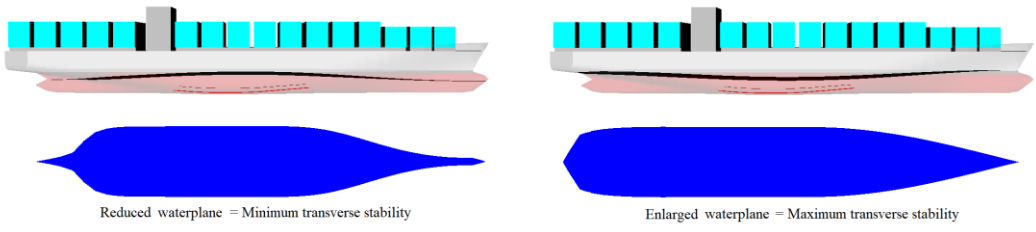

Figure 4 - Waterplanes for wave crests centred at perpendiculars (right) and amidship (left)

Thus, when the variation of transverse stability occurs twice within a roll period, parametric roll develops (parametric synchronism condition). IMO (2021b) states that when the ship rolls while the wave passes through, the increased stability (GM) provides stronger pushback. Thus, as the ship returns to the upright position, the additional pushback provided by the increased stability leads to an increase of the roll velocity. If at this time, the wave crest is centred amidship, the ship's stability is at its lowest while the roll velocity is at her maximum, leading the ship to roll further to the opposite side. Then, if the maximum roll angle is reached when the wave crests are located at perpendiculars, the ship stability is maximum, and the roll cycle starts again. It has to be noted that no direct transverse excitation is provided to the ship during the parametric amplification of the roll motion. The following conditions are required for parametric roll to develop:

- The ship sails in head, following seas or in bow\stern-quartering seas
- The wavelength is comparable to the length of the ship
- Both the hull geometry and the wave profile provide a sufficient variation of the transverse stability
- The ship's roll period is twice the wave encounter period
- The roll damping is sufficiently low

The roll damping is a key factor of parametric roll. Large bilge keels significantly increase the roll damping. However, it does not permit to avoid parametric roll. It only reduces the amplitude of the roll motion. Thus, large roll damping may permit to avoid undesirable consequences of the phenomenon of parametric roll. However, equipping vessels with such large bilge keels increases the hull resistance and thus the fuel consumption. Consequently, this solution is not favoured by ship owners for economic and environmental matters.

Parametric roll requires that the variation of transverse stability occurs twice within a roll period to develop. On regular waves, the variation of the transverse stability is directly linked to the encounter wave frequency. Thus, the wave encounter frequency (denoted by ω_e) equal to twice the ship's natural roll frequency (denoted by ω_0), Equation 1 is the fundamental condition for parametric roll to develop. Consequently, it is possible to calculate the vessel speed for which this condition is met in longitudinal seas (denoted by V_{PR}), Equation 2 (demonstrated by Grinnaert, 2017; IMO, 2020a). This condition is referred as parametric synchronism.

$$\omega_e = 2\omega_0 \quad (1)$$

$$V_{PR} = \left| \frac{2\lambda}{T_0} \sqrt{\frac{GM_{mean}}{GM_0}} - \sqrt{\frac{g\lambda}{2\pi}} \right| \quad (2)$$

λ	(m)	Wavelength
T_0	(s)	Natural roll period in calm water
GM_{mean}	(m)	Mean GM in longitudinal waves
GM_0	(m)	GM in calm water
g	($m.s^{-2}$)	Acceleration of gravity

However, the phenomenon of parametric roll does not appear only at this single speed. The speed range for which parametric rolls may appear depends on the magnitude of the stability variation induced by the wave encounter (IMO, 2021b). As stated by Grinnaert et al. (2017), parametric roll appears for a speed range which can be analytically calculated in regular wave. This speed range

is referred as lock-in-field. Assuming linear GZ, Kerwin (1955) and then Grinnaert (2017) stated that the lock-in-field is centred on the speed for which the condition of parametric synchronism is verified (Equation 1). Within the lock-in field, the ship's roll period is locked to twice the encountered wave period. The speed (V_{PR}) for which the condition of parametric synchronism is verified is calculated using Equation 2, it can be expressed as well as follows:

$$V_{PR} = (2\omega_0 - \omega_w)\frac{g}{{\omega_w}^2} \quad 3$$

Where ω_w denotes the wave frequency.

The bandwidth of lock-in-field is provided analytically from a dimensionless speed by Grinnaert et al. (2017). The formula proposed by Grinnaert is traduced as a speed range δV, bounding the lock-in-field from V_{PR} - δV to V_{PR} + δV. δV is calculated as follows:

$$\delta V = \frac{g}{\omega_w}\left(\frac{\delta GM \omega_0}{2GM_{mean}\omega_w}\right) \quad 4$$

Demonstration of Equation 4 is provided in Annex 3.

δGM denotes the half variation of transverse stability between minimum and maximum GM (denoted by GM_{min} and GM_{max}, respectively) and calculated as follows:

$$\delta GM = \frac{1}{2}(GM_{max} - GM_{min}) \quad 5$$

As example, Figure 5 shows the roll amplitudes calculated with a 1-DoF time-domain solver as a function of the speed for the C11-class container ship (presented in Annex 4) known for its vulnerability toward parametric roll (France et al., 2003). The speed range corresponding to a non-zero roll amplitude is the lock-in-field. The speed corresponding to the condition of parametric synchronism (V_{PR}) is plotted in Figure 5, as well as the speed range calculated from Equation 4 (δV). The natural roll frequency is equal to 0.299 rad.s^{-1} and the wave frequency is equal to 0.485 rad.s^{-1}. Thus, V_{PR} is calculated using Equation 3 and is equal to 4.77 m.s^{-1}. Here, GM_{mean} is equal to 2.967 metres and δGM is equal to 0.9495 metre. Thus, δV calculated using Equation 4 is equal to 4 m.s^{-1}. It is observed that the analytical calculation of the lock-in-field slightly differs from the one obtains from 1-DoF simulations. In this case, simulations results considering either linear or non-linear GZ provide identical bandwidth of the lock-in field. The roll amplitudes calculated considering linear GZ exceed 70 degrees in some cases, which is not represented here in favour of a better vision of the lock-in-field (Figure 5). The analytical calculation of the lock-in-field relies on a linear GZ assumption (Equation 4). It is observed that no matter the assumptions considered (linear and non-linear GZ) in the simulations, the analytically calculated bandwidth of the lock-in field is estimated with an acceptable accuracy. The damping coefficients considered to realise the simulations are estimated using Ikeda method (Ikeda, 1978; Kawahara, 2009). However, assuming linear damping, the bandwidth of the lock-in-field does not depend on the damping coefficients (Equation 4).

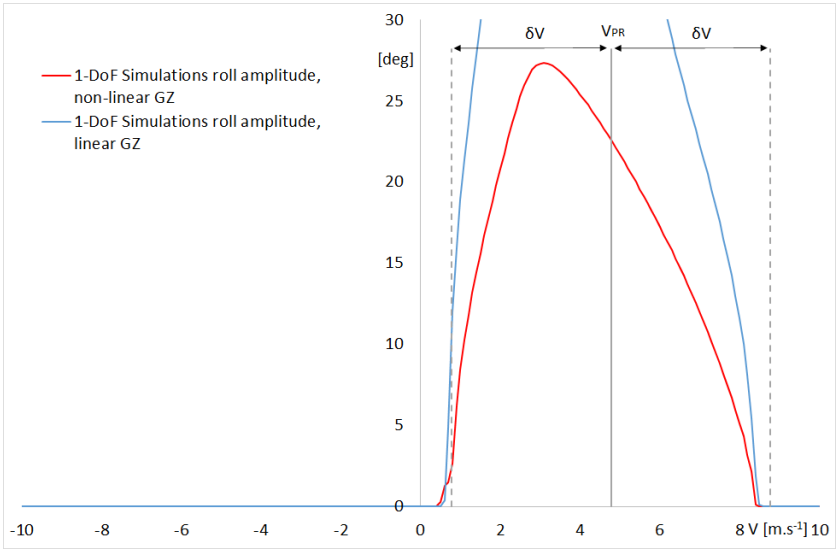

Figure 5 - Bandwidth of the lock-in-field

In addition, the bandwidth of the lock-in field depends on the magnitude of the GM variation (IMO, 2021b) which is directly linked to the wave height. As the wave height increases, the lock-in field gets larger. Outside of the lock-in field, parametric roll does not exist. Figure 6 shows the roll amplitude reached within the lock-in field on three different wave heights equal to 3, 4.4 and 6 metres, with δGM equal to 1.23, 1.90 and 2.53 m, respectively. It is observed that the mean and the half variation of GM varies. Thus, the bandwidth of the lock-in field varies as well. The bandwidth of the lock-in field increases as the wave height gets larger.

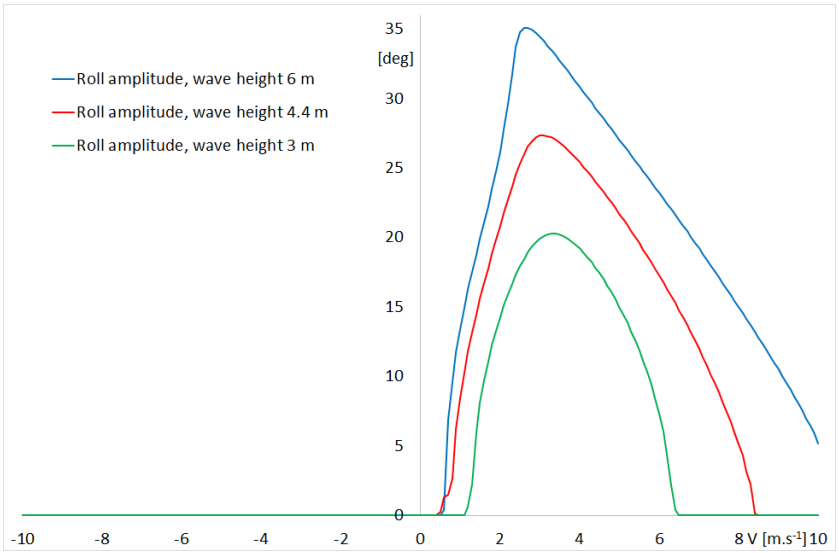

Figure 6 - Bandwidth of the lock-in field for 3 different wave heights

When parametric roll develops, the consequences depend on the reached roll amplitude. Thus, if the roll damping is sufficient to limit the roll amplitude, parametric roll may appear without undesired consequences. Thus, a quantitative assessment of the parametric roll is required. Such assessment can be conducted using a time-domain solver.

1.2. TIME-DOMAIN SIMULATION ASSESSMENT

1.2.1. One-degree-of-freedom assessment

A 1-DoF time-domain solver is one of the easiest methods to solve the equation of the roll motion. The linearised roll motion equation can be expressed as follows:

$$J_{44}\ddot{\varphi} + B_{44}\dot{\varphi} + WGM_0\varphi = F_{ext} \quad (6)$$

φ	(rad)	Roll angle
$\dot{\varphi}$	(rad.s^{-1})	Roll velocity
$\ddot{\varphi}$	(rad.s^{-2})	Roll acceleration
J_{44}	(kg.m^2)	Roll moment of inertia
B_{44}	(N.m.s.rad^{-1})	Roll damping coefficient
W	(N)	Ship's weight
F_{ext}	(N.m)	External forces

Here it considered that the roll moment of inertia is constant and that the roll damping coefficient varies with the roll amplitude. The transverse stability is linearised as $GM_0*\varphi$ which assumes that the waterplane area does not vary in waves. The external forces can be provided by waves, wind, tug … However, when assessing parametric roll, since there is no direct wave excitation from the wave in longitudinal seas, the external forces are equal to zero.

The waterplane area varies with the waves running along the ship's hull. Therefore, the transverse stability (GM and GZ) varies consequently. Assuming linear GZ and a sinusoidal roll motion, a simple way to define the variations of GM and GZ in time-domain is:

$$GM(t) = GM_{mean} + \delta GM.cos(\omega_e.t) \quad (7)$$

$$GZ(\varphi;t) = (GM_{mean} + \delta GM.cos(\omega_e.t))\varphi \quad (8)$$

In addition, parametric roll can be seen as a parametric oscillator system (Section 1.1). Thus, introducing the variation of the transverse stability (Equation 8) in Equation 6 leads to:

$$J_{44}\ddot{\varphi} + B_{44}\dot{\varphi} + W\left(GM_{mean} + \delta GM.cos(\omega_e.t)\right)\varphi = 0 \quad (9)$$

GM_{mean}	(m)	Average value of all GM in waves

In this equation, the variation of the stability through time is calculated using the mean GM value in wave and its half variation. Thus, it is required to use a hydrostatic solver able to handle the metacentric height in waves. Figure 7 presents an example of the difference between the cosine approximation of the transverse stability variation (Equation 7) and the actual value in waves.

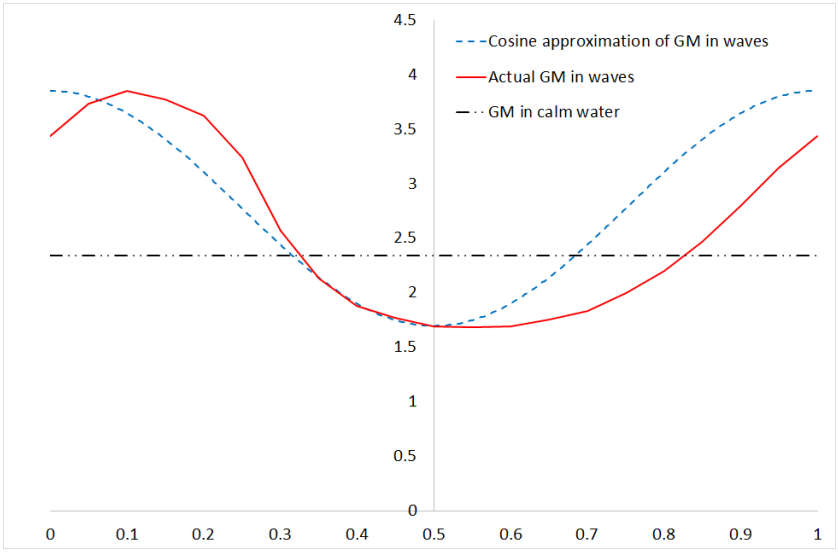

Figure 7 – Variation of the metacentric height as a function of the wave crest position in a fixed ship coordinate

It is observed that the maximum GM width is larger for actual values and the minimum GM width is smaller for the real values. As well, a shift in wave position is observed between the analytic definition of GM (Equation 7) and the actual GM. Thus, the variation of the transverse stability in waves should preferably be used. It can be introduced in the differential equation 9, leading to:

$$J_{44}\ddot{\varphi} + B_{44}\dot{\varphi} + WGZ(\varphi, t) = 0 \qquad 10$$

Where GZ(φ,t) in metre denotes the righting arm as a function of the roll angle φ varying in time according to the encounter frequency and B_{44} is function of the roll amplitude. Thus, the hydrostatic solver has to be able to calculate the righting lever arm for any position of the wave along the hull. An example of a two-dimension representation of the GZ curves in waves is provided for 10 positions of the waves along the ship, Figure 8. The associated three-dimension dimensionless representation is provided in Figure 9, for the C11-class container ship at a draught equal to 10 metres and a KG equal to 19 metres.

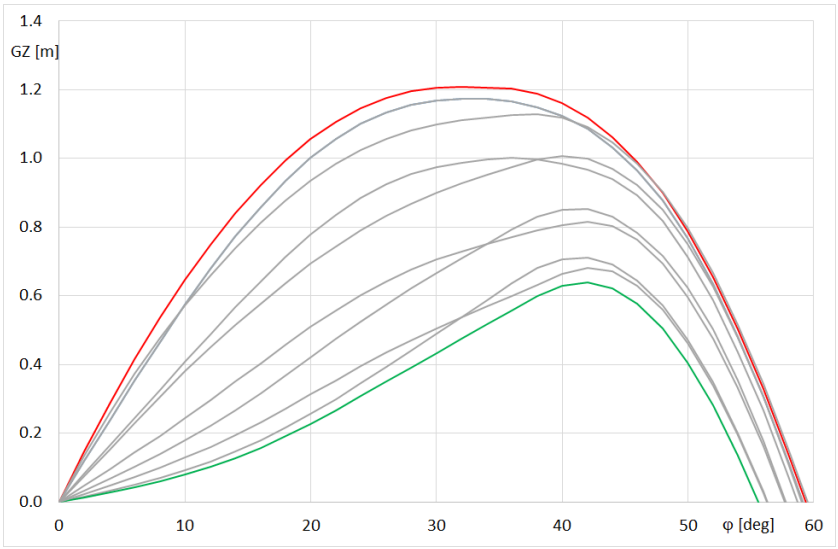

Figure 8 – Two-dimension representation of the restoring moment as a function and heel angle for 10 wave positions

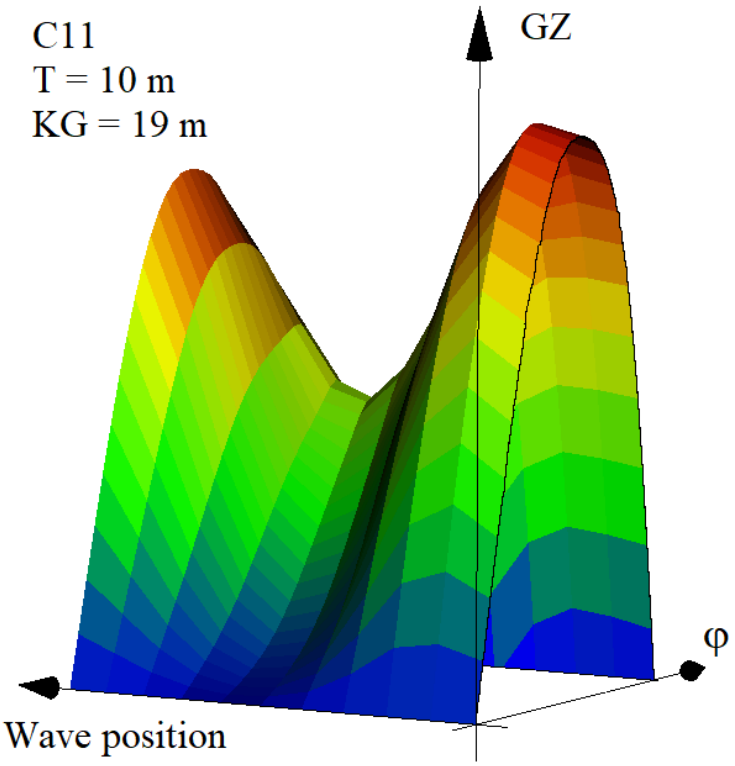

Figure 9 - Three-dimension representation of the restoring lever as a function of the wave position and of the heel angle, equivalent to the one presented in Figure 8

The one-degree-of-freedom parametric roll differential equations 9 and 10 have no analytic solution. Thus, a numerical method is required to solve them. Several numerical solving solutions such as Euler method, Runge-Kutta of order 2, 4 or 4.5 can be used. Euler method is easy to implement, however it is known for its poor accuracy since it diverges after few periods. Runge-Kutta methods provide an acceptable accuracy and should preferably be used. A mathematical implementation of the solving of Equation 10 with the method of Runge-Kutta at 4^{th} order is provided by Grinnaert (2017).

Throughout this PhD thesis, time-domain simulations in 1-DoF are conducted using a time-domain solver referred as "1-DoF" and solving of the differential Equation 10 with the Runge-Kutta 4^{th} order method. This time-domain solver was built in Excel by Grinnaert within the scope of his PhD (Grinnaert, 2017) and improved within the scope of this PhD. The user guide associated to this time-domain solver is presented in Annex 7. The GZ curves in waves are pre-computed with the hydrostatic solver Calcoque (Grinnaert et al., 2015). Calcoque is a real three-dimension hydrostatic code computing the equilibrium and the transverse stability in both calm water and regular longitudinal waves. Thus, the ship model is not directly required to use the time-domain solver. The one-degree-of-freedom time-domain solver permits to simulate parametric roll motions of the ships in longitudinal regular waves.

The 1-DoF time-domain solver can either solve numerically the parametric roll differential equation considering linear and non-linear GZ (equations 9 and 10, respectively). It considers a constant roll moment of inertia (J_{44}) during the simulation. Thus, the value of J_{44} provided by the user should include the added mass from the radiation forces. The roll damping coefficient B_{44} can either be automatically estimated during the simulation using Ikeda method (Ikeda, 1978; Kawahara, 2009) or imposed by the user as a linear and a quadratic roll damping coefficient (B_{Lin} in $N.m.s.rad^{-1}$ and B_{Quad} in $N.m.s^2.rad^{-2}$, respectively). When the roll damping is imposed by the

user, Equation 10 is replaced by Equation 11. B_{Lin} and B_{Quad} must be provided for the considered speed.

$$J_{44}\ddot{\varphi} + B_{Lin}\dot{\varphi} + B_{Quad}\dot{\varphi}|\dot{\varphi}| + WGZ(\varphi, t) = 0 \quad 11$$

Solving Equation 11 permits to reproduce simulations obtained from model tests.

Prior to realise the simulations, the speed for which the first mode of parametric roll should appear is pre-calculated using Equation 3. The ships natural roll frequency is estimated using the following Equation:

$$\omega_0 = \sqrt{\frac{W.GM_{Mean}}{J_{44}}} \quad 12$$

When realising simulations with this 1-DoF time-domain solver within this PhD thesis, the time step is set between one 30th and one 60th of the natural roll period of the ship, in accordance with the recommendations formulated by Peters et al, (2015) and by the IMO (2016) toward the Second Generation Intact Stability Criteria.

Since this solver is limited to 1-DoF, it does not consider the coupling between the different degrees of freedom. In addition, this solver is limited to longitudinal seas (no direct excitation). Therefore, the ship's motions prediction accuracy is lower than the one of a time-domain solver handling several degrees of freedom.

1.2.2. Several-degree-of-freedom assessment

A ship sailing at sea can experience motions in 6 degrees of freedom (Figure 10). Thus, complex time-domain solvers considering all 6 degrees of freedoms exist. Such solvers consider the coupling between each degree of freedom in the motion equation. Thus, no specific equation for parametric roll is required, a 6 DoF equation of the motion is provided instead (Equation 13, here illustrated as a linear equation). When assessing the phenomenon of parametric roll, the International Maritime Organisation recommends to consider at least heave, roll, and pitch (IMO, 2020a; IMO, 2021b). The addition of heave and pitch degrees of freedom may reduce the variation of stability in waves, leading to a narrowest lock-in field and reduced roll amplitudes (Spyrou, 2000). The other 3 degrees of freedom are considered to have less influence on parametric roll motions through coupling.

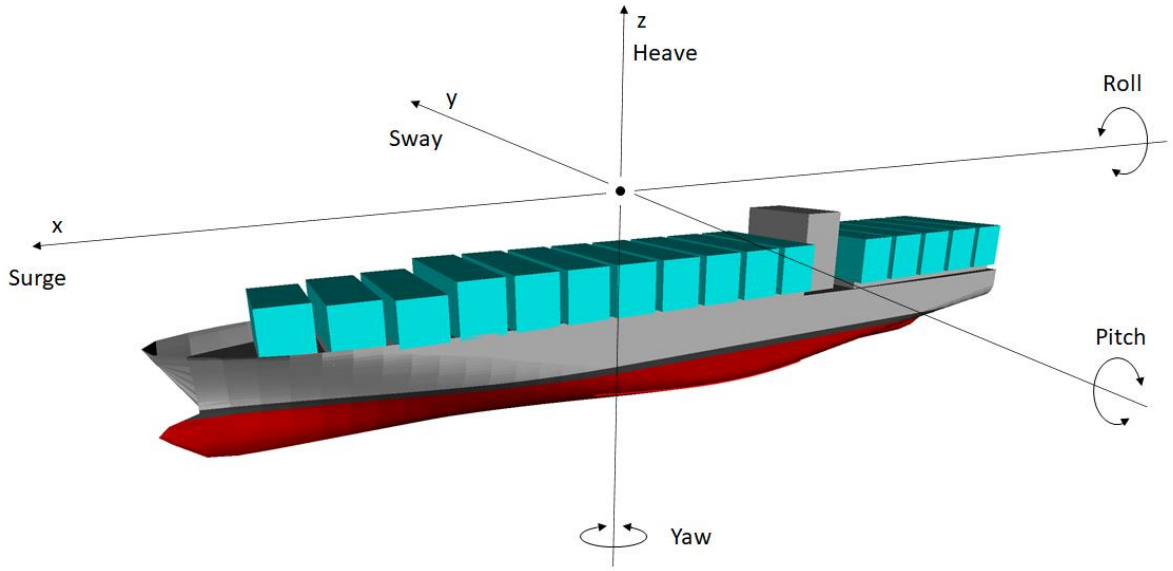

Figure 10 - The ship six degrees of freedom

$$[Inertia] \times [\ddot{X}] + [Damping] \times [\dot{X}] + [Stiffness] \times [X] = [F_{ext}] \quad 13$$

[X]	(m; rad)	6-dimension vector, position
$[\dot{X}]$	($m.s^{-1}$; $rad.s^{-1}$)	6-dimension vector, velocity
$[\ddot{X}]$	($m.s^{-2}$; $rad.s^{-2}$)	6-dimension vector, acceleration
[Inertia]	(kg; $kg.m^2$; kg.m)	6*6 matrix, inertia
[Damping]	($N.s.m^{-1}$; $N.m.s.rad^{-1}$; N.s)	6*6 matrix, damping
[Stiffness]	($N.m^{-1}$; N.m; N)	6*6 matrix, stiffness
[F_{ext}]	(N; N.m)	6-dimension vector, external forces

Hydrodynamic software able to reproduce the ship motions in complex sea state in 6-DoF were developed jointly from governments, private companies, class societies and Towing tank research facilities. Known ones are LAMP-2 (US Navy, ABS), Fredyn (CRNav, MARIN), Hydrostar ++ (BV), NLOAD3D (ABS), Wasim (DNV) and X-Dyn. Those software or equivalent ones are required to assess parametric roll level 3 (direct assessment) of the IMO second generation intact stability criteria (IMO, 2020a), presented in Section 1.3.1. A validation of the simulated roll motions toward a parametric roll direct assessment is provided by Kapsenberg et al. (2019) for 5 of the solvers mentioned hereabove. It shows that the estimation of the roll damping between the solver is unreliable. However, when avoiding this problem with measured values, the five hydrodynamic solvers provide little variations (Kapsenberg et al., 2019). Kapsenberg et al. (2020) provide a comparison of 4 of the solvers mentioned hereabove, within the scope of a work for the Cooperative Research Ships (CRS) community. This comparison is conducted through roll decay, forced roll tests and in irregular longitudinal sea state to compare the distribution of parametric roll events.

The hydrodynamic time-domain solver Fredyn is used within the scope of this PhD thesis. Fredyn is developed by the Cooperative Research Navies (CRNav) consortium. Fredyn features presented hereafter are available in detailed in its full documentation (CRN, 2021; MARIN, 2009a, MARIN 2009b). Fredyn requires to be coupled to another software in charge of the pre-computation of

the radiation and diffraction forces. It aims to realise a database of the radiation and diffraction forces in order to reduce computational time. The software Shipmo (MARIN, 2013) is used when strip theory is considered to calculate those forces, requiring to provide a section file of the hull geometry. Alternatively, the software PanShip (MARIN, 2012) can be used when panel method is considered, requiring to provide a mesh file of the hull geometry. Both are based on a potential flow theory; such methods are presented by Bertram (2000). Within this PhD, the software Shipmo was used to pre-compute hydrodynamic forces.

The radiation forces in time-domain are divided in added mass component and damping component which are equivalents to the ones used in frequency domain. They are calculated in the 3-DoF of the plan of each hull section (sway, heave, roll) as a function of the motion frequency based on linear strip theory. This theory is applicable to vessels which length-over-breadth ratio is larger than 6.5. This is the case of most container ships.

The diffraction forces are pre-calculated by Haskind method (MARIN, 2009a) using linear strip theory. Shipmo creates a database providing the linear transfer functions of the diffraction forces and moments as a function of the wave frequency, relative wave direction and ship speed. The transfer functions are considered independent of roll and pitch.

In Fredyn all 6-DoF can be set free. All couplings between DoF are taken into account in the matrix representation of the system, except the one between roll and yaw. The motion equation in 6 DoF is based on the Newton's second law. The vessel is considered to be infinitely stiff. A linear approach is applied to potential forces, they can be split and superposed (Froude-Krylov, radiation and diffraction effects). The viscous forces are added to the potential forces. The interaction between the vessel and the waves it creates are not considered. The wave profile without perturbation is used to compute the relative water height along the hull and to calculate the associated Froude Krylov forces.

Froude-Krylov forces calculation is realised at each time step. The wetted surface area and the position of the centre of buoyancy are calculated for each section as a function of the draught and list. This approach permits a fast calculation of those forces when conducting time-domain simulations (restoring and excitation due to waves).

The propulsion forces are calculated in calm water based on the instantaneous water speed in the vicinity of the propeller. Required data are provided by the user as a J, KT table. J defines the advance ratio (function of the speed, propeller diameter and propeller revolution per minute) and KT defines the propeller thrust coefficient (Bertram, 2000).

The forces applied on the appendages (rudder) are calculated at each time-step considering their shape and the local speed.

A large number of inputs is provided to simulate the environmental and loading conditions as close as the ones encountered. It permits to perform high-fidelity simulations on real sea states. However, it can be a hard task to evaluate some inputs with a sufficient accuracy to reproduce the motions observed in real case.

The combination of a ship model and a 6-DoF solver is a digital twin of the real ship. It enables engineers to reproduce numerically as accurately as possible the ships motions in complex sea states. Thus, such solvers are used to evaluate the ship seaworthiness.

1.3. GLOBAL ASSESSMENT

The global assessments aim to state if vessel is sensitive to the phenomenon of parametric roll, and if so, to provide roll polar plots to avoid the worse combinations of course and speed for pre-

defined loading and environmental conditions. Here-after, the regulatory parametric roll assessment provided by the IMO is presented, in addition to the assessment procedures provided by Bureau Veritas and American Bureau of Shipping. The Bureau Veritas assessment procedure has partially been implemented within the scope of this PhD thesis.

1.3.1. IMO, MSC.1/Circ.1627: Interim guidelines on the second generation intact stability criteria

Accidents in waves highlighted the insufficiency of the first generation intact stability criteria of the IMO contained into IS code 2008 (IMO, 2008). To avoid those accidents, the International Maritime Organisation decided to work on new criteria in 2007 (Grinnaert et al., 2017; Francescutto, 2015). This new regulation named Second-Generation Intact Stability Criteria (denoted by SGISCs) were finalized in 2020 (IMO, 2020a). The explanatory notes of the regulation are under finalisation at the time of the submission of this PhD thesis. At this time, the SGISCs are not mandatory. However, shipyards are encouraged by the IMO to apply those criteria to be familiar with them and to validate their use. Five failure modes in waves are considered:

- Dead ship condition
- Excessive acceleration
- Pure loss of stability
- Parametric roll
- Surf riding and broaching

For each failure mode, a three-level approach is proposed. The assessed vessel must comply with at least one level for each failure mode. If the vessel does not comply with the regulation for one or more failure mode, it is possible to provide Operational Measures to reduce the risk of appearance of the phenomenon. The first level is based on a simplified physical deterministic approach, guarantying a large safety margin. The second level is based on a more accurate physical probabilistic approach and is supposed to reduce the safety margin obtained with the level-one criteria. The third level is a direct assessment which consists in numerical simulations of the motions of the ship in waves. Finally, Operational Measures can be introduced if the vessel does not comply with the requirement of any of the three levels.

Level One and Level Two assess at least each loading condition defined in the stability booklet. The direct stability assessment proposed as level three is realised for predefined loading conditions and proposes to interpolate results in between to realise roll polar plots for further operational use. Operational Measures can be applied to the vessel if she does not fulfil the criteria to reduce the risk based on the results of the direct assessment. If the vessel fulfils one criterion, a safe zone defined by acceptable values of GM, draught and trim is to be provided. Any of the four alternatives may be applied first. Thus, as an example, level 2 can be applied without assessing level 1. A simplified scheme of the application structure of the SGISCs is provided by the IMO (Figure 11, IMO, 2020a).

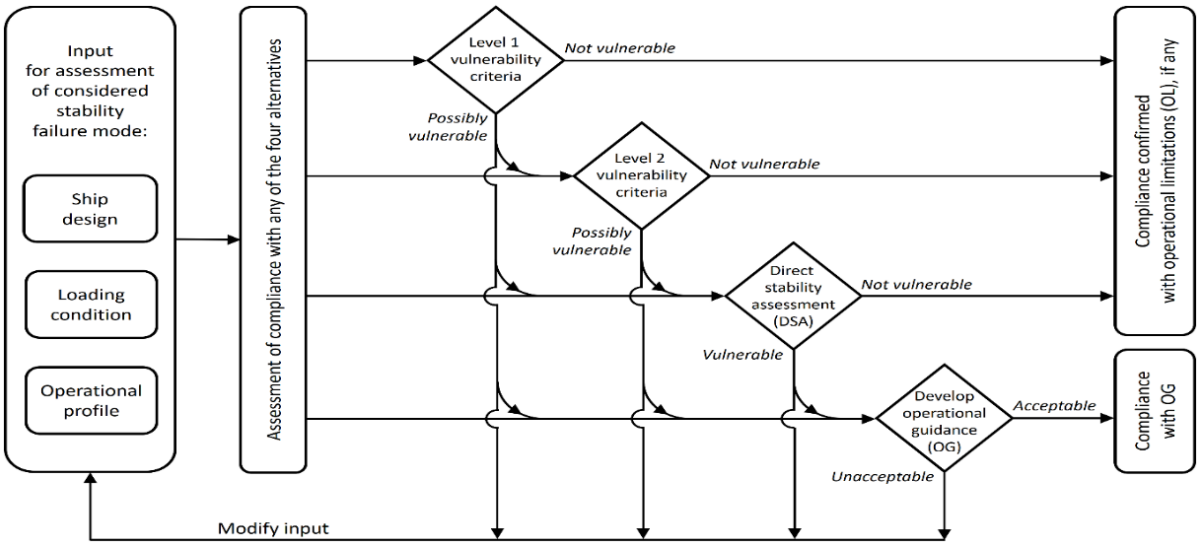

Figure 11 - Simplified scheme of the application structure of the SGISCs (IMO, 2020a)

The regulatory criteria of levels 1 and 2 of parametric roll are described hereafter.

Level 1

The level-one criterion consists of a static study of parametric roll. It considers the metacentric height (GM) in calm water and the amplitude of variation of the metacentric height (δGM_1). Two conditions must be simultaneously verified to fulfil the criterion (Equations 14 and 15).

$$\frac{\delta GM_1}{GM} \leq R_{PR} \tag{14}$$

$$\frac{\nabla_D - \nabla}{A_W(D-d)} \geq 1 \tag{15}$$

∇_D (m^3) Volume of displacement at a draught equal to D at zero trim

∇ (m^3) Volume of displacement corresponding to the loading condition under consideration

D (m) Moulded depth as defined in IS Code 2008 (IMO, 2008)

d (m) Mean draught amidships in calm water for the loading condition under consideration (denoted by d by IMO and by T outside of this section throughout the PhD thesis)

A_W (m^2) Waterplane area at the draught equal to d

R_{PR} (-) Coefficient regarding the roll damping, if the ship has sharp bilge keels to be taken as 1.87, otherwise to be calculated as follows:

If $C_{m,full} > 0.96$

$$R_{PR} = 0.17 + 0.425\left(\frac{100A_K}{LB}\right) \tag{16}$$

If $0.94 \leq C_{m,full} \leq 0.96$

$$R_{PR} = 0.17 + \left(10.625C_{m,full} - 9.775\right)\left(\frac{100A_K}{LB}\right) \tag{17}$$

If $0.94 < C_{m,full}$

$$R_{PR} = 0.17 + 0.2125\left(\frac{100A_K}{LB}\right) \quad 18$$

The ratio $100A_K/LB$ should not exceed 4.

$C_{m,full}$ (-) Midship section coefficient of the fully loaded departure condition in calm water

L (m) Ship length as defined in Is code 2008

B (m) Breadth, moulded

A_K (m^2) Total overall area of the bilge keels

Equation 14 compares the non-dimensional variation of the stability on wave with a predefined value considered acceptable by the regulation- denoted by R_{PR}. The maximum value allowed by the regulation depends on the hull shape and considers the added roll damping provided by the vessel's bilge keels. Equation 14 is geometrically and physically relevant only if Equation 15 is fulfilled. Otherwise, the ship hull form does not permit to assess the vulnerability of the vessel through level 1 criteria, such as illustrated in Figure 12. Equations 16 to 18 shows that R_{PR} increases linearly with the bilge keels area. As an example, the C11-class container ship (presented in Annex 4) known for its vulnerability to parametric roll presents a $C_{m,full}$ equal to 0.972. In this condition Equation 16 is to be applied. The maximum R_{PR} value that can be calculated is 1.87 which is reached for a bilge keel area of 420 m^2 since $100A_K/LB$ should not exceed 4. In practice the vessel presents a bilge keel area of 43.3 m^2 which leads to R_{PR} equal to 0.37.

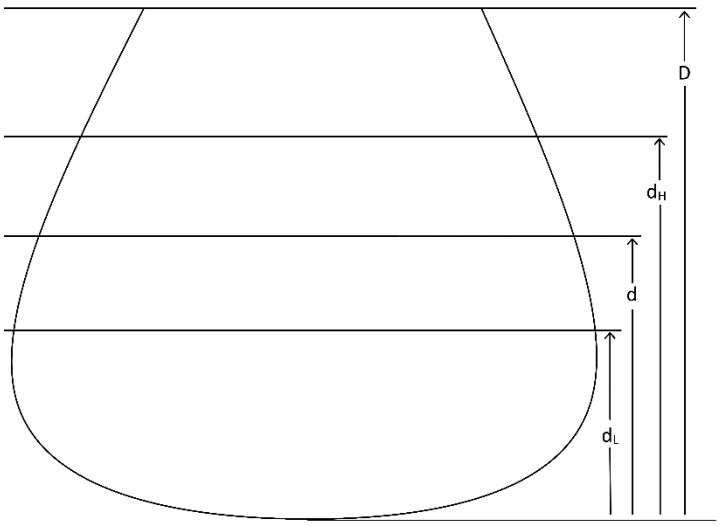

Figure 12 - Hull form which does not satisfy Equation 15

The amplitude of the variation of the metacentric height δGM_1 in metre is calculated as follows:

$$\delta GM_1 = \frac{I_{TH} - I_{TL}}{2\nabla} \quad 19$$

I_{TH} (m^4) Transverse moment of inertia of the waterplane at the draught d_H

I_{TL} (m^4) Transverse moment of inertia of the waterplane at the draught d_L

It is considered that the minimum and maximum moments of inertia of the waterplane area in longitudinal waves are respectively equal to that of parallel waterplanes at a lowest draught d_L and at a highest draught d_H. Both draughts are calculated as follows:

$$d_L = d - min\left(d - 0.25d_{full}; \frac{LS_W}{2}\right) \quad 20$$

$$d_H = d + min\left(D - d; \frac{LS_W}{2}\right) \quad 21$$

S_W (-) Wave steepness, to be taken as 0.0167

As presented in Equation 20, the minimum draught on waves cannot be lower than the quarter of the full loaded draught. As well in Equation 21, the maximum draught on waves cannot be larger than the vessel depth.

This static method considers a relevant environmental case for parametric roll with a longitudinal wave of length (λ) equals to the length of the ship defined in the IS code 2008 as the length between perpendiculars and of wave steepness 0.0167. The wave height is calculated by multiplying the wave length by the wave steepness. Figure 13 presents the waterplanes at draught d, d_H and d_L for a general case. Figure 14 presents the water plan area of a 14400-TEU container vessel at d_H and d_L. It is observed that an important variation of the waterplane area appears on the specified wave for this vessel.

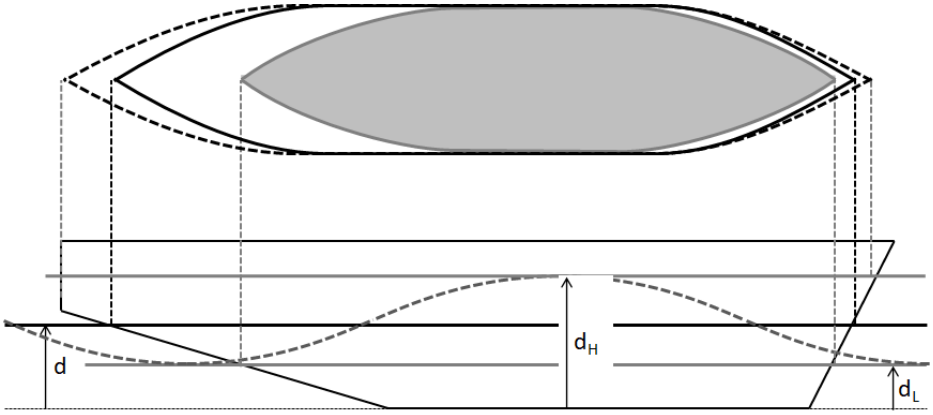

Figure 13 - Parallel waterplane at d_H and d_L (Grinnaert, 2017)

Figure 14 - Parallel waterplanes at d_H (blue) and d_L (red), 14400 TEU

Level 2

If the ship fulfils level 1 there is no need to assess level 2. As well, level 2 can be assessed without assessing level 1. Level 2 is based on two independent checks corresponding to two independent probabilistic approaches. The ship is considered not to be vulnerable to parametric roll if she complies with any of those two checks:

First check

This first check is a static study of the ship stability in waves. It is based on two conditions and considers a reduced wave scatter diagram. The vessel is considered not to be vulnerable to parametric roll is C1 is not larger than 0.06, C1 is calculated as follows:

$$C_1 = \sum_{i=1}^{16} W_i C_i \quad (22)$$

W_i Weighting factor for the considered wave, available in Table 2.

C_i Equal to 0 if any of the conditions 1 or 2 is satisfied (hereafter), 1 otherwise.

Sixteen waves presented in Table 2 are considered and defined by a wave height H_i and a wavelength λ_j and associated with a weighting factor W_i. This reduced wave scatter table is calculated from the wave scatter diagram provided by the International Association of Classification Societies (IACS, 2001). The wavelength λ is calculated (Equation 23) using the zero-crossing period T_Z with the infinite depth formula, considering a Bretschneider sea spectrum. The wave height is calculated as the average height of the weighted waves at T_z multiplied by a coefficient k_{PR} equal to 0.7 (Equation 24). The weighting factor is calculated as the sum of the weighting factors of all sea states at T_z (Equation 25).

$$\lambda = \frac{g(1.0864.T_Z)^2}{2\pi} \quad (23)$$

$$H_i = \frac{k_{PR}}{W_i} \sum_{j=1}^{17} W_{i,j} H_{i,j} \quad (24)$$

$$W_i = \sum_{j=1}^{17} W_{i,j} \quad (25)$$

$W_{i,j}$ and $H_{i,j}$ are respectively the weighting factor and the wave height and are to be taken from the IACS wave scatter diagram (IACS, 2001).

Wave case number	Weight factor W_i	Wavelength (m) λ_j	Wave height (m) H_i
1	0.000013	22.574	0.350
2	0.001654	37.316	0.495
3	0.020912	55.743	0.857
4	0.092799	77.857	1.295
5	0.199218	103.655	1.732
6	0.248788	133.139	2.205
7	0.208699	166.309	2.697
8	0.128984	203.164	3.176
9	0.062446	243.705	3.625
10	0.024790	287.931	4.040
11	0.008367	335.843	4.421
12	0.002473	387.440	4.769
13	0.000658	442.723	5.097
14	0.000158	501.691	5.370
15	0.000034	564.345	5.621
16	0.000007	630.684	5.950

Table 2 - Reduced waves scatter table, IMO, 2020a

For each wave of Table 2, 10 positions of the ship on the wave regularly distributed are considered with a step of $0.1\lambda_i$ forward and aft from amidship. Any hydrostatic solver able to balance the ship in trim and sinkage on longitudinal waves can be used to calculate the 10 metacentric heights, corresponding to the 10 positions of the wave along the ship. The average value of GM in waves

is calculated and the minimum and maximum values of GM are used to calculate the half GM variation. This discretisation is supposed to be sufficient to obtain the maximum and minimum metacentric height on the wave with an acceptable accuracy.

1st condition

$$GM(H_i, \lambda_i) > 0 \qquad and \qquad \frac{\delta GM(H_i, \lambda_i)}{GM(H_i, \lambda_i)} < R_{PR} \tag{26}$$

R_{PR}	(-)	As defined in level-one criterion
$GM(H_i,\lambda_i)$	(m)	Average value of the 10 metacentric heights, corresponding to the loading condition under consideration, considering the ship balanced in sinkage and trim on a series of waves characterized by a wave height H_i and a wavelength λ_i
$\delta GM(H_i,\lambda_i)$	(m)	One-half the difference between the maximum and minimum values of the metacentric height, corresponding to the loading condition under consideration, considering the ship balanced in sinkage and trim on a series of waves characterized by a wave height H_i, and a wavelength λ_i

This first condition verifies that the metacentric height in wave remains positive and that the non-dimensional variation of the transverse stability is acceptable for all considered waves. The vessel is considered to be vulnerable to parametric roll if C1 is larger than 0.06. Then, if the vessel does not fulfil one or more conditions for wave cases numbered 4 to 9, she will not fulfil the first check (Table 2).

2nd condition

$$V_{PRi} > V_s \qquad with \qquad V_{PRi} = \left| \frac{2\lambda_i}{T_0} \sqrt{\frac{GM(H_i, \lambda_i)}{GM}} - \sqrt{g \frac{\lambda_i}{2\pi}} \right| \tag{27}$$

V_{PRi}	($m.s^{-1}$)	Speed corresponding to the first mode of parametric roll resonance (the encounter frequency is twice the natural roll frequency)
Vs	($m.s^{-1}$)	Ship service speed
T_0	(s)	Natural roll period
GM	(m)	Metacentric height in calm water

This condition is based on the vessel speed. It considers that if the vessel cannot sail fast enough to reach the first mode of parametric roll resonance, she is not subject to it. The mathematical proof of Equation 27 is presented by Grinnaert (2017, Annex 3).

Thus, this first probabilistic approach considers 16 waves on which the vessel is assessed. The vessel is considered to be not subject to parametric roll on each wave if she cannot reach the speed corresponding to the one of appearance of the first mode of parametric roll or if the non-dimensional variation of the transverse metacentric height in wave and is sufficiently low. The vessel is considered not vulnerable to parametric roll if the check C1 (Equation 22) calculated from all 16 waves is not greater than 0.06.

Second check

The second check of level two is assessed if the first check is not fulfilled. It relies on a statistical study as well, considering dynamic ship roll in longitudinal waves.

C2 coefficient is associated to the second check. The vessel is considered not to be vulnerable to parametric roll if C2 is not greater than R_{PR2} = 0.025. C2 is calculated considering the maximum roll

angle of the ship on equivalent sinusoidal waves for each non-zero-weighted waves of the wave scatter diagram (IACS, 2001), considering 13 speeds (12 + zero speed) in both head and following seas. For a given speed and a given wave, the maximum roll angle is determined by solving the one-degree-of-freedom differential equation of parametric roll, Equation 10, rewritten hereunder:

$$J44\ddot{\varphi} + B44\dot{\varphi} + WGZ(\varphi, t) = 0 \quad (10)$$

φ	(rad)	Roll angle
J_{44}	(kg.m^2)	Roll moment of inertia, including added mass
B_{44}	(N.m.s.rad^{-1})	Damping coefficient, function of the roll amplitude
W	(N)	Ship's weight
GZ(φ,t)	(m)	Righting arm, function of both the roll angle φ and time t, varying with the wave encounter frequency

The 1 DoF time-domain simulations can be conducted considering 10 GZ curves in waves calculated for the ship balanced in trim and sinkage as presented previously.

C2 coefficient is calculated as follows:

$$C_2 = \left[\sum_{i=1}^{12} C_2(V_i, \beta_h) + \frac{1}{2}\{C_2(0, \beta_h) + C_2(0, \beta_f)\} + \sum_{i=1}^{12} C_2(V_i, \beta_f)\right]/25 \quad (28)$$

$$V_i = K_i V_s \quad (29)$$

$C_2(V_i,\beta_h)$	(-)	Coefficient $C_2(V_i,\beta)$ for ship sails in head waves with a speed equal to V_i
$C_2(V_i,\beta_f)$	(-)	Coefficient $C_2(V_i,\beta)$ for ship sails in following waves with a speed equal to V_i
V_i	(knt)	Vessel speed
K_i	(-)	To be taken in Table 3, to calculate the vessel speed

i	K_i
1	1.0
2	0.991
3	0.966
4	0.924
5	0.866
6	0.793
7	0.707
8	0.609
9	0.500
10	0.383
11	0.259
12	0.131

Table 3 - K_i factor for calculation of vessel speeds

For zero speed case, Equation 28 considers two different computations in head and following seas.

$C_2(V_i,\beta)$ is calculated as follows:

$$C_2(V_i, \beta) = \sum_{i=1}^{N} W_i C_{S,i} \quad (30)$$

W_i (-) Weighting Factor, available in (IACS, 2001) (divided by 100,000)

$C_{S,i}$ (-) Equal to 1 if the maximum roll angle is larger than 25 degrees, 0 otherwise.

In order to simplify the calculation of stability in waves, the Grim effective wave concept is considered (Grim, 1961). This concept consists of replacing an irregular sea state defined by a zero-crossing period (T_Z) and a significant height (H_S) as provided in the IACS scatter diagram (IACS, 2001) by a single equivalent sinusoidal wave which length is equal to that of the ship. The height of the resulting effective wave is denoted here by H_{ri}. Its calculation is presented by Grinnaert (2017, Annex 3) and in the explanatory notes of the SGISCs (IMO, 2021a).

Thus, 11 wave cases are considered to compute the maximum roll angle as follows:

Wavelength; $\lambda = L$

Wave height; $h_j = 0.01jL$, with $j=0,1,\ldots,10$

For each wave height h_j, the maximum roll angle is calculated by solving Equation 10. Then for each non-zero weighted wave in the scatter diagram (IACS, 2001) characterized by its effective wave height H_{ri}, the maximum roll angle is interpolated between the 11 maximum roll angles previously calculated on the 11 waves. If the maximum roll angle is larger than 25 degrees, then C2 = 1, 0 otherwise.

Finally, this second check considers that the vessel is not vulnerable to parametric roll if the probability to encounter conditions leading to roll amplitudes larger than 25 degrees is lower than 0.025. It considers that the vessel sails as much in head and following seas and all speeds are evenly weighted.

Example of 1st and 2nd levels

Figure 15 presents the minimum allowable GM curve (GM_{min}) associated with the 1st generation intact stability criteria (IMO, 2008) of the 350-metre container vessel (Hyundai Heavy Industries, 2017), and the minimum allowable GM curves associated with the Level-1 and Level-2 criteria of the second-generation intact stability criteria (IMO, 2020a). GM_{min} is the lowest value of GM for which the vessel complies with all considered criteria. The loading condition reported in the stability booklet are plotted as black circles. The operational loading conditions reported by the shipowner are plotted as blue dots. It is observed that the Level-1 criterion is very conservative and does not reflect the operational GM range of the vessel in some cases. The first check of Level-2 criterion is less conservative but does not represent most of the loading cases defined in the stability booklet. The second check of Level-2 criterion is less conservative than the criteria proposed in the 1st generation intact stability code (IMO, 2008) for the ship on ballast condition (draught lower than 9.5 metres). When new criteria will enter into force, the ships will not be considered as vulnerable to parametric roll in this area. Between 9.5 and 16.5 metres the new criteria are slightly more stringent than the first-generation criteria. All loading conditions defined in the stability booklet complies with the second check of the Level-2 criterion. Consequently, is not necessary to conduct the parametric roll direct assessment (level 3) for this vessel.

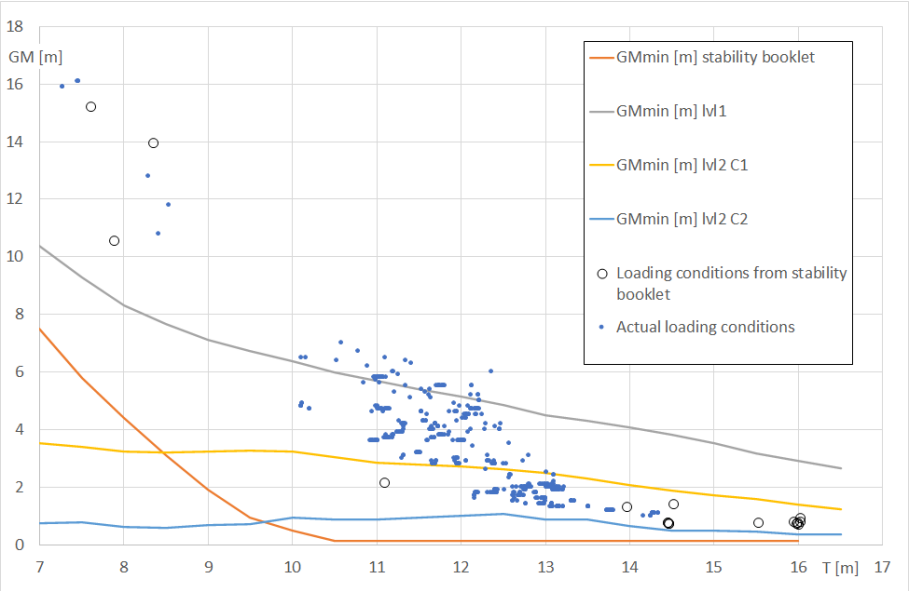

Figure 15 - Example of GM_{min} curves for a 350-metre container vessel

Level 3

Level Three is a direct assessment of the ship motions in waves considering all failure modes. The complexity of Level Three is higher than Level One and Level Two. It is conducted by hydrodynamics engineers and requires specific numerical tools such as the ones are available in numerical towsing tanks. The criteria consider that the average stability failure rate shall not exceed 2.6×10^{-3} per ship per year.

Two methods are proposed to estimate the ship motion in waves:

- Model test
- Numerical simulations

Since the stability failures are rare, long simulations or long model tests must be performed. Therefore, a combination of model tests and numerical simulations can be agreed by the Administration. Both methods must adequately replicate the ship motions in waves. The procedures specified by IMO (2020a) must be followed for pre- and post-process of the direct assessment. The software selected to perform numerical simulations shall be validated qualitatively and quantitatively. Such software solves the equations of the motion of the ship sailing in waves.

Three different assessments can equivalently be performed in this direct assessment:

- Full probabilistic assessment
- Assessment using probabilistic criteria in design situations
- Assessment using deterministic criteria in design situations

Both probabilistic assessments consider a stability failure if the maximum roll angle is larger than 40 degrees or if the lateral acceleration exceeds 9.81 $m.s^{-2}$ at any position on the ship where a human may stay. Deterministic assessment considers half of these values.

Waves

The waves should be modelled by sea states defined with their zero-crossing period T_z and their significant height H_S. The mathematical model of the waves must be hydrodynamically and statistically valid and allow the calculation of the hydrodynamic forces. Brestshneider wave energy spectrum and cosine square wave spreading function are recommended.

Roll damping and mathematical modelling

Roll damping model may be defined from roll decay tests, forced roll tests, CFD computations on the vessel, CFD computations on similar vessels or from empirical formulae (eg: Ikeda, 1978; Kawahara, 2009). It should include wave, lift, vortex, and skin friction components. Model test is the preferred source of information. Special care must be provided to avoid considering some components more than once. When using software, the Froude-Krylov forces are calculated using body-exact formulation (Lewis's form method should not be used) with the strip theory (each station is computed independently) or 3D panel theory. Radiation and diffraction forces are to be computed from either approximate coefficient, body linear solution or body-exact solution. Hydrodynamic reactions are approximated for sway forces, roll and yaw moment by either coefficient derived from model test, CFD computations, empirical formulae, or empirical database. The propeller thrust is to be calculated from coefficients based on model test (J, K_T curves).

Software validation for parametric roll

Software shall be qualitatively and quantitatively validated. Qualitative validation checks that software correctly reproduces the failure modes, while quantitative validation determines the degree of prediction of failure modes. Both qualitative and quantitative requirements are described by IMO (2020a). For parametric roll failure mode, ship motion simulations should at least include the following three degrees of freedom: heave, roll and pitch. Fredyn software (Kapsenberg et al., 2019; Kapsenberg et al., 2020) complies with the requirements exposed hereabove.

Full probabilistic assessment

The criterion is based on the mean-long term rate of the stability failure, calculated as the weighting average over all conditions. The conditions to be tested shall cover all non-zero weighted waves of the IACS wave scatter diagram (2001). The speeds must be regularly distributed from 0 to the service speed. The relative wave heading is to be regularly distributed. All loading cases from the stability booklet shall be tested. This requires a large number of simulations. The mean stability failure mode should not exceed 2.6×10^{-8} s^{-1} to satisfy the requirement.

Assessment using probabilistic criteria in design situations

The probabilistic assessment with design situation is based on probabilistic criteria with a reduced number of cases. Only zero speed is considered in head and following seas with a reduced wave scatter diagram available in the SGISc (IMO, 2020a). It is considered that a stability failure shall not appear more than once every 2 hours in design see states with a probability density of 10^{-5} $(m.s)^{-1}$.

Assessment using deterministic criteria in design situations

Since deterministic criterion is less accurate, the ship is considered to fail at least one failure mode if the roll angle is larger than 20 degrees or if lateral acceleration is larger than 4.905 $m.s^{-1}$. The criterion considers the mean 3 hours maximum roll angle. At least 15 hours of simulation for each case are to be carried out. The average value of the 5 mean 3-hours-maximum roll angles is calculated. All waves of a second reduced scatter diagram available in the SGISCs (IMO, 2020a) are to be tested with a probability density of 7×10^{-5} $(m.s)^{-1}$. Loading conditions are the ones defined in the stability booklet. The speed is considered null. Head and following wave directions are considered.

Operational measures

A vessel not complying with any of the three levels can sail with restrictions. In this case, Operational Measures shall be defined (IMO, 2020a; Petacco and Gualeni, 2020; Petacco and Gualeni, 2021). The Operational Measures can be both Operational Limitations and Operational Guidance. Operational Limitations focus on restrictions on the sailing area, wave heights, and on the seasons where the probability of occurrence of unfavourable sea state is too important.

Operational Guidance aims to define precisely the possible encountered sea states, loading conditions, speeds and headings corresponding to an acceptable failure rate. Thus, Operational Guidance provides to the master operational tools to avoid high risk situations for the operational lifetime of the vessel, based on the forecasted weather without predefined limitations of sailing areas and/or seasons (eg: roll polar plots).

1.3.2. BV, NR 667: Parametric roll assessment

Bureau Veritas proposes to assess the vulnerability of container ships toward parametric roll. The procedure is defined in NR 667 (BV, 2019b) and relies on a full assessment of the ship motions on pre-defined loading and environmental conditions. Time-domain simulations in real sea state in at least 3 degrees of freedom (heave, roll and pitch) are conducted. Other failure modes may be considered simultaneously if the required degrees of freedom are taken into account in the simulations. The aim is to provide user friendly roll polar plots (go and no-go areas) to the master for each pre-defined loading and sea state condition, by comparing the roll amplitude obtained from simulations and the maximum roll angle acceptable by the lashing of the containers.

Bureau Veritas proposes two class notations:

- PaRoll1, for container ships without any anti-rolling device or only using bilge keels as anti-rolling devices.
- PaRoll2, for container ships using anti-roll devices such as anti-roll tank, stabilizer fins or any other anti-rolling devices other than bilge keels.

Those class notation have not been assigned yet to any vessel since no complete parametric roll assessment using NR 667 was conducted. Since most container vessel do not have any other anti-roll device than bilge keels, containers ships would have the class notation PaRoll1 if the assessment is completed.

In this assessment the ship motions are to be computed using a non-linear time-domain hydrodynamic code. The Froude-Krylov forces are to be calculated by applying the pressure of the undisturbed incoming wave to the hull on every wet panel at any time step. Data used for roll damping calibration can be obtained from roll decay test, forced roll test or CFD computations. Non-linearities of the roll damping should be considered and can be modelled with a linear and a quadratic coefficient.

In order to ensure a maximum repeatability, the following information for pre- and post-treatment of the simulations are specified (sea states, speeds, loading conditions):

Sea states

The sea state input parameters are calculated from Table 4. This table is derived from the IACS wave scatter diagram (IACS, 2001). NI 638 (BV, 2019a), Appendix 1, provides the procedure to calculate this table, from the probability of appearance of the waves with the considered characteristics in 25 years. This table is referred as the 25th year contour.

T_Z (s)	4.5	5.5	6.5	7.5	8.5	9.5	10.5	11.5	12.5	13.5	14.5	15.5	16.5	17.5
H_S (m)	2.4	5.5	8.4	10.9	12.9	14.4	15.4	15.9	16.1	16.0	15.4	14.6	13.1	10.7

Table 4 - 25 Year contour, calculated from IACS scatter diagram (2001), according to NI 638 (BV, 2019a)

T_Z (s) Average zero up-crossing wave period

H_S (m) Significant wave height

Each sea state is modelled with a Pierson-Moskowitz spectrum denoted by $S_\eta(\omega,\beta)$ as defined in the NI 638 (BV, 2019a, section 2). The sea state definition (Equation 31) is the multiplication the monodirectional Pierson-Moskowitz spectrum (Equation 32) by a 90 degrees spreading function denoted by $G(\beta)$ as follows:

$$S_\eta(\omega,\beta) = S_\eta(\omega)G(\beta) \quad 31$$

$$S_\eta(\omega) = \frac{5{\omega_p}^4{H_s}^2}{16{\omega_w}^5}.exp\left[-1.25\left(\frac{\omega_p}{\omega_w}\right)^4\right] \quad 32$$

Where:

$S_\eta(\omega,\beta)$	($m^2.rad^{-1}.s$)	Wave energy density spectrum including directional spreading
ω_w	($rad.s^{-1}$)	Wave frequency
ω_p	($rad.s^{-1}$)	Peak frequency, calculated as follows for a considered spectrum:

$$\omega_p = \frac{2\pi}{T_p} = \frac{2\pi}{1.408T_z} \quad 33$$

A "cos^n" type spreading function is to be used (Equation 34 and 35), as defined in (BV, 2019a).

When $|\beta| \leq 90°$

$$G(\beta) = \frac{\pi}{180}.\frac{\Gamma\left(\frac{n}{2}+1\right)}{\sqrt{\pi}\Gamma\left(\frac{n}{2}+\frac{1}{2}\right)}.cos^n(\beta) \quad 34$$

When $|\beta| \geq 90°$

$$G(\beta) = 0 \quad 35$$

Where:

β	(deg)	Wave heading relative to the ship axis
n	(-)	Spreading parameter, Bureau Veritas recommends to consider the use of n = 8

Simulation's software require the number of directions in which the spreading function generates monodirectional sea states (denoted by N). Bureau Veritas recommends using N = 21 for a sufficient spreading range. The range of ± 90 degrees recommended by BV is especially discussed in Section 3.3 of this PhD thesis.

The numerical simulations are carried out for waves coming from 0 degree (following seas) to 180 degrees (head seas) with a maximum increment of 15 degrees. The roll polar plots are symmetric, thus only half of it can be computed, representing at least 13 directions to consider. For each wave period (T_z) provided in Table 4, the significant wave height to be taken into account must vary from zero up to the significant height specified in the 25-year contour table. The significant wave height step to consider is left to the appreciation of the person conducting the assessment. An example is provided in Table 5 with a significant height step set to one metre. This represents 178 sea states to be assessed:

T_Z (s)	4.5	5.5	6.5	7.5	8.5	9.5	10.5	11.5	12.5	13.5	14.5	15.5	16.5	17.5
	1	1	1	1	1	1	1	1	1	1	1	1	1	1
	2	2	2	2	2	2	2	2	2	2	2	2	2	2
	2.4	3	3	3	3	3	3	3	3	3	3	3	3	3
		4	4	4	4	4	4	4	4	4	4	4	4	4
		5	5	5	5	5	5	5	5	5	5	5	5	5
		5.5	6	6	6	6	6	6	6	6	6	6	6	6
			7	7	7	7	7	7	7	7	7	7	7	7
			8	8	8	8	8	8	8	8	8	8	8	8
H_S (m)			8.4	9	9	9	9	9	9	9	9	9	9	9
				10	10	10	10	10	10	10	10	10	10	10
				10.9	11	11	11	11	11	11	11	11	11	10.7
					12	12	12	12	12	12	12	12	12	
					12.9	13	13	13	13	13	13	13	13	
						14	14	14	14	14	14	14	13.1	
						14.4	15	15	15	15	15	14.6		
							15.4	15.9	16	16	15.4			
									16.1					

Table 5 – Example of sea states to be assessed, NR 667, step of 1 metre

Speed

The selected ship's speeds should cover the entire range of service speed from zero up to the maximum service speed (zero-speed must be considered). The maximum speed increment should be no more than 5 knots. An example is provided in Table 6 for a vessel which maximum speed is 24.6 knots considering the maximum allowed speed step. This represents 6 speeds to be assessed:

Speed [kn]	0	5	10	15	20	24.6

Table 6 – Example of the selected speed, NR 667, maximum service speed 24.6 knots

Loading condition

A loading condition is defined as a couple of values of draught (denoted by T) and metacentric height (denoted by GM). Several loading conditions are defined in the stability booklet. The GM corresponding to the smallest value of the GM of all loading conditions is denoted here by $GM_{min.book}$. The maximum value is denoted by $GM_{max.book}$. The draught associated with these metacentric heights are denoted by $T_{GMmin.book}$ and $T_{GMmax.book}$, respectively.

The loading conditions to be tested are defined from ($GM_{min.book}$,$T_{GMmin.book}$) to ($GM_{max.book}$,$T_{GMmax.book}$) as (GM_i,T_{GMi}). The first loading condition is ($GM_{min.book}$, $T_{GMmin.book}$) and the other couples are calculated as follows:

$$GM_{i+1} = \left(\Delta f \frac{0.825\pi}{\sqrt{g}} B + \sqrt{GM_i}\right)^2 \qquad 36$$

Where:

GM_i	(m)	Metacentric height at step i with the first step begin $GM_1 = GM_{min.book}$
GM_{i+1}	(m)	Metacentric height of the step i+1
Δf	(s^{-1})	Step coefficient, not to be larger than 0.015 s^{-1}
B	(m)	Breadth, moulded
g	(m. s^{-2})	Gravity, equal to 9.81 m.s^{-2}

T_{GMi} associated to GM_i is calculated by linear interpolation between ($GM_{min.book}$, $T_{GMmin.book}$) and ($GM_{max.book}$, $T_{GMmax.book}$). As an example, for a vessel for which minimum GM provided in the stability booklet is equal to 0.7 metre and its maximum GM is equal to 20 metres, considering the maximum allowed value of Δf, 8 loading conditions are to be assessed (the breadth of the vessel is equal to 48 metres), Table 7.

GM [m]	0.70	2.05	4.11	6.89	10.37	14.56	19.46	20.00
T [m]	16.00	14.98	13.43	11.35	8.73	5.58	1.90	1.49

Table 7 - Example of the selected loading conditions, NR 667

Simulation duration

For each combination of loading condition, wave height, wave period, wave heading and ship speed, simulations should be repeated at least 20 times with the same wave spectrum and different sets of initial phase angles. The duration of the simulation should not be less than 1 hour for each combination. The maximum roll angle to consider for each combination is the one-hour maximum roll angle with a probability of exceedance of 0.5 (denoted by θ_{sh}). Thus θ_{sh} is the median of the 20 maximum roll angles. In this sub-section θ denotes the roll angle in accordance with BV, while outside of this sub-section θ denotes the pitch angle in accordance with the ITTC Symbols and Terminology List (ITTC, 2021b).

The time step directly influences the number of points of the simulation. A compromise must be chosen between an acceptable accuracy and the duration of computation. When discussing with the engineer in charge of this topic at Bureau veritas, the author was informed that the value of 0.3 seconds is recommended after a sensitivity study conducted by BV.

Two simplifications to reduce the number of simulations are proposed (BV, 2019b). If θ_{sh} is lower than 5 degrees for a selected H_S and a selected wave period, the simulations for lower H_S (at constant wave periods) are not to be carried out. θ_{sh} related to those non assessed cases are considered to be lower than 5 degrees. If the one-hour maximum roll angle with a probability of exceedance of 0.5 is larger than the maximum acceptable roll angle for a given H_S, the simulations for larger values of H_S (at constant wave period) are not to be carried out and the related maximum roll angles are considered to be larger than the computed θ_{sh}. This second simplification can only be realised if a maximum allowable roll angle is defined prior calculations. Operationally, the choice of the maximum allowable roll angle can be left to the ship's master. Thus, in this case, this second simplification cannot be assumed and all cases for larger H_S must be assessed.

Criteria

The parametric roll assessment defined in NR667 (BV, 2019b) relies on the difference between a three to six degrees-of-freedom roll assessment providing prediction of the ship motions in waves and a linear frequential assessment which is a long-term study computing the maximum roll angle that the lashing can suffer before it breaks.

The one-hour maximum roll angle with a probability of exceedance of 0.5 (θ_{sh}) calculated from 20 one-hour simulations is compared to the maximum roll value from the associated linear frequential assessment in order to realise roll polar plots with acceptable and non-acceptable areas. The vessel complies with the requirement if Equation 37 is fulfilled:

$$\theta_{sh} < \frac{\theta_{PR}}{\gamma_{PR}} \qquad 37$$

With:

γ_{PR} (-) Conversion factor taken equal to 1.6. This factor permits to switch from a long-term study to a short-term study. The value should be reviewed in the next version of the NR 667 to be published after submission of this PhD. The author has not found any validation regarding this value.

θ_{PR} (deg) Parametric roll angle threshold, equal to θ_{lash} as defined in NR625 (BV, 2020a), chapter 4 section 1, and depending on the class notation defined in NR467 (BV, 2020b), part F, chapter 11, section 5:

For container vessels tagged with class notation LASHING:

$$\theta_{PR} = \theta_{lash} = f_{ART}\theta \quad (38)$$

For container vessels tagged with class notation LASHING-WW:

$$\theta_{PR} = \theta_{lash} = \frac{H_{WW}}{H} f_{ART}\theta \quad (39)$$

For container vessels tagged with class notation LASHING (specific area):

$$\theta_{PR} = \theta_{lash} = \frac{H_{RA}}{H} f_{ART}\theta \quad (40)$$

For container vessels without additional class notation:

$$\theta_{PR} = \theta \quad (41)$$

If the vessel has more than one class (LASHING and LASHING (specific area) for example), a different set of polar plots must be provided for each additional class.

H_{WW} (m) Wave parameter calculated from LASHING-WW (NR 625 section 3 and 14 (BV, 2020a))

H_{RA} (m) Wave parameter calculated from LASHING (specific area) (NR 625 section 3 and 14 (BV,2020a))

H (m) Wave parameter calculated from LASHING (NR 625 section 3 (BV, 2020a))

f_{ART} (-) Roll reduction factor, equal to 1 if the ship has no passive free-surface anti-roll tank (denoted by ART), otherwise calculated as follows:

$$f_{ART} = \frac{\theta_{ART}}{\theta_{wo-ART}} \quad (42)$$

θ_{ART} (deg) Extreme long-term roll angle (25 years return period for the North-Atlantic scatter diagram) from direct calculation including the effect of ART

$\theta_{wo\text{-}ART}$ (deg) Extreme long-term roll angle (25 years return period for the North-Atlantic scatter diagram) from direct calculation without the effect of ART

θ (deg) Roll angle as defined in Chapter 4, section 3 (BV, 2020a), calculated for unrestricted navigation as follows:

$$\theta = n\frac{9000(1{,}25 - 0{,}025T_\theta)}{(B+75)\pi} f_{fa} f_{BK} \quad (43)$$

and not less than

$$\theta = n\frac{1862}{(B+75)}f_{fa}f_{BK} \quad 44$$

n	(-)	Equal to 1 for unrestricted navigation (see (BV, 2020a) if coastal navigation only)
f_{fa}	(-)	Equal to 1 for the current strength assessment
f_{BK}	(-)	Equal to 1 if the ship has bilge keels, 1.2 otherwise
T_θ	(s)	Roll period, calculated according to the following formula:

$$T_\theta = \frac{2.3\pi k_{xx}}{\sqrt{g.GM}} \quad 45$$

k_{xx}	(m)	Roll radius of inertia, denoted radius of gyration in NR 667 (BV, 2019a), 0.45B for ballast condition, 0.35B otherwise
GM	(m)	Metacentric height, 0.18B for ballast condition, 0.07B otherwise

Both Equations 43 and 45 are available in the IACS Common Structural Rules (IACS, 2022). In addition, the procedure to calculate the parametric roll angle threshold (θ_{PR}) should be reviewed in the updated version of the NR667.

The assumptions considered here to estimate the radius of inertia (k_{xx}) can be disused since the assessed typical loading conditions are known. Thus, the container repartition leading to this draught and GM is estimated. In consequence, more accurate values of the radii of inertia can be calculated. This topic has been assessed in more details by Grin et al. (2016).

As mentioned above, to realise user-friendly roll polar plots, only two colours are used, defining go or no-go areas depending on the criterion expressed in Equation 37. This choice can be discussed since the Officer Of the Watch may alter course or speed to be at the border of the dangerous area. However, the maximum roll angle that the vessel can reach is not mentioned. Even if lashing can theoretically sustain the corresponding roll angles, the vessel will endure higher stress.

This assessment permits to compute roll polar plots for predefined loading conditions and sea states. Operationally, the roll polar plots closest to the actual conditions is displayed. The selection is realised considering the loading conditions and the natural roll period of the vessel. No interpolations between roll polar plots are conducted since some physical phenomena are not linear.

1.3.3. ABS, Guide for the assessment of parametric roll resonance in the design of container carriers

American Bureau of Sipping (ABS) proposes to assess the vulnerability of container ships toward parametric roll. ABS assessment (2019) is structured in three levels like the method proposed by the IMO. The technical background of the ABS assessment (2019) is discussed by shin et al. (2004).

The first-level assessment is a static study of parametric roll, based on the work of Shin et al. presented in 2004 (Shin et al., 2004). The second-level assessment is based on one-degree-of-freedom simulations to obtain the maximum roll angle on pre-defined sea states. The third-level assessment is based on at least three-degree-of-freedom simulations to determine the maximum roll angle in several environmental and loading conditions to realise operational roll polar plots.

First-level assessment

This first-level assessment is based on a static study of the ship sailing on a longitudinal sinusoidal wave with a forward speed. It assesses a single condition which according to ABS, will most likely lead to the development of parametric roll. Based on empirical formulae, the assessment concludes if the vessel can be subject to parametric roll.

For this single condition assessment, a sinusoidal wave of length equals to the ship's length between perpendiculars ($L_{PP} = \lambda$) is considered. The wave height is calculated by linear interpolation in Table 8 (Shin et al., 2004), calculated from the IACS Scatter diagram (IACS, 2001). The wave height cannot be greater than H_{Max} according to Equation 46. The wave frequency (ω_W) is directly related to the length of the wave (λ) in infinite depth as expressed in Equation 47.

Wave length λ [m]	50	100	150	200	250	300	350	400	450
Wave height H_W [m]	5.9	11.6	14.2	15.1	15.2	14.6	13.6	12	9.9

Table 8 - Wave heights (Shin et al., 2004)

$$H_{Max} = 2(D_m - T_m) \quad 46$$

$$\omega_W = \frac{2\pi}{T_W} = 2\pi\sqrt{\frac{g}{2\pi\lambda}} \quad 47$$

D_m (m) Moulded depth amidships

T_m (m) Moulded draught amidships

ABS recommends to consider at least 21 waves crest positions equally spaced. An easy method based on Bonjean curves permits to calculate the GM of the vessel in waves for the 21 positions of the wave (the number of waves positions is greater than the one proposed in the IMO assessment since the method to calculate the GM in waves is more simple). This method is described by Shin et al. (2004) and by ABS (2019). This method does not consider the hydrostatic balance of the vessel, since it is assumed that the vessel's draught in wave is equal to the one in calm water, trim and heave are not balanced. Thus, a simple numerical model of the hull geometry is required. GM in waves is considered to determine GM_{max} as the maximum GM, GM_{min} as the minimum GM, GM_{ampl} as half of the difference between GM_{max} and GM_{min} Equation 48, GM_{mean} as the mean value of GM_{max} and GM_{min} Equation 49.

$$GM_{ampl} = 0.5(GM_{max} - GM_{min}) \quad 48$$

$$GM_{mean} = 0.5(GM_{max} + GM_{min}) \quad 49$$

Both GM_{ampl} and GM_{mean} are expressed in terms of frequency respectively using empirical Equation 50 and 51. The natural roll frequency in calm water is calculated according to Equation 52 in absence of other available data. All frequencies are expressed in rad.s^{-1}. The constant 7.85 is equal to 2π divided by 0.8 as mentioned by Shin et al. (2004).

$$\omega_{ampl} = \frac{7.85\sqrt{GM_{apml}}}{B} \quad 50$$

$$\omega_{mean} = \frac{7.85\sqrt{GM_{mean}}}{B} \quad 51$$

$$\omega_0 = \frac{7.854\sqrt{GM}}{B} \quad 52$$

Prior to apply the first-level assessment criteria, a check on the vessel's speed is realised. If $2\omega_{Mean}$ is larger than $\omega_{W,}$ then parametrical resonance is expected in head seas. The vessel speed which will the most likely lead to the development of parametric roll (V_{PR} in knots) is calculated according to Equation 53 (demonstrated in Annex 3):

$$V_{PR} = \frac{19.06|2\omega_{mean} - \omega_W|}{{\omega_W}^2} \quad 53$$

If the maximum service speed (denoted by V_{Max}) is larger than V_{PR} then the first-level criteria is applied at V_{PR} ($V_S = V_{PR}$, V_S denotes the vessel speed). If V_{Max} is smaller than V_{PR}, the vessel speed is set to the maximum service speed $V_S = V_{Max}$. A new wavelength is calculated for this speed to lead to an encounter frequency to be near twice the natural roll frequency (Equations 54 and 55).

$$\omega_W = \frac{\sqrt{(96.23 + 78.48 V_S \omega_{mean})} - 9.807}{2V_S} \quad 54$$

$$\lambda = \frac{61.61}{{\omega_W}^2} \quad 55$$

All GM in waves are re-computed for this new environmental condition. The associated wave height must be linearly interpolated once more for the new wavelength in Table 8.

Both encounter frequencies in head and following seas are calculated, respectively denoted by $\omega_{e.h}$ and $\omega_{e.f}$), respectively with Equation 56 and 57 in rad.s^{-1}.

$$\omega_{e.h} = \omega_W + 0.0524 \cdot V_s \cdot {\omega_W}^2 \quad 56$$

$$\omega_{e.f} = \omega_W - 0.0524 \cdot V_s \cdot {\omega_W}^2 \quad 57$$

An estimation of the ship's roll damping is required to assesses its capacity to sustain the roll motion. A linear roll damping coefficient should be obtained by a roll decay test performed by ABS. Alternatively, the linear roll damping coefficient is assumed to be a fraction of critical damping as:

$$\mu = 0.3 \quad 58$$

- Two parameter criterion "p" and "q" are computed as follows in the conditions previously stated. If the $V_s = V_{PR}$ then this single condition is assumed. Otherwise, two conditions must be assessed, the first one for $V_s = V_{Max}$ and $\lambda = L_{PP}$ and the second one for the re-calculated λ leading to the highest probability of parametric roll at $V_s = V_{Max}$

$$p = \frac{{\omega_{mean}}^2 - (\mu \cdot \omega_0)^2}{{\omega_e}^2} \quad 59$$

$$q = \frac{{\omega_{ampl}}^2}{{\omega_e}^2} \quad 60$$

Thus, the Mathieu differential equation of parametric roll can be expressed as a function of p and q. Bounded or unbounded solutions appear for different combinations of p and q. Those solutions are plotted on Figure 16 known as Mathieu stability chart (Hayashi, 1985). Bounded solutions are represented by the white areas and unbounded solutions are represented by the shaded areas (IMO, 2021a).

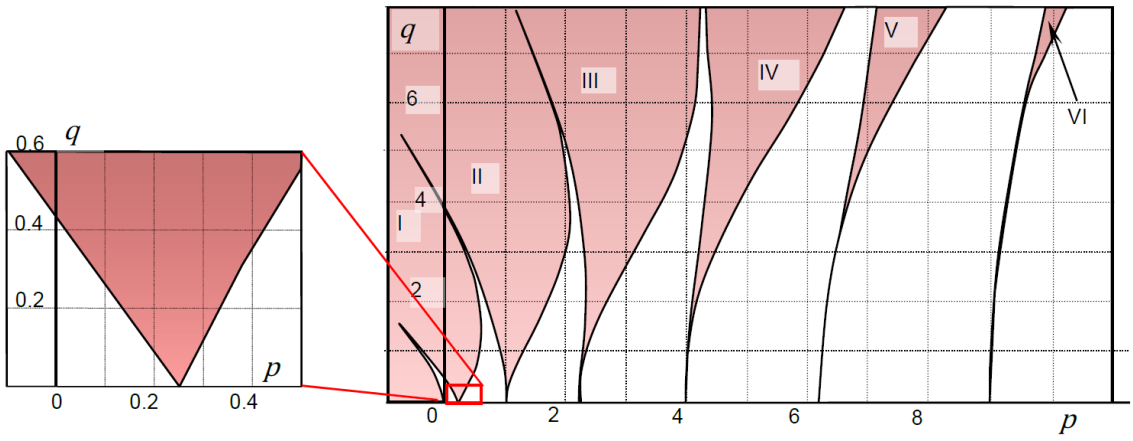

Figure 16 - Mathieu stability chart (credit: IMO, 2021a)

Several instability zones appear. The first zone intersects the q-axis exactly at p = 0.25, corresponding to an encounter frequency over roll frequency ratio equal to 2. The boundaries in p of the first instability zone are approximated by Hayashi (1985). Thus, the first criterion of the first-level assessment checks if p is within the interval leading to unbounded roll motions, inequality 61.

$$\frac{1}{4}-\frac{q}{2}-\frac{q^2}{8}+\frac{q^3}{32}-\frac{1}{3}\cdot\frac{q^4}{128}\leq p\leq\frac{1}{4}+\frac{q}{2} \qquad 61$$

If the condition is fulfilled, the vessel may be subject to parametric roll. Otherwise, the vessel may not be vulnerable to parametric roll. In this case, the second criterion of the first-level assessment can be conducted, with regards to the roll damping, using inequality 62.

$$\mu\frac{\omega_0}{\omega_e}<q\cdot k_1\cdot k_2\sqrt{1-{k_3}^2} \qquad 62$$

Where:

$$k_1=1-0.1875q^2 \qquad 63$$

$$k_2=1.002p+0.16q+0.759 \qquad 64$$

$$k_3=\frac{q^2-16+\sqrt{q^4+352q^2+1024p}}{16q} \qquad 65$$

If k_3 is larger than 1, then the damping criterion (inequality 62) is considered as not satisfied.

If k_3 is lower than 1 and inequality 62 is not satisfied, then the vessel vulnerability to parametric roll is unlikely.

If both inequality 61 and 62 are satisfied, then the vessel is considered as vulnerable to parametric roll. Then, the second-level assessment (qualified as severity criterion) must be applied.

It must be noticed that the second criterion of first-level is based on the vessel roll damping which is assumed to be a fraction of the critical roll damping if no roll decay test is validated by ABS. Thus, such approximation is conservative and leads to consider vessels as subject to parametric roll in most cases.

Second-level assessment

Second-level asses the severity of parametric roll using a simplified numerical procedure. This procedure solves numerically the roll motion equation in one degree of freedom (Equation 66, equivalent to Equation 10), with non-linear restoring term taking into account the variation of stability in waves. The simulation is to be conducted for a sinusoidal wave of length equal to the one of the ships and of height calculated by linear interpolation in Table 8.

$$\ddot{\varphi} + 2\mu\omega_0\dot{\varphi} + {\omega_0}^2 f(\varphi, t) = 0 \qquad 66$$

Actual GZ curves on waves should be considered. Such GZ curves on waves can be calculated by a hydrostatic solver for 15 to 18 wave position and 12 to 15 heel angles (while the IMO equivalent assessment presented in Section 1.3.1 considers only 10 positions and does not introduce any requirement considering the number of heel angles). Here, ABS does not introduce any requirements about hydrostatic equilibrium when calculating each GZ curve (while, IMO procedure requires the ship to be balance in trim and sinkage). It provides a two-dimension table of GZ, that can be presented as a tree dimension surface (wave position along the hull, heel angle and GZ). An example of this representation is provided in Figure 17.

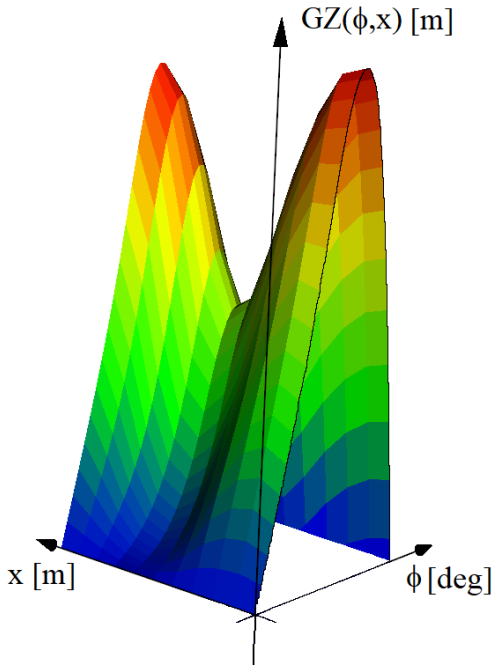

Figure 17 - Restoring moment as a function of wave position and heel angle

The restoring term f(φ,t) is based on a two-dimensional interpolation of the GZ curves and the use of the following formula:

$$f(\varphi, t) = \frac{sign(\varphi)}{GM_0} GZ(|\varphi|, t) \qquad 67$$

GM_0 (m) GM in calm water

sign(φ) (-) Equal to 1 when φ is positive and -1 when φ is negative

The position of the wave crest in the associated cartesian coordinate system along the hull (x) during the simulation is calculated using the following formula:

$$x = V \cdot t - L \cdot floor\left(\frac{V \cdot t}{\lambda}\right) \qquad 68$$

The function floor is defined as the largest integer number lower than the argument.

V (knots) Encounter speed calculated as follows:

In Head seas:

$$V = V_S + 0.159 \cdot \omega_W \cdot \lambda \quad (69)$$

In Following seas:

$$V = V_S - 0.159 \cdot \omega_W \cdot \lambda \quad (70)$$

If model test approved by ABS are available, the corresponding roll damping coefficient should be used. Otherwise, the simplified numerical procedure must be realised for the following range of roll damping coefficients. Such arbitrary range of roll damping coefficients does not consider the actual available roll damping devices fitted on the vessel such as bilge keels or anti roll tanks. Thus, the use of this range of damping coefficient may be conservative.

$$\mu = 0.03, 0.05, 0.075, 0.10 \quad (71)$$

Simulations are to be carried out for several ahead speeds covering the entire range leading to parametric roll, within the operating range. At least seven speeds are to be assessed. The following two speeds must be included:

$$V_1 = \frac{19.06 \cdot |2\omega_0 - \omega_W|}{{\omega_W}^2} \quad (72)$$

$$V_2 = \frac{19.06 \cdot |2\omega_{Mean} - \omega_W|}{{\omega_W}^2} \quad (73)$$

V_1 is the speed corresponding to the first mode of parametric roll (V_{PR}) calculated from the natural roll frequency (ω_0). V_2 is the speed corresponding to the first mode of parametric roll (V_{PR}) calculated from the roll frequency obtained from the mean value of GM in waves (ω_{Mean}, Equation 51; GM_{mean}, Equation 49). GM values used to calculate GM_{mean} must be extracted from the same hydrostatic solver than the one used to compute the GZ curves, or directly from the GZ curves.

When performing simulations, at least 20 roll periods must be observed before stopping it, in order to reach a roll steady state. The initial roll angle should be set up to 5 degrees, to speed up the possible development of parametric roll. Several combinations of initial roll angle and roll velocity are to be assessed, as those initial parameters can modify the final simulation roll amplitude.

As an example, if for each considered speed, 10 different set of initial conditions are assessed. This represents a total of 70 simulations to be carried out for one loading condition. If no roll decay test validated by ABS are available, 4 values of the roll damping should be considered, leading to a total of 280 simulations. Each simulation can be performed in only a few seconds. Any available commercial numerical software able to handle such differential equation can be used.

If all simulations simultaneously result in time series similar to the one of a roll decay, then the vessel is considered to be not vulnerable to parametric roll. Otherwise, if at least one roll time series, leads to a steady state roll amplitude lower than 15 degrees and larger than the initial roll angle, then the parametric roll at this particular condition may be considered as acceptable. Finally, if at least one roll time series leads to a steady state roll amplitude larger than 15 degrees or if unlimited increase of the roll motion is observed, then parametric roll should be considered as “severe”. In this case, the third-level assessment is conducted.

It should be noticed that without roll decay test from which the roll damping coefficient is calculated it is required to assess 4 values of the roll damping, in which low values of the roll

damping is to be considered. With the use of such roll damping coefficients, the vessel is expected to roll further than 15 degrees. Thus, without specific roll damping coefficient calculation most vessel will likely suffer from “severe” parametric roll and will thus require to be assessed through the third-level.

Third-level assessment

The third level assessment is the most complete and difficult level proposed by ABS to assess parametric roll. This level is a direct assessment based on simulations in irregular sea states in at least 3 degrees of freedom (heave, roll and pitch). To perform this assessment, software must be able to compute hydrostatics forces, Froude-Krylov forces and moments along the instantaneous submerged body. Software should be capable of taking into account the eddy making and viscous components of roll damping as external inputs from roll decay test. Such simulation system is partially described by Shin et al. (2003). Fredyn software (CRNav) and Hydrostar (BV) complies these requirements. Both were evaluated by Kapsenberg et al. (2019).

The simulations should be performed for loading cases available in the trim and stability booklet. No further indications on the selection of those loading cases are provided by ABS. Irregular sea state should be modelled either by a Bretschnieder or a JONSWAP spectrum, for sea states 6 and above. Thus, it is assumed that for sea states lower than 6 it is not required to assess the vulnerability of the vessel toward parametric roll. The use of such sea state definition can be criticized since it provides ranges of period and wave height. The user can select any combination of H_S and T_Z within the range defined by the sea state. Therefore, two different users would not consider the same couple H_S/T_Z and the results will then not be comparable. The simulations should be performed for long-crested waves with no spreading function. This assumption makes the simulations faster than with short-crested waves. The set of frequency used to represent the considered sea state should cover the entire spectral range. The frequency range should be wide enough to contain all values higher than 1% of the maximum spectral density. The wave elevation obtained in the time series by the set of frequency must be statistically representative. For evenly distributed frequency, the frequency step is to be calculated as provided by Equation 74, in which T_R denotes the duration of the simulation in seconds.

$$\delta\omega = \frac{2\pi}{T_R} \qquad 74$$

This definition of the frequency step to be set in the time-domain solver implies that the definition of the frequency is linearly linked to the duration of the simulation, limiting the simulation duration. The range of wave directions should be taken from 0 degree to 180 degrees with a 15 degrees increment (13 directions). The speed range should cover the entire range of service speeds, with a recommended increment of 5 knots.

For each loading condition, environmental sea state and speed, each simulation must be performed at least 5 times with different phase angles. Each simulation must be at least 12 minutes long, for a total time in each condition of minimum 1 hour. Each time series provides a maximum roll angle. The maximum roll angle for one environmental and loading condition is considered to be the maximum of all 5 runs.

Here, if simulations of 12 minutes are conducted, then the sea spectrum frequency discretisation according to Equation 74 is about equal to $8.73*10^{-3}$ rad.s^{-1}. Regarding the large number of simulations realised within the scope of this PhD, the author observed that a 12-minute run may not be sufficiently long for parametric roll to appear, even if conducted several times. Moreover, the sea spectrum frequency discretisation is selected with regards to the simulation duration.

Thus, it is computationally heavy to increase the simulation duration, even if the ABS procedure permits to realise longer simulations ("at least 12-minutes").

Results should be presented as polar plots, with areas of different colours for maximum roll angle exceeding 22.5 degrees. The anti-roll devices such as bilge keels or anti-roll tank are to be considered sufficient if a maximum of 10 degrees change in course and/or 10% change of speed is sufficient to get out of the considered dangerous area. In this case, it can be considered that parametric roll is qualified as "under control". The master should be provided with a hard copy or electronic copy of the roll polar plots.

ABS should approve the plan of simulations prior to realise them. Thus, this assessment cannot be performed without ABS support.

1.4. REAL-TIME ASSESSEMENT

Following the accidents of the C11-class container ship *APL China* (France et al., 2003) and the *Maersk Carolina* (Carmel, 2006), both due to parametric roll, insurers asked the shipowners to take measures to avoid such failure to appear (Dølhie, 2006). The request aimed to develop operational solutions to significantly reduce the frequency and the severity of those accidents. Three of such solutions are presented hereafter. Nevertheless, efforts to prevent the appearance of such phenomenon are continuously undertaken by the maritime actors. As an example, the TOP TIER project (Koning et al., 2022) recently proposed an open guidance for operational use by the crew to avoid dangerous situations (TOP TIER, 2022).

1.4.1. Operational routing

Operational routing is widely used now days. It consists in finding the most adequate route for the vessel regarding among others the forecasted weather along the route. For seafarers it becomes a continuous update of the passage planning. Operational routing is used by a large number of maritime companies to reduce fuel consumption, avoid heavy weather, and keep schedule. The routing can either be externalised to private companies or realised within the company. In this second case, it can be realised onboard or by a dedicated team ashore. Software used to realise such routing can be provided by external companies such as ABB (OCTOPUS software), StormGeo (BVS, BONVOYAGE software), DTN (SPOS onboard software), or DNV (ARCS software) as examples. Other dedicated software can be developed internally by shipowners to focus on specific parameter or to be able to consider its own specific inputs, such as weather forecast sources. Several types of routing can be realised with the aim to focus on time efficiency (due to narrow band availability time), fuel consumption (use of current) or roll motions (avoid container loss, heavy acceleration). The predicted roll motions along the route are based on the loading condition and the weather forecast. This estimation is either based on database computed from time-domain simulations or real-time calculation using more simplifying assumptions. Thus, all software will not be able to predict specific phenomenon such as parametric roll.

Figure 18 presents an example of weather routing from Rotterdam (Netherlands) to Huston (USA). Two routes were generated by the weather routing software. The red route is generated to lead to the shortest time taking into account only a limit on the encountered wave height. The blue route is generated when considering thresholds on the ship responses (such as roll and pitch motions) with regards to the forecasted weather. It shows that considering the ship motion response can lengthen the route. However, it reduces the forecasted risk of encountering undesired ship motions.

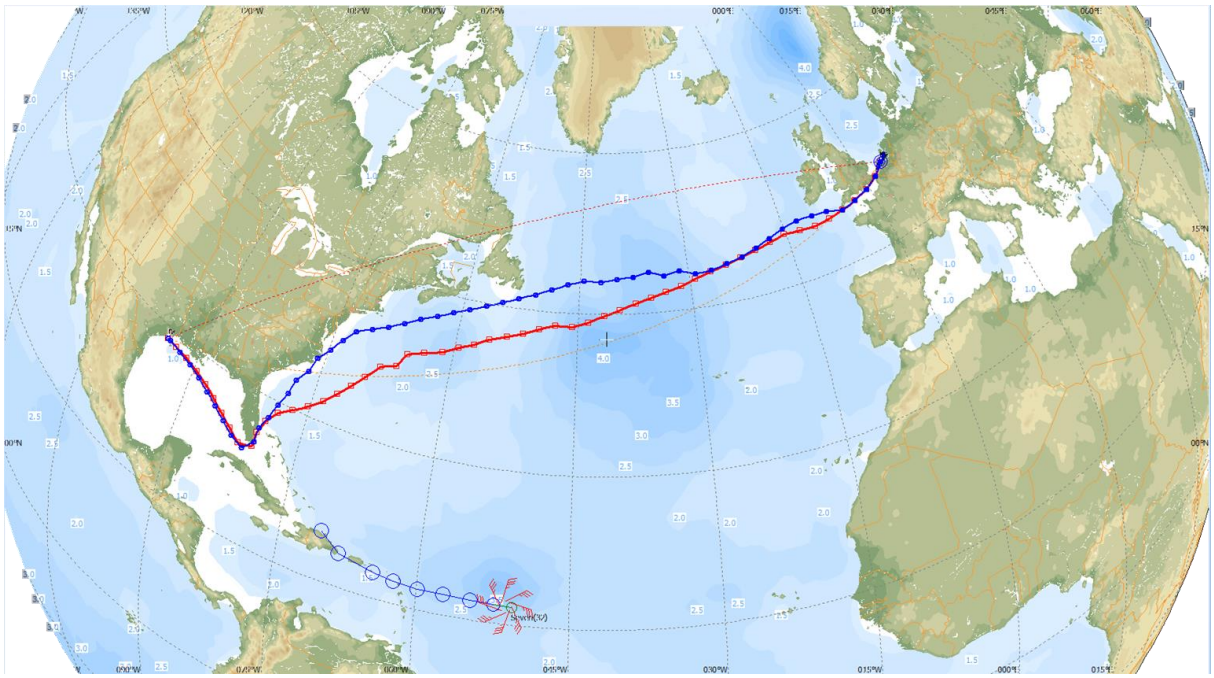

Figure 18 - Weather routing (credit: ABB)

1.4.2. MSC.1/Circ.1228: Revised guidance to the master for avoiding dangerous situations in following and quartering seas

The International Maritime Organization (IMO) has provided revised open guidance to avoid dangerous phenomenon such as parametric roll. This circular 1228 (IMO, 2007a) replaces the circular 707 (IMO, 1995) which did not provide sufficient effective operational guidance to avoid the appearance of stability failures in waves. Thus, the revised circular 1228 provides details on the appearance of each failure modes in waves assessed by the second generations intact stability criteria (IMO, 2020a), except excessive accelerations. This operational guidance provides a user-friendly diagram to be operationally used by the Officer Of the Watch (denoted hereafter by OOW) to estimate graphically the wave encounter period (denoted by T_E, key factor of the appearance of most stability failures in waves), Figure 19. The required inputs are the vessel speed, the wave period, and the relative course to the wave. The OOW can as well use the corresponding formula, Equation 75.

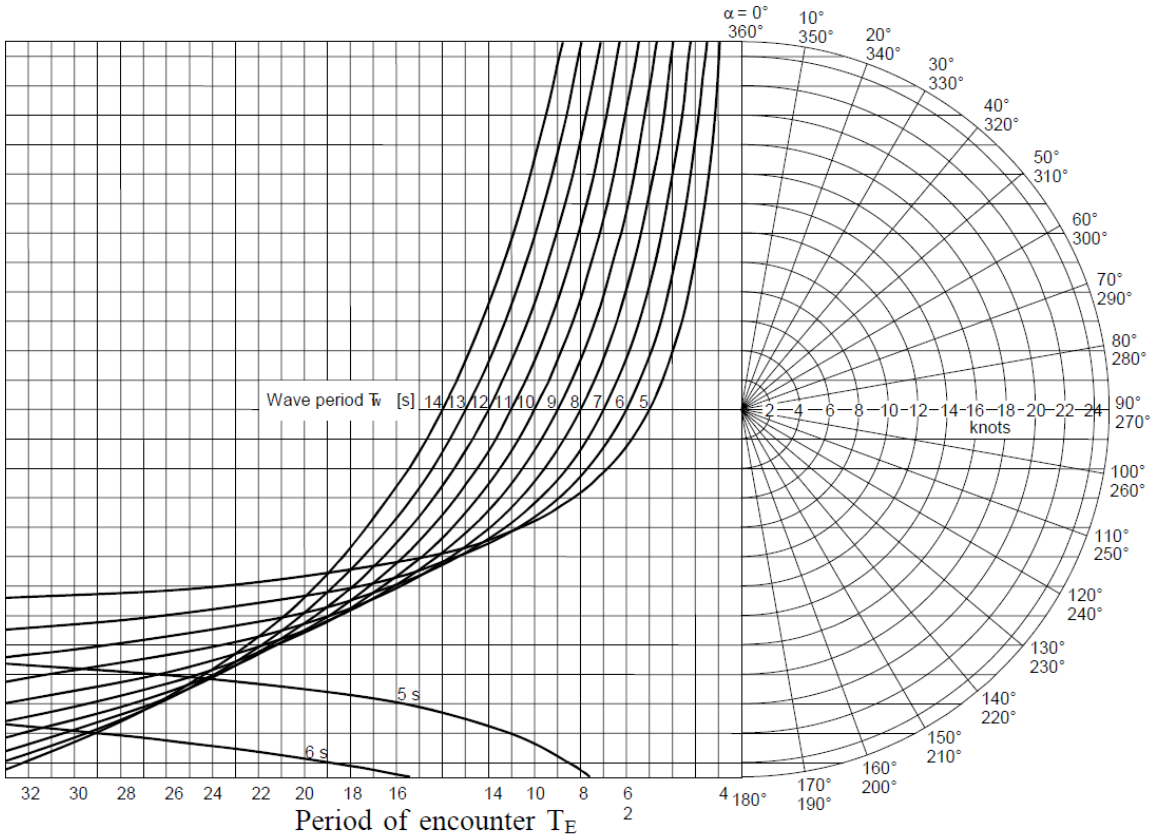

Figure 19 - Determination of the period of encounter T_E, IMO (2007a)

$$T_E = \frac{3{T_W}^2}{3T_W + V\cos\beta} \qquad 75$$

T_W (s) Wave period

β (rad) Wave heading relative the ship axis

V (knots) Actual ship speed in knots

A sub-section is dedicated specifically to each phenomenon. The operational guidance provides, when available, a graphic representation of the recommendations as generic polar diagrams presenting the dangerous zones in which the OOW should not sail to avoid the considered stability failure. It provides recommendations on how to avoid the appearance of parametric roll based on the wave directions, wave encounter period and the ship natural roll period. This revised open guidance permits to rise the attention of the OOW on the topic of stability failure in waves. This is a first step towards a regulatory real-time assessment of the risks.

Operationally, the dangerous zones provided by the guidance can be displayed onboard by operational software. However, the revised guidance does not provide an evaluation of the risk regarding the severity of phenomena or the occurrence rate when the vessel is in a dangerous zone. As well, it does not provide any advice on the actions to undertake when large roll motions appear consecutively to a stability failure. Thus, the OOW must avoid as much as possible such situations. In order to avoid excessive course and/or speed alterations, the shipowners more and more invest in automatic real-time detection devices to warn efficiently the OOW of the existing danger.

1.4.3. Real-time detection

The content of this section has been submitted to the Journal of Ship Research (Luthy et al., 2022d). Within the scope of a paper relative to an improvement of the method to detect parametric roll in real time.

Two onboard solutions are rapidly developed to answer the request of the insurer in 2006 to take measures to avoid such failure to appear. The first one is developed by SeaSense and named SeaSense Monitoring (Nielsen et al., 2006). It is based on the estimation of the sea spectrum through the onboard sensor signals. The other one is developed by Amarcon's (part of ABB Group) and named OCTOPUS Resonance (Acomi et al., 2016). This onboard real-time solution provides roll polar plots based on the forecasted environmental conditions and the ship loading condition. It also provides a real-time analysis of the ship motions based on the inertial unit data to warn the Officer Of the Watch when the roll motion is assessed as due to parametric roll (ABB, 2012). Both solutions are developed by private groups. The methods implemented in their software are not public. Thus, the scientific community proposed some reflections on how to assess this phenomenon in real time.

First, Holden et al. (2007) proposed to evaluate parametric roll based on the roll time series data. It estimates the eigenvalues of a linear second-order oscillatory system and issues an alarm when the eigenvalue gets out of the stability region. This method is fitted for regular seas. Thus, it cannot be used operationally on real sea state with acceptable relevance.

Then McCue and Bulian (2007) attempt to detect the increase of the roll amplitude due to parametric roll based on a finite time Lyapunov exponent. They mention that an alarm to warn the Officer Of the Watch could be fitted on the behaviour of the Lyapunov exponent. This method presents very interesting results. However, according to Galeazzi et al. (2013), it did not provide sufficiently robust results on real data. No trace of onboard implementation of this method has been found by the author.

Another approach based on a Generalized Likelihood Ratio Test (GLRT) for non-gaussian signals is proposed by Galeazzi et al. (2009b). Galeazzi's team studied the coupling between the vertical motions of the ship (heave and pitch) and the roll motion to detect energy flows (Galeazzi et al., 2009a). They found a pattern between the pitch motion and the roll motion leading to parametric roll. The associated amplification of the roll motion is predicted using a dedicated detector based on a recursive GLRT. The false alarm rate observed with this method in beam seas due to synchronous roll is assessed (Galeazzi et al., 2013). This method is implemented onboard ships under the name PAROLL, standing for imProuve sAfety towaRds parametric Roll appLying reaL-time detection. It has been validated through full-scale data on a 2800-TEU container ship and a large car carrier over respectively 2 years and 1 year of data (Galeazzi, 2014). This validation provides results showing that parametric roll is detected more than 70 % of the time when the roll motions are larger than 10 degrees. It is stated that it provides a very low false alarm rate, without statement of the real values observed on those data. The parametric roll identification method proposed by Galeazzi et al. (2009b) are covered by patents pending EP 09157857.5 and US 61/169,154.

González at al. (2011) attempt to forecast parametric roll with multilayer perceptron neutral network approach. This approach was used to realise predictions at 5, 10 and 20 seconds in advance. It provides accurate results in regular seas and very promising results in irregular seas.

Yu et al. (2016, 2018) developed an early parametric roll detection algorithm based on incremental real-time Hilbert-Huang transform technique. The method focusses on the abrupt variation of the roll frequency when the vessel suffers from parametric roll. This method has been validated on

model test and coupled to a rudder roll stabilization to lower the parametric roll amplitude. The detection method provides a very good detection rate in head seas. However, a significant false alarm rate results from the Hilbert-Huang transform technique itself. This short false alarm can be ignored (Yu et al., 2018). The author is not aware of any validation of the false alarm rate in beam seas.

Acanfora et al. (2018) developed a method to detect large roll motions due to parametric and synchronous phenomena based on the roll over pitch period ratio. This method can be used in real time as a warning system (Acanfora and Balsamo, 2020).

Real-time parametric roll detection methods are commonly based on the study of the ship motions. Thus, most methods do not require any ship model and can be used without customization to any type of ship. Those motion-based methods are event detection system providing a warning to the Officer Of the Watch when parametric roll develops. They permit to the Officer Of the Watch to be informed prior the largest roll motions appears and to react in consequence.

The first-generation warning systems provide a risk prediction depending on the hull geometry, loading condition and environmental condition (IMO, 2020a; BV, 2019b; ABS, 2019), such as roll polar plots (methods presented in Section 1.3). Those roll polar plots permit the ship's master to avoid the most dangerous areas and to adopt the safest operating combination of course and speed in heavy weather. Thus, both first-generation warning systems and real-time assessment solutions are complementary and should be coupled to be more efficient.

CHAPTER 2. ENERGY METHOD

This chapter presents an innovative energy method to calculate the amplitude of parametric roll in regular longitudinal seas at any speed, considering non-linear transverse stability. First, the phenomenon of parametric roll is presented from energy point of view. Then, the variation of the transverse stability on longitudinal waves is studied, leading to the introduction of the notion of shift angle, modulating the parametric exciting energy, and the estimation of its value. The energy method is detailed and an example of its implementation on the well-known C11-class container ship is provided. Finally, results and the limits of use of the method are discussed.

The content of this chapter has been presented at the 1st International Conference on the Stability and Safety of Ships and Ocean Vehicles, held in Glasgow (UK) in June 2021 (Luthy et al., 2021b) and in the Journal Ocean Engineering (Luthy et al., 2022c).

2.1. INTRODUCTION

As presented in Chapter 1, several methods to estimate the parametric roll amplitude exist. This phenomenon can be assessed using several means such as model tests, time-domain simulations in 1 to 6 degrees of freedom (DoF) or real-time evaluation. The international maritime organisation (IMO), through the second-generation intact stability criteria presented in Section 1.3.1 (IMO, 2020a) aims to reduce the occurrence rate of this phenomenon. Nayfeh (1981) presented an averaging method which providing the parametric roll amplitude through an analytical solution for non-linear oscillators. A polynomial fit of the mean transverse righting lever (GZ) in longitudinal wave is required. An averaging method based on this work has been intended to the IMO to assess the vessel vulnerability regarding parametric roll through level-2 criterion in the second-generation intact stability criteria (SGICs), (IMO, 2015). However, this method has not been adopted in favour of 1-DoF time-domain simulations (IMO, 2020a). In 1955, Kerwin (1955) presented the first analysis of the phenomenon in 1-DoF, based on energy considerations. He demonstrated that in regular longitudinal waves, a roll steady state is reached when the exciting energy provided by longitudinal waves to the vessel in parametric condition (denoted by E_E) is equal to the damping energy dissipated by the hull throughout the roll motion (denoted by E_D), as presented in Figure 20.

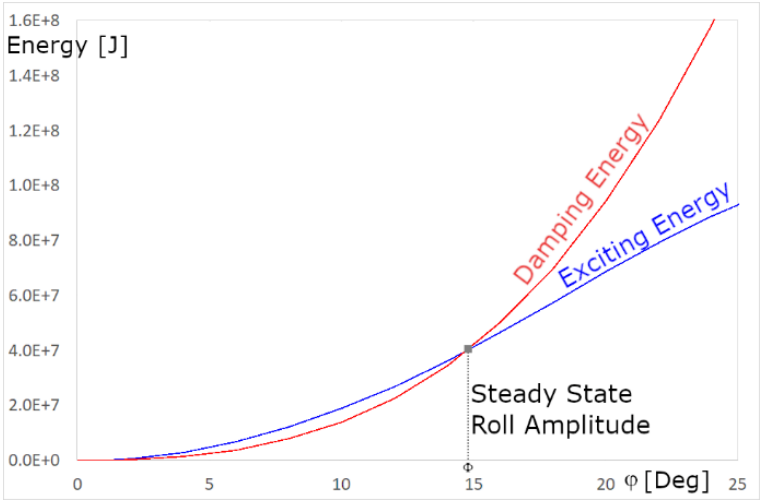

Figure 20 – Energy balance

Grinnaert extends the research of Kerwin in 2017 and proposes an improved method providing the steady state roll amplitude in resonance conditions considering linear GZ (Grinnaert et al., 2017; Grinnaert, 2017). He compares the results with the ones obtained from a 1-DoF

time-domain routine solving numerically Equation 9, using Runge-Kutta method. He demonstrates that the steady state roll amplitude can be analytically calculated in linear GZ at resonance condition. In this condition, the wave encounter frequency (denoted by ω_e) is equal to twice the natural roll frequency (denoted by ω_0).

Grinnaert proposes to estimate the maximum roll amplitude (denoted by Φ) for any speed empirically, based on the one calculated in resonance condition (Equation 76, Grinnaert et al., 2017). The results depend on a triggering coefficient (k), empirically chosen. The results obtained for different triggering coefficients (k) are provided in Figure 21. This was an attempt to calculate the steady state roll amplitude within the lock-in field (defined in section 1.1) without simulation.

$$\Phi = \Phi_{VPR} \cos^k \left(\pi \left(2 - \frac{\omega_e}{\omega_0} \right) \frac{GM}{\delta GM} \right) \qquad 76$$

Where Φ_{VPR} denotes the roll amplitude calculated at the synchronism speed (ie in resonance condition). k equal 0.5 has been identified by Grinnaert (2017) to provide the most relevant results compared to 1-DoF time-domain simulations.

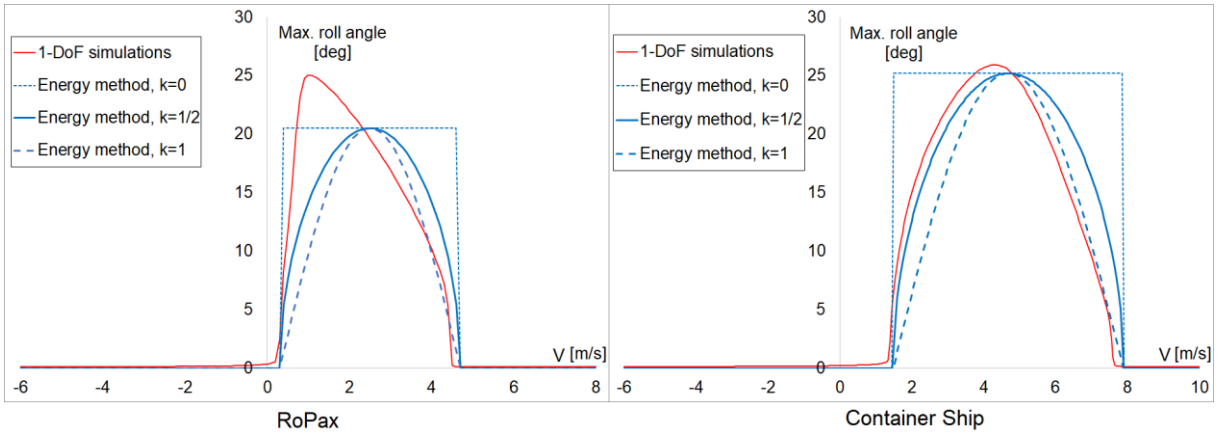

Figure 21 - Maximum roll angle versus speed, influence of exponent in energy method (Grinnaert, 2017)

The energy method is extended to non-linear domain in 2021 in resonance condition (Luthy et al., 2021b) and then extended to any other speed, Ocean Engineering 2022 (Luthy et al., 2022c). Complete energy method and results are presented here-after.

2.2. VARIATION OF THE TRANSVERSE STABILITY

2.2.1. Instantaneous variation of the transverse stability

Parametric roll considering Instantaneous variation of the transverse stability

When the vessel is sailing in head or following seas, a variation of the waterplane area appears. As presented in Chapter 1, this variation leads to a variation of the transverse stability. Container ships are wall-sided amidship and flare-sided at the stern and at the bow. Considering this hull shape and a wave having a length equal to the one of the ship, a container ship presents its maximum transverse stability when the wave crests are located near the ship's perpendiculars and its minimum transverse stability when the wave crest is located amidship. In this sub-sub-section, instantaneous variation of the transverse stability is assumed. This assumption leads to consider the maximum possible parametric exciting energy. At maximum roll angle on both side (denoted by φ_{max}), the vessel switches from GZ curve associated with GM_{min} (GZ_{min} curve)

to GZ curve associated with GM_{max} (GZ_{max} curve); When crossing the angle of stable equilibrium ($\varphi = 0$), she switches from GZ_{max} to GZ_{min}. At φ_{max} the roll energy is fully potential (denoted by E_P). The instantaneous variation from GZ_{min} to GZ_{max} increases the potential energy. Assuming that the vessel has no damping, at $\varphi = 0$ she has converted her potential energy into kinetic energy (denoted by E_K) and switches from GZ_{max} to GZ_{min}. The roll motion continues on GZ_{min} on the opposite side until the next maximum roll angle is reached. At this angle, the potential energy increases by switching instantaneously from GZ_{min} to GZ_{max}. The roll potential energy is equal to the area under the GZ curve multiplied by the ship's weight (IMO, 1985). Thus, the area under the GZ curve is representative of the roll potential energy. Therefore, the area under GZ_{max} curve up to the maximum roll angle (denoted by $\varphi_{max.n}$, red area in Figure 22 and Figure 24) is equal to the area under GZ_{min} curve up to the maximum roll angle reached on the opposite side at the next half period (denoted by $\varphi_{max.n+1}$, green area in Figure 22 and Figure 24). This is an energy explanation of the amplification of the roll motion due to the variation of the transverse stability twice in a roll period known as parametric roll.

Instantaneous variation of the transverse stability, linear GZ

If linear GZ is assumed, the roll potential energy can be calculated analytically. Its expression at $\varphi_{max.n}$ after switching instantaneously from GM_{min} to GM_{max} (denoted by $E_{P.n}$) is:

$$E_{P.n} = \frac{1}{2} W . GM_{max} . {\varphi_{max.n}}^2 \qquad 77$$

Then, the expression of the roll potential energy at $\varphi_{max.n+1}$ before switching instantaneously from GM_{min} to GM_{max} (denoted by $E_{P.n+1}$) is:

$$E_{P.n+1} = \frac{1}{2} W . GM_{min} . {\varphi_{max.n+1}}^2 \qquad 78$$

$E_{P.n+1}$ is equal to $E_{P.n}$, therefore $\varphi_{max.n+1}$ can be analytically calculated as:

$$\varphi_{max.n+1} = \varphi_{max.n} \sqrt{\frac{GM_{max}}{GM_{min}}} \qquad 79$$

Figure 22 represents the parametric amplification of the roll motion defined in Equation 79.

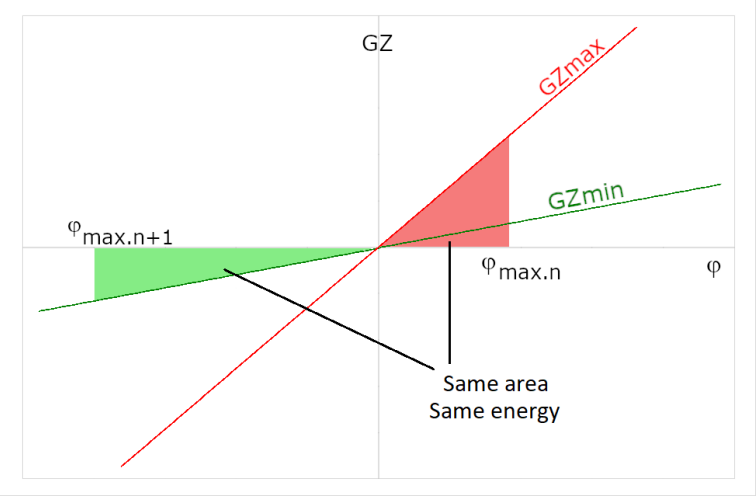

Figure 22 - Amplification of the roll angle due to instantaneous variation of transverse stability, linear GZ

Due to the succession of the encounter of waves, if no damping is assumed, the phenomenon continues until the vessel capsizes. Otherwise, a roll steady state is reached when both damping and exciting energies are equal (Kerwin, 1955, Grinnaert et al., 2017), Figure 20. Thus, the exciting energy is defined as the energy provided by the wave due to the variation of the transverse stability during half a period. In these conditions the exciting energy E_E is defined as the ship's weight multiplied by the area between linear GZ_{min} and GZ_{max} curves (denoted hereunder by Area) up to the steady state roll amplitude (denoted by Φ):

$$E_E = W.Area = W.\delta GM.\Phi^2 \qquad 80$$

Instantaneous variation of the transverse stability, non-linear GZ

When considering non-linear GZ and instantaneous variation of stability, the exciting energy is defined as the ship's weight multiplied by the area between GZ curves up to the roll amplitude Φ (red area in Figure 23).

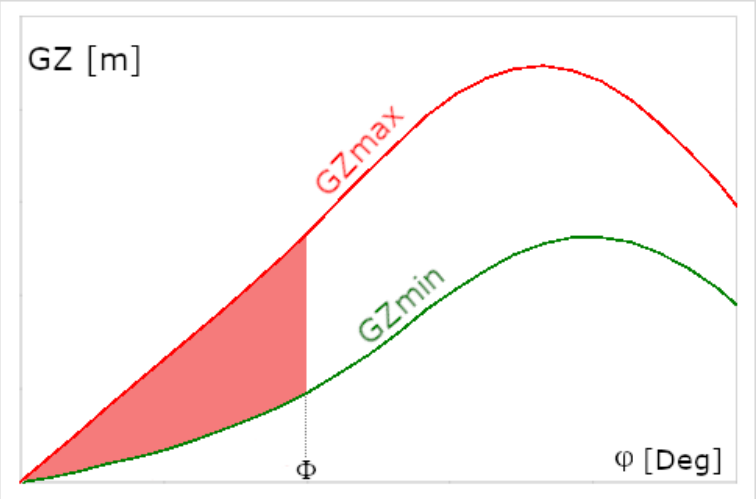

Figure 23 – Area representing the exciting energy assuming instantaneous variation of stability

The same energy consideration than the one in linear GZ is conducted. If no damping is assumed, the roll angle reached during the next half roll period is calculated as follows:

$$\int_0^{\varphi_{max.n+1}} GZ_{min}(\varphi)\, d\varphi = \int_0^{\varphi_{max.n}} GZ_{max}(\varphi)\, d\varphi \qquad 81$$

Figure 24 represents the parametric amplification of the roll motion defined in Equation 81.

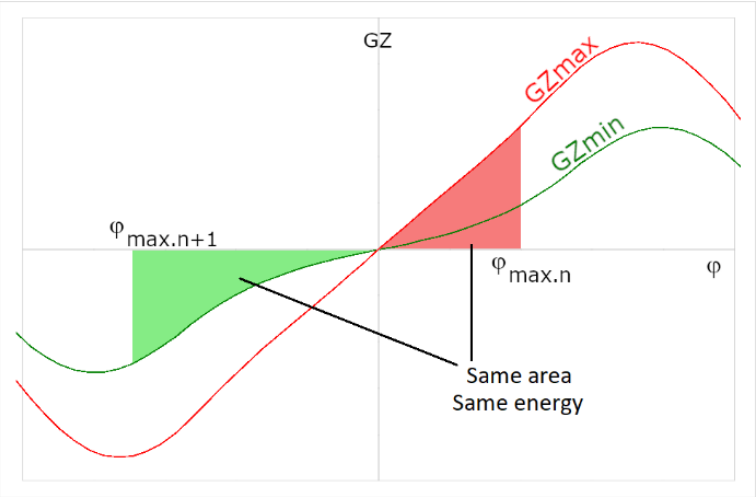

Figure 24 - Amplification of the roll angle due to instantaneous variation of transverse stability, non-linear GZ

Thus, this easily understandable explanation can be used in maritime academies to explain the amplification of the roll motion and the appearance of a steady state of parametric roll when the ship sails in longitudinal waves such as her transverse stability vary twice in a roll period.

2.2.2. Continuous variation of the transverse stability

The waterplane area varies continuously with the waves running along the ship's hull. Therefore, the variation of the transverse stability (GM and GZ) is not instantaneous. Assuming linear GZ and a sinusoidal roll motion, the variations of GM and GZ in time-domain are expressed respectively by Equations 7 and 8 (Section 1.2.2), and rewritten hereunder:

$$GM(t) = GM_{mean} + \delta GM.cos(\omega_e.t) \qquad 7$$

$$GZ(\varphi;t) = (GM_{mean} + \delta GM.cos(\omega_e.t))\varphi \qquad 8$$

GZ(φ,t) is bounded by GZ_{max} and GZ_{min}. During half a roll period, GZ(φ; t) describes a lobe in a [φ; GZ] coordinate system (Figure 25). The area of this lobe is lower than the triangular area bounded by GZ_{min} and GZ_{max} curves from 0 to the maximum roll angle. Thus, the exciting energy assuming continuous variation of the transverse stability is lower than the on assuming instantaneous variation. The shape of the lobe depends on the delay between the GM variation and the roll motion. The remarkable points of the lobe presented in Table 9 are obtained by delaying the GM variation of π/2 in Equation 7, which becomes:

$$GM(t) = GM_{mean} - \delta GM.sin(\omega_e.t) \qquad 82$$

The associated lobe is shown by Figure 25.

t [s]	φ(t) [deg]	GM(t) [m]
0	0	GM_{mean}
$T_0/8$	$\sqrt{2}/2\ \Phi$	GM_{min}
$T_0/4$	Φ	GM_{mean}
$3T_0/8$	$\sqrt{2}/2\ \Phi$	GM_{max}
$T_0/2$	0	GM_{mean}

Table 9 - Remarkable points of the lobe described by GZ(φ; t)

Figure 25 - Point (φ,GZ) describing a lobe during half a period

The area of the lobe is analytically calculated with Equation 83. Minus sign is introduced to obtain a positive area since the lobe described by the point [φ; GZ] on a half period (denoted by $T_\varphi/2$) is turning counterclockwise in this system (Figure 25).

$$Area_{Lobe} = -\oint_{\frac{T_\varphi}{2}} GZ(\varphi; t)\, d\varphi \qquad 83$$

Introducing trigonometric identities and Equation 82 in Equation 83 and considering linear GZ, lead to the following expression of the lobe area:

$$Area_{Lobe} = \frac{\Phi^2 . \delta GM . \pi}{4} \qquad 84$$

Therefore, the lobe area is analytically calculable (Equation 84, demonstrated in Annex 3) as well as the area between linear GZ curves considering instant variation of GM (Equation 80). The ratio between both areas provides a coefficient denoted by C (Equation 85) permitting to pass analytically from the energy considering instantaneous variation of the transverse stability to the one considering continuous variation, assuming linear GZ (Figure 26).

$$C = \frac{Area_{Lobe}}{Area_{inst}} = \frac{E_{E.lobe}}{E_{E.inst}} = \frac{\pi}{4} \qquad 85$$

$Area_{inst}$ correspond to "Area" in Equation 80; here indexed with "inst" since it corresponds to the area when considering the instantaneous variation of the transverse stability, same for the exciting energy E_E.

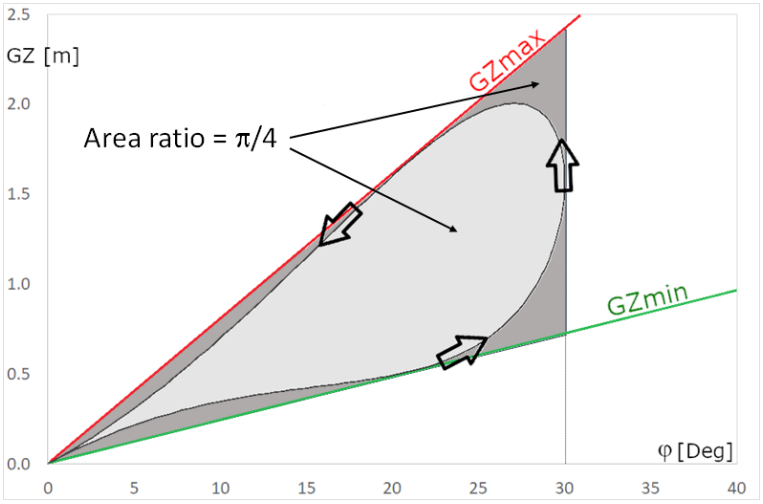

Figure 26 – Ratio of the areas considering instantaneous and continuous variation of GZ

Same reasoning is conducted when assuming nonlinear GZ curves. Figure 27 presents the area between the GZ curves in waves (left, instantaneous variation) and the one of the lobe (right, continuous variation) assuming non-linear GZ curves. GZ curves on waves are not analytically described, therefore the lobe described in coordinate [φ; GZ] by GZ(t) on half period can only be defined numerically.

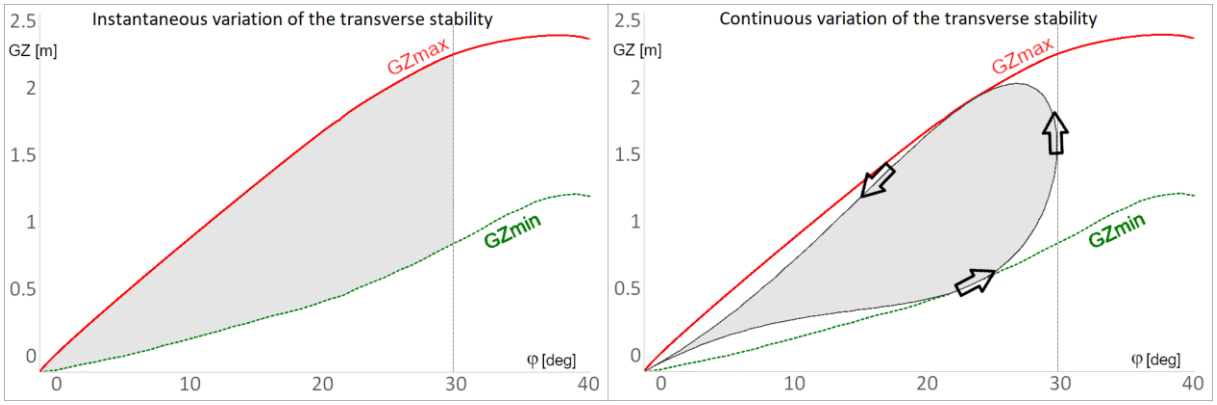

Figure 27 - Area developed by the transverse stability considering instantaneous (left) and continuous (right) variation of the transverse stability on regular wave

2.3. SHIFT ANGLE

2.3.1. Definition of the shift angle

In this Chapter the roll motion is assumed to be sinusoidal and defined by Equation 86 in steady state. In longitudinal waves, when steady state is reached, it is observed that the transverse stability variation in waves is in phase with the roll motion for a specific speed depending on the hull geometry and the wave shape, and not in phase for the other speeds. This speed can differ from the one associated to the resonance condition. Since GM variation in waves may not be in phase with the roll motion (Figure 28), the shift angle (denoted by α) is introduced in the GM variation equation.

$$\varphi(t) = \Phi . \sin\left(\frac{\omega_e}{2} t\right) \qquad 86$$

$$GM(t) = GM_{mean} + \delta GM.cos(\omega_e.t + \alpha) \quad (87)$$

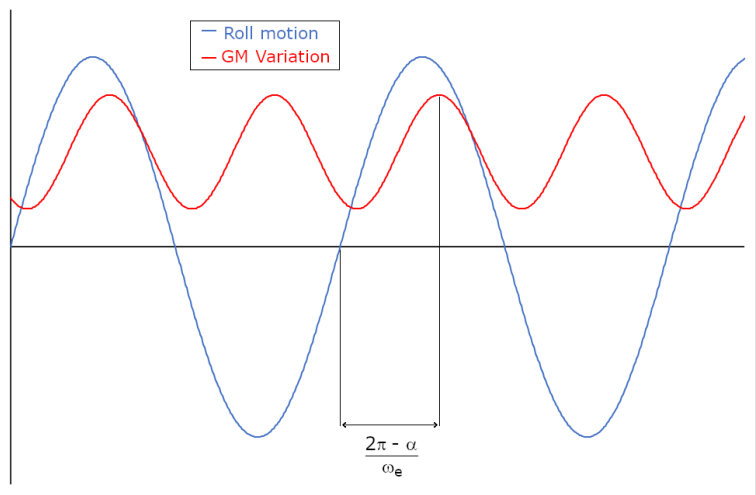

Figure 28 - Temporal representation of the shift angle

As stated by Grinnaert (2017), the maximum exciting energy occurs when the shift angle is equal to $\pi/2$. Other values of the shift angle, representing different delays between the roll motion and the variation of stability, leads to a distortion of the lobe. Figure 29 presents the lobe for a shift angle equal to $\pi/2$. Figure 30 presents the lobe for a shift angle equal to $3\pi/4$ (grey area) and π (light grey line); the variation of GZ is in retard compared to the shift angle providing the maximum energy. Figure 31 presents the lobe for a shift angle equal to $\pi/4$ (grey area) and 0 (light grey line); the variation of GZ is in advance. When the shift angle is equal to 0 or π, the lobe area and the exciting energy are null.

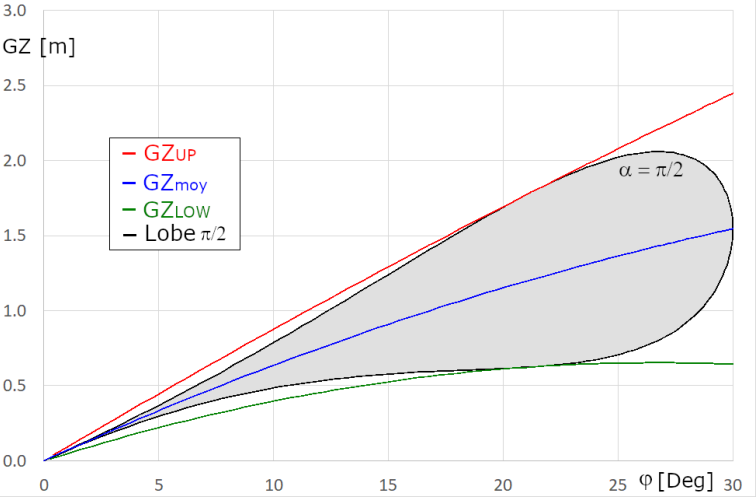

Figure 29 – Lobe for a shift angle equal to $\pi/2$

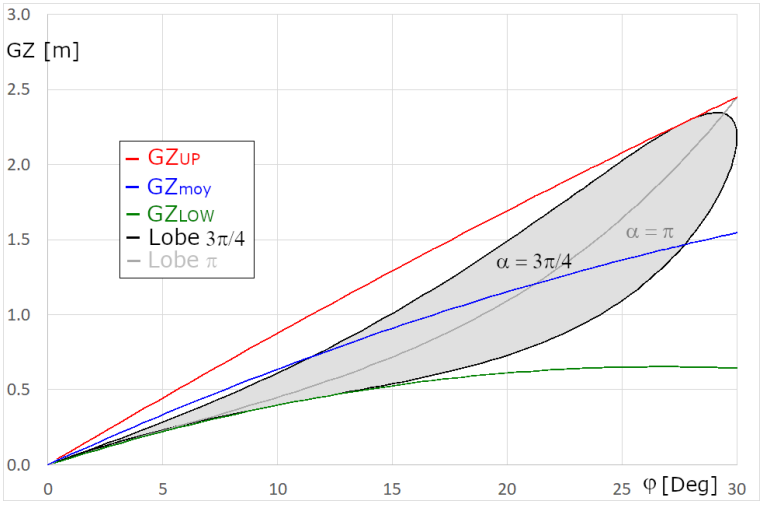

Figure 30 – Lobe developed for a shift angle equal to $3\pi/4$ and flat lobe resulting from a shift angle equal to π

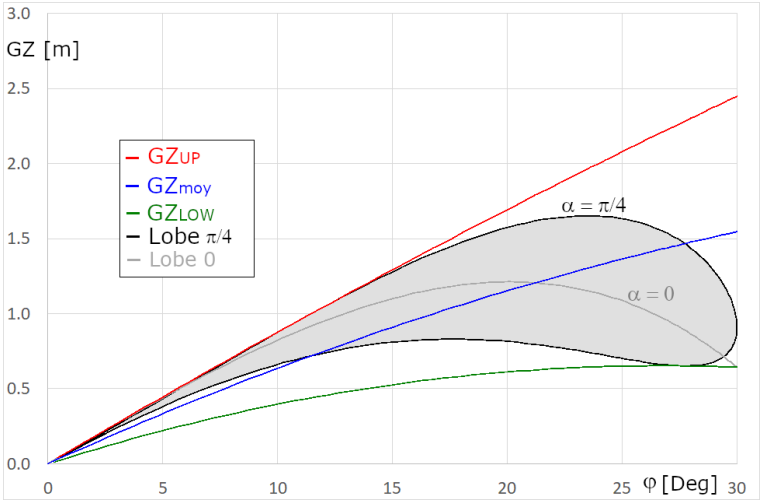

Figure 31 - Lobe developed for a shift angle equal to $\pi/4$ and flat lobe resulting from a shift angle equal to 0

The shift angle has a direct and major influence on the shape of the lobe and its area. The more the shift angle distant from $\pi/2$ is, the less the wave encounter provides energy.

2.3.2. Required notions to the estimation of the shift angle

The phenomenon of parametric roll in resonance condition is simulated by a 1-DOF time-domain solver using a Runge-Kutta method, such as the on presented in Section 1.1. The variation of stability is imposed in the solver as a function of the time. The shift angle can be observed by calculating the delay between the resulting roll motion and the variation of stability when steady state is reached (Figure 28). First, simulations in resonance condition on several ships known for their different vulnerability to parametric roll are conducted. The analysis of the resulting shift angles leads to the conclusion that the value of the shift angle is obviously linked to the shape of the GZ curves on waves. Therefore, two coefficients denoted by MEAN and OPEN are defined to characterize their shape. The coefficient MEAN characterizes the overall linearity. The coefficient OPEN characterizes the “opening” of the GZ curves. The following preliminary notions have to be introduced to calculate these coefficients:

- The GZ curves on wave are calculated using a hydrostatic solver for different positions of the ship relative to the wave. X denotes the position of the wave crest relative to the aft perpendicular and varies from 0 to the wavelength (denoted by λ), Figure 32. The positions

must be regularly spaced. It is recommended to use at least 10 positions, such as proposed by the IMO (2020a) in level 2 criterion. The number of positions must be even. Figure 33 shows 10 GZ curves calculated in these conditions.

- The GZ curves associated with these positions are identified by a real number K defined as:

$$K = \frac{X}{\lambda} \qquad 88$$

GZ_K denotes the GZ curves associated with K.

- $GZ_{mean}(\varphi)$ is defined as the average value of all $GZ_K(\varphi)$.
- A "pair of GZ curves" denotes two GZ curves associated with K and K + 0.5. Both considered GZ curves are obtained for two positions of the wave crest shifted of $\lambda/2$.
- The area of a pair of GZ curves is defined as the area between both curves up to a considered roll amplitude.
- GZ_{UP} and GZ_{LOW} respectively denote the upper and lower GZ curves of the pair presenting the greatest area.
- K_{UP} denotes the number K associated with GZ_{UP}.

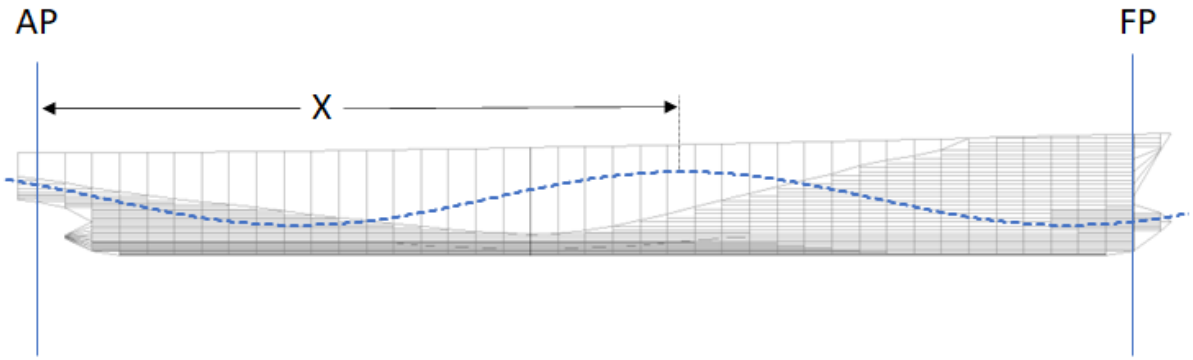

Figure 32 - Position of the wave crest relative to the aft perpendicular

For a considered roll amplitude, GZ_{max} and GZ_{min} curves are not systematically the more relevant GZ curves to consider because they may not be associated in the same pair, or they may not develop the greatest area. Since the ship speed does not vary (1-DoF), the wave is regular and the roll period is twice the encounter period, both curves bounding the lobe are shifted of 0.5 in K. As an example, Table 10 presents the area of each pair of GZ curves of Figure 33 corresponding to a frigate rolling with an amplitude of 38 degrees. The pair [0.1; 0.6] is the one developing the greatest area and defines GZ_{UP} and GZ_{LOW}. At 38 degrees, the highest value of GZ is associated with K = 0.3 and the lowest value of GZ is associated with K = 0.8. The area developed by these GZ curves up to 38 degrees is 56% lower than the one developed by the pair [0.1; 0.6]. The area developed by the highest and lowest values of GZ for all roll angles up to 38 degrees, switching from a curve to another one when necessary, is 12% higher than the one of the pair [0.1; 0.6]. However, considering this area is a physical nonsense. In the example of Figure 33, GZ_{UP} and GZ_{LOW} are associated with GM_{max} and GM_{min}, respectively. However, this configuration is not systematic.

Pair of GZ curves	Area of the pair up to 38 deg [m.rad]	Difference with the pair of greatest area
0; 0.5	0.0458	-19%
0.1; 0.6	0.0568	0%
0.2; 0.7	0.0498	-12%
0.3; 0.8	0.0247	-56%
0.4; 0.9	0.0144	-75%
Max-Min for all roll angles	0.0636	+12%

Table 10 - Excitation area domain function of the GZ couple curves

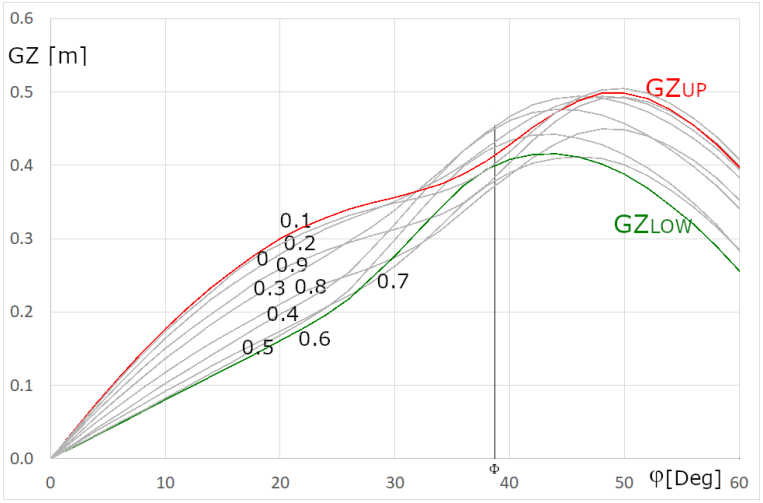

Figure 33 - GZ curves on waves

Both coefficients MEAN and OPEN are function of the considered steady state roll amplitude (Φ). The first coefficient, denoted by MEAN, characterizes the linearity of the GZ_{mean} curve up to Φ. It is defined as the ratio of the area under the straight line from the origin point up to the point $GZ_{mean}(\Phi)$ over the area under GZ_{mean} curve up to Φ (Equation 89, Figure 34).

$$MEAN(\Phi) = \frac{\Phi . GZ_{mean}(\Phi)}{2\int_0^{\Phi} GZ_{mean}(\varphi)d\varphi} \quad 89$$

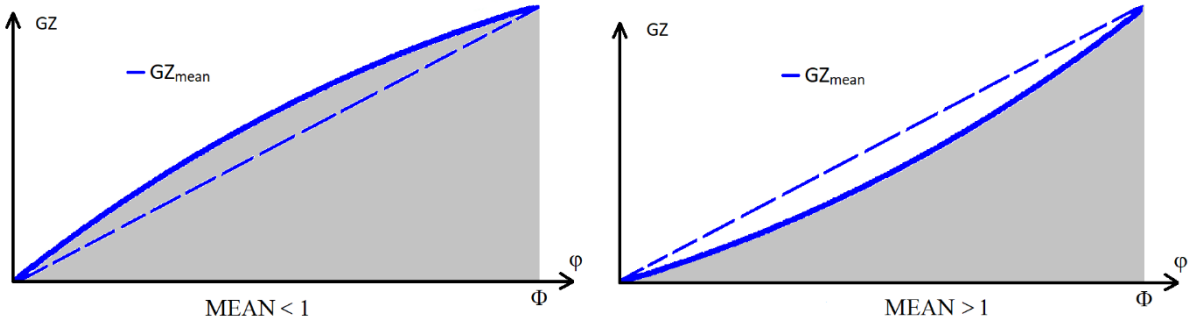

Figure 34 - Graphical representation of MEAN coefficient

The second coefficient, denoted by OPEN, characterizes the "opening" of the pair of GZ curves developing the greatest area (GZ_{UP} and GZ_{LOW}). It is defined as the ratio of the area of the triangle

defined by $GZ_{UP}(\Phi)$, $GZ_{LOW}(\Phi)$ and the origin point over the area of the pair formed by GZ_{UP} and GZ_{LOW} up to the roll amplitude Φ (Equation 90, Figure 35):

$$OPEN(\Phi) = \frac{\Phi\left(GZ_{UP}(\Phi) - GZ_{LOW}(\Phi)\right)}{2\int_0^{\Phi}\left(GZ_{UP}(\varphi) - GZ_{LOW}(\varphi)\right)d\varphi} \quad 90$$

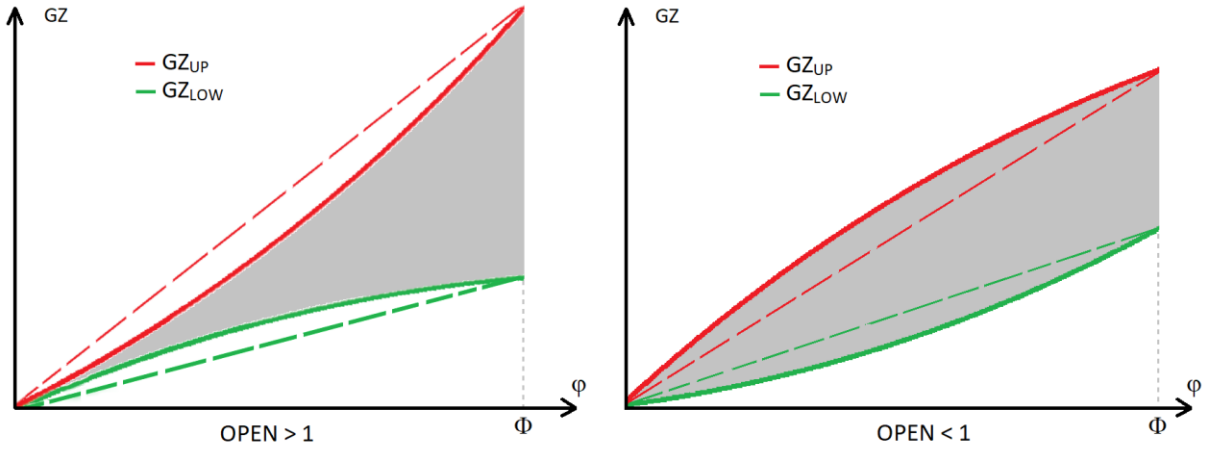

Figure 35 - Graphical representation of OPEN coefficient

It can be noted that linear GZ varying in time with the encounter frequency as stated in Equation 8 leads to coefficient MEAN and OPEN both equal to 1.

Since GZ curves directly depend on the hull shape, the coefficients MEAN and OPEN also reflect it. Therefore, the couple [MEAN; OPEN] varies significantly when considering different types of ships. Figure 36 shows the repartition of couples [MEAN; OPEN] for four different ships, at different draughts and for a large spectrum of values of KG.

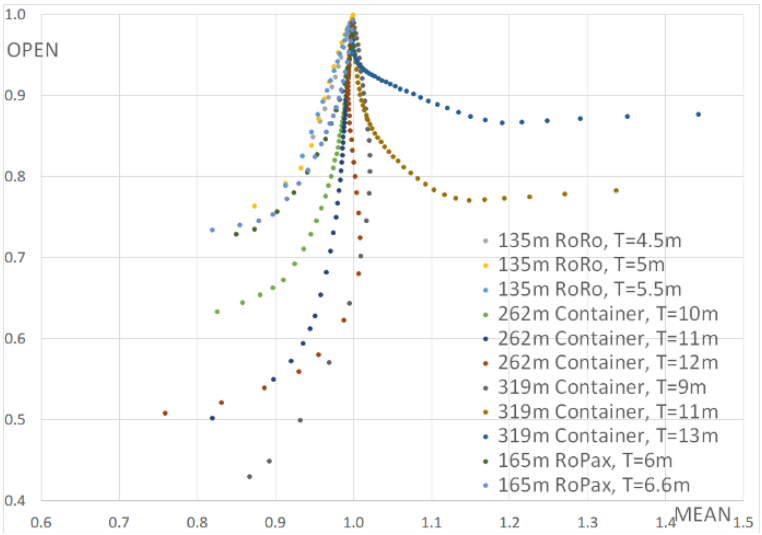

Figure 36 - Couple [MEAN; OPEN] for different ships

2.3.3. Observation

The couple [MEAN; OPEN] presented above is calculated at the end of each 1-DoF simulation for the steady state roll amplitude and associated with the calculated value of the shift angle. The shift angle is calculated as follows:

$$\alpha = \left(t_{\varphi.UpLast}.\omega_e - 2\pi.K_{UP}\right).mod(\pi) \qquad 91$$

Where $t_{\varphi.UpLast}$ denotes the time of the last zero-up-crossing roll angle. K_{UP} is identified for the steady state roll amplitude observed at the end of the simulation as defined previously. Thus, reference points [MEAN; OPEN; α] are extracted from the results obtained with the time-domain solver. However, the shift angle is not constant for all vessel speeds. Figure 37 shows the steady state roll amplitude and the roll period calculated for the C11-class container ship using a 1-DoF time-domain solver. A typical evolution of the shift angle within the lock-in field (speed range within parametric roll appears, defined in Section 1.1) is represented in this figure. The shift angle is not defined outside the lock-in-field since the ratio between the encounter frequency and the roll frequency is not locked to 2. The shape of the evolution of the shift angle as a function of the speed depends mostly on the type of vessel, of the GZ curves in waves and of the loading condition. The shift angle is provided as a function of a dimensionless speed within the lock-in field to permit its comparison for different vessels. The dimensionless speed (denoted by γ) varies from -1 to +1, and is calculated as follows:

$$\gamma = \frac{\mathrm{V} - V_{PR}}{\delta \mathrm{V}} \qquad 92$$

Where V denotes the vessel speed.

Therefore, a fourth dimension is added to the reference points [MEAN; OPEN; α; γ]. The reference points are calculated for different vessels, in different loading conditions, and on several waves, creating a database of reference points.

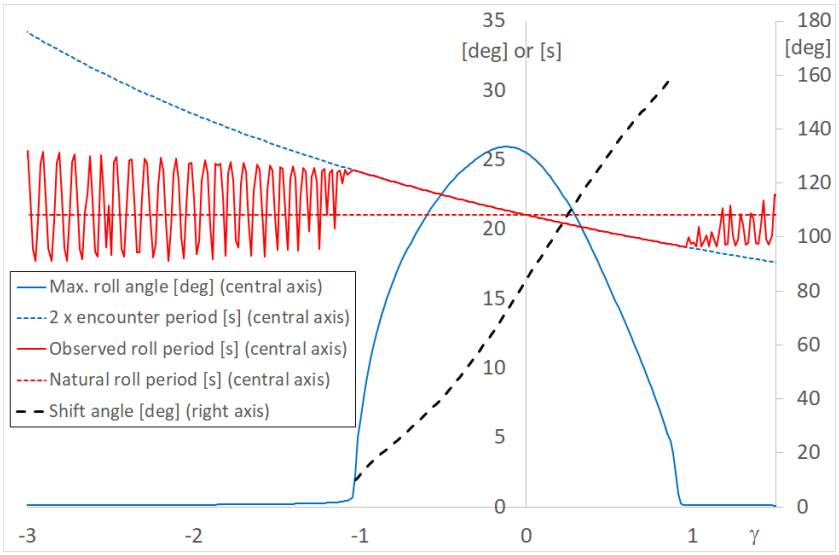

Figure 37 - Evolution of the shift angle in the lock-in field as a function of the dimensionless speed

2.3.4. Estimation of the shift angle

A surface is developed on the database reference points for different values of dimensionless speeds. For each speed, this surface is fitted using a third-degree polynomial equation in two dimensions (Equation 93; Figure 38). The coefficients of the fit are optimized using a least-square method. This fitted surface permits an easy estimation of the shift angle for any values of MEAN and OPEN. The resulting shift angles is named “fitted shift angle” and is bounded by 0 and π (Equation 93). Reference points are excluded from the database if both coefficients MEAN and OPEN are equal to 1 or if the steady state roll amplitude is not reached. The author recommends

using a discretisation of the dimensionless speed of 0.1 or thinner and not to consider γ near the boundaries of the lock-in field where the number of reference points is not sufficient to obtain a proper fitted surface.

$$\alpha = \frac{\pi}{180}(C + a1.MEAN + a2.OPEN + a3.MEAN^2 + a4.MEAN.OPEN + a5.OPEN^2 + a6.MEAN^3 + a7.MEAN^2.OPEN + a8.OPEN^2.MEAN + a9.OPEN^3) \quad 93$$

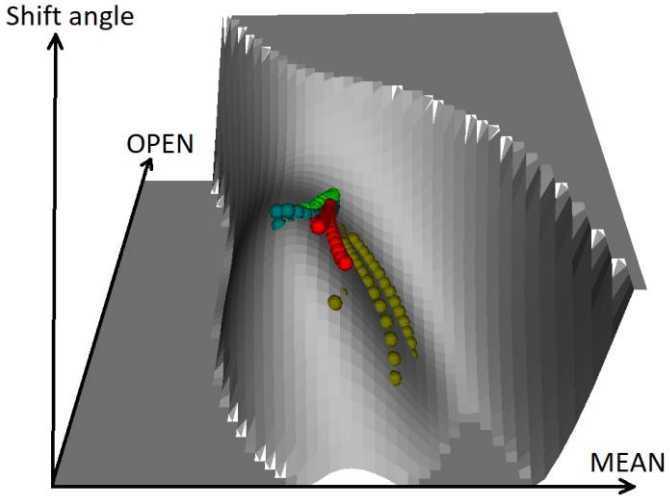

Figure 38 - 3-dimensional representation a fit of the shift angle for a given γ

As example, Table 11 provides the coefficients of the fitted surfaces calculated from references points of 6 container vessels, one RoRo vessel, one RoPax vessel and one tanker, considering 2 to 3 draughts and a large spectrum of values of KG for each ship, representing a total of 3256 reference points. Among the 6 container vessels, the C11-class container ship known for her vulnerability to parametric roll (France et al., 2003) is considered. The number of reference points per surface depends on the dimensionless speed since some points are irrelevant. In the vicinity of γ = 1 and γ = -1, the number of relevant reference points is insufficient to build a fitted surface for γ = 0.9 and γ = -0.9. The lowest number of points used to build one fit is 98. These fitted surfaces are identified as the general fits throughout this PhD thesis since they do not focus on a single type of ship.

V \ Coef	C	a1	a2	a3	a4	a5	a6	a7	a8	a9	Number of reference points
-1.0	0.0	0.0	0.0	0.0	0.0	0.0	0.0	0.0	0.0	0.0	0
-0.8	334.7	781.9	-2558.5	3889.1	-8395.7	7790.3	-548.1	-4569.0	9956.7	-6650.1	200
-0.7	62.4	2477.0	-3259.9	2125.2	-9014.3	8971.4	-1304.4	248.3	5193.5	-5462.7	205
-0.6	-264	1058.5	-17.8	341.4	-2161.6	1049.4	-864.7	720.4	1205.6	-1023.6	207
-0.5	-3347.3	13769.7	-3184.6	-14101.5	-396.6	4013.8	3036.4	5456.9	-5712.4	517.1	208
-0.4	638.3	1831.5	-3936.1	-3286.3	3517.3	2678.8	1050.9	-702.3	-899.0	-838.8	210
-0.3	-5261.8	17861.6	-1267.5	-16666.0	-3912.3	3892.1	3912.2	5543.4	-3922.1	-118.9	209
-0.2	-2499.1	13079.8	-5536.7	-15134.8	3879.4	4416.5	4996.0	-99.2	-1904.7	-1132.2	210
-0.1	-3993.1	18858.8	-7176.2	-20633.2	3585.8	6485.7	5712.5	3641.1	-6098.6	-310.8	210
0	-5197.2	20512.6	-5221.4	-22348.4	4302	3911.7	7029.3	886.3	-3480.5	-316.4	209
0.1	-7997.9	26420	-2382.6	-24220.7	-5065.8	6155.1	6417.3	5306.3	-3306.2	-1242.6	208
0.2	-6953.5	24701.3	-3902.5	-20593.1	-9702.8	10608.1	4523.5	7934.9	-3822.9	-2703.6	204
0.3	-2524.6	21374.8	-14634.4	-18952.3	-6177.6	20333.1	3859.1	8382.6	-6209.3	-5354.3	203
0.4	1689.5	23577.4	-30553.4	-24097.7	771.7	33346	5034.8	9838.7	-11527.3	-7973.8	196
0.5	3827.5	25121.3	-38829.8	-27263.1	4928.5	39415.2	4859.3	13624.6	-17989.7	-7578.9	185
0.6	-13.7	27640.1	-29601.8	-23527.3	-8312.0	37061.1	1963.0	19018.3	-16847.8	-7258.2	160
0.7	-16757.8	48267.2	-669.4	-25555.7	-46063.8	28146	-1768.8	33333.9	-13225.5	-5574.2	134
0.8	-117788.0	124268.9	225141.4	-36751.6	-171056.5	-135791.5	-7470.2	64597.2	12269.3	42724.1	98
1.0	180	0.0	0.0	0.0	0.0	0.0	0.0	0.0	0.0	0.0	0

Table 11 - Values of the coefficients of the general fits of the shift angle

2.4. METHOD

2.4.1. Assumptions

The extended energy method is based on the following assumptions:

1. The vessel is symmetrical, and its centre of gravity is located on the centreline. Thus, the angle of equilibrium is $\varphi = 0$.
2. The steady state roll motion is sinusoidal.
3. The vessel is sailing on a regular wave at constant speed.
4. The vessel is rolling at half the encounter frequency within the lock-in field (Grinnaert et al., 2017).
5. At steady state, the exciting energy and the damping energy are equal (Kerwin, 1955; Grinnaert et al., 2017), no larger roll angle can appear further on.
6. The roll damping is non-linear. It can be estimated using IKEDA method (Ikeda, 1978; Kawahara, 2009)

Parametric roll may lead to large roll motions. Thus, the consideration of non-linear GZ is recommended by the IMO in the second-generation intact stability criteria (2020a) and by Peters et al. (2015). Indeed, the energy method considers the non-linear GZ to increase its accuracy. The assumptions 1, 3 and 6 are formulated in parametric roll level 2 assessment of the SGISCs (IMO, 2020a).

Assumption 1 is close to reality since the vessel is ballasted to sail without list. Assumption 2 is important since it is required to calculate the lobe and the damping energy from the half phase diagram. This assumption is close to reality when parametric roll is fully developed on longitudinal regular waves as observed on calculated time series. Regular waves are representative for long swell which can be encountered at sea, even if fully developed sea states are often encountered in open water. Assumption 3 is considered when assessing parametric roll in time domain in one (level 2 criteria) or even three degrees of freedom (direct assessment) since surge is frozen (IMO, 2020a). As specified by IMO in SGISCs (IMO, 2020a), when realising a full parametric roll study from time-domain simulations, at least, heave, roll and pitch motions should be considered. Indeed, surge motion is not considered as especially affecting parametric roll. Assumption 4 is systematically observed for any vessel assessed in 1-DoF simulations on regular waves. This assumption is also admitted by most of parametric roll Real-time identification methods since they considered the ratio of the roll over pitch period equal to 2. However, the author do not have sufficient full-scale data where parametric roll appeared on regular waves to conclude if assumption 4 is also observed in reality. Finally, assumption 5 is verified as long as the environmental and loading conditions are not modified.

2.4.2. Exciting energy

The exciting energy is calculated based on the area of the lobe described by the variation of the transverse stability.

It has been analytically demonstrated considering linear GZ that the area of the lobe is equal to the area between the linear GZ curves up to the considered roll angle multiplied by a ratio C equal to $\pi/4$. However, the shift angle leads to a distortion of the lobe. Thus, hereafter this simplification ratio of $\pi/4$ is not assumed when considering non-linear GZ. However, it will be verified in Section 2.5 that this simplification always provides conservative results.

The calculation of the exciting energy requires to numerically construct the lobe described by the variation of the transverse stability point after point while considering the estimation of the shift angle. Thus, an accurate estimation of the lobe is required. To obtain such an accuracy, the shift angle has to be estimated as accurately as possible. Therefore, the shift angle fits are used to provide this estimation at any roll angle and speed.

For one vessel in a specific loading condition, the GZ curves on longitudinal waves are calculated for several positions of the wave along the hull. In this study, GZ curves in waves are calculated by the hydrostatic solver presented by Grinnaert et al. (2015). This solver provides the righting lever of the ship balanced in trim and sinkage on longitudinal static waves, for any required heel angle and any position of the ship relative to the wave crest, such as specified by the SGISCs (IMO, 2020a). However, any other solver providing the GZ curves in longitudinal waves is adapted to the energy method presented here. GZ curves are defined numerically as $GZ_K(\varphi)$ from 0 up to a maximum roll angle which will be a limit for the energy method. Examples of 3-dimension representation of the GZ curves in waves are shown in Figure 9 page 24 and Figure 17 page 47 (here the wave crest position X is replaced by K).

Each point of the GZ curves is seen as a possible steady state roll amplitude (denoted by Φ_p). K_{UP} and both coefficients MEAN and OPEN are calculated from the pair $[GZ_{UP}; GZ_{LOW}]$ identified for each possible steady state roll amplitude. For any dimensionless ship speed, each possible steady state roll amplitude, is associated to a possible shift angle (denoted by α_p) using Equation 93, calculated with the same discretisation angle than the GZ curves (where "p" stands for possible). For speeds other than the ones considered to build the fitted surfaces, a linear interpolation between both adjacent fitted shift angles is applied. For each possible steady state roll amplitude

Φ_p, the lobe described by GZ(t) in the coordinate system [φ; GZ] is constructed for N points for half a roll period (denoted by $T_r/2$). Where N is an integer set by the user. The higher N is, the more accurate the lobe description is. The author recommends to use at least N = 100. For each point of the lobe indexed by i (from 0 to N), the roll angle φ(i) is provided by Equation 94 and GZ(φ(i); K(i)) is calculated by double interpolation in φ and in K, with K(i) calculated according to Equation 95.

$$\varphi(i) = \Phi . \sin\left(\frac{\pi . i}{N}\right) \quad 94$$

$$K(i) = \left(\frac{\alpha}{2\pi} + K_{UP} + \frac{i}{N}\right) mod(1) \quad 95$$

The area of the lobe (denoted by A_P) is calculated for each couple [Φ_p; α_p] using Green Riemann method (an implementation of this method is proposed by Grinnaert, 2017) or any equivalent method. Those integration methods can be used since the lobe is closed at the origin point (0; 0), thanks to the assumption of the centre of gravity located on the centre line. The introduction of the shift angle estimated from the fit in the expression of K(i) (Equation 95) leads to the construction of the lobe distorted by the shift angle as it can be seen in Figure 29, Figure 30 or Figure 31. The exciting energy (denoted by E_E) for each Φ_p is finally obtained by multiplying the area of the lobe (A_P) by the vessel's weight (W), Equation 96.

$$E_E = -W \int_{\frac{T_\varphi}{2}} GZ\big(\varphi(i); K(i)\big) d\varphi \quad 96$$

The roll period (T_φ) is analytically calculated as a function of the speed within the lock-in field since it is directly locked to twice the encounter period (denoted by T_e). At the beginning of half a roll period, the vessel is considered at the upright position. After a quarter of period the vessel reaches the maximum roll angle. Since the definition of the shift angle is a shift between the roll angle and the GZ variation, it can be introduced in the equation of motion to state on which GZ curve is the vessel at the upright condition. In other words, it is possible to see it as a delay between the position of the wave along the hull and her impact on the ship stability. This is valid only if a constant speed is assumed (no surge oscillations, 1 DoF).

2.4.3. Damping energy

The damping energy is calculated considering the assumption of a sinusoidal roll motion when the steady state is reached. Therefore, the roll angle versus roll speed diagram can be defined analytically (Figure 39). The area of this diagram is the image of the damping energy (Equation 97). The damping energy is calculated for the same possible steady state roll amplitudes Φ_P than the exciting energy (Equation 99).

$$E_D(\Phi_P) = B_{44} \int_{\frac{T_\varphi}{2}} \dot{\varphi} d\varphi \quad 97$$

$$\dot{\varphi}(t) = \omega \Phi_P \cos(\omega t) \quad 98$$

$$E_D(\Phi_P) = \frac{{\Phi_P}^2 {\omega_e}^2 T_e B_{44}}{8} = \frac{{\Phi_P}^2 \omega B_{44} \pi}{2} \quad 99$$

In this method, the damping coefficient B_{44} is required as a function of the roll amplitude. This coefficient can be calculated empirically according to a simplified method (Ikeda et al., 1978; Kawahara et al., 2009) for each possible steady state roll amplitude Φ_P. Any other method providing B_{44} can be used, such as results from model test or CFD. In such cases, the damping coefficient is most of the time expressed as a linear and a quadratic coefficients (B_{Lin}, B_{Quad}). Equation 100 provides an equivalent damping coefficient B_{44} as a function of the roll amplitude (ITTC, 2011). For any dimensionless speed different than 0, ω_0 is replaced by the actual roll frequency ω.

$$B_{44}(\Phi_P) = B_{Lin} + \frac{8}{3\pi}\omega\Phi_P B_{Quad} \qquad 100$$

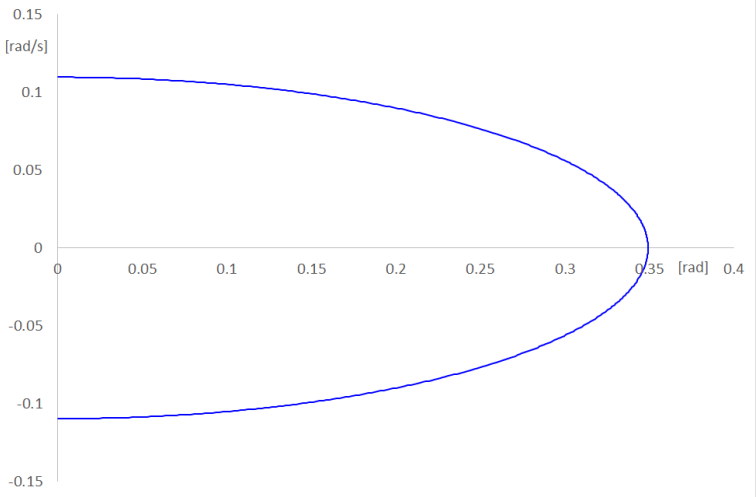

Figure 39 - Roll speed versus roll angle diagram

2.4.4. Energy balance

The roll steady state appears when both damping and exciting energies are equal. The corresponding roll amplitude can be graphically identified (Figure 20, page 55) or numerically calculated. The energy method provides one unstable solution at 0 degree and one stable solution at Φ. It can happen that no intersection between the exciting and the damping energies appears. In this case, the steady state roll amplitude is lower than the roll angle of the first non-zero point of the GZ curves if the damping energy is larger than the exciting energy. Otherwise, if the exciting energy is larger than the damping energy, the roll amplitude is larger than the maximum roll angle considered in the GZ curves.

In addition, the energy method permits to state if a roll steady state is reached during a simulation and in consequence stop the simulation to avoid unnecessary computational time:

If $E_E = E_D$, a roll steady state is reached

If $E_E > E_D$, the roll amplitude increases

If $E_E < E_D$, the roll amplitude decreases

As an example, Table 12 presents the exciting energy and the damping energy calculated at the end of four time-domain simulations where the energy method is considered to conclude on the simulation duration (1500 points per simulation). The simulations are conducted with the C11-class container ship on sinusoidal longitudinal waves at synchronism speed with a time step

chosen by the user. At the end of the simulation a steady state may not be reached. The damping energy is then calculated from the area of the half phase diagram associated with the last half roll period using Green-Riemann method.

Time step [s]	KG [m]	E_E / E_D %	Φ [deg]	Observations	Φ observed with infinite sim. duration [deg]
0.07735	15	118.5%	11.88	Simulation is not long enough	15.03
0.1547	15	101.8%	14.68	Simulation is not long enough	15.03
0.3094	15	99.7%	15.05	The simulation is long enough, a steady state appears at Φ	15.05
1.0812	20	194%	>70	The vessel capsized	>70

Table 12 - Simulation duration example, energy consideration

The simulation presented in Table 12 have been run again in the same conditions (same time step as well) until a steady state is reached or until the vessel capsizes. It shows that the conclusion obtained with energy considerations are correct. The difference of 0.02 degrees observed between the two first simulations and the third one is due to the chosen time step and the numerical calculation method (Runge-Kutta method).

2.4.5. Example of implementation of the method

A detailed example of implementation of the energy method is provided for the C11-class container ship sailing on regular longitudinal sinusoidal wave of length equal to the one of ship and of steepness equal to 0.0167. The draught of the vessel is 12 metres, the height of the centre of gravity above base line is 17.2 metres. The GZ curves in wave associated to this situation are calculated using the Calcoque software (Grinnaert et al., 2015), and provided in Table 13. In these conditions the mean metacentric height calculated from the 10 GZ curves in waves is equal to 3.25 metres. The synchronism speed corresponding to the first mode of parametric roll resonance is calculated using Equation 3, and equal to 5.92 $m.s^{-1}$. The bandwidth of the lock in field is calculated using Equation 4. The selected speed for this example is 6.53 $m.s^{-1}$, equivalent to a dimensionless speed of γ = +0.2. Thus, within the lock-in field, the vessel roll period is locked to twice the encounter period. The encounter period corresponding to a forward vessel speed of 6.53 $m.s^{-1}$ in head sea is 9.79 seconds. In consequence, the roll period is locked to 19.58 seconds.

φ \ K	0	0.1	0.2	0.3	0.4	0.5	0.6	0.7	0.8	0.9	1
0	0.000	0.000	0.000	0.000	0.000	0.000	0.000	0.000	0.000	0.000	0.000
2	0.156	0.168	0.161	0.140	0.093	0.068	0.062	0.071	0.091	0.122	0.156
4	0.312	0.334	0.320	0.275	0.186	0.137	0.125	0.142	0.183	0.245	0.312
6	0.464	0.496	0.473	0.403	0.282	0.207	0.189	0.214	0.277	0.369	0.464
8	0.613	0.653	0.619	0.524	0.378	0.278	0.256	0.288	0.372	0.495	0.613
10	0.760	0.805	0.758	0.639	0.473	0.352	0.324	0.365	0.470	0.622	0.760
12	0.905	0.952	0.891	0.751	0.568	0.429	0.396	0.445	0.570	0.751	0.905
14	1.048	1.094	1.019	0.860	0.663	0.509	0.471	0.529	0.675	0.881	1.048
16	1.189	1.233	1.145	0.968	0.758	0.594	0.551	0.617	0.783	1.012	1.189
18	1.327	1.367	1.267	1.076	0.855	0.683	0.636	0.710	0.895	1.143	1.327
20	1.462	1.498	1.387	1.184	0.955	0.778	0.726	0.808	1.011	1.273	1.462
22	1.593	1.623	1.504	1.291	1.056	0.876	0.822	0.911	1.129	1.402	1.593
24	1.720	1.745	1.618	1.399	1.160	0.979	0.923	1.018	1.248	1.529	1.720
26	1.842	1.861	1.728	1.506	1.266	1.085	1.029	1.128	1.367	1.652	1.842
28	1.958	1.972	1.835	1.612	1.374	1.194	1.138	1.241	1.485	1.772	1.958
30	2.066	2.077	1.938	1.718	1.484	1.306	1.251	1.355	1.602	1.887	2.066
32	2.159	2.166	2.034	1.822	1.592	1.417	1.365	1.470	1.717	1.991	2.159
34	2.232	2.232	2.112	1.914	1.687	1.513	1.467	1.582	1.825	2.080	2.232
36	2.279	2.275	2.167	1.984	1.761	1.589	1.550	1.679	1.918	2.150	2.279
38	2.300	2.293	2.195	2.027	1.811	1.642	1.610	1.747	1.982	2.193	2.300
40	2.296	2.285	2.197	2.043	1.836	1.670	1.642	1.780	2.008	2.206	2.296
42	2.263	2.251	2.170	2.028	1.835	1.673	1.646	1.781	1.998	2.183	2.263
44	2.199	2.187	2.112	1.982	1.805	1.651	1.624	1.753	1.957	2.126	2.199
46	2.108	2.095	2.027	1.909	1.748	1.605	1.577	1.698	1.889	2.042	2.108
48	1.992	1.980	1.918	1.811	1.665	1.536	1.506	1.619	1.796	1.933	1.992
50	1.857	1.844	1.789	1.693	1.562	1.442	1.414	1.519	1.681	1.804	1.857
52	1.704	1.691	1.642	1.557	1.438	1.328	1.301	1.398	1.546	1.657	1.704
54	1.535	1.523	1.479	1.404	1.297	1.195	1.169	1.257	1.395	1.494	1.535
56	1.353	1.341	1.303	1.238	1.141	1.045	1.019	1.101	1.227	1.318	1.353
58	1.160	1.147	1.116	1.059	0.969	0.878	0.853	0.929	1.047	1.130	1.160
60	0.956	0.944	0.918	0.868	0.785	0.697	0.672	0.743	0.854	0.931	0.956
62	0.745	0.732	0.711	0.667	0.587	0.502	0.478	0.545	0.650	0.722	0.745
64	0.525	0.514	0.497	0.456	0.379	0.295	0.272	0.336	0.437	0.505	0.525
66	0.299	0.289	0.275	0.238	0.160	0.077	0.055	0.116	0.214	0.280	0.299
68	0.067	0.059	0.048	0.011	-0.069	-0.148	-0.169	-0.111	-0.016	0.049	0.067
70	-0.170	-0.176	-0.185	-0.223	-0.305	-0.381	-0.401	-0.346	-0.254	-0.188	-0.170

Table 13 - Example, C11, GZ curves in waves, T = 12 m, KG = 17.2 m, $\lambda = L_{PP}$, $S_W = 0.0167$

The roll damping is estimated with the method provided by Ikeda (1978) and Kawahara (2009). The damping energy is calculated using Equation 99 considering a roll period locked to 19.58 seconds for each angle in Table 13, seen as possible roll amplitude (Φ_P). The resulting values of the damping coefficient and damping energy are provided in Table 14 up to Φ_P = 30 degrees.

Φ_P [deg]	B_{44} [N.m.s/rad]	E_D [J]
0	412215968	618
2	475050560	285055
4	546433033	1311553
6	622993959	3364459
8	704410958	6762930
10	790237861	11854594
12	879908458	19007668
14	972744000	28601149
16	1067964371	41013381
18	1164702678	56609449
20	1262022909	75727928
22	1358940137	98667593
24	1454442676	125674723
26	1547515477	156931650
28	1637164032	192547153
30	1722437990	232549253

Table 14 - Example, damping calculation

For each possible roll amplitude (Φ_P), the pair of GZ curves (associated to K and K + 0.5) presenting the greatest area up to Φ_P is identified. Then, the coefficients MEAN and OPEN are calculated (respectively Equation 89 and 90). The shift angle is calculated for each Φ_P using the fit (Equation 93) and the coefficients provided in Table 11 for the dimensionless speed of γ = +0.2, results are provided in Table 15.

Φ_P [deg]	MEAN	OPEN	Shift angle [deg]
0	1.000	1.000	0.00
2	1.000	1.000	89.47
4	0.999	0.994	91.47
6	0.996	0.984	94.52
8	0.994	0.970	97.68
10	0.993	0.955	100.33
12	0.992	0.938	102.19
14	0.992	0.921	103.05
16	0.993	0.903	103.11
18	0.995	0.883	102.58
20	0.997	0.862	101.72
22	0.999	0.838	100.78
24	1.001	0.812	99.99
26	1.001	0.784	99.79
28	1.002	0.754	100.68
30	1.001	0.723	103.35

Table 15 - Example, estimation of the shift angle from the fit

Using these values of the shift angle, a lobe is defined for each possible roll amplitude. The area of each lobe and the associated exciting energy are calculated. Finally, the steady state parametric roll amplitude is calculated at the intersection of the of the exciting and the damping energies (Table 16, Figure 40).

Φ_P [deg]	E_E [J]	E_D [J]
0	0	0
2	1046081	294986
4	4174377	1359356
6	9304379	3491512
8	16252005	7025659
10	24774896	12325815
12	34651855	19777560
14	45789147	29777761
16	58111174	42722601
18	71514463	58994379
20	85851540	78947635
Intersection of E_E and E_D between 20 and 22 degrees		
22	100912500	102895230
24	116292809	131095058
26	131626739	163738045
28	146181289	200938100
30	158386516	242724567

Table 16 - Example, energy calculations

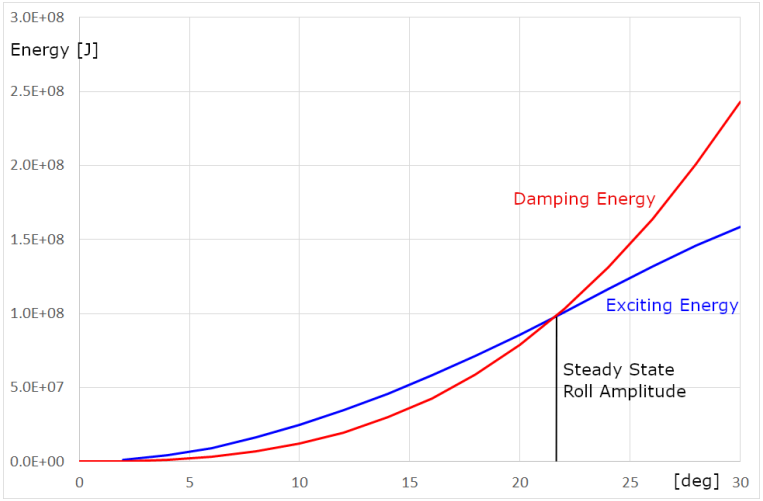

Figure 40 - Example, energy balance

In this example, steady-state roll amplitude calculated with the energy method, is equal to 21.55 degrees. The steady-state roll amplitude reached for an equivalent 1DoF time-domain simulation in the same conditions is equal to 21.07 degrees. Here, the energy method provides an estimation of the steady state roll amplitude with an acceptable accuracy.

2.5. RESULTS

First, this section presents the validation of a possible conservative simplification of the energy method based on the conservative ratio C (introduced in Section 2.2.2). It aims to validate considering non-linear GZ that the coefficient C = π/4 is a conservative ratio which permits an easy calculation of a conservative lobe area.

Then, results obtained from the energy method for several types of ships in different conditions are presented and discussed. The results are compared with the ones obtained from a 1-DoF

time-domain solver solving numerically Equation 10 (page 23), and rewritten hereunder, using Runge-Kutta method, such as realised in the example presented in Section 2.4.5. The nonlinear roll damping coefficient (B_{44}) is recalculated at each time step as a function of the roll amplitude.

$$J_{44}\ddot{\varphi} + B_{44}\dot{\varphi} + WGZ(\varphi, t) = 0 \qquad 10$$

Finally, the possible use of the method and its limits are discussed.

2.5.1. Validation of a possible conservative simplification of the energy method

The ratio of the area the lobe described by the variation of the transverse stability up to Φ on half a period on the area described by the GZ_{UP} and GZ_{LOW} up to Φ is analytically demonstrated to be equal to $\pi/4$ considering linear GZ (denoted by C in section 2.2.2), Equation 85. A validation study is realised to conclude if this ratio can be applied considering nonlinear GZ. The study is conducted on 2 container vessel, 1 tanker, 1 RoRo vessel and one passenger vessel. Time-domain simulations are conducted at V_{PR} (where the value of the shift angle should be close to $\pi/2$) on sinusoidal waves of length equal to the one of ship and of steepness 0.0167. When steady state is reached, the area of the conservative pair of GZ curves (GZ_{UP} and GZ_{LOW}) and the one of the lobe are calculated. Table 17 present the most significant results obtained in this study. It is observed that the ratio $C/(\pi/4)$ is lower than 100 %. If the shift angle (α) is distant from $\pi/2$ the shape of the lobe is distorted, reducing the lobe are (for a constant roll amplitude), thus C decreases as α is distant from $\pi/2$. It is possible to conclude that $\pi/4$ is a conservative result to switch from the instantaneous variation of the transverse stability to the continuous transverse stability assumptions. Thus, the ratio $\pi/4$ could be used to switch from the area between GZ_{UP} and GZL_{OW} up to Φ to a conservative area of the lobe. This significantly simplifies the method (no consideration of the shift angle), it could be used as a first step to provide conservative results in case of implementation for further regulatory assessment.

Vessel	Draught [m]	KG [m]	Φ [deg]	Area of the pair of GZ curves up to Φ [m.rad]	Area of the lobe up to Φ [m.rad]	C	C/(π/4) %
C11 class	12	16	21.68	0.2166	0.7798	0.7798	99.3%
C11 class	12	17	28.70	0.3794	0.7786	0.7786	99.1%
8600 TEU	13	15	21.32	0.2055	0.7800	0.7800	99.3%
8600 TEU	13	16	26.61	0.3200	0.7794	0.7794	99.2%
227.5-metre tanker	11	12	11.53	0.0078	0.7692	0.7692	97.9%
227.5-metre tanker	11	13	25.00	0.0366	0.7814	0.7814	99.5%
KTH RoRo	5.5	10	4.72	0.0075	0.7733	0.7733	98.5%
Passenger vessel	6.6	12	12.79	0.0528	0.7784	0.7784	99.1%

Table 17 - Validation of the C coefficient, non-linear GZ, synchronism condition

2.5.2. Results

The results obtained with the energy method presented in this section are calculated using the fit of the shift angle available in Table 11. The roll amplitudes calculated with the energy method are compared with the ones reached during time-domain simulations in the same conditions (same loading condition and damping) when a steady state appears. Results are provided as functions of the speed. Negative speed values represent a vessel sailing with a forward speed in following seas.

The method and the proposed fits are tested on 8 vessels (five container vessels, one RoPax, one tanker, one frigate). The tanker, the frigate and one container vessel are not the ones considered to build the fit of the shift angle. The tested vessels were used to build the fit of the shift angle. Each vessel is assessed for a range of KG values for which the minimum GM in waves is no less than 0.2 metre, representing a total of 171 conditions. Within the lock-in field, the average absolute root mean square deviation is 1.34 degrees, the minimum encountered deviation is 0.14 degree, and the maximum is 7.38 degrees. Among those cases, the most representatives are detailed hereafter.

Figure 41 presents the results obtained for the 262-metre container vessel which has been used to build the fits of the shift angle (C11-class container ship). The vessel is sailing on sinusoidal regular waves. The energy method provides accurate results compared to the one obtained during 1-DoF simulations. Results for the lowest speeds in the lock-in field are less accurate than it could be expected. The absolute root mean square deviation in the lock-in field is 1.54 degree.

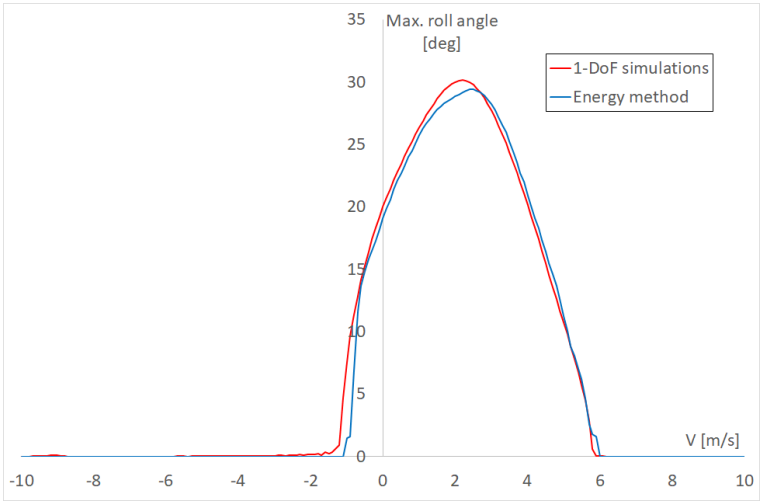

Figure 41 - Parametric roll amplitude of a 262-metre container vessel on sinusoidal regular waves

Figure 42 presents the results obtained for a 180-metre container vessel which has also been used to build the fits of the shift angle. The vessel is sailing on non-sinusoidal regular waves. The results obtained with the energy method are very accurate in the whole lock-in field. The absolute root mean square deviation in the lock-in field is 0.54 degree.

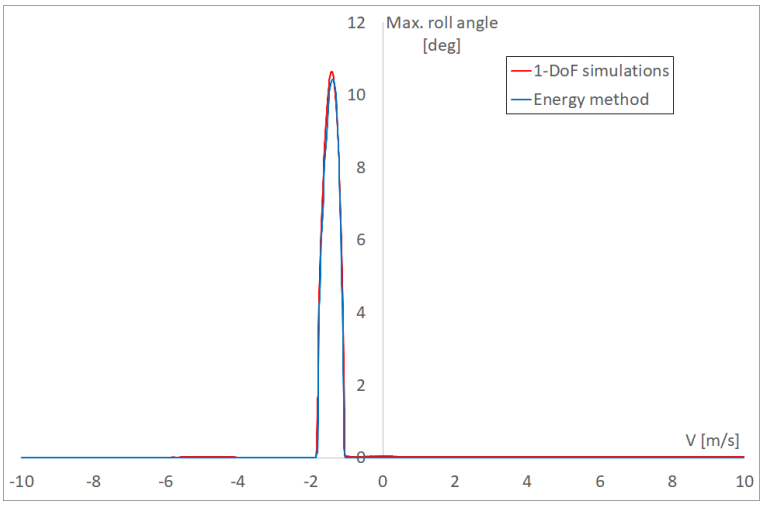

Figure 42 - Parametric roll amplitude of a 180-metre container vessel on non-sinusoidal regular waves

Figure 43 presents equivalent results obtained for a 319-metre container vessel that has not been used to build the fits of the shift angle. The study is stopped at the maximum vessel speed even if the theorical lock-in field extends further. The estimated roll amplitude using the energy method is accurate even for a vessel which was not used to build the fit of the shift angle. As observed previously, the accuracy decreases at the borders of the lock-in field. The absolute root mean square deviation in the lock-in field (up to the maximum vessel speed) is 0.83 degree.

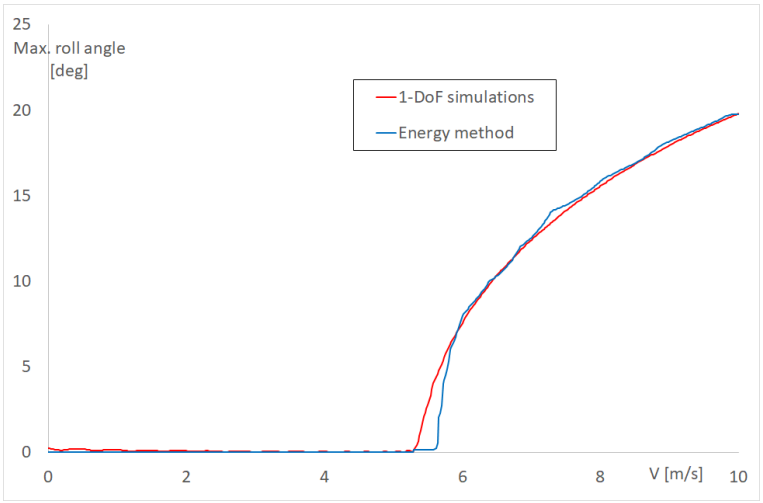

Figure 43 - Parametric roll amplitude of a 319-metre container vessel on sinusoidal regular waves

Figure 44 presents the results obtained for a 331-metre container vessel that has not been used to build the fits of the shift angle. The energy method is not as accurate as expected. A second implementation of the energy method is conducted, using the shift angle observed at the end of the 1-DoF simulations as a forced entry. This significantly increases the accuracy of the method.

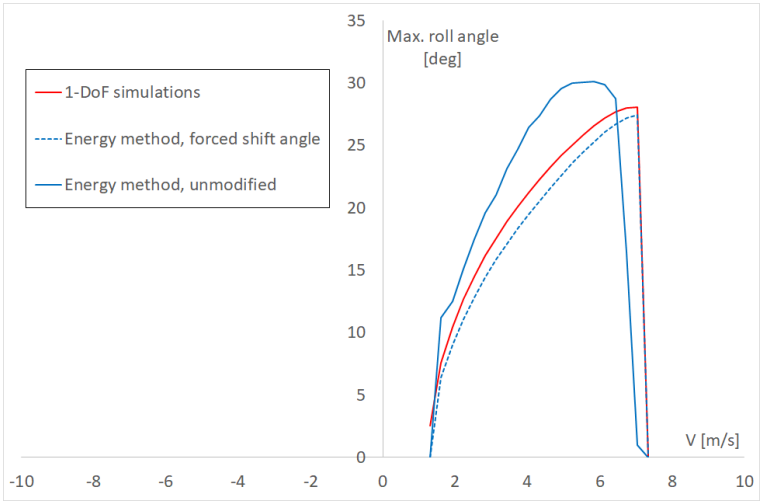

Figure 44 - Parametric roll amplitude of a 311-metre container vessel, influence of the shift angle

Table 18 provides some other remarkable results obtained on the C11-class container ship presented in Figure 41. She is sailing on a sinusoidal wave which length is equal to the one of the ship and of steepness equal to 0.0167 such as specified by IMO (2020a).

GM on calm water [m]	Minimum GM in waves [m]	Dimensionless speed γ [-]	Roll amplitude from simulations [deg]	Roll amplitude energy method [deg]	Observation
0.226	-1.067	0.2	Capsize	29.6	GM_{min} is negative
1.325	0.033	0	38.53	37.05	$GM_{min} < 0.2$
2.225	0.933	0	29.9	29.4	$GM_{min} > 0.2$

Table 18 - Some remarkable cases on container vessel

Figure 45 represents the evolution of the exciting and damping energies as functions of the roll amplitude for the last line of Table 18.

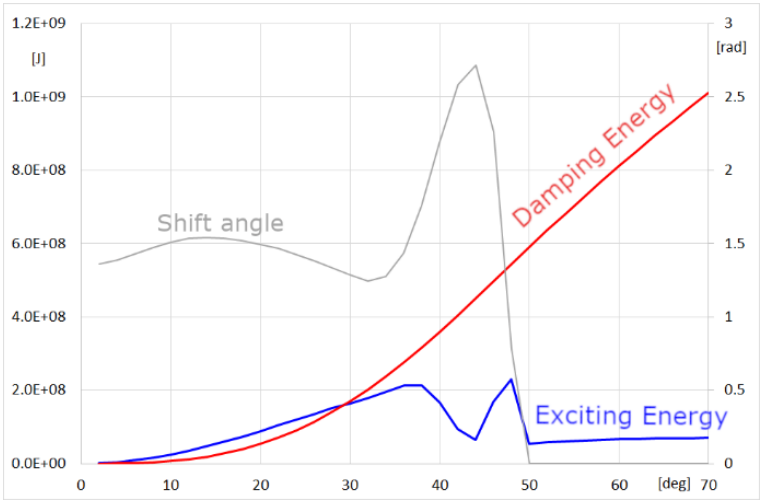

Figure 45 - Damping and exciting energies and fitted α as a function of the roll amplitude

Figure 41 and Figure 42 validate the use of the energy method for vessels which are used to build the fit of the shift angle. The method provides in those cases an accurate evaluation of the steady state roll amplitude. Figure 43 validates the use of the method even for vessel which are not used

to build the fit. However, this type of vessel is considered in the fit (container vessel). Figure 41 and Figure 43 present a less accurate estimation of the roll amplitude for extremely low dimensionless speeds. This poor of accuracy may be explained as follows:

- The value of the shift angle calculated from the fit is not accurate for speeds near the boundaries of the lock-in field since fewer relevant reference points were used to build the fit.
- An estimation of the shift angle from the fit resulting to a value near 0 or π lowers the exciting energy, leading to a smaller roll amplitude estimation.
- The calculated bandwidth of the lock-in field may not be accurate since it is analytically calculated based on linear assumptions as presented in Equation 4. Thus, it may slightly differ of the bandwidth resulting from non-linear simulations.

Table 18 presents some remarkable cases which require further explanations. For the first case, the 262-metre container vessel capsizes during the simulation. However, the energy method does not detect it. An erroneous estimation of the roll amplitude appears when minimum GM in waves is negative even if the average GM in waves or the GM in calm water remain positive. Therefore, minimum GM in waves should not be negative when using the energy method, it is a restrictive criterion. The second case in Table 18 presents a positive minimum GM in waves. However, the accuracy of the method is poor. The roll amplitude resulting from the energy method is equal to 37.05 degrees, this value is larger than the angle of maximum GZ in waves which is 34 degrees. Therefore, if the roll amplitude resulting from energy method is larger than the angle of maximum GZ, the energy method should not be considered as relevant. Both restrictions of use appear due to a wrong estimation of the coefficients MEAN and OPEN in those cases.

The third case presented in Table 18 is also available in (Luthy et al., 2021b), with an estimated value of the roll amplitude based on the energy method equal to 29.7 degrees. Using the fit provided in Table 11, the estimated roll amplitude is 29.4 degrees. The difference is a consequence of the chosen fit of the shift angle. The fit is based on a larger number of vessels than the one presented by Luthy et al. (2021b) and therefore may lead to less accurate results; however, it can be used for a greater range of vessel type. The fit presented by Luthy et al. (2021b) is not reported in this PhD since it only considers the dimensionless speed $\gamma = 0$.

Figure 44 shows that in some cases, the energy method is not as accurate as it could be expected, due to an insufficiently accurate estimation of the shift angle. When a more accurate value of the shift angle is used as forced input, the accuracy of the estimated roll amplitude increases significantly, from an absolute root mean square deviation of 7.38 degrees to 1.51 degree. Therefore, the quality of the fit of the shift angle is the key factor of an accurate estimation of the roll amplitude. The sustainability of the method and of the fit has been assessed resulting in an average absolute deviation of 1.34 degrees. The accuracy of the method depends on the accuracy of estimation of the shift angle. Therefore, the author recommends to use one set of fits per ship type (container vessel, RoRo, RoPax, Tanker, frigate…) to estimate as accurately as possible the shift angle and consequently the roll amplitude.

2.5.3. Possible use and limits

The energy method provides accurate results within the boundaries of its limit of use.

When minimum GM on wave is negative, OPEN coefficient is not designed to consider it, this leads to a poor estimation of the shift angle and then to an insufficiently accurate estimation of the roll amplitude. Moreover, negative values of minimum GM on wave can lead to erroneous results such

as the one presented in the first line of Table 18. Thus, it is recommended by the author not to use the energy method if the GM_{min} in waves is smaller than 0.2 metre.

Figure 45 shows that at large angles, the shift angle estimated from the fit does not make sense, since MEAN and OPEN are not representative of the shape of the GZ curves when the angle of maximum GZ is overreached. Here, the maximum of the GZ curves is reached at 38 degrees. Therefore, the exciting energy is not accurately estimated. At those large angles, assuming that the roll motion is sinusoidal and that the vessel rolls at her natural frequency may not be relevant. When reaching angles further than the angle of maximum GZ, the roll frequency may significantly differ, then the estimation of the damping energy is less accurate since it is based on the roll frequency.

The accuracy of the energy method relies on the accuracy of the estimation of the shift angle (Figure 44). Thus, the method should not be used if the fit of the shift angle is not in accordance with the type of vessel which is assessed.

The energy method does not consider other modes of parametric roll since the lock-in field is calculated for the first mode only. The method could be extended to other modes. However, the other modes are not assessed either in the second-generation intact stability code (IMO, 2020a) since they do not provide sufficient energy to lead to dangerous roll amplitudes (Grinnaert, 2017).

The energy method can be seen as an alternative to the averaging method (IMO, 2015). The energy method considers real GZ in longitudinal waves while the averaging method considers both the polynomial fit of the mean GZ curve in wave and the metacentric height variation. The energy method could also be submitted as an alternative to time-domain simulations for level 2 of the parametric roll criterion in the second-generation intact stability criteria (IMO, 2020a). In this case, two sub levels could be considered. The first sublevel would consider the area between the GZ curves and the conservative ratio of $\pi/4$ to calculate the exciting energy considering nonlinear GZ. The second sublevel would consider a specific fits of the shift angle per ship type.

CHAPTER 3. 6-DEGREE-OF-FREEDOM SOLVER TO ASSESS PARAMETRIC ROLL

Time-domain simulations requires a large number of inputs. Its complexity permits to simulate a wide diversity of environmental and loading conditions. However, providing accurately each input parameter may be complex in some cases.

This chapter presents the results of some works conducted with the aim to validate and increase the relevance of the time-domain simulations inputs. First, an iterative method to calculate the roll damping coefficients to be set in the solver to reproduce roll decay time series obtained from other sources is presented. Then, a study on the relevance of the probability of appearance of a sea states for the considered sailing area is realised based on the data provided by the European Copernicus Marine Service. Detailed research on the most conservative spreading angle to be considered when realising operational roll polar plots are presented, considering either monodirectional waves or fully developed sea states. Finally, the relevance of the loading case selection performed when realising operational roll polar plots is presented.

3.1. ESTIMATION OF THE ROLL DAMPING COEFFICIENTS

3.1.1. Documented Method

Different methods are proposed in the literature to estimate the roll damping coefficients (Haddara, 2005; Falzarano, 2015; ITTC, 2021a), either based on model tests or calculated from empirical formulas. The IMO (2020a) recommends to use full scale or model tests to obtain the most accurate results. If no roll decay tests are available, the recommended method is CFD. CFD is undeniably the most accurate numerical method to estimate roll damping (Irkal et al., 2016). However, if CFD results are not available, any other empirical method within their application limits can be used (IMO, 2020a). Such empirical method was used in the previous chapter to estimate a non-linear roll damping coefficient B_{44} for each roll angle (Ikeda).

The most accurate methods to obtain the roll damping coefficient are free roll decay tests or forced roll tests. The advantages and inconvenience of roll decays and forced roll tests associated to their roll damping estimation methods are discussed by Wassermann (2016). When model free roll decay time series are provided, the Froude similarity is considered to upscale the results prior applying any method to calculate the ship roll damping. Froude (1872) proposed the first method to obtain the roll damping coefficients based on a quadratic model. According to Fernandes and Oliveira (2009), this well documented method was probably used by most model basins in the world. However, this method may lead to confusing results when assessing hulls with a flat bottom (Fernandes and Oliveira, 2009). Thus, other methods appeared to obtain an improved accuracy. One of them is the logarithmic decrement of roll peak (Hua, 2009; ITTC, 2021a), which provides an estimation of the roll damping coefficients based on the observed peak amplitude decrement. Parameter identification technique (PIT) is another one, based on the assumption of a 1-DoF approximation fitted by 6 parameters (including the damping coefficients) (Bulian, 2003, IMO, 2006, Sun, 2019) or alternatively based on time-dependent second-degree polynomial fit (Söder, 2012). The PIT consists in fitting the input parameters to reduce the error between the analytic solution of the roll motion and the reference free roll decay time series at all times, based on a root mean square method. Thus, the PIT method provides roll damping coefficients to be used in any solver.

Those methods provide roll damping coefficients which can be used in any solver. However, when providing those damping coefficients to a time-domain solver, it is rare that the resulting roll decay

matches exactly the reference free roll decay. Thus, an iterative method is presented here-after to obtain the exact roll damping coefficients to be provided as input of the solver to match as close as possible to the reference free roll decay tests.

The content of this Section has been presented at the 1st International Conference on the Stability and Safety of Ships and Ocean Vehicles (STAB&S), held in Glasgow (UK) in June 2021 (Luthy et al., 2021a).

3.1.2. Improved method

This section presents an iterative method permitting to estimate the roll damping coefficient from a free roll decay time series. The method is based on the identification of the parameters having an influence on roll damping without considering any analytical equation of the roll motion (such as the PIT does it with a 1-DoF equation). The method can be used in any solver without introducing any added assumptions. Contrary to PIT, the method proposed here consist in a numerical identification of parameters within an iterative process. Thus, the method to provide roll damping coefficient especially fitted for the solver in which the iterative process is conducted. Therefore, the resulting roll damping coefficients will differ if the iterative process is run in another solver. This method can be used to reproduce model test or to realise the exact same simulation in two different solvers which do not share the same assumptions. The method requires approximate initial values to be set in the time-domain solver. Two parameters are triggered to overlap the simulated free roll decay time series on the reference one provided by model test or by another time-domain solver. First, the different possibilities to obtain initial approximative values are presented. Then the iterative method permitting to obtain accurate roll damping coefficients is described. Finally, a validation of the method considering a model test as reference free roll decay time series is provided.

An example is provided along the presentation of the method. The reference free roll decay used in this example is obtained from the 6-DoF time-domain solver Fredyn (presented in Section 1.2.2) simulating the C11-class container ship at a draught equal to 12 m. The iterative process is conducted in the 1-DoF time-domain solver, presented in section 1.2.1, for the same ship.

Input parameter

Initial input parameter values must be provided to the time-domain solver to reproduce the reference free roll decay time series. The input parameters must be set to reproduce as close as possible the conditions in which the reference free roll decay time series was obtained. Three parameters must be especially estimated prior to the first simulation: the roll moment of inertia (denoted by J_{44}), the linear damping coefficient (B_{Lin}) and the quadratic damping coefficient (B_{Quad}).

In some solvers roll inertia J_{44} is provided as the roll radius of inertia denoted by k_{xx}. In such case, it can be estimated using empirical formula, provided by ITTC (2017), Equation 101 (dry roll radius of inertia).

$$k_{xx} = \left(\frac{1}{12} \begin{matrix} \left(0.4(B + \mathrm{D})^2 + 0.6(B^2 + D^2)\right) \\ -(\mathrm{T} - 0.5\mathrm{D} - KG_W)^2 \end{matrix} \right)^{\frac{1}{2}} \qquad 101$$

K_{xx}	(m)	Roll radius of inertia
B	(m)	Ship's breadth
D	(m)	Depth
T	(m)	Draught

KG_W (m) Height of the centre of gravity above the water surface

If those information are not available, ITTC (2017) recommends the value of k_{xx} to be taken between 35 and 45 % of the ship's breadth. J_{44} is estimated either from the roll radius of inertia, Equation 102, or extracted from the roll period (denoted by T_φ) measured on the reference free roll decay time series, Equation 103. In the example, T_φ is measured on the reference free roll decay and equal to 20.08 s, W is equal to $7.201*10^8$ N and GM is equal to 3.225 m. J_{44} is extracted using Equation 103 and is equal to $2.373*10^{10}$ kg.m^2.

$$J_{44} = {k_{xx}}^2 \Delta \quad 102$$

$$J_{44} = W.GM_0 \left(\frac{T_\varphi}{2\pi}\right)^2 \quad 103$$

Δ (t) Ship's displacement

W (N) Ship's weight

GM_0 (m) Metacentric height in clam water

J_{44} (kg.m^2) Roll inertia

A special care should be provided to not to count certain terms twice, in particular the added mass (force of radiation, in phase with acceleration). Therefore, it is necessary to differentiate well the added mass from pure mass inertia.

The first estimation of the value of the roll damping coefficients can be conducted using any documented methods such as the logarithmic decrement of the peak's (Hua, 2009) or the parameter identification technique (Bulian, 2003, IMO, 2006, Sun, 2019). More the initial estimated values are close to the final ones, less iterations will be required and faster the process will be. Arbitrary values can be used alternatively. However, the number of iterations may increase. In the example, B_{Lin} and B_{Quad} are estimated using the CAC method (Hua, 2009) and are respectively equal to $2.513*10^8$ N.m.s.rad^{-1} and $7.322*10^9$ N.m.s^2.rad^{-2}.

Those three initial input parameter values are hereafter denoted by $J_{44.INI}$, $B_{Lin.INI}$ and $B_{Quad.INI}$. Initial roll angle (denoted by φ_0) and initial roll speed are to be set identically to the ones of the reference free roll decay. When the reference roll time series is provided from model test, the initial roll angle is taken at the second or third maximum roll amplitude (where roll speed is null) to avoid any perturbation in the roll period due to the experiment process. The iterative method can start with this set of initial input parameters.

Two-parameter iterative identification method

The two-parameter iterative identification method aims to overlap a free roll decay simulation on a reference free roll decay time series, no matter the number of degrees of freedom nor the assumptions. Both roll damping coefficient are triggered, both have a major influence on the simulated free roll decay time series. The linear roll damping coefficient impacts predominantly the roll amplitude at small roll angles. The quadratic roll damping coefficient impacts predominantly the roll amplitude at large roll angles. Therefore, each parameter is triggered based on their major influence. An as accurate as possible value of the roll inertia should be provided since it directly impacts the roll period, as mentioned in the previous sub-section.

A two-parameter iterative identification method requires to conduct several simulations with different set of inputs.

- The final roll amplitude of the reference free roll decay is seen as a target to trigger the linear roll damping coefficient (Figure 46). Thus, the simulation duration should be at least equal to the one of the reference free roll decay.
- The 3rd to the Nth maximum roll peak amplitude (positive or negative) of the reference free roll decay are seen as targets to trigger the quadratic roll damping coefficient (Figure 46). N can be adjusted depending on the reference free roll decay duration and on the roll amplitudes. If the initial roll angle is too small, quadratic damping coefficient has low influence.

When the reference free roll decay is obtained from model test, a moving average on 1/10th of the roll period can be used to reduce the noise. The time of each roll peak observed on this corrected time series is used to find the value of the maximum roll angle at the peak on the reference time series, avoiding to consider the noise perturbations (Figure 46).

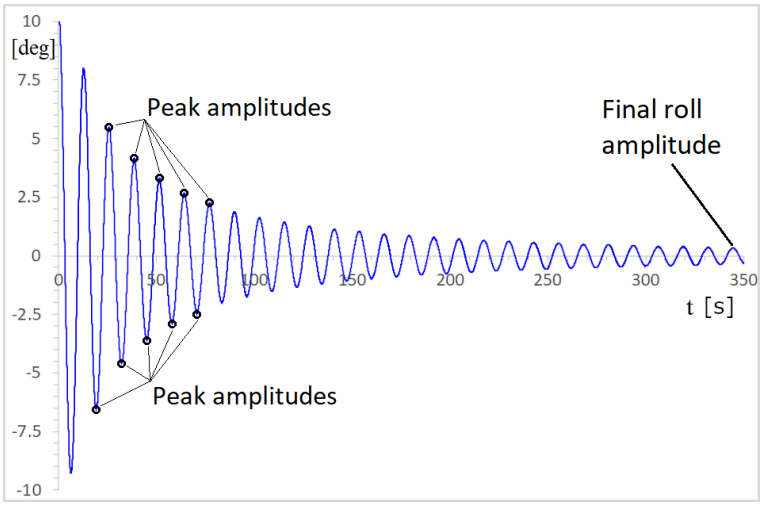

Figure 46 - Triggered parameters

Boundaries are set as tolerance intervals for the final roll amplitude and for the peaks. The tolerance intervals can either be set as a percentage of the values or as absolute values. Thus, the final accuracy is directly triggered by the user. In the example, the tolerances are set to 1 % for the peak roll amplitudes and 0.1 % for the final roll amplitude. One simulation is performed at each iteration. Figure 47 presents the free roll decay obtained with the initial parameters and compared to the reference free roll decay. Figure 47 shows that the final roll amplitude seems to be within an acceptable accuracy compared to the one of the reference free roll decay. However, it seems that the peak's amplitude are larger than the one of the reference free roll decay at large roll amplitudes.

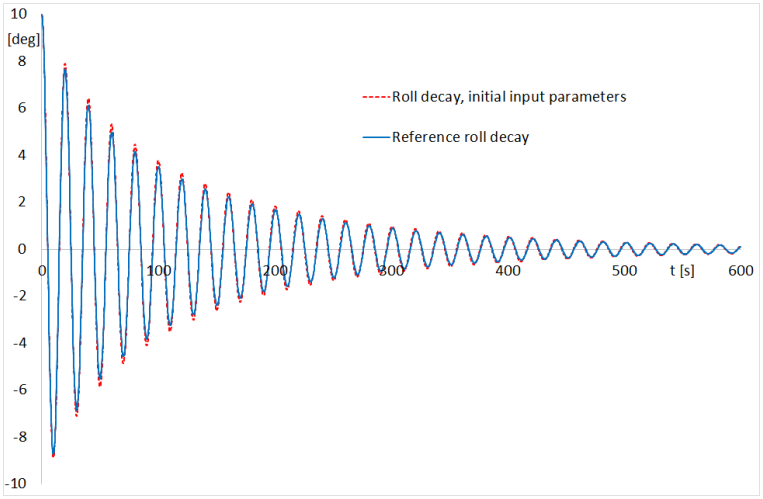

Figure 47 - Reference roll decay and simulated one with initial parameters

A first group of iterations is performed to trigger the linear coefficient regarding the error on the final roll amplitude. The linear coefficient is increased if the final roll amplitude is larger than the one of the reference free roll decay, otherwise decreased. In the example (Figure 47), the final roll amplitude after the first simulation (run with the initial parameters) is within the tolerance. Therefore, in this case no additional iteration is required to trigger the linear roll damping coefficient in a first time.

A second group of iterations is performed to trigger the quadratic coefficient regarding the errors at the peaks. The quadratic coefficient is increased if the peaks roll amplitudes are larger than the ones of the reference free roll decay, otherwise decreased. In addition, if the condition on the final roll amplitude is not met anymore, a new iteration process of the linear damping coefficient is realised within the iteration process of the quadratic coefficient. Figure 48 presents the final free roll decay simulated after this second iteration process. In the example, the final roll damping coefficients calculated with the iteration process are $B_{Lin} = 2.513*10^{8}$ N.m.s.rad^{-1} and $B_{Quad} = 9.092*10^{9}$ N.m.s^{2}.rad^{-2}.

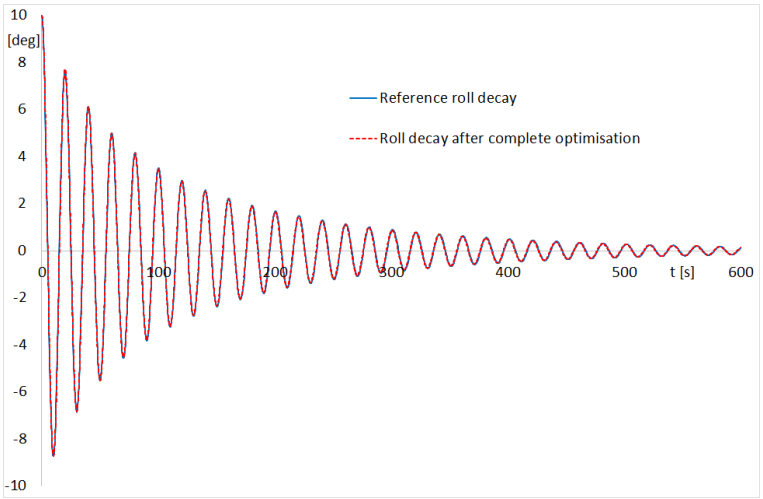

Figure 48 - Reference roll decay and final simulated roll decay after the complete two-parameter iterative process

Validation on model free roll decay

A validation of the iterative method is conducted on a free roll decay obtained on a naval ship at the French DGA TH model basin. The time series is extracted using photogrammetry technique.

The roll decay time series duration is shortened to start on a maximum roll angle (φ_0). The roll inertia to be set in the simulator is calculated from the roll period observed on the reference roll decay using Equation 103. Initial roll damping coefficients are estimated using CAC method (Hua, 2009). Figure 49 presents the reference time series and the 1 -DoF simulated roll decay obtained at the end of the iterative process. The simulated roll decay overlaps the reference within tolerance interval set by the user as 0.1 percent of the final roll amplitude and 1 percent of the roll peaks (from the 3rd to the 8th peak).

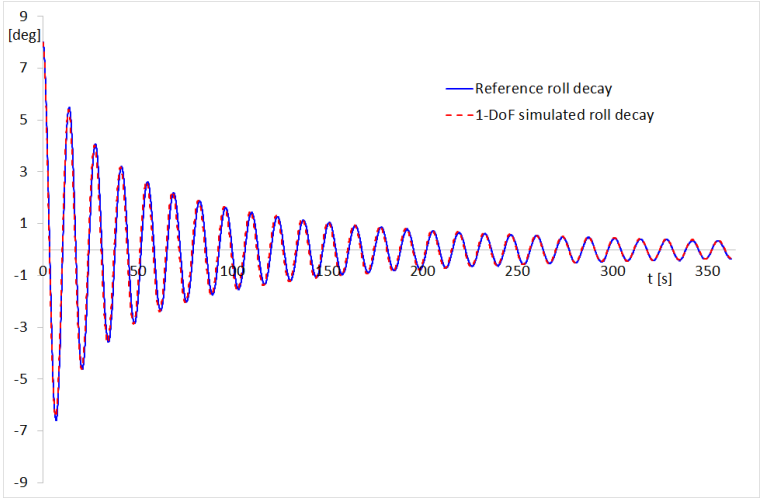

Figure 49 - Reference model test roll decay and final simulated roll decay after the complete two-parameter iterative process (naval ship)

The roll damping coefficients to be set in the simulator are accurately estimated. Applicable limits should be set since the roll inertia is not triggered. The value of the roll inertia provided as input of the simulation must be estimated accurately. This method should be used in solvers considering added mass with caution, since the estimation methods do not differentiate the pure mass and the added mass (some terms may be counted twice). If the targeted accuracy is too stringent, the method may not find any solution.

It can be noticed that the two parameter iterative identification method is easy to implement in any solver. However, the resulting roll damping coefficients differ from a solver to another since both may not use the same assumptions and numerical processes. Thus, the resulting damping coefficients are especially calculated for the solver in which the iterative process is conducted. The roll damping coefficients resulting from the iterative process represents the behaviour of the model as reference (numerical model, model test or full-scale data) but does not reflect its physical or numerical complexity. Thus, the model used in the time-domain solver can be less complex than the one used to provide the reference free roll decay.

The two-parameter iterative identification method can be used between two different numerical solvers to overlap the roll decay time series they provide. Thus, two different set of roll damping coefficients are obtained (one set per solver). Within this PhD thesis, the C11-class container ship has been modelled and simulated in both 1-DoF solver (Section 1.2.1) and 6-DoF solver Fredyn (Section 1.2.2). The two-parameter iterative identification method has been used to validate the damping coefficients used as inputs in Fredyn, considering a roll decay time series from the 1-DoF time-domain solver as reference. The reference roll decay was obtained using Ikeda method to estimate the roll damping of the ship, considering her bilge keels. The iterative process has permit to set the damping without bilge keels in the 6-DoF solver with an acceptable accuracy. In addition, the use of this iterative method has permitted to compare the results of both solvers.

The two-parameters iterative identification method is preferably used in 1-DoF time-domain solvers since the roll inertia is not triggered. The accuracy of the method and its use in complex solver require to trigger a larger number of inputs.

DGA TH developed an algorithm that can operate an optimization process with Fredyn (6-DoF solver) using a Bayesian optimization. This method includes the roll inertia as a third parameter to be triggered. This method has been assessed with full scale free roll decay and provide results with an acceptable accuracy. This method has been presented in a joint paper during STAB&S 2021 conference (Luthy et al., 2021a).

3.2. SEA STATES

Most parametric roll global assessment presented in Section 1.3 consider as inputs the sea states provided by the IACS wave scatter diagram (2001) or derived from it. The data used to calculate this table of probability of appearance is based on years of wave observation in North Atlantic. The last update of this table has been realised more than 20 years ago in 2001. Moreover, some vessels sail in other regions. Thus, this section aims to provide a method to compute a regional wave scatter diagram based on the data provided by the Copernicus Marine Environment and Monitoring Service (CMEMS).

3.2.1. Copernicus Marine Environment and Monitoring Service data

Several means are available to measure sea states. In-Situ data can be obtained through wave buoys which can provide high fidelity local information in real time. As well In-Situ data can be obtained by the mean of visual observation. The International Comprehensive Ocean-Atmosphere Dataset (ICOAD) host those measurements since 1662 until present days. Such periodic and local data is not sufficient to establish statistical results worldwide. Thus, to obtain more results in a short period of time on a wide area, satellite observations are realised. The measurements realised with such technology have been validated and provide now accurate measurements of wave height and direction. The full-time geographical coverage offered by the satellite constellation dedicated to the observation of the oceans permits to obtain worldwide data of extreme sea states with a greater occurrence rate than from visual or buoy observation. Models have been developed to extrapolate results for left over areas where no data is provided at the exact time of the measurements and to forecast the evolution of the sea states on short term. Thus, the models are adjusted with the new data every time it is provided (several times per day). Since their commissioning day, such model provides high resolution and fidelity data to establish wave scatter diagram for specific areas.

The Copernicus Marine Environment Monitoring Service (CMEMS) is the marine component of the European Union Copernicus program (European Commission, 2015). It provides open-access data, support, expertise, and services on Oceans. The CMEMS aims to serve the international legal commitments related to ocean governance (European Commission, 2016). As well it provides an open data set for scientific research with variable geographical and time resolution. The provided products go from the sea salinity, water temperature, waves height to winds specifications. Each product provides data at several stage of treatment depending on the required output. The data provided go from the raw satellite output up to fully developed georeferenced products. The data is collected by a dedicated constellation of satellites known as “Sentinels” which provides information for all Copernicus program and from some other third-party satellites known as “contributing space mission”. For the CMEMS and more precisely on the evaluation of the sea state, several third-party satellites are used (Jason 3, Saral, Cryosat-2 and CFOSAT). In this field,

France is one of the most advanced countries with China. Their collaboration has led to the CFOSAT mission which have permit to launch the Chinese-French Oceanography SATellite (CFOSAT) in 2018. This mission aims to monitor the ocean surface wind and waves on a global scale, in order to improve the ocean dynamics modelling and prediction. This satellite is equipped with an innovative wave scatterometer which allows to monitor and investigate the wave surface (SWIM). SWIM is the first space radar mainly dedicated to the measurement of ocean waves directional spectra. It can provide a 2-dimension wave spectrum, the significant wave height, the peak direction, and the peak wavenumber for cells of 70 km $\times$ 90 km. Even with such satellite technologies and satellite coverage, a wave model is required to provide the different products and increase the geographical coverage and the resolution. Thus, the CMEMS has decided to use Météo France WAve Model (MFWAM) to model the sea states. The model (WAM) used by Météo France is described in Dynamics and modelling of ocean waves (Komen et al., 1994). The satellite data are used to readjust the model to provide an estimation as accurate as possible. The estimations are validated by in-situ (non-space) data such as buoys data.

The sea state product which has been selected in this study to establish wave scatter diagram is denoted by GLOBAL_ANALYSIS_FORECAST_WAV_001_027. This product is built with the use of wave model from Météo France and assimilate the date provided from the SWIM-nadir system fitted on CFOSAT (Aouf, 2020). It provides among others values the 3-hourly instantaneous values for the significant wave height, the peak wave period and the direction of the sea states (Dalphinet et al., 2022). The accuracy of the values has been validated by comparison with the results obtained from buoy located in North America from January to May 2020. The results presented a bias as small as 2 cm on the significant wave height with a scatter index of 13.8 %. As well the results presented a bias of 0.33 seconds on the wave peak period with a scatter index of 12.6 % (Aouf, 2020). This product is updated twice-daily and provide forecast up to 10 days. It has a geographical resolution of 1/12° (about 8 km) at the Equateur and a temporal resolution of 3 hours. The data can be downloaded with this resolution worldwide or for on any geographical sub-region up to a maximum latitude of $\pm$ 80 degrees. The time frame is to be selected; the online data is available since 2020 up to nowadays.

3.2.2. Establishment of the wave scatter diagrams

This Sub-Section presents the method to calculate wave scatter diagram for any area based on the CMEMS product GLOBAL_ANALYSIS_FORECAST_WAV_001_027 presented above.

The wave scatter diagram needs to be comparable to the existing ones. Thus, join distribution scatter diagram with significant wave height and zero-up crossing period is selected. The geographic resolution of 1/12° of the selected product permits to create scatter diagram for specific sub-region or even along any navigation route. Thus, the product is now downloadable for any sub-region for the selected time frame. The first step is to download the data for the sub-region as close as the one that will be studied and on the time frame for which the statistical study will be conducted. Then it is required to resize the geographic sub-region. In the case of a study on a wide area, resizing the sub-region can be realised by selecting the boundaries latitudes and longitudes. In the case of a study along a route, it is proposed to select a margin error along which the vessel may sail. In this case, each cell (8 km by 8 km) which crosses the route have to be taken into account. By the end of this PhD, the CMEMS should realise an update on the website to enable direct download of data along a route. If the selected sub-region crosses land, a special care should be provided to avoid considering erroneous values in the study.

Once each cell part of the sub-region is defined and the time frame is validated, the values which are interesting to realise the scatter diagram may be considered. In this study, the required values

are the significant wave height and the zero-up crossing period. Both are directly provided by the selected product. A grid on the joint distribution is selected to realise the scatter diagram. The IACS (2001) has select a grid beginning at 0.5 metre up to 16.5 metres in wave height with a step of 1 metre (the provided value is the mean value, for example 11.5 metres refers to heights from 11 to 12 metres), the grid begins at 1.5 s up to 18.5 s in wave period. The same grid can be used or refined if desired by the user. The values provided in each cell at each time step are observed to increment the corresponding cell of the joint distribution grid. Once all available values have been assessed, the scatter diagram is divided by the total number of point and multiplied by 100 000 for a presentation similar to the one of IACS rec 34 (2001).

Thus, this method permits to obtain a dedicated scatter diagram for any area or line on which the vessel is sailing, from free open-access data. The study is only limited by the time frame on which the data is available. Thus, at this time, the longest period which can be treated is the latest two and half years. Thus, with time, the data set will become more complete and extensive studies will be possible. An example is presented here-after.

3.2.3. Establishment of a North Atlantic wave scatter diagram

The method presented hereabove has been implemented by students from the French Naval Academy within the scope of their end of studies' project (Gnalo et al., 2021). The aim is to validate the method and to compare the scatter diagram it provides with the one provided by IACS (2001) for North Atlantic.

The IACS scatter diagram (2001) provided in Table 20 has been built for a twenty-year return period with data over 100 years old up to 2001. Four geographical subs-regions in the North-Atlantic were considered by the IACS (Figure 50), which are sub region 8, 9, 15 and 16. The geographical definition of those 4 subs-regions is provided in Table 19. Thus, the comparison will be conducted on the same geographical region. However, the data from the Copernicus program do not extend on the same time frame. Thus, the data selected for this study covers the entire years 2019 and 2020. The scatter diagram established with this method is presented in Table 21. It shows that no higher wave than 15 metres were observed during this period. Smaller and shorter waves occurred more often on this two-year data set. The difference can be explained by the shorter period and thus a lower occurrence rate of extreme events.

Some other validations realised with this method and comparisons of scatter diagrams from the winter and summer seasons of 2019 and 2020 are available in the report of Gnalo et al. (2021). As well route scatter diagrams are provided in this report.

Thus, the method to realise wave scatter diagrams for specific areas based on the CMEMS data is relevant. This method can be used to realise specific wave scatter diagrams for each vessel based on its sailing area. The sub-region scatter diagrams can then be used for a global assessment of the vulnerability of the vessel within this region. Results from such sub-region study can be used as well to select accurately the sea states to be considered to realise operational roll polar plots. The author proposes to use this method to provide an adapted wave scatter diagram when geographical operational measures are intended within the scope of the Second Generation Intact Stability Criteria (IMO, 2020a).

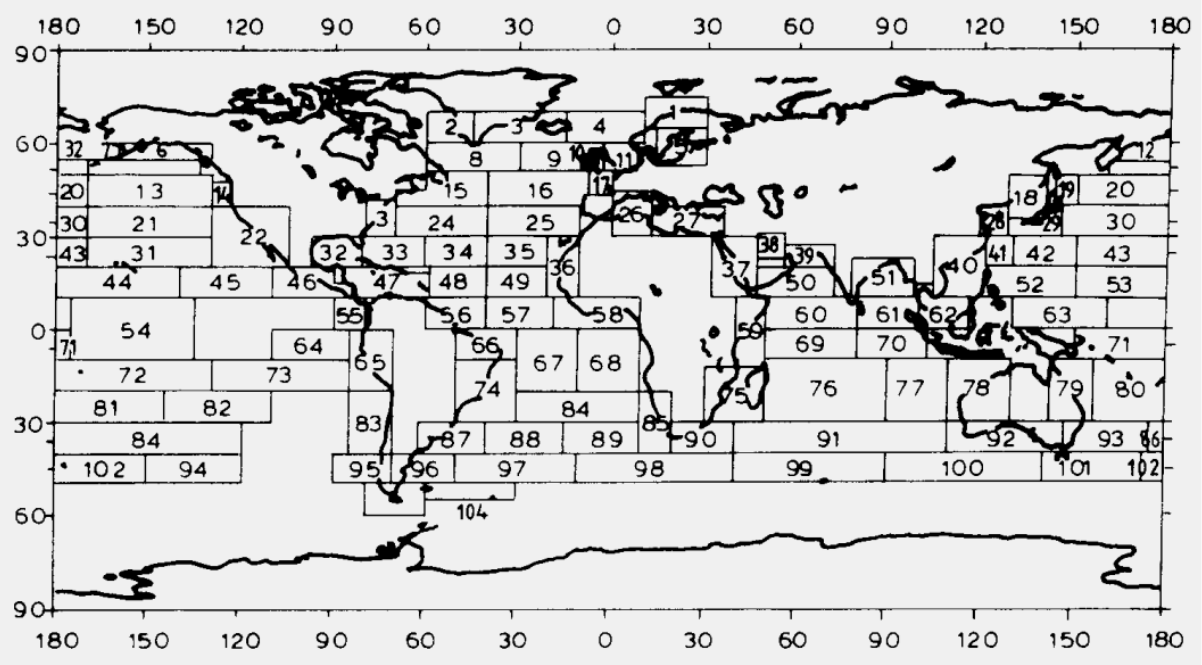

Figure 50 - Sub-Region division by the IACS (2001)

Sub-region n°	latitude inf [deg]	Latitude sup [deg]	Longitude inf [deg]	Longitude sup [deg]	Sub-region area [km²]	Number of cells
8	48	60	-30	-60	4344731.7	67886
9	48	60	-5	-30	3620609.7	56572
15	40	48	-40	-70	2932378.9	45818
16	40	48	-10	-40	2932378.9	45818
Total					13830099	216095

Table 19 - Definition of the North Atlantic Sub-Regions

H_S [m] \Tz [s]	1.5	2.5	3.5	4.5	5.5	6.5	7.5	8.5	9.5	10.5	11.5	12.5	13.5	14.5	15.5	16.5	17.5	18.5	Sum
0.5	0.0	0.0	1.3	133.7	865.6	1186.0	634.2	186.3	36.9	5.6	0.7	0.1	0.0	0.0	0.0	0.0	0.0	0.0	3050
1.5	0.0	0.0	0.0	29.3	986.0	4976.0	7738.0	5569.7	2375.7	703.5	160.7	30.5	5.1	0.8	0.1	0.0	0.0	0.0	22575
2.5	0.0	0.0	0.0	2.2	197.5	2158.8	6230.0	7449.5	4860.4	2066	644.5	160.2	33.7	6.3	1.1	0.2	0.0	0.0	23810
3.5	0.0	0.0	0.0	0.2	34.9	695.5	3226.5	5675.0	5099.1	2838	1114.1	337.7	84.3	18.2	3.5	0.6	0.1	0.0	19128
4.5	0.0	0.0	0.0	0.0	6.0	196.1	1354.3	3288.5	3857.5	2685.5	1275.2	455.1	130.9	31.9	6.9	1.3	0.2	0.0	13289
5.5	0.0	0.0	0.0	0.0	1.0	51.0	498.4	1602.9	2372.7	2008.3	1126.0	463.6	150.9	41.0	9.7	2.1	0.4	0.1	8328
6.5	0.0	0.0	0.0	0.0	0.2	12.6	167	690.3	1257.9	1268.6	825.9	386.8	140.8	42.2	10.9	2.5	0.5	0.1	4806
7.5	0.0	0.0	0.0	0.0	0.0	3.0	52.1	270.1	594.4	703.2	524.9	276.7	111.7	36.7	10.2	2.5	0.6	0.1	2586
8.5	0.0	0.0	0.0	0.0	0.0	0.7	15.4	97.9	255.9	350.6	296.9	174.6	77.6	27.7	8.4	2.2	0.5	0.1	1309
9.5	0.0	0.0	0.0	0.0	0.0	0.2	4.3	33.2	101.9	159.9	152.2	99.2	48.3	18.7	6.1	1.7	0.4	0.1	626
10.5	0.0	0.0	0.0	0.0	0.0	0.0	1.2	10.7	37.9	67.5	71.7	51.5	27.3	11.4	4.0	1.2	0.3	0.1	285
11.5	0.0	0.0	0.0	0.0	0.0	0.0	0.3	3.3	13.3	26.6	31.4	24.7	14.2	6.4	2.4	0.7	0.2	0.1	124
12.5	0.0	0.0	0.0	0.0	0.0	0.0	0.1	1.0	4.4	9.9	12.8	11.0	6.8	3.3	1.3	0.4	0.1	0.0	51
13.5	0.0	0.0	0.0	0.0	0.0	0.0	0.0	0.3	1.4	3.5	5.0	4.6	3.1	1.6	0.7	0.2	0.1	0.0	21
14.5	0.0	0.0	0.0	0.0	0.0	0.0	0.0	0.1	0.4	1.2	1.8	1.8	1.3	0.7	0.3	0.1	0.0	0.0	8
15.5	0.0	0.0	0.0	0.0	0.0	0.0	0.0	0.0	0.1	0.4	0.6	0.7	0.5	0.3	0.1	0.1	0.0	0.0	3
16.5	0.0	0.0	0.0	0.0	0.0	0.0	0.0	0.0	0.0	0.1	0.2	0.2	0.2	0.1	0.1	0.0	0.0	0.0	1
Sum	0	0	1	165	2091	9280	19922	24879	20870	12898	6245	2479	837	247	66	16	3	1	100000

Table 20 - IACS North-Atlantic scatter diagram

H_S [m] \Tz [s]	1.5	2.5	3.5	4.5	5.5	6.5	7.5	8.5	9.5	10.5	11.5	12.5	13.5	14.5	15.5	16.5	17.5	18.5	sum
0.5	43.3	198.1	337.5	677.8	890.3	571.1	325.7	361.4	203.5	88.3	53.7	20.7	4.5	0.9	0.0	0.0	0.0	0.0	3777
1.5	0.0	24.2	1623.9	4673.1	7303.1	7073.9	2969.6	1687.7	949.4	448.7	292.0	124.1	18.5	3.7	0.0	0.0	0.0	0.0	27192
2.5	0.0	0.0	33.0	2088.7	5816.3	7692.8	5196.2	2937.4	1880.2	772.3	309.5	101.7	24.4	6.1	0.0	0.0	0.0	0.0	26859
3.5	0.0	0.0	0.0	108.9	2372.2	5547.5	5171.3	3649.7	2009.0	826.0	318.6	123.8	37.5	2.9	0.0	0.0	0.0	0.0	20168
4.5	0.0	0.0	0.0	0.2	226.9	2325.6	3694.1	2854.3	1620.7	620.1	174.0	47.7	9.0	1.5	0.0	0.0	0.0	0.0	11574
5.5	0.0	0.0	0.0	0.0	3.2	267.5	1916.4	2088.0	1117.9	350.6	100.2	33.5	7.3	0.8	0.0	0.0	0.0	0.0	5885
6.5	0.0	0.0	0.0	0.0	0.0	10.0	355.0	1102.8	785.5	269.3	72.1	27.6	4.3	0.2	0.0	0.0	0.0	0.0	2627
7.5	0.0	0.0	0.0	0.0	0.0	0.4	28.3	316.9	481.0	194.2	59.1	22.7	0.9	0.0	0.0	0.0	0.0	0.0	1103
8.5	0.0	0.0	0.0	0.0	0.0	0.1	2.0	49.0	237.7	131.7	46.0	14.1	0.6	0.0	0.0	0.0	0.0	0.0	481
9.5	0.0	0.0	0.0	0.0	0.0	0.0	0.2	4.3	63.0	100.0	38.2	7.2	0.6	0.0	0.0	0.0	0.0	0.0	214
10.5	0.0	0.0	0.0	0.0	0.0	0.0	0.0	0.4	7.5	45.2	28.7	3.6	0.3	0.0	0.0	0.0	0.0	0.0	86
11.5	0.0	0.0	0.0	0.0	0.0	0.0	0.0	0.0	0.3	7.7	14.5	2.7	0.1	0.0	0.0	0.0	0.0	0.0	25
12.5	0.0	0.0	0.0	0.0	0.0	0.0	0.0	0.0	0.0	0.4	5.7	1.8	0.0	0.0	0.0	0.0	0.0	0.0	8
13.5	0.0	0.0	0.0	0.0	0.0	0.0	0.0	0.0	0.0	0.0	0.5	0.5	0.0	0.0	0.0	0.0	0.0	0.0	1
14.5	0.0	0.0	0.0	0.0	0.0	0.0	0.0	0.0	0.0	0.0	0.0	0.0	0.0	0.0	0.0	0.0	0.0	0.0	0
15.5	0.0	0.0	0.0	0.0	0.0	0.0	0.0	0.0	0.0	0.0	0.0	0.0	0.0	0.0	0.0	0.0	0.0	0.0	0
16.5	0.0	0.0	0.0	0.0	0.0	0.0	0.0	0.0	0.0	0.0	0.0	0.0	0.0	0.0	0.0	0.0	0.0	0.0	0
sum	43	222	1995	7549	16612	23489	19659	15052	9356	3855	1513	532	108	16	0	0	0	0	100000

Table 21 - North-Atlantic scatter diagram based on 2019-2020 data from CNEMS (Gnalo et al., 2021)

3.3. SPREADING ANGLE

As seen in the previous section (3.2), a se state is defined by its significant wave height and wave period. However, the definition of a monodirectional sea state is not relevant in most cases if the aim is to reproduced what is observed in reality. Thus, to solve this issue, a spreading function is introduced. This reflects how the sea state is spread aside the main wave direction. It is associated to the spreading angle which is the angle on which this spreading occurs on both sides of the main wave direction. The spreading angle is hardly operationally measured from the bridge. In most cases only the main direction of the waves can be estimated. Thus, the information provided to the Officer Of the Watch on the possible vessel roll motions (roll polar plots or equivalent), based on his evaluation of the sea state must be conservative. Therefore, when evaluating the vessel seaworthiness by realizing operational roll polar plots, simulations in 6 degrees of freedom (DoF) should be conducted considering the most conservative spreading angle. The study presented in this sub-section aims to define the most conservative spreading angle.

When conducting time-domain simulations, the spreading is defined as the spreading angle (denoted by $\Delta\alpha$), the discrete number of waves directions (denoted by N) and the spreading function, defined as the repartition of energy on each discreet wave direction. A usual spreading function is the "cos^n" function, where n = 8 such as recommended by Bureau Veritas (2019b). The more the number of wave directions is large, the more the computation of the vessel motions is time consuming.

First the method to generate equivalent set of waves developing the same energy is proposed and validated. The implementation of the set of waves in the time-domain solver is validated by comparison with its analytical description. Then method to evaluate the influence of the spreading angle on the motion of the vessel is presented. This evaluation is performed with 6-degree-of-freedom simulations realised with the time-domain solver Fredyn. Finally, the results are compared and discussed, and the most conservative spreading angle is identified.

The study of the spreading angle presented in this sub-section has been partially presented at the 18th International Ship Stability Workshop, held in Gdańsk (Poland) in September 2022 (Luthy et al., 2022a). Additional studies on real sea states will be presented at the 18th conference des Journées de l'Hydrodynamiques, held in Poitiers (France) in November 2022 (Luthy et al., 2022e), accepted on abstract, and presented here-after.

3.3.1. Equivalent set of waves

Definition of the reference wave, sea state

A monodirectional sinusoidal wave or a monodirectional sea state are defined as references. A set of spread waves or a set of spread sea states are calculated from theses references.

Reference sinusoidal wave

A sinusoidal monochromatic wave of length and steepness (denoted here after by S_w) arbitrary chosen is considered as reference (Figure 51). The energy developed by this wave is calculated using Equation 104.

$$E_0 = \frac{1}{8}\rho g {H_0}^2 \qquad 104$$

E_0	$J.m^{-2}$	Energy of the reference wave
ρ	$kg.m^{-3}$	Water density
g	$m.s^{-2}$	Gravity acceleration

H_0 m Reference sinusoidal wave height

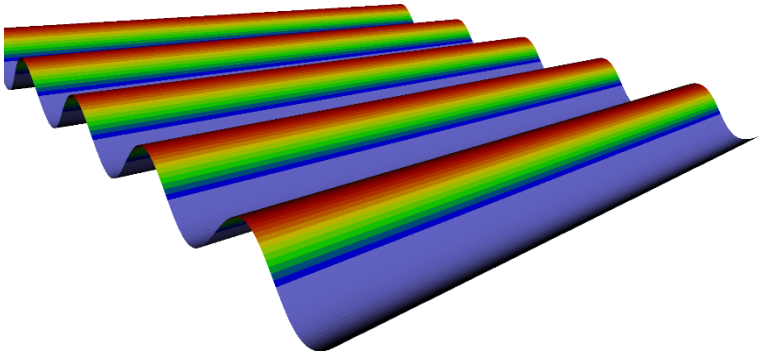

Figure 51 – Reference sinusoidal wave

The energy of the reference wave is calculated, and equivalent set of waves are built to develop the same energy.

Reference sea state

A sea state can be considered as well as reference. In this case, a monodirectional Pierson-Moskowitz spectrum (Equation 105, equivalent to Equation 32 page 39) is considered to describe it (Molin, 2002), defined with a reference significant height (H_S) and a reference up-crossing period (T_Z).

$$S(\omega) = \frac{1}{4\pi} {H_s}^2 \left(\frac{2\pi}{T_z}\right)^4 \omega^{-5} e^{-\frac{1}{\pi}\left(\frac{2\pi}{T_z}\right)^4 \omega^{-4}} \qquad 105$$

Where, ω denotes the frequency.

In this formula it is observed that the spectrum amplitude is proportional to the square of significant wave height for a given up-crossing period.

Equivalent set of waves

A set of waves is defined as the overlay of several monochromatic sinusoidal waves of different heights coming from several directions, or of several monodirectional Pierson-Moskowitz spectra.

Method, general case

The energy developed by the reference wave (or sea state) is distributed to each component of the set of waves. The number of directions (denoted by N) is calculated depending on the spreading angle ($\Delta\alpha$) to obtain a maximum spacing of 10 degrees between two adjacent directions. N shall be odd to keep a wave component in the main direction. The resulting spacing (denoted by $\delta\alpha$) is calculated using Equation 106. As example, for a spreading angle of ± 30 degrees, N is equal to 7 and $\delta\alpha$ is equal to 10 degrees. The main direction is identical to the one of the reference wave and the other directions are calculated relative to this main direction, using the spreading angle and the number of considered directions.

$$\delta\alpha = \frac{2\Delta\alpha}{N-1} \qquad 106$$

The energy of the reference wave E_0 (Equation 104) is distributed in the N directions based on a cos^n spreading function (BV, 2019b). When considering a reference sea state, the reference energy is the one developed by the entire sea spectrum (the area under the spectrum reflects the energy developed by the sea state). Thus, N areas are defined within the range [-π/2; +π/2] under the cos^n function. The sum of the N areas is equivalent to the total energy E_0. Each area is

associated to its own direction (denoted by α_i in radian, where i defines the direction index) and to its percentage χ_i of the total area (Equation 107).

$$\chi_i = \frac{A_i}{A_{tot}} \qquad 107$$

Where A_i denotes the area under the cos^n spreading function associated to the i^{th} direction, A_{tot} denotes the overall area under the cos^n spreading function from - $\pi/2$ to $\pi/2$

Figure 52 provides a graphic representation of the areas to consider associated to the wave directions for a spreading angle of ± 30 degrees and 7 wave directions (N = 7) with a cos^8 spreading function. In this example, the main wave direction is equal to 0.

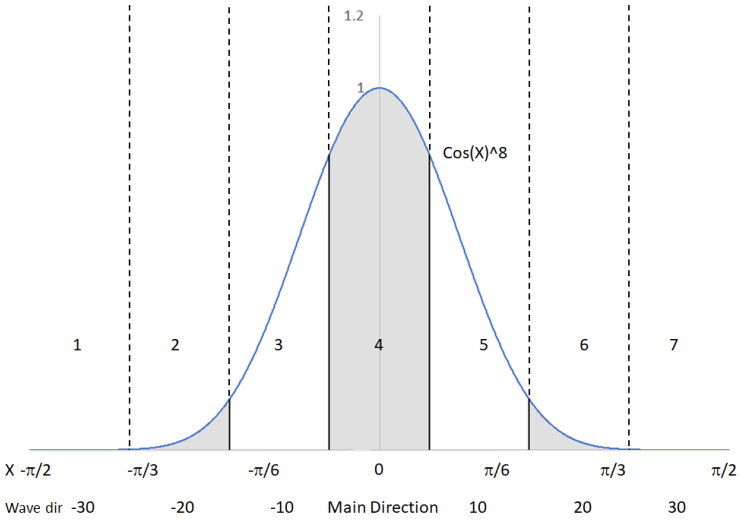

Figure 52 - Energy distribution

Method, additional measures for sinusoidal waves

Here is presented how to calculate an equivalent set of waves for any spreading angle when considering a monochromatic sinusoidal wave as reference.

A monochromatic sinusoidal wave of length equal to the one of the reference and of height H_i is associated to each wave direction α_i. The wave height H_i is calculated considering the energy repartition (Equation 108 and 109).

$$\chi_i E_0 = \frac{1}{8}\rho g {H_i}^2 \qquad 108$$

$$H_i = \sqrt{\frac{\chi_i E_0}{\frac{1}{8}\rho g}} = \sqrt{\chi_i} H_0 \qquad 109$$

The total energy developed by the equivalent set of waves (composed of N waves) is equal to the one of the reference wave.

Method, additional measures for sea states

Here is presented how to calculate an equivalent set of sea state for any spreading angle when considering a sea state as reference.

A sea state of period equal to the one of the reference T_z and of significant height H_{Si} is associated to each direction α_i. The spectrum of the sea state associated to the i^{th} direction is defined using Equation 105. χ_i is calculated for each direction as presented above and the significant wave height

H_{Si} is calculated considering this energy repartition. Equation 109, defined hereabove for the case of sinusoidal waves, also provides the significant wave height associated to each direction in the case of a real sea state (H_i and H_0 are replaced by H_{Si} and the reference significant wave height, respectively).

The sea spectrum for each direction is defined using Equation 105. The sum of the areas under the N spectra, defining all together the spread sea state, is equal to the area under the reference spectrum. Defining the same energy on a considered surface.

Analytical description of multidirectional sinusoidal wave field

When a monochromatic sinusoidal wave is considered as reference, the set of waves can either be analytically described (as the equation of the free water surface) or entered as input in a time-domain solver. The comparison of both permits to validate the implementation of the set of waves in the time-domain solver. A native wave phase angle is programmed in the time-domain solver Fredyn. This native phase angle (denoted by γ) is identified for 7 wave directions (denoted by β) throughout simulations without any ship (only the waves are simulated), Table 22. Those values are fitted using a 3rd degree polynomial equation presenting a correlation coefficient equal to 1 (Equation 110).

Relative angle β [rad]	Native phase angle [%T]
0	0
0.5236	0.06202
1.0472	0.24031
1.5708	0.48062
2.0944	0.72093
2.6180	0.89922
3.1416	0.96124

Table 22 – Native wave phase angle

$$\gamma_i = 2\pi(-0.069|\beta_i|^3 + 0.3252\beta_i^2 - 0.0347|\beta_i| + 0.0002) \quad 110$$

Where β_i denotes the wave direction of the i^{th} wave relative to the main wave direction.

The native phase angle (denoted by γ) is reintroduced in the analytical description of the free water surface in a cartesian system (x; y), provided in Equation 111.

$$\eta(x; y; t) = \sum_{i=1}^{N} \frac{H_i}{2} cos(kx\, cos(\beta_i) + ky\, sin(\beta_i) - \omega t - \gamma_i) \quad 111$$

η	m	Elevation of the free water surface relative to calm water
k	(rad.m^{-1})	Wave number (same value for each direction)
ω	(rad.s^{-1})	Wave frequency (same value for each direction)
γ_i	(rad)	Phase angle associated to the i^{th} direction, native from Fredyn
x	(m)	x coordinates of the observer in the cartesian system
y	(m)	y coordinate of the observer in the cartesian system
t	(s)	Time

Validation of the representation in the time-domain solver

The description of the set of waves is compared to the one provided by Equation 111 to validate the implementation of the set of waves in the time-domain solver. The mean observed error between the simulation and the analytical description is equal to 1 cm. The maximum observed error is equal to 5 cm. As an example, Figure 53 represents the free water surface amplitude for an equivalent set of waves composed of 5 waves (5 directions) from - 90 to + 90 degrees from the main direction, based on a reference wave of length λ. The amplitude of free surface is analytically obtained by varying the time element in Equation 111 for different positions of the observer. Figure 54 represents the elevation of the free surface at t = 0 for the same set of waves. The blue grey surface defines the limit of the free surface in calm water ($\eta = 0$). Figure 53 and Figure 54 are provided for a field of $2\lambda * 2\lambda$.

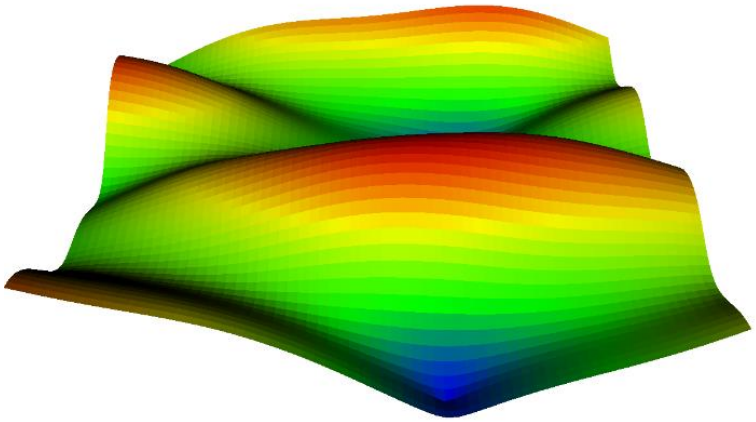

Figure 53 - Free surface amplitude

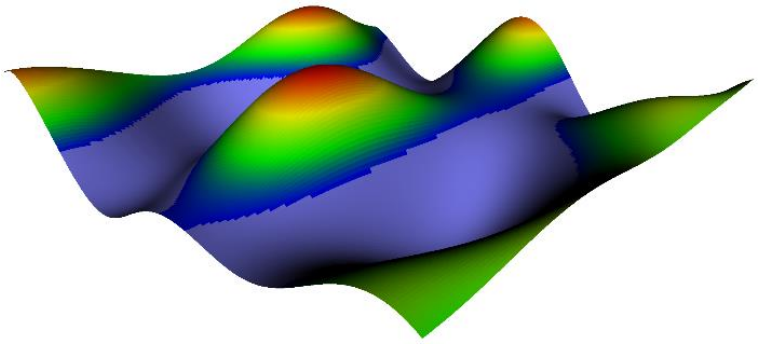

Figure 54 - Instantaneous free surface

Results obtained in the time-domain solver are almost identical (less than 1% of difference) to the one obtained with the analytical description. Each set of waves used in the solver Fredyn throughout this sub-section is validated as presented hereabove.

Such validation cannot be realised when considering real sea states. Thus, the generation of equivalent sea states are validated by comparison of the equivalent spectra. An example is provided for a reference sea state of significant height equal to 5 metres and of up-crossing period equal to 12 s (the mean period is equal to 13.03 s). First the reference sea spectrum is defined using Equation 105 and the area under this spectrum is calculated (Figure 55). The area under this spectrum between 0.24 and 0.85 rad.s^{-1} is equal to 1.491 m^2 (red area). The spreading angle is set to $\pm$ 30 degrees. 7 sea state directions are considered with a cos^8 repartition function. The 7 sea

state directions and the energy repartition for each direction are calculated using the method presented above. The significant height of each sea state in each direction is calculated using Equation 109. Each resulting sea spectrum is defined using Equation 105 and the area under each spectrum is calculated (Table 23). The sum of the areas under the spectra associated to all directions is equal to 1.491 m^2. Thus, both reference and equivalent sea state develop the same energy. Finally, the same calculation is performed with the data extracted from the output file of the time-domain solver. This result to the same energy. This validates the implementation of the spread sea state in the time-domain solver.

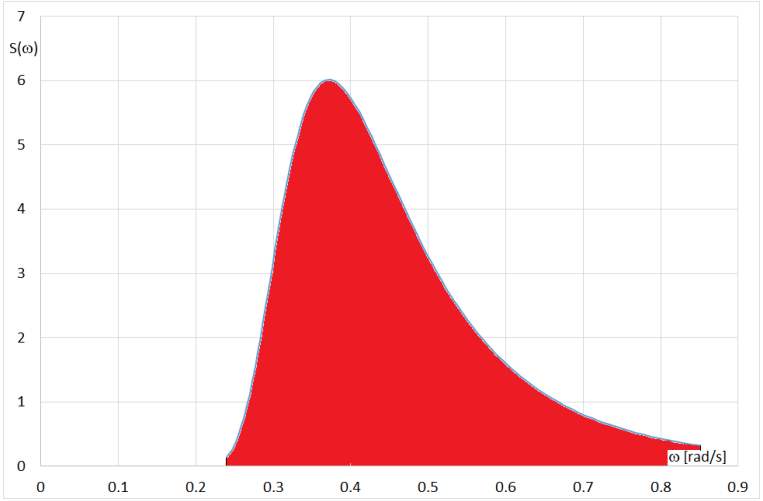

Figure 55 - Pierson-Moskowitz sea spectrum, T_z = 12 s, H_S = 5 m

Heading [deg]	H_{Si} [m]	Area under i^{th} spectrum [m^2]
-30	0.043522	0.000113
-20	0.708589	0.029958
-10	2.424645	0.350772
Main direction	3.497744	0.729969
+10	2.424645	0.350772
+20	0.708589	0.029958
+30	0.043522	0.000113
sum		1.491655

Table 23 - Example of equivalent spread sea state

3.3.2. Influence of the spreading angle on the roll motion, monochromatic sinusoidal waves

Simulation conditions

Simulations on a container ship are conducted for several set of regular waves (Table 24), using the time-domain solver Fredyn. Each simulation is one hour long. Since there is no possibility to change the phase of the wave in each direction, a unique simulation is sufficient to obtain a representative maximum roll angle for each set of waves, loading condition, heading and speed.

Case n°	Spreading angle [deg]	Number of waves	Comment
1	0	1	Reference
2	± 30	7	-
3	± 90	21	-

Table 24 - Set of waves parameters

The vessel selected for this study is the C11-class container ship of length equal to 262 m, known for her vulnerability to parametric roll (France et al., 2003). Three different loading conditions are considered, corresponding to draughts of 10, 11 and 12 metres. The reference wave is of length equal to the one the ship and of steepness 0.0167. A second reference wave of steepness 0.025 is also considered for the draught of 12 metres.

Roll polar plots

Roll polar plots representing the 1-hour maximum roll angle are realised for the sets of waves presented in Table 24. The speed discretisation is 0.5 $m.s^{-1}$ from 0 to 10 $m.s^{-1}$ and the heading discretisation is 7.5 degrees from head sea to following sea. Half of the roll polar plots is calculated since the results are symmetrical (symmetrical hull shape, centre of gravity located on the centreline).

The maximum roll angles obtained on the different set of waves presented in Table 25 are compared one with another, for each reference wave and loading condition. Special care is provided when heavy roll motions appear to detect parametric roll: If the roll period is nearly twice the pitch period (image of the encounter period) when the maximum roll angle is reached, then the maximum roll angle is considered to be consecutive to the phenomenon of parametric roll. The boundaries of the parametric roll domain (in which the maximum roll angle is considered to be due to parametric roll) are overlayed with a black line on the roll polar plots. This permits to take a closer look to the influence of the spreading angle on the parametric roll domain. This domain can be seen as a two 2-dimension lock-in-field (Section 1.1) function of both the speed and heading.

The results are provided as roll polar plots presenting the maximum roll angle observed during one-hour simulations in 6-DoF. Three loading conditions are evaluated, representing a total of 11025 simulations. Figure 56 to Figure 58 present the roll polar plots obtained for the C11-class container ship with a draught of 12 m, a KG of 18 m, for the three sets of waves presented in Table 24, considering a reference sinusoidal wave of steepness 0.0167.

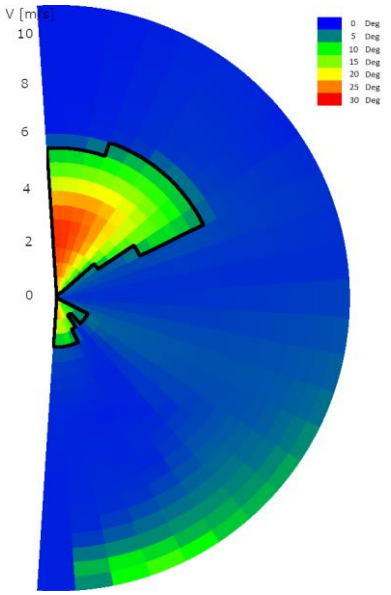

Figure 56 - Roll polar plot, case n°1 (reference wave)

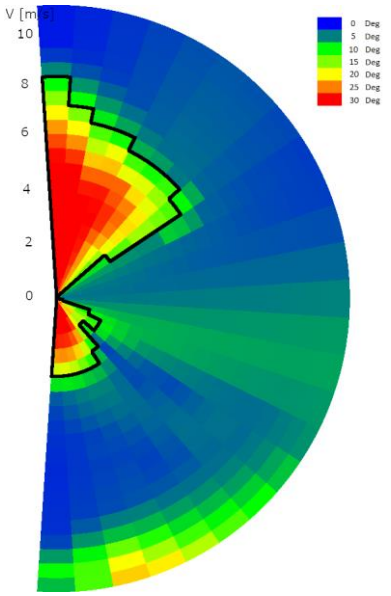

Figure 57 - Roll polar plot, case n°2 (spreading $\pm$ 30 degrees)

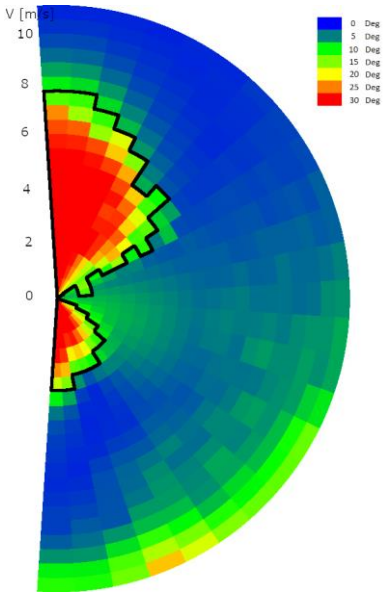

Figure 58 - Roll polar plot, case n°3 (spreading ± 90 degrees)

The simulation is performed three times, for the three spreading cases (0 degree, ± 30 degrees, ± 90 degrees). The spreading case leading to the highest value of the maximum roll angle is identified, for each speed and heading in the polar plot. Table 25 presents the results obtained for each loading condition and wave steepness. The column "±90° v. ±30°" presents the percentage of simulations for which the maximum roll angle observed with a spreading angle of ± 90 degrees is larger than the one obtained with a spreading angle of ± 30 degrees. As well, columns "±90° v. 0°" and "±30° v. 0°" present the percentage of simulations for which the maximum roll angle observed with a spreading angle of ± 90 and ± 30 degrees is larger than the one obtained without spreading angle, respectively.

For speeds lower than 2.5 $m.s^{-1}$ the vessel may not keep her course in waves. Therefore, simulations in 5-DoF with frozen yaw are conducted in addition to the one in 6-DoF and lead to equivalent results.

Draught [m]	KG [m]	Wave Steepness	±90° v. ±30°	±90° v. 0°
12	18	0.0167	62%	95%
12	18	0.025	69%	87%
12	17	0.0167	80%	97%
12	17	0.025	71%	93%
11	18	0.0167	66%	95%
10	19	0.0167	74%	96%
10	17	0.0167	76%	99%
Average			71%	95%

Table 25 - Compared percentage of maximum roll angle

The method used to build equivalent sets of waves developing an equivalent energy is validated for each selected case in the time-domain solver. The roll polar plots presented in Figure 56 to Figure 58 refer to the first line of Table 25. In this case, 62 % of the maximum roll angles are larger when the spreading angle is ± 90 degrees than when the spreading angle is ± 30 degrees, and 95 % of the cases larger than the ones without any spreading. In average (for all the conditions in Table 25), 71 % of the maximum roll angle are larger when the spreading angle is ± 90 degrees than when the spreading angle of ± 30 degrees, and 95 % of the cases larger than the ones without any spreading.

The wavelength is equal to the ship's length. This maximizes the appearance of parametric roll in longitudinal seas. The ratio of the wavelength over ship's breadth is equal to 6.6, which is too large to observe synchronous roll in beam seas.

In theory, considering parametric roll, the case without spreading (monodirectional wave) should lead to the largest GM variation in head seas, and therefore to the largest roll angle. However, results are counterintuitive: The largest roll angles are mostly observed when a non-zero spreading angle is considered.

Figure 56 to Figure 58 show that parametric roll domain (contoured in black) extends when the spreading angle increases. This extension of parametric roll domain is observed in all cases assessed in Table 25.

Therefore, considering sinusoidal waves as reference waves, the spreading angle leading to the largest roll angle is $\pm$ 90 degrees. Thus, here, it is identified as the most conservative spreading angle.

3.3.3. Influence of the spreading angle on the roll motion, real sea states

Simulations conditions

A study of the spreading angle equivalent to the one realised based on sinusoidal waves is realised for several reference sea states. The spreading angles considered are the ones presented in Table 24. Here, a unique simulation is not sufficient to obtain a representative maximum roll angle for each set of waves, loading condition, vessel heading and speed. Thus, the median of the maximum roll angle on 20 simulations of 1 hour with different seeds is considered as recommended by BV (NR 667, 2019b).

In this study, the simulations are conducted on the C11-class container ship. The draught is set to 12 metres. Two loading conditions representing a KG of 17 and 18 metres are assessed. Two reference sea states are considered and described in Table 26. The probability of occurrence presented in this table is the one provided in the IACS Rec.34 (IACS, 2001).

Sea state n°	H_S [m]	Tz [s]	Occurrence Probability
1	5	13	300 / 100 000
2	8	10	468.9 / 100 000

Table 26 - Sea state definition

Roll polar plots

Roll polar plots representing the median 1-hour maximum roll angle of 20 simulations are realised for the spreading angles considered in Table 24. The speed discretisation is 2 $m.s^{-1}$ from 2 to 10 $m.s^{-1}$ and the heading discretisation is 15 degrees from head sea to following sea. Half of the roll polar plot is calculated since the results are symmetrical. This represents 1300 simulations for each combination of loading and environmental conditions. The method used to build the equivalent sea states developing the same energy is validated for each case in the time-domain solver by comparison of the total energy with the one of reference (Section 3.3.1). The median one 1-hour maximum roll angle for each combination of course and speed is the one displayed on the roll polar plots.

The roll polar plots obtained on the sea state number 2 with a KG of 18 metres are presented hereafter. Figure 59 presents the roll polar plot obtained without spreading, Figure 60 presents the roll polar plot obtained for a spreading of $\pm$ 30 degrees and Figure 61 presents the roll polar

plot obtained for a spreading of ± 90 degrees. The black line in Figure 59 (without spreading) corresponds to the combinations of course and speed associated to the highest risk of encountering parametric roll, based on the period of peak of the monodirectional spectrum and the formula of the encounter period provided by the IMO (2007a).

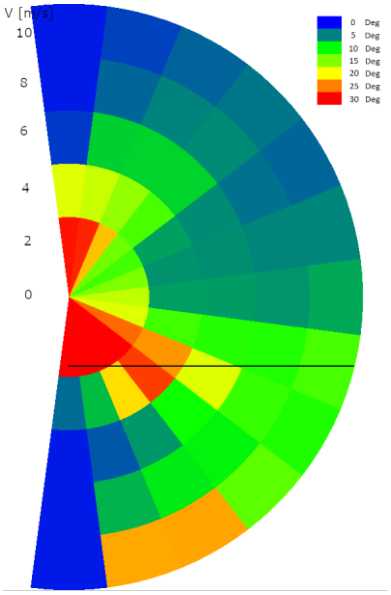

Figure 59 - Roll polar plot, case n°1 (reference spectrum)

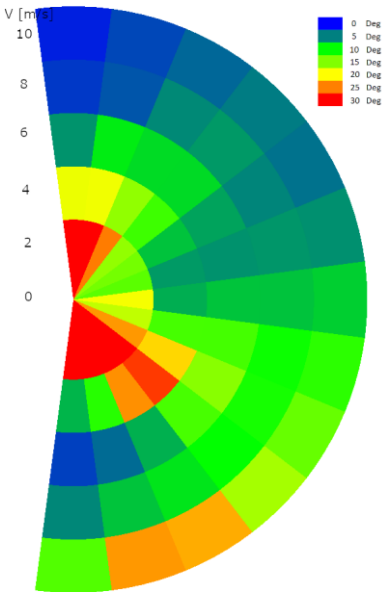

Figure 60 - Roll polar plot, case n°2 (spreading ± 30 degrees)

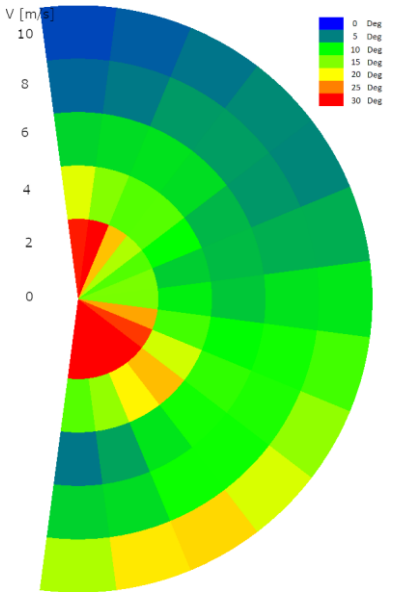

Figure 61 - Roll polar plot, case n°3 (spreading ± 90 degrees)

Figure 59 to Figure 61 shows that the increase of the spreading angle tends to increase the width of combinations of course and speed leading to heavy roll motions. However, this study in real sea state shows that the maximum roll angles, reached for combinations of course and speed where parametric or synchronous roll may appear, decrease with the increase of the spreading angle. This conclusion was more expected to the author than the one observed on sinusoidal waves.

The median 1-hour maximum roll angles calculated for each combination of course and speed are compared for each spreading angle (as presented in Table 25 for the study considering sinusoidal waves as reference). The results are presented in Table 27. The results show that the spreading angle of ± 90 degrees provides in average the most conservative roll amplitudes. The numerical results lead to the same conclusions than the one observed for the study considering sinusoidal waves.

KG [m]	Sea state case	±90° v. ±30°	±90° v. 0°	±30° v. 0°
17	1	69.2%	70.8%	76.9%
17	2	66.2%	72.3%	67.7%
18	1	67.7%	78.5%	70.8%
18	2	66.2%	73.8%	80.0%
Average		66.7%	73.9%	73.9%

Table 27 - Compared percentage of mean maximum roll angle

This study leads to the conclusion that the most conservative spreading angle is ± 90 degrees in most of the cases. Thus, a spreading angle of ± 90 degrees should be considered as the most conservative one when realising simulations to build operational roll polar plots.

3.4. LOADING CASE SELECTION

The loading cases selected to realise operational roll polar plots are rarely the current one of the ship at the time of its use. Since no interpolation of the roll amplitudes can be realised between two or more roll polar plots (non-linear phenomena), the selected loading cases should be as representative as possible of the ones that the vessel will encounter in its entire life. The assessment presented in Section 1.3 propose to select the loading conditions along a straight line

starting from the point defined by the minimum GM and maximum draught to point defined by the maximum GM and minimum draught provided in the stability booklet. Those extreme loading conditions are usually encountered in the stability booklet for both conditions fully loaded with cargo and supply at departure, and empty cargo on ballast at arrival with 10% supply. Such method permits to cover the entire theoretical range of loading conditions that the vessel might encounter while under service, defined by the regulation (D211 for a French-flagged vessel (Affaires Maritimes, 2019)). However, statistically it is not under those extreme loading conditions that the vessel mainly sails in her lifetime. Nowadays, as presented in the introduction of this PhD thesis, the number of container ships raises due to a continuous growing freight demand. The increasing number of container vessels (718 ordered container ships on the 31st of December 2021 according to Barry Rogliano Sales (BRS, 2022)) and the aim to reduce costs lead to build large vessel series. Thus, it is proposed hereafter to identify relevant operational loading cases from existing data of sister ships or from vessel series with similar hull shape rather than from theoretical loading cases. It can be noticed that such identification of relevant inputs based on operational cases from vessel series or from similar ships already exists when selecting the damping coefficients in a regulatory framework (IMO, 2020a, Section 3.3.2).

The vessel series loading case study includes all data provided from sister ships. The data is checked to avoid taking into account erroneous results such as mis reporting. The loading cases are summarised as ship displacement and GM (including free surface effects if such correction applies). Within the scope of this PhD, three vessel series were assessed based on the data collected from real departure and arrival conditions, representing a total of 2665 loading conditions. The study covers the entire range of displacement. The displacement range is sectioned in 10 to 20 intervals depending on the total number of loading cases available. For each vessel series, 10 % of the total number of loading case are considered as extreme. In each interval, the 5 % lowest and 5 % largest GM values are considered as extreme. A polynomial trend curve is fitted on the remaining 90 % loading cases. This trend curve is used to select operational loading cases. A upper and a lower trend curves are fitted on their respective 5 % extreme loading conditions. Thus, both equations bound the operational GM. This method permits to select the operational loading cases along an operational mean trend curve (instead of a theoretical straight line) and for each displacement to obtain representative extreme encountered metacentric heights.

Figure 62 presents a dimensionless example of the operational cases which have been selected, their associated trend curves (mean trend curve in green, upper in orange, lower in blue) and the straight line assumed in most global assessment in red (Section 1.3). Results are provided as dimension-less data since numerical values are left confidential by the ship owner.

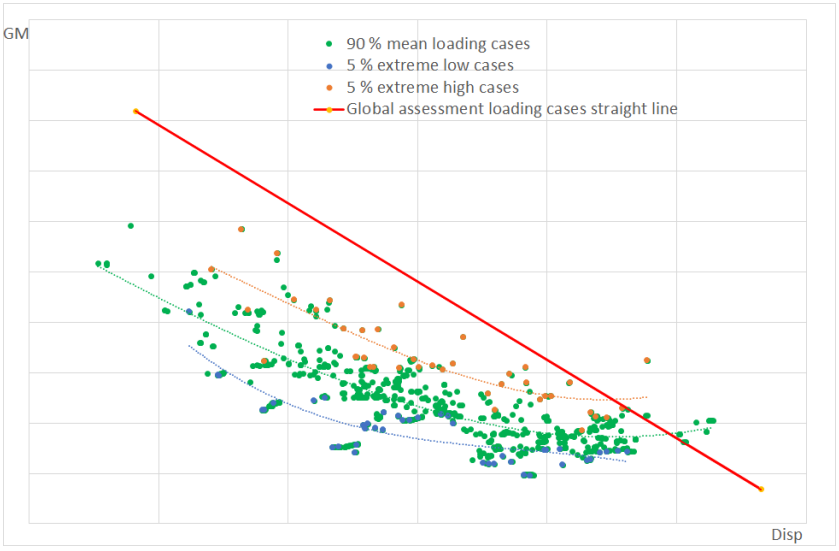

Figure 62 – Loading cases trend curves compared to BV assessment

Finally, if the number of loading conditions needs to be reduced even further (limited computational time), the loading cases are selected based on their frequency of appearance for a combined displacement (or draught) and GM. In this case the number of considered loading cases must be empirically selected (denoted by N). The data set is sliced in N sets of data equivalently spaced in GM from the minimum to the maximum GM. Thus, each sub data set does not present an equivalent number of loading cases. A simple barycentre permits to provide statistically the N most representatives loading conditions. The same data set of loading conditions used in Figure 62 is used to select with this method 3 operational loading conditions (red triangle), shown in Figure 63.

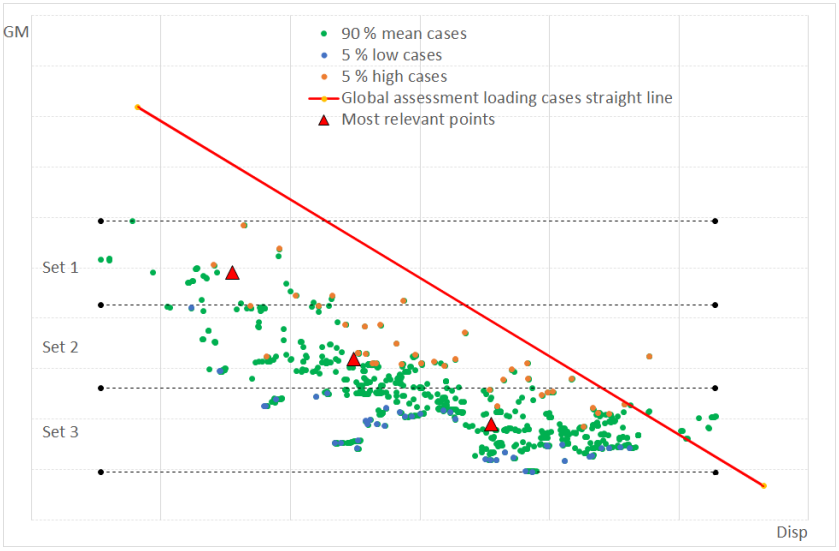

Figure 63 – Selection of three operational relevant loading cases

Thus, both easy-to-use methods provide relevant operational loading conditions inputs (displacement or draught and GM) to realise operational roll polar plots.

When discussing with engineers in charge to select operational loading cases, it appears that nowadays, more and more private companies ask the ship owner if they can provide real loading cases in order to select more accurately operational loading conditions instead of the one calculated from a theoretical point a view. This is especially relevant when realising operational

roll polar plots. However, no engineers provided their method to select the most relevant loading cases based on this operational dataset.

The *Maersk Essen* lost 750 containers at sea in 2021 (DMAIB, 2022). According to onboard software, the vessel was sailing safely. However, this estimation was unreliable since the forecasted weather was not the one encountered. In the report, the DMAIB encourages companies and authorities to explore and experiment solutions to avoid parametric roll based on real-time conditions rather than forecast.

Several methods to detect parametric roll in real time exist and are briefly presented in Section 1.4.3. This chapter presents an innovative real-time detection method based on physical conditions required for parametric roll to appear. It also proposes an alarm associated to the detection of parametric roll. A validation of the method and its associated alarm is provided. The content of this chapter has been submitted the Journal of Ship Research (Luthy et al., 2022d).

4.1. METHOD

4.1.1. Parametric roll coefficients

This innovative parametric roll detection method is based on a single coefficient denoted hereafter « C ». C coefficient is the multiplication of three coefficients $\widehat{C1}$, $\widehat{C2}$ and $\widehat{C3}$ (non-dimensional, denoted here after with a hat, Equation 112), reflections of the three-dimensional coefficient C1, C2 and C3, respectively. Each coefficient directly reflects a physical condition required for parametric roll to appear. Thus, each coefficient takes a non-zero value when the required condition is met. The three coefficients $\widehat{C1}$, $\widehat{C2}$ and $\widehat{C3}$ are evenly weighted. The coefficient C is calculated by multiplying the three coefficients together, Equation 112.

$$C = \widehat{C1} \times \widehat{C2} \times \widehat{C3} \qquad 112$$

The three coefficients are calculated from the data provided by the inertial unit or any other equivalent data, such as time-domain simulation results. Discrete signals of the roll and pitch time series are required.

- Coefficient C1 is based on the ratio of the up-crossing roll period (denoted by $T_{UP.\varphi}$) over the up-crossing pitch period (denoted by $T_{UP.\theta}$), Equation 113. C1 reflects the well-known physical condition required for parametric roll to appear. Usually, the roll period is compared to the encountered period, since it is assumed that the pitch period is equal to the encounter period (IMO, 2007a). The coefficient $\widehat{C1}$ is the normalized coefficient C1. $\widehat{C1}$ takes the value of 1 when the roll over pitch period ratio is equal to 2.

$$If\ C1 = \frac{T_{Z.\varphi}}{T_{Z.\theta}} = 2\ then\ \widehat{C1} = 1 \qquad 113$$

  In beam seas, it is observed that this period ratio may be, such as in head seas, equal to 2. However, according to the definition of parametric roll (IMO, 2020a), this phenomenon cannot appear in beam seas since there is no variation of the transverse stability. However, some phenomena other than parametric roll can lead to a period ratio equal to 2, especially in beam seas. Thus, other physical conditions must be considered to qualify the roll motion as due to parametric roll.
- Coefficient C2 is equal to the ratio of the peak roll period (denoted by $T_{P.\varphi}$) over the up-crossing roll period (denoted by $T_{UP.\varphi}$), Equation 114. The peak roll period represents the

period of successive peaks in the roll time series. When the roll motion is sinusoidal, the peak roll period is equal to the up-crossing period. It is observed that this ratio is around 1 when parametric roll appears. This ratio differs from 1 when the roll energy is not sufficient to overcome the energy provided by beam waves. In real sea state, the roll time series tends to become sinusoidal when parametric roll appears. Therefore, coefficient $\widehat{C2}$ is equal to 1 when C2 value is between 0.8 and 1.2 and equal to zero otherwise.

$$If\ C2 = \frac{T_{P.\varphi}}{T_{Z.\varphi}} \in [0.8; 1.2]\ then\ \widehat{C2} = 1, else\ \widehat{C2} = 0 \qquad 114$$

- Coefficient C3 is based on the phase shift between the roll and the pitch motion. This phase shift is measured between both time series at the up crossing of each time series. This delay reflects the shift angle defined in Chapter 2. If the phase shift is almost null, then $\widehat{C3}$ takes the value of 1. The notion of up-crossing is defined in the next sub-section.

To avoid discontinuities in the coefficient C and weight their bandwidth of influence, coefficients C1 and C3 are calculated using a normal distribution, Equation 115. The normal distribution is selected for its simplicity since it is triggers by two parameters only. The value of the parameters of the normal laws were empirically selected based on the results observed on sinusoidal waves.

$$P(x) = \frac{1}{\sigma.\sqrt{2\pi}} e^{-\frac{1}{2}\left(\frac{x-\mu}{\sigma}\right)^2} \qquad 115$$

σ Square root of the variance, standard deviation

μ Expectation

x Current assessed value

$\widehat{C1}$ and $\widehat{C3}$ are respectively obtained by dividing C1 and C3 by the value of the associated normal distributions where x is equal to the expectation. Therefore, $\widehat{C1}$ and $\widehat{C3}$ varies from 0 to 1.

Coefficient C1

Coefficient C1 is based on the ratio of the up-crossing roll period (denoted by $T_{UP.\varphi}$) over the up-crossing pitch period (denoted by $T_{UP.\theta}$), Equation 113. Coefficient C1 reflects the period coupling which appears when parametric roll occurs. It is demonstrated that within the lock-in field (speed range within parametric rolls appears, Section 1.1) the roll period is locked to twice the encounter period in regular waves (Grinnaert, 2017). The up-crossing periods are measured on the time series. The references for the up-cross are the values calculated from the hydrostatic balance in calm water, heel angle for $T_{UP.\varphi}$ and trim angle for $T_{UP.\theta}$. For each example provided hereafter, the ship is balanced at zero trim and zero heel in calm water. At each time step, the current value is compared with the previous one. If the previous value is lower than the reference value and the current value is larger than this reference, then a linear interpolation is realised to calculate the up-crossing time (t_{UP}), Figure 64. This method is used on both roll and pitch time series. The up-crossing period (T_{UP}) is calculated between two successive t_{UP} and is updated at each new up-crossing.

The pitch period is highly influenced by the encounter of waves due to the high stiffness of the longitudinal stability. Thus, this method assumes that the pitch period is equal to the encounter period (IMO, 2007a). The ratio of the roll period over the pitch period ($T_{UP.\varphi}/T_{UP.\theta}$) is around two when the first mode of parametric roll appears. Rapid variations of the pitch period may occur. Consequently, considering a single pitch up-crossing period may not be significant to accurately provide a representative estimation of the encounter period (Figure 65). Thus, two values of the up-crossing pitch period are calculated. The first pitch period is defined as a single up-crossing

period ($T_{UP.\theta 1}$). The second up-crossing pitch period is defined as the mean of the latest two up-crossing pitch period ($\overline{T_{UP.\theta 2}}$). The ratios of the roll period on both pitch periods are calculated. The pitch period leading to the period ratio presenting the lowest risk of parametric roll is considered (the farthest value from 2).

A normal distribution is applied to the period ratio with an expectation equal to 2 ($\mu = 2$) and a standard deviation of 0.25 ($\sigma = 0.25$). Applying theses values to μ and σ in Equation 115 leads to Equation 116. Coefficient $\widehat{C1}$, varying from 0 to 1, is obtained by dividing C1 by the value of the normal distribution calculated for $T_{UP.\varphi}/T_{UP.\theta} = 2$, Equation 117. The value of the standard deviation has been selected to obtain a value of the coefficient $\widehat{C1}$ equal to 0.6 when the period ratio is equal to 1.75 or 2.25 (Table 28).

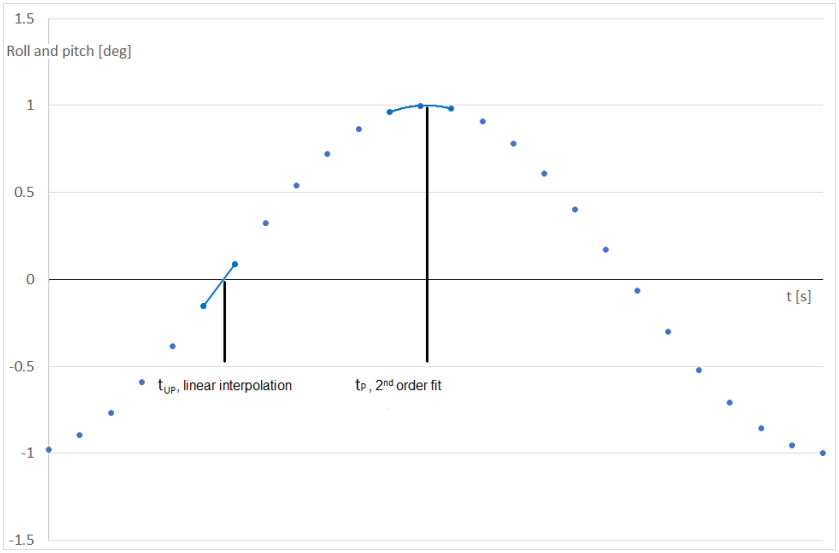

Figure 64 - Up-crossing time t_{UP} and time of the peak t_{Peak}

$T_{UP.\varphi}/T_{UP.\theta}$	$(T_{UP.\varphi}/T_{UP.\theta})$-2	$\widehat{C1}$
1.25	-0.75	0.0111
1.50	-0.50	0.1353
1.75	-0.25	0.6065
2.00	0.00	1.0000
2.25	0.25	0.6065
2.50	0.50	0.1353
2.75	0.75	0.0111

Table 28 - $\widehat{C1}$ value for significative roll over pitch period ratio

C1 coefficient is expressed as follows, Equation 116.

$$C1 = \frac{4}{\sqrt{2\pi}} e^{-8\left(\frac{T_{UP.\varphi}}{T_{UP.\theta}}-2\right)^2} \qquad 116$$

Finally, the value of C1 is divided by the one calculated for $T_{UP.\varphi}/T_{UP.\theta} = 2$ to obtain $\widehat{C1}$ coefficient varying from 0 to 1, Equation 117.

$$\widehat{C1} = \frac{\sqrt{2\pi}}{4} C1 = e^{-8\left(\frac{T_{UP.\varphi}}{T_{UP.\theta}}-2\right)^2} \qquad 117$$

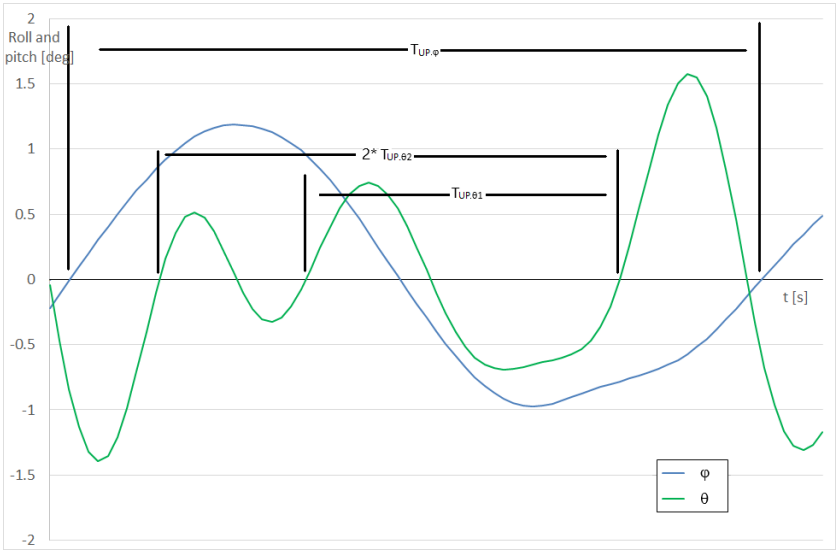

Figure 65 - Example of large variations of the pitch period during one roll period

Coefficient C2

Coefficient C2 is equal to the ratio of the peak roll period (denoted by $T_{P.\varphi}$) over the up-crossing roll period ($T_{UP.\varphi}$), Equation 114. Both periods may differ, as shown in Figure 66. Coefficient C2 reflects the effect of beam waves which do not lead to any parametric excitation. Despite Ikeda et al. (2005) stated that parametric excitation can appear in beam waves if the heave motion has sufficient magnitude to lead to large variation of the waterplane and of the transverse stability, the method considers that no parametric excitation can appear in beam seas due to the high stiffness of the heave motion. Moreover, the second-generation intact stability criteria (IMO, 2020a) do not consider the case of parametric roll in beam seas. When the vessel encounters beam waves, they modify instantaneously the roll motion. The up-crossing period is calculated as presented in the previous sub-section. The peak period is calculated on half a period between two consecutive peaks (one positive and one negative or one negative and one positive). There can be several peaks' periods within one up-crossing period. Three consecutive points in the roll time series are considered to identify the peaks. If the absolute value of the 1st point ($|\varphi_1|$) is lower than the absolute value of the second point ($|\varphi_2|$) and the absolute value of the 3rd point (current value, aka the latest value acquired during real-time assessment) is as well lower than $|\varphi_2|$, then φ_2 is a local maximum (Equation 118), Figure 64.

$$If\ |\varphi_1| < |\varphi_2| > |\varphi_3|\ then\ \varphi_2\ is\ a\ local\ maximum \qquad 118$$

The discretisation of the roll time series may significantly reduce the accuracy of the local maximum. Thus, the accuracy is guaranteed by fitting a parabola on the three points (Equations 119 and 120). The time of the local maximum (t_{Peak}) is calculated by Equation 121.

$$\begin{cases} ax_1{}^2 + bx_1 + c = Phi_1 \\ ax_2{}^2 + bx_2 + c = Phi_2 \\ ax_3{}^2 + bx_3 + c = Phi_3 \end{cases} \quad 119$$

$$y = ax^2 + bx + c \quad 120$$

$$t_{\text{Peak}} = \frac{-b}{2a} \quad 121$$

The peak period (denoted by T_P) is obtained by multiplying by two the time between two consecutive peaks (positive and negative or negative and positive, respectively denoted by $t_{Peak.n}$ and $t_{Peak.n+1}$), Equation 122.

$$T_P = 2(t_{Peak.n+1} - t_{Peak.n}) \quad 122$$

In Figure 66, $T_{UP.\varphi1}$ is graphically almost equal to $T_{P.\varphi1}$ during the first oscillation. During the second oscillation, $T_{UP.\varphi2}$ is graphically larger than $T_{P.\varphi2}$. This second situation is mostly observed in beam seas or when the energy provided by the wave is insufficient for parametric roll to develop. It is observed that when parametric roll develops, only one positive peak and one negative peak are observed in each roll period. In this case, the peak period is equal to the up-crossing period. Thus, if the ratio of the peak period over the up-crossing period is between 0.8 and 1.2, then the coefficient $\widehat{C2}$ takes the value of 1, otherwise it takes the value of 0, Equation 114. The bandwidth [0.8; 1.2] is empirically selected based on large amount of roll time series.

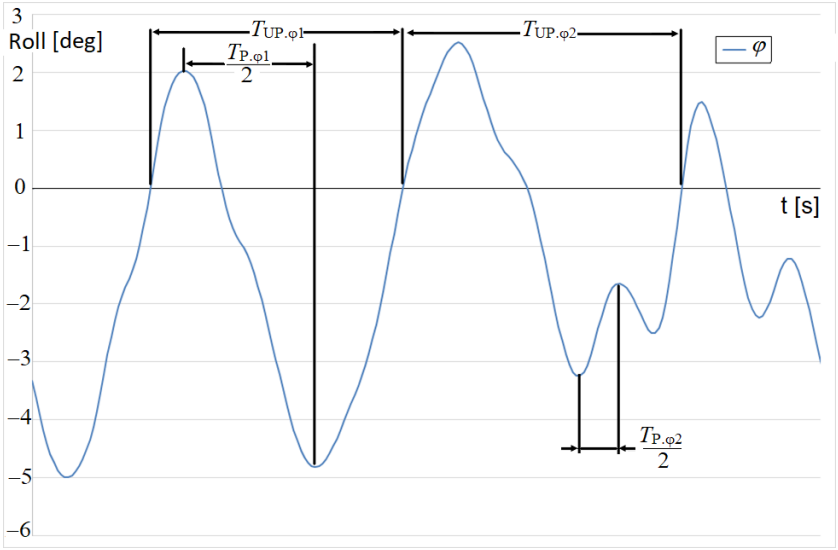

Figure 66 - Roll time series on real sea state, peak and up-crossing period

Coefficient C3

Coefficient C3 is based on the phase shift between the roll motion and the pitch motion. Thus, coefficient C3 reflects the phase shift between the variation of the transverse stability and the roll motion, defined as shift angle which triggers the amplitude of parametric roll (Grinnaert, 2017; Luthy et al., 2021b; Luthy et al., 2022c), Chapter 2. Thus, if the phase shift does not correspond to the condition required for parametric roll to appear, then parametric roll is not the phenomenon leading to the observed increase of the roll amplitude. The roll time series and the pitch time series do not have the same period. Therefore, the phase shift between them is not constant (unless a roll steady state appears in regular waves). The duration δt between the up cross time of both

time series (roll and pitch) reflects the phase shift. This duration is hereafter denoted by delay. When a roll up-crossing is detected, the delay δt1 is calculated between the latest pitch up-crossing time ($t_{UP.\theta 1}$) and the time of the roll up-crossing ($t_{UP.\varphi}$). If the delay δt1 is lower than $T_{UP.\varphi}/16$, then this delay can immediately be considered to update $\widehat{C3}$. Otherwise, it is required to wait for the next pitch up-cross and to measure the delay δt2 between the time of this second pitch up cross $t_{UP.\theta 2}$ and $t_{UP.\varphi}$. The lowest absolute value of δt1 and δt2 is considered and denoted hereafter by δt. Figure 4 presents a graphic example in which δt1 is larger than $T_{UP.\varphi}/16$, thus δt2 must be considered. Here, δt2 is lower than δt1, then δt2 is the delay which shall be considered, such as δt = δt2.

The ratio of the roll period over the pitch period has been observed for a wide range of ships, loading conditions and waves (H_S, T_P, direction), studied throughout more than 10,000 hours of simulation. This ratio has never been observed to be larger than 8. Therefore, it is not necessary to wait for a second pitch up cross if δt1 is lower than $T_{UP.\varphi}/16$ to update $\widehat{C3}$ (the absolute value of δt2 will be larger than δt1).

Parametric roll appears when the roll and pitch motions are in phase (δt is null). Therefore, a standard normal distribution is applied (expectation is null) to δt to calculate C3. The standard deviation (denoted by σ) varies at each new measurement of the up-cross roll period (Equation 123). Coefficient C3 is expressed by Equation 124.

$$\sigma = \frac{T_{\mathrm{UP}.\varphi}}{8} \qquad 123$$

$$C3 = \frac{8}{T_{\mathrm{UP}.\varphi}\sqrt{2\pi}} e^{-32\left(\frac{\delta t}{T_{\mathrm{UP}.\varphi}}\right)^2} \qquad 124$$

Finally, coefficient $\widehat{C3}$ varying from 0 to 1 is obtained by dividing C3 by the value of the standard normal distribution for δt = 0, Equation 125.

$$\widehat{C3} = T_{\mathrm{UP}.\varphi}\sqrt{2\pi}\frac{C3}{8} = e^{-32\left(\frac{\delta t}{T_{\mathrm{UP}.\varphi}}\right)^2} \qquad 125$$

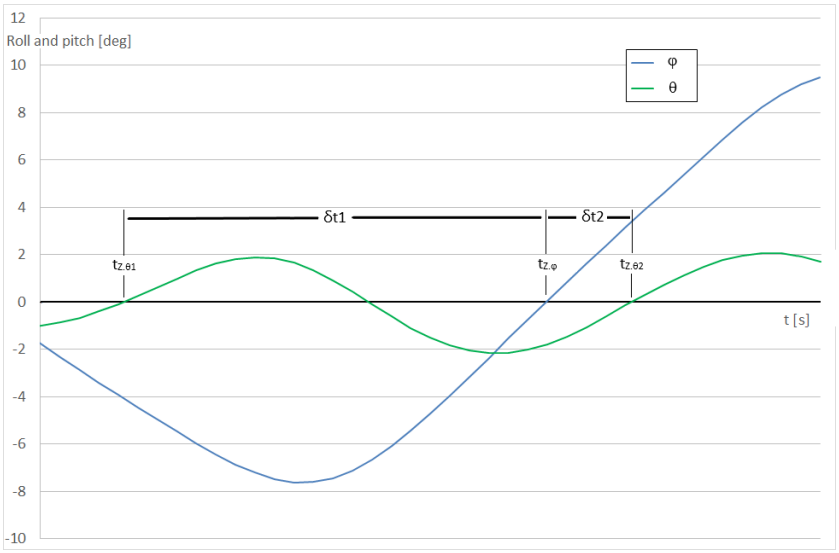

Figure 67 - Delay measurement between two time series

Parametric roll appears when the variation of the transverse stability is important. On a regular longitudinal wave which length is equal to the one of the ship, for typical container hull shape

(wall sided amidship and flared at the bow and the stern), the maximum waterplane inertia (and thus maximum transverse stability) appears when the wave crests are located on the ship's ends, and the minimum waterplane inertia (and thus minimum transverse stability) appears when the wave crest is located amidship (Section 1.1). However, when the actual GM on wave is compared to its cosine approximation (Equation 7), it is observed that maximum and minimum transverse stability does not appear exactly for the wave centred on the perpendiculars and amidship (IMO, 2021a), respectively. For a vessel balanced at zero-trim in calm water, the maximum and minimum transverse stability in waves appear almost when the trim is null. Considering that in real sea state each wave component has a direct influence on the transverse stability, the pitch motion varies in accordance with the waves. Thus, it is assumed that regardless the shape of the incoming waves (on a real sea state) the maximum and minimum transverse stability appears almost when the trim is null, such as in regular waves. According to the definition of parametric roll provided by the IMO (2021b) and presented in Section 1.1 of this PhD thesis, if the transverse stability is the least when the ship returns to the upright position, then the ships will roll further on the opposite side due to the less resistance to heeling (amplifying the roll motions). Therefore, theoretically, parametric roll develops mostly when the temporal shift (δt) between the up-cross of the pitch motion and the up-cross of the roll motion is null, or almost null. Thus, the expectation of the normal law applied for the calculation of coefficient C3 is null.

4.1.2. Coefficient C and onboard alarm

The three coefficients $\widehat{C1}$, $\widehat{C2}$ and $\widehat{C3}$ are each based on physical conditions required for parametric roll to develop. Therefore, the three coefficients are evenly weighted. The coefficient C is the multiplication of the coefficients $\widehat{C1}$, $\widehat{C2}$ and $\widehat{C3}$ (Equation 112). Coefficient C varies from 0 to 1. To avoid fluctuating values of the coefficient C due to real sea state, a smoothing algorithm is introduced with a moving average on a half natural roll period.

The coefficient C itself does not directly consider the roll amplitude; it reflects the motion as being due to parametric roll. Therefore, parametric roll can be detected even for small roll amplitudes providing an early detection of parametric roll. However, warning the Officer Of the Watch when the roll amplitude is too low may conduct to realise unnecessary manoeuvres. Thus, a roll amplitude threshold is operationally combined to the coefficient C. The threshold can be modified. If the roll amplitude is lower than the threshold, then the coefficient C takes the value of 0. The author recommends to use a roll amplitude threshold of 3 degrees such as usually implemented onboard.

The Officer Of the Watch cannot keep his\her attention on the evolution of the coefficient C during his\her watch. Therefore, a parametric roll alarm is implemented to warn the Officer Of the Watch of the existing danger. This alarm arises when the ships motions are assessed as due to parametric roll if the coefficient C is larger than 0.4 during more than a time interval Δt. The time interval, Δt, should be determined as the maximum value of half a natural roll period and 15 seconds. Those values of the time interval have been empirically chosen regarding the results obtained in regular sea states with the aim to provide sufficient time for the crew to respond to the roll amplification in the opinion of the author. Thus, the alarm appears one roll period after the first signs of the detection of the phenomenon (half a roll period due to the moving average and half a roll period to arise the alarm).

4.2. NUMERICAL VALIDATIONS

4.2.1. Test of the method in regular wave

In this sub-sub-section, the parametric roll detection method is tested in longitudinal seas and beam regular waves using 6-DoF simulations of several container ships. The tests are conducted with Fredyn (CRN, 2021).

Figure 68 presents an example of time series obtained from a simulation realised on the C11-class container ship on longitudinal sinusoidal waves of length equal to the one of the ship (262 metres) and of steepness equal to 1/60. The ship is sailing at 5 $m.s^{-1}$ with a KG equal to 18 metres and a draught equal to 12 metres (this value of the draught is considered in all examples provided in this chapter). The ship motions are assessed using the method presented in Section 4.1. The loading condition corresponds to a balance at zero trim and zero heel in calm water. At the beginning of the simulation, the coefficient C is null since there is no sufficient data to calculate it. Once enough data is provided (at least enough time to calculate one up-cross roll period), the coefficient C increases significantly. In this case, coefficient $\widehat{C3}$ limits the coefficient C since both $\widehat{C1}$ and $\widehat{C2}$ are equal to 1. An almost linear increase of the coefficient C is observed. This is due to the moving average. From 50 to 80 seconds, the coefficient C is larger than 0.4 (limit to start counting before the alarm), however the operational roll amplitude threshold set to 3 degrees is not reached. After 80 seconds, the roll amplitude is larger than the threshold, and the coefficient C value is larger than 0.4. 15 seconds later, the parametric roll alarm is raised (here 15 seconds is selected since the natural roll period is smaller than 30 seconds). In this case, the alarm is raised for a roll amplitude between 3 and 4 degrees. The Officer Of the Watch may react consequently. In this case the method identifies correctly that the roll motion is due to parametric roll. Even if the C11-class container ship can suffer from parametric roll up to 35 degrees (ITTC, 2021c), the roll amplitude presented in this figure is limited to 8 degrees to show that the method is able to detect parametric roll before large roll motions occur.

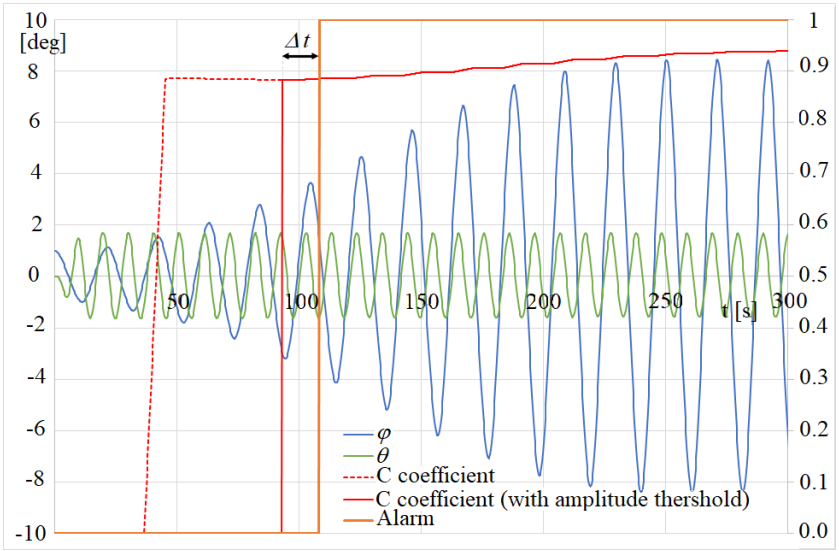

Figure 68 - C coefficient and associated alarm in head sea, regular waves

The method is also tested in beam regular waves, where synchronous roll may develop, and no parametric roll can appear. Thus, the coefficient C is expected to remain lower than the threshold of 0.4. Figure 69 presents the time series obtained for a simulation on the C11-class container ship sailing in beam sinusoidal waves of period equal to the ship's natural roll period and of height

equal to 7 metres. The ship is sailing at 3 m.s^{-1} with a KG equal to 16.5 metres. In this condition, synchronous roll appears, leading to roll amplitudes larger than the one presented in Figure 68. The coefficient *C* remains under the threshold used to qualify the roll as parametric. Therefore, on regular waves the coefficient C correctly discriminate the parametric roll from the synchronous roll. The results show the robustness of the method against synchronous roll in regular waves. Since the method is intended to be fitted onboard, such tests in regular waves are not sufficient. Tests and validation in real sea state are required.

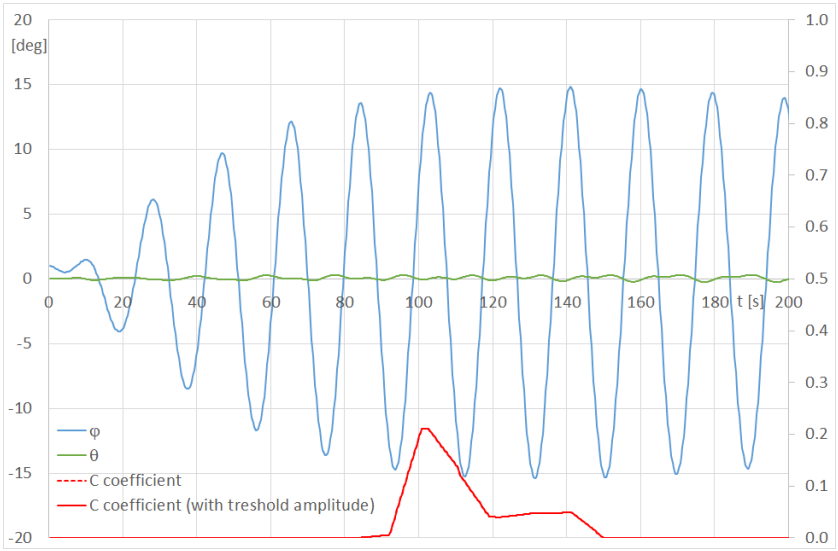

Figure 69 - C coefficient in beam seas, regular waves

4.2.2. Test of the method in irregular waves

A test of the parametric roll detection method is conducted in real sea states. Real sea state conditions where parametric roll may appear are selected in head and following seas. The sea state is modelled with a monodirectional Pierson-Moskowitz spectrum. The evolution of the coefficient C during the simulations is monitored. As an example, Figure 70 presents the evolution of the coefficient C for the C11-class container ship in monodirectional real sea state in head seas with a zero-up crossing period equal to 11.6 seconds and a significant height equal to 7 metres. The ship sails at 4.5 m.s^{-1} with a KG equal to 18 metres. In this condition, without any transverse excitation, the only type of roll motion which may appear is parametric. The coefficient $\widehat{C1}$ representing the ratio between the roll and the pitch period is not null during almost the whole simulation. $\widehat{C2}$ is equal to 1 during the whole simulation since no beam wave are encountered. The coefficient C grows significantly when the roll amplitude increases unexpectedly, even when the roll amplitude remains relatively low. Considering only $\widehat{C1}$ to detect parametric roll would lead to an over detection. The addition of $\widehat{C3}$ in the process permits to discriminate the parametric roll episodes with a higher accuracy. During this one-hour simulation, the parametric roll alarm would have arisen 7 times. Therefore, in this example, the coefficient C correctly identifies parametric roll in head seas. Results in following seas are similar to the one obtained in head seas.

The test is then conducted in beam sea. The sea state is selected to lead to roll amplitudes larger than the ones observed in head seas. The sea state is modelled with a monodirectional Pierson-Moskowitz spectrum. As an example, Figure 71 presents the results obtain for the C11-class container ship in beam real sea state with a zero-up crossing period equal to 13 seconds and a significant height equal to 9 metres. The ship sails at 7.5 m.s^{-1} with a KG equal to 16 metres. The coefficient C is expected to remain lower than the threshold of 0.4 during the whole simulation since no parametric roll can appear. In Figure 71, the coefficient $\widehat{C1}$ representing the

ratio between the roll and the pitch period is not null on several occasions. Thus, in beam real sea state, the roll period may almost be twice the pitch period as when parametric roll appears. Coefficients $\widehat{C2}$ and $\widehat{C3}$ moderate the global coefficient C when no parametric roll should be detected. It is observed that the coefficient C presents non-zero values during this one-hour simulation in beam seas. Here, the non-zero values of the coefficient C are not significant since no parametric roll alarm would arise. Thus, this test in beam seas shows that the method correctly qualifies the roll motion as not due to parametric roll.

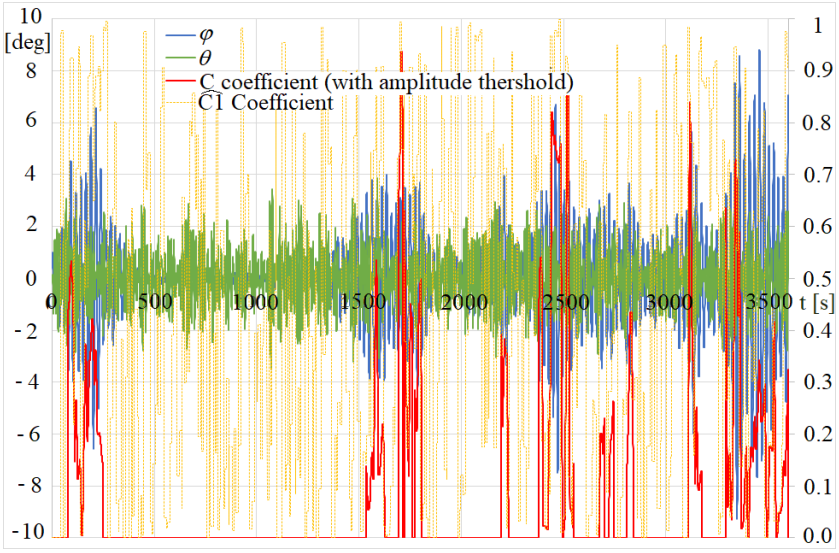

Figure 70 - C coefficient in head seas, real sea state

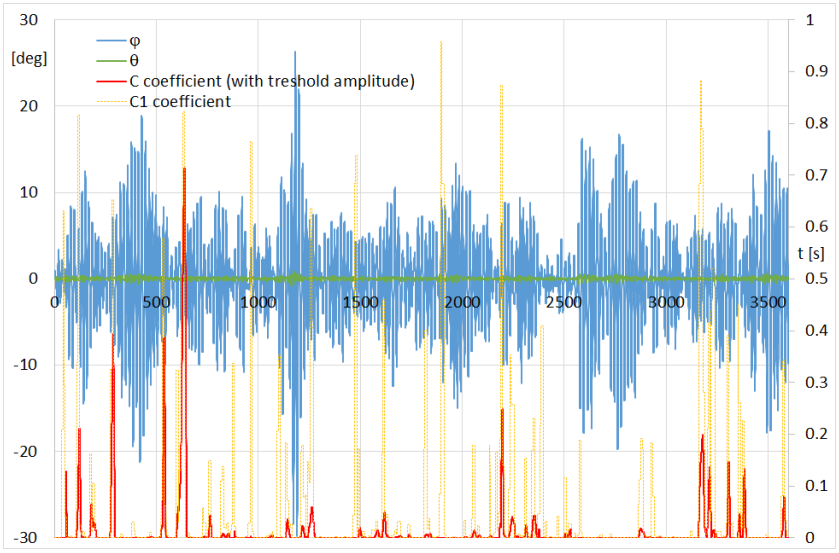

Figure 71 - C coefficient in beam seas, real sea state

4.2.3. Statistical validation of the parametric roll alarm

A statistical validation of the alarm associated to the method is conducted from the results of a large number of simulations realized on the C11-class container ship, known for her vulnerability to parametric roll (France et al., 2003). The loading condition corresponds to zero trim and zero heel in calm sea, with a draught of 12 metres and a KG of 18 metres. The environmental conditions are modelled with a monodirectional Pierson-Moskowitz spectrum. The wave period varies from 6 to 14 seconds with a step of 0.2 second. The significant wave height varies from 4 to 9 metres with a step of 1 metre. The ship's speed varies from 4 to 9 m s^{-1} with a step of 0.5 m s^{-1}. Several

seeds for phase angles are used in some cases. This represents 3816 simulations to conduct for each ship's relative direction to the wave. Each simulation is one-hour long.

The 3816 simulations are conducted in head seas to assess the relevance of the parametric roll detection. As well, the 3816 simulations are conducted in beam seas to establish the false-alarm rate. The simulations are conducted in 5 DoF (frozen yaw) to prevent from any undesired course alteration due to the waves. This guaranties that the roll motion encountered in head sea can only be due to parametric roll and that no parametric roll can appear in beam seas. To assess the alarm relevance during each simulation, the number of times the alarm is encountered during each one-hour simulation is compared to the number of times the roll amplitude gets above a threshold. To avoid counting twice a single roll episode, several methods are proposed in the Second-Generation Intact Stability Criteria by the IMO (2020a) when considering the direct counting of events in level 3. Here, a hysteresis on the roll amplitude with an upper threshold and lower threshold is considered to avoid counting twice a single roll episode or the same alarm. In this study, two roll amplitude hysteresis are considered. The first hysteresis considers a roll episode to begin when the roll amplitude gets larger than 5 degrees (upper threshold) and ends when the roll amplitude decreases under 2.5 degrees (lower threshold), denoted hereafter by Hysteresis 1, represented in Figure 72. The second hysteresis considers a roll episode to begin when the roll amplitude gets larger than 10 degrees (upper threshold) and ends when the roll amplitude decreases under 5 degrees (lower threshold), denoted hereafter by Hysteresis 2. Each roll episode is studied independently.

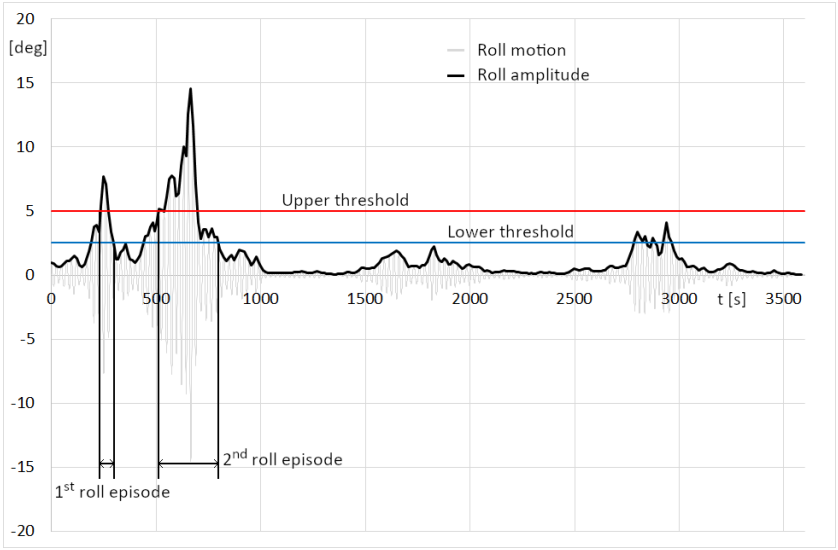

Figure 72 - Roll episodes identified with a hysteresis

In head seas, if a parametric roll alarm appears during a roll episode, then the parametric roll detection is considered to be successful for this roll episode. If no parametric roll alarm appears during the considered roll episode, then the parametric roll detection is considered to fail. The assessment in head seas provides the relevance of the method. Parametric roll is mostly observed in sea states modelled with a significant height larger than 6 metres and a period larger than 8 seconds (Figure 73).

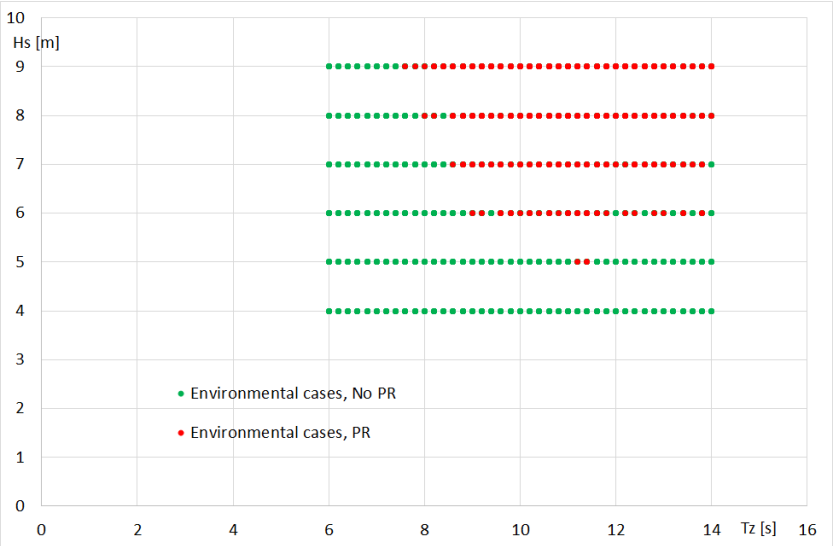

Figure 73 - Environmental cases leading to parametric roll in head seas

In beam seas, if a parametric roll alarm appears during a roll episode, then the parametric roll detection is considered to fail (false alarm). The assessment in beam seas provides the false-alarm rate.

Table 29 provides the results of this statistical study on the C11-class container ship. In head seas, parametric roll alarm arises more than 84 % of the time when the roll amplitude gets above 5 degrees. As well, parametric roll alarm arises more than 88 % of the time when the roll amplitude gets above 10 degrees. Therefore, the method efficiently detects parametric roll in real sea state. In beam seas, parametric roll alarm arises less than 4 % of the time when the roll amplitude gets above 5 degrees. As well, the alarm arises less than 1.5 % of the time when the roll amplitude gets above 10 degrees. In beam seas, the false alarm rate decreases when the hysteresis increases. Therefore, the physics behind the coefficient C and its associated alarm reflect that the heavy motions in beam seas are not due to parametric roll.

Study \ Test	Detection alarm rate (Hysteresis 1) [%]	Detection alarm rate (Hysteresis 2) [%]
Head seas	84.3	88.6
Beam seas	3.7	1.5

Table 29 - Statistical study of the relevance of parametric roll alarm

The same simulations are conducted in 5-DoF on the C11-class container ship presenting a draught of 12 metres and a KG of 16 metres. The results of those 3816 simulations in head seas present a maximum roll amplitude of 5.8 degrees. On all the simulations, Hysteresis 2 (minimum roll amplitude 10 degrees) is never reached and Hysteresis 1 (minimum roll amplitude 5 degrees) is reached twice. No parametric roll is detected during any simulation. Thus, it is considered that parametric roll did not occur enough to detect it. The results of the 3816 simulations in beam seas presents a maximum roll amplitude of 31.5 degrees. Thus Hysteresis 1 and 2 are reached many times. Parametric roll is detected on several occasions. The false detections rate is 1.6 % and 1.2 % for Hysteresis 1 and 2, respectively. Thus, for this loading condition, the false alarm rate in beam seas is less than 2 %. In head seas the roll motion did not lead to the detection of parametric roll (roll amplitudes less than 6 degrees). Thus, the parametric roll alarm provides irrelevant detections with a low rate in beam seas when large roll amplitudes are detected, and does not provide irrelevant detections in head seas for small roll amplitudes.

Moreover, an equivalent study is conducted on a 227.5-metre tanker vessel. The hull form is assessed as not subject to parametric roll with regards to IMO SGISC level 1 parametric roll criterion (IMO, 2020a; Grinnaert, 2017). A total of 5112 combinations of speed and environmental condition is assessed. During the simulations in head seas, no roll motion larger than 1.1 degree (initial roll angle 1 degree) is observed. No parametric roll is detected. During the simulations in beam seas, roll motions up to 38 degrees were observed. Parametric roll was detected more than 50 % of the time. Here the detection method does not provide relevant results. Thus, the detection method is not designed for this hull shape. Further investigation on the coupling of pitch and roll motions in beam seas for this type of vessel should be conducted to improve the method. This work was not realised within this PhD thesis since the work focuses on container ships for the benefit of CMA CGM.

4.3. REAL SCALE VALIDATION

The parametric roll detection method and its associated alarm are validated on a real-case time series. This operational validation is realised on a 2.5-day data set extracted from the inertial unit of a 349.5-m container ship (beam 51.2 m, design draft 14 m, design speed 22 knots) crossing the Pacific Ocean during winter season. During this period, the ship sailed at a constant speed. The ship encountered heavy weather with wave height varying from 3 to 5.5 metres. The ship suffered roll motions up to 13 degrees. Due to the large roll motions, the master decided to alter course significantly for 5.5 hours (50 degrees) and then came back to the original route. Therefore, this course alteration led to a modification of the encounter wave frequency, providing an interesting data set to assess the parametric roll detection method. The evolution of the environmental conditions during these 2.5 days is obtained from the open-access data provided by the Copernicus Marine Services. The main wave heading (defined as the heading of the primary swell) is extracted from the product "GLOBAL_ANALYSIS_FORECAST_WAV_001_027" (described in detailed in Section 3.2.1) for each point on the vessel's route. The relative wave heading is calculated from the vessel heading and main wave heading. This data set permits to validate that the method correctly identifies the periods during which parametric roll appears.

Figure 74 presents the roll-amplitude time series calculated from this data set. The pitch time series (not displayed) is considered to apply the parametric roll detection method presented in Section 4.1. The author reasonably believe that the ship experienced parametric roll on several occasions during these 2.5 days since the relative wave heading permits to this phenomenon to develop. The onboard warning system, monitoring data of the inertial unit, qualified the ship motions as due to parametric roll. Onboard warning system is not displayed here due to confidentiality. The study of the time series permits to display the parametric roll alarm proposed in this PhD thesis. The ship's heading is the one provided by the gyrocompass and the relative heading is calculated as presented above. During those 2.5 days, the ship initially rolls moderately with an amplitude from 6 to 8 degrees. During this first period, the parametric roll detection method presented in this paper leads to numerous alarms, warning the Officer Of the Watch of the existing danger. During this period the vessel sailed almost in head sea, relative to primary swell. A course alteration of 10 degrees was then engaged to follow the planned route and the new heading (100 degrees) was kept constant for 1.5 day. During this period, the roll motions led to roll amplitudes up to 13 degrees. The parametric roll alarm appears a few times. The danger was not constant since the relative heading to the wave was not constant. Between 20000 and 45000 seconds, an unexpected large variation of the relative heading is observed. Since the relative heading is calculated for the primary swell only, the author assumes that in this case the secondary swell, characterized with a different heading, became predominant and then was

identified as the primary swell during this period. The master altered course of 50 degrees for 5.5 hours, and then came back to the original route. During this period, the roll motion decreased by half, and the method does not detect any parametric roll. The onboard warning system did not qualify the roll motion as due to parametric roll during this period as well. The ship came back to the original route by altering course of 60 degrees. The roll motions increased once more up to 9 degrees. The method does not detect this roll motion as due to parametric roll and thus does not arise any alarm.

The method operationally identifies parametric roll and warns the Officer Of the Watch. No alarm arises when the course is altered and the ship is no longer in condition of parametric roll. Therefore, in this operational case study, the method and the associated alarm are relevant.

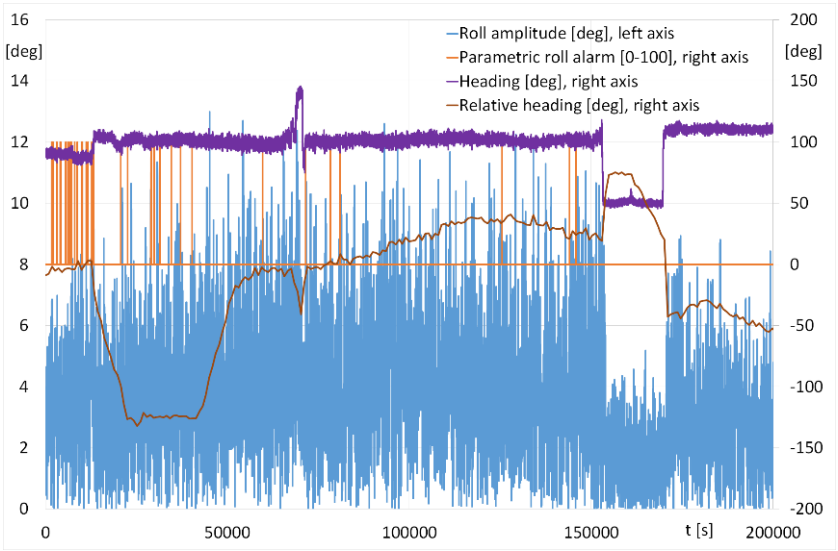

Figure 74 - Operational assessment of the parametric roll detection method

4.4. PARTIAL CONCLUSION

The assessment of the roll motion does not depend on the roll amplitude. Thus, this method permits to qualify the roll motion as due to parametric roll even for low roll amplitudes. An alarm is associated to the global coefficient permitting to warn the Officer Of the Watch of the existing danger. The method is tested in longitudinal and beam regular waves. This shows that no parametric roll is detected in transverse seas. The method and the associated alarm are tested and validated in irregular seas on a large number of simulations, providing relevant results. A statistical evaluation of their relevance is conducted based on 3618 hours of simulations in head and re-conducted in beam seas on a container ship. The alarm detection rate in head seas is larger than 80 % and the false alarm rate in beam seas is lower than 4 %. An equivalent study is conducted on a tanker, where no parametric roll is observed in head seas, while more than 50 % of false alarm are observed in beam seas. Finally, the method and the alarm are assessed on a real operational case where parametric roll developed (large container ship).

The method presents a relevant identification of the periods during which parametric roll appears. Further study can be conducted on the improvement of the method to reduce the false alarm rate by adapting bandwidth of the coefficients for each type of ship and hull. Furthermore, the normalization of the coefficient C2 by a normal law with a specific standard deviation for each type of ship and hull could be another interesting improvement.

DNV reported that in case of heavy weather leading to heavy roll motions a prudent captain would come to head sea and reduce speed (DNV, 2005). However, it is in longitudinal seas (head and following seas) that parametric roll can appear.

This chapter presents an evaluation of the most relevant manoeuvre to undertake after the parametric roll detection to avoid undesired roll motions. First, the method used to evaluate the efficiency of the manoeuvre is presented and validated. Then, a statistical study of the efficiency of several possible manoeuvres which could be executed by the Officer Of the Watch is conducted on the C11-class container ship. Based on those results, the most relevant manoeuvre to execute when unexpected heavy roll motions in head or following seas appear is identified.

Galeazzi et al. (2009c), Breu (2013) and Holden et al. (2012) conducted similar works based on frequency detuning with the aim to avoid large roll motions consecutive to both parametric and synchronous resonances.

5.1. ASSESSMENT METHOD

Most study on parametric roll are focused on the identification of the phenomenon (see Section 1.4 and Chapter 4). However, very few information are provided to the crew on how to operationally react when the phenomenon is detected. The masters and the Officer Of the Watch often ask themselves “what would have happened if I had engaged another manoeuvre ?”. Simulations permits to reproduce several times the exact same conditions and provide an answer on the efficiency of different manoeuvres. Thus, the aim of this study is to select the most relevant manoeuvre to execute when parametric roll appears. This assessment method has been partly presented at the 18th International Ship Stability Workshop, held in Gdańsk (Poland) in September 2022 (Luthy et al., 2022b).

To conduct this study, the method selected to detect parametric roll is the one presented in Chapter 4. Simulations are realised using the time-domain solver Fredyn. This solver has been validated trough manoeuvring tests in calm water, in regular and irregular waves (Quadvlieg et al., 2019). The simulations are conducted in 6 degrees of freedom with course and speed autopilots. Each simulation is one hour long. The simulation begins with the autopilot set to head seas to maximise the probability of appearance of parametric roll. A first simulation without any manoeuvre is performed. When parametric roll is detected on this first simulation prior half an hour, then the initial conditions (environmental, loading, speed) are memorised. Hereafter, those simulations without manoeuvre are denoted reference simulations. The time at which the parametric roll alarm rises on the reference simulation is denoted t_{Alarm}. When the Officer Of the Watch is warned of the appearance of parametric roll, 20 seconds are left to the crew to select and begin a manoeuvre (denoted hereafter t_{start}), Equation 126. The reference simulations are run again several times to assess the effects of all possible manoeuvres. The simulations prior t_{start} are strictly identical to the one of reference, then the possible manoeuvre is engaged. The manoeuvre assessed in this study are course alterations and speed modifications.

$$t_{start} = t_{Alarm} + 20 \qquad 126$$

5.1.1. Course alteration

A course alteration modifies the encounter period which is a key parameter of the appearance of parametric roll. Modifying the ship course of few degrees will not significantly modify the encounter period. Table 30 presents the course alterations assessed in this study.

Short Name	Course alteration [deg]
C+22.5	22.5
C+45	45
C+67.5	67.5
C+90	90

Table 30 - Course alterations

The turn ratio is validated prior to simulate course alterations. The course alterations are realised by modifying the heading setting in the autopilot at t_{start}. It is verified in calm water that a course alteration leads to a loss of speed which is compensated in a second time by the speed autopilot. As well the course alteration in calm water leads to heel. Thus, this course alteration is not exactly representative of the reality since the OOW would have to increase the propeller rotational speed while altering course to keep speed. In the simulation the action of the OOW on the engine is replaced by the speed autopilot. However, this permits to consider the efficiency of the course alteration independently of the speed modification.

Figure 75 provides an example of a 30 degrees course alteration simulated on the C11-class container ship in calm water. It is observed that the course autopilot permits to realise efficiently the course alteration. The speed begins to decrease when the vessel alters her course, then the speed autopilot compensates the loss to resume the speed. During this manoeuvre the C11 rolls up to about 2 degrees.

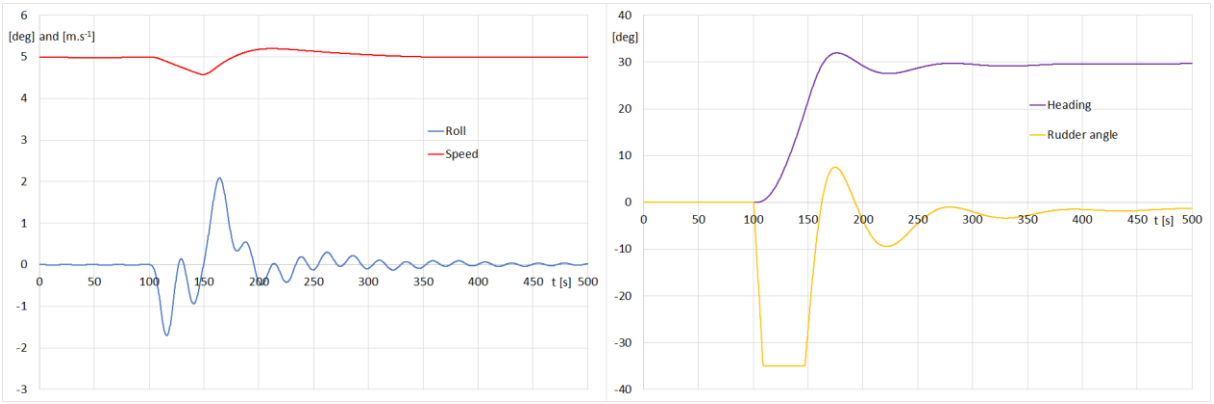

Figure 75 - Course alteration in calm water

5.1.2. Speed modification

The ship speed directly influences the encounter period, especially when sailing in head or following seas and then has a direct impact on the parametric roll response. The speed modification is realised by modifying the speed setting in the autopilot at t_{start}. The propeller rotational speed (in revolutions per minute, denoted by RPM) is consequently automatically adjusted. Thus, the vessel maximum speed is limited by maximum RPM of the engine. The engine loading sequence is not considered in this study. However, the resistance curve triggers the speed variation. Table 31 presents the speed modifications which are assessed in this study.

Short Name	Speed modification [m.s-1]	Comments
V+2.5	+2.5	Increases roll damping
V-2.5	-2.5	Reduces roll damping

Table 31 - Speed modifications

5.1.3. Assessment method, example on a single case

The manoeuvre assessment method has been validated and preliminary results were provided on a naval vessel and published within the scope of this thesis during the 18th International Ship Stability Workshop 2022 in Gdansk (Luthy et al., 2022b). In this sub-sub-section, an example of the manoeuvre assessment method and some results are presented on the C11-class container ship. In this example the discretisation of the course alteration has been increased and the value of the speed modification reduced. The ship's roll damping coefficients are calculated using Ikeda's method (Ikeda, 1978, Kawahara, 2009). The simulations are conducted on a sea state modelled with a Pierson-Moskowitz spectrum of significant height equal to 8 metres and of zero up crossing period equal to 12 seconds (peak period 16.9 seconds). A "cos^8" spreading function is considered (BV, 2019b) and a spreading angle of $\pm$ 90 degrees to simulate real sea state. The assessed manoeuvres are the one presented in Table 30 and Table 31.

The simulations are 5000 seconds long and begin with the autopilot set to head seas and the speed adjusted at 7.5 $m.s^{-1}$. A first simulation without any manoeuvre is performed, during which the first parametric roll detection alarm, using the method described in Chapter 4, rises at 1328.8 seconds (t_{Alarm}). The crew reaction time is added to calculate the time of the beginning of the manoeuvre (1348.8 s). The simulation is run again several times to assess the effects of all manoeuvres presented in Table 1 and Table 2.

Figure 76 presents the reference simulation and two manoeuvres with a course alteration of respectively 22.5 and 45 degrees. Figure 77 presents the reference simulation and two manoeuvres with a course alteration of respectively 45 and 90 degrees. Figure 78 presents the reference simulation and two manoeuvres with a speed modification of respectively + 2.5 and – 2.5 $m.s^{-1}$.

Table 32 presents results of the roll amplitudes reached during each simulation. Three roll amplitudes are presented. The first roll amplitude represents the maximum roll amplitude reached during the entire simulation and denoted by ΦSim. The second one represents the roll amplitude reached around t_{start} and denoted by ΦPR. The third one is the maximum roll amplitude reached once the manoeuvre is completed on the final part of the simulation and denoted by Φ2ndPart. On the reference time series ΦSim, ΦPR and Φ2ndPart are respectively denoted ΦSimRef, ΦPRRef, Φ2ndPartRef and are illustrated in Figure 76.

A comparison of those roll amplitudes with the ones observed on the reference simulation is provided in Table 33. The results are provided as a fraction of the amplitude observed on the roll time series of the reference simulation during the same time interval. The right column of Table 33 compares the roll amplitude reached during the final part of the simulation (Φ2ndPart) with the roll amplitude reached around t_{start} on the reference time series (PRRef).

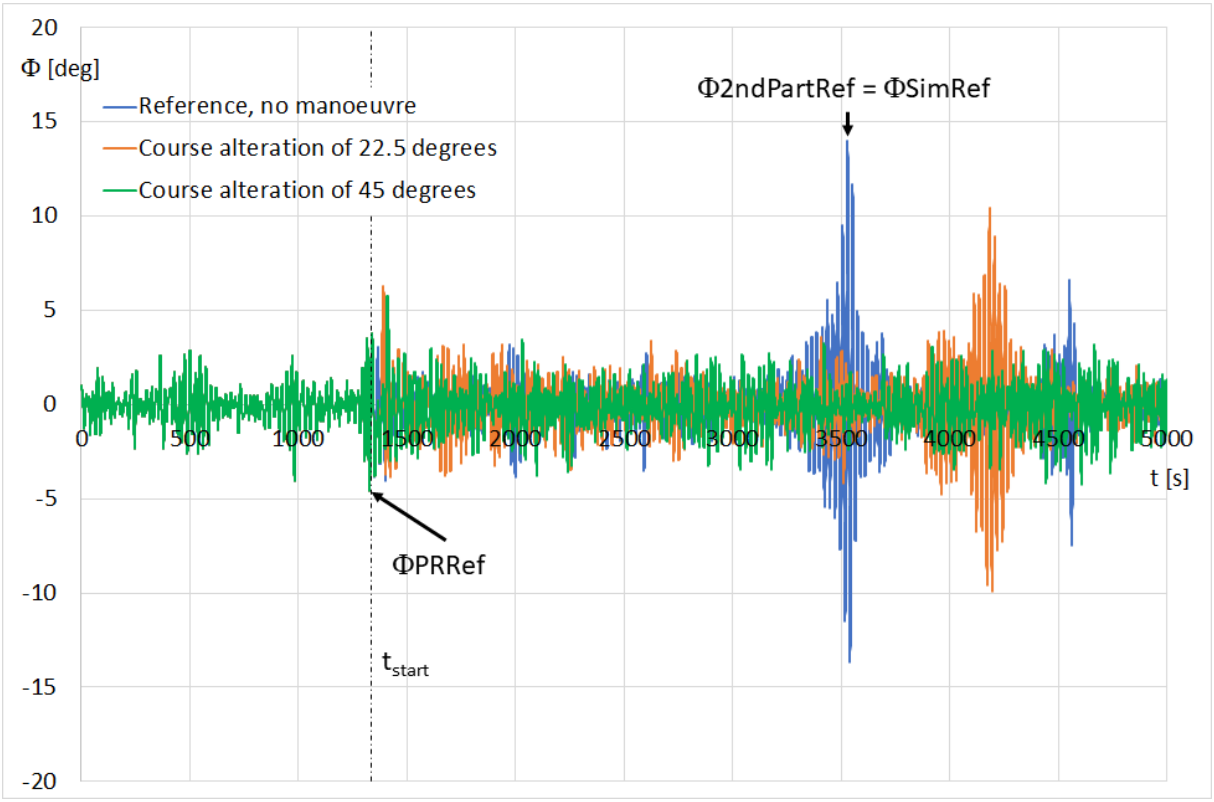

Figure 76 - Effect of limited course alterations on the roll motion

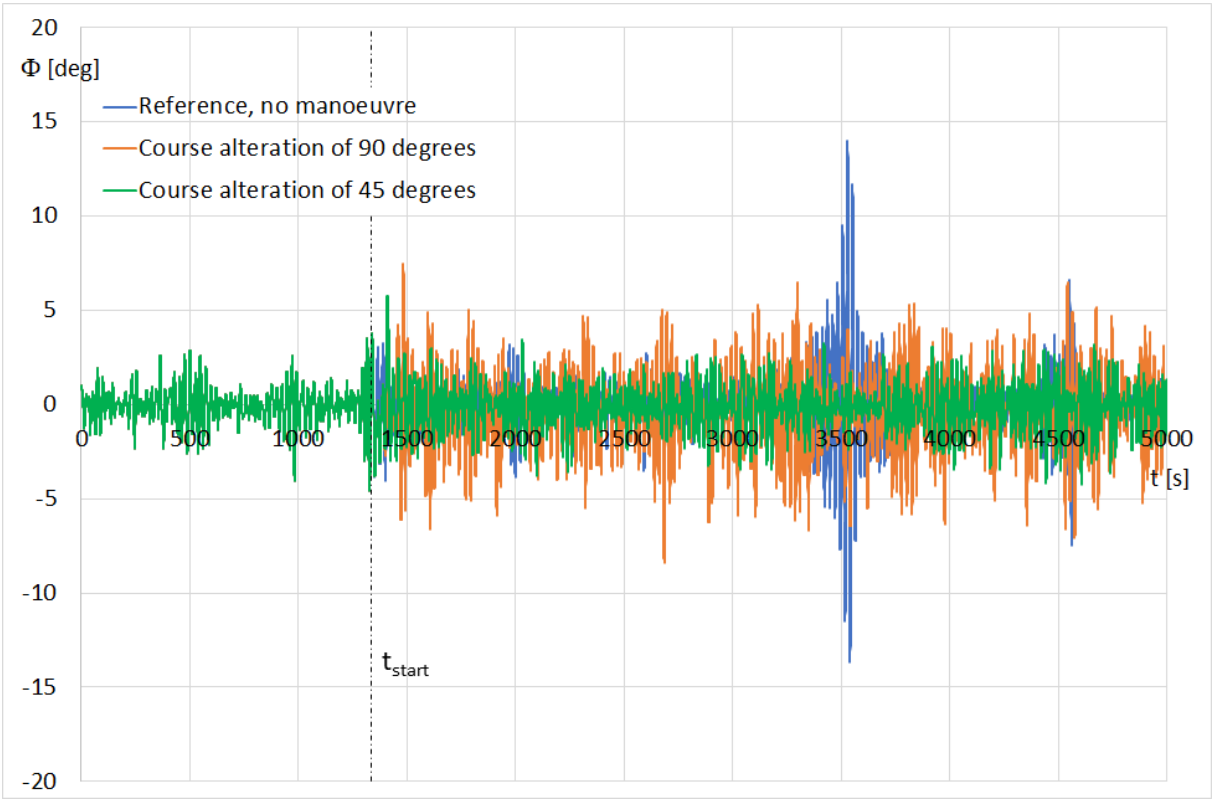

Figure 77 - Effect of large course alterations on the roll motion

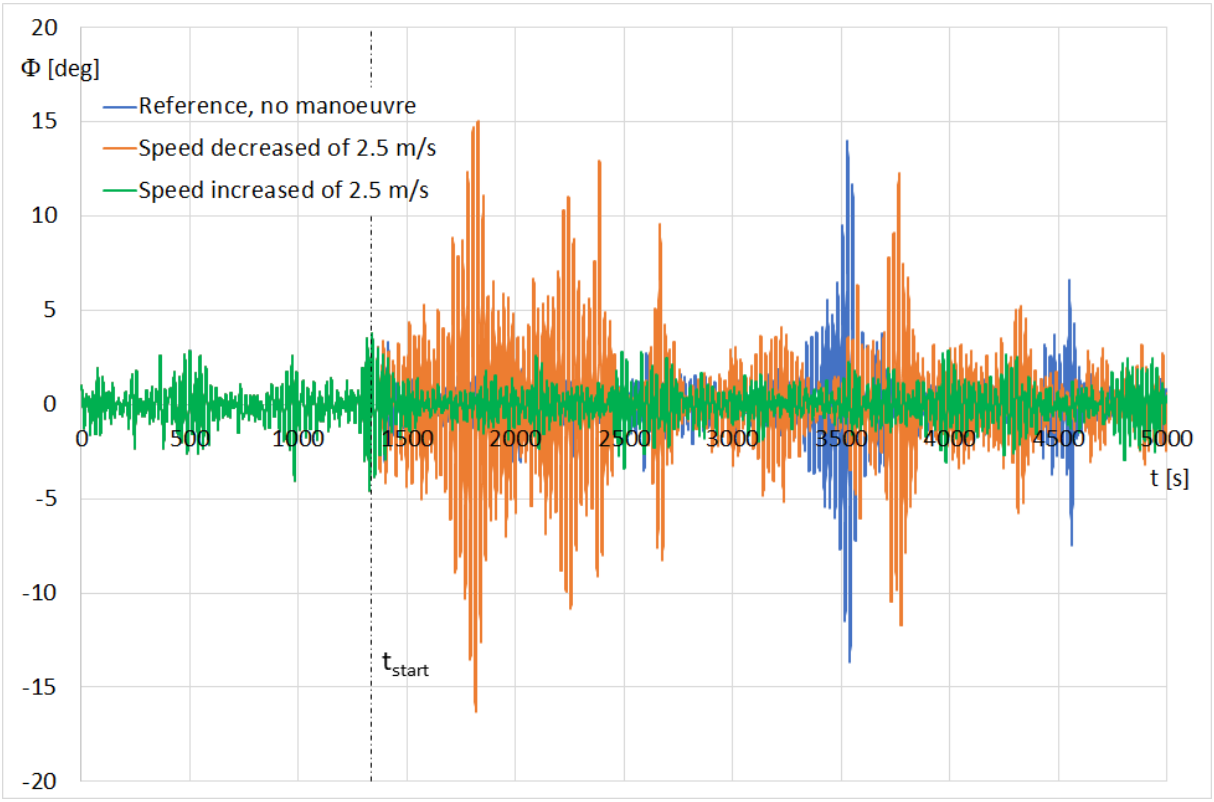

Figure 78 - Effect of speed modification on the roll motion

Sim	ΦSim [deg]	ΦPR [deg]	Φ2ndPart [deg]
Ref	13.97 = ΦSimRef	4.52 = ΦPRRef	13.97 = Φ2ndPartRef
C+22.5	10.46	6.24	10.46
C+45	5.73	5.73	4.20
C+67.5	6.91	4.52	6.91
C+90	8.36	4.52	8.36
V-2.5	16.26	4.52	16.26
V+2.5	4.52	4.52	3.43

Table 32 – Roll amplitudes

Sim	ΦSim / ΦSimRef	ΦPR / ΦPRRef	Φ2ndPart / Φ2ndPartRef	Φ2ndPart / ΦPRRef
Ref	100%	100%	100%	309%
C+22.5	75%	138%	75%	231%
C+45	41%	127%	30%	93%
C+67.5	49%	100%	49%	153%
C+90	60%	100%	60%	185%
V-2.5	116%	100%	116%	360%
V+2.5	32%	100%	25%	76%

Table 33 - Roll amplitudes relative to the ones of reference

It is observed in Figure 76, Figure 77 and Table 32 that the roll amplitude reached at the time of the manoeuvre (ΦPR) is large when a limited course alteration is realised. This may be due to the rapid modification of the rudder position.

Figure 76 shows that a course alteration of 22.5 degrees is not sufficient to avoid parametric roll to appear after manoeuvre is engaged, since another parametric roll episode is observed between 4000 and 4500 seconds. This parametric roll episode leads to roll amplitude more than twice larger than the one reached around t_{start}. However, the roll amplitude reached after the manoeuvre is 15 % smaller than the one reached on the reference simulation.

In this example, a course alteration of 45 degrees permits to avoid the appearance of severe roll motion due to parametric roll. The roll amplitude reached after the course alteration decreases significantly and no roll amplitude larger than the one reached at the time of the manoeuvre is observed. The roll amplitude reached after the manoeuvre is 70 % smaller than the one observed if no manoeuvre is engaged (Table 33).

Figure 77 shows that a course alteration of 90 degrees leads to larger roll motions than the ones observed after a course alteration of 45 degrees. A slight modification of the roll period is observed. Therefore, those heavy roll motions are not a consequence of parametric roll since the ship is sailing in beam sea. They may be due to the phenomenon of synchronous roll. A course alteration of 67.5 degrees (not displayed) leads as well to larger roll amplitudes than the one observed after a course alteration of 45 degrees (Table 32 and Table 33). This may be due to synchronous roll since the sea state is defined with spreading.

In this case, a course alteration may permit to avoid large roll amplitudes. A limited course alteration does not permit to avoid the appearance of parametric roll and a large course alteration may lead to synchronous roll.

Figure 78 shows that a speed reduction of 2.5 $m.s^{-1}$ leads to larger roll amplitudes than the ones of the reference (without manoeuvre). Even if the speed reduction alters the encounter period, the phenomenon of parametric roll still appears and leads to large roll motions, probably due to the roll damping reduction. In this case, when the ship increases her speed, no more parametric roll is encountered. The maximum roll amplitudes are significantly smaller than the one of reference (Table 32 and Table 33).

A modification of 2.5 $m.s^{-1}$ does not seem sufficient to alter the encounter period sufficiently to avoid the appearance of parametric roll. When the ship speed is reduced, the roll damping decreases, amplifying the roll motions. Thus, a speed reduction should be avoided. When the ship speed is increased, the roll damping increases consequently, limiting the ship roll motions. These results should be handled with care since the speed reduction and increase are simulated faster than in reality. Therefore, this speed increase would in reality present a longer transient state, during which the roll motion may be closer to the one of the reference simulation.

The effects of each manoeuvre have been separately assessed for this specific case in real sea state. It concludes that for the case presented in this sub-sub-section, the most effective manoeuvre is a course alteration of 45 degrees.

5.2. PROBABILITY OF AVOIDING THE WORSE ROLL AMPLITUDE

A single case, such as presented in Section 5.1.3, is not sufficient to state that a course alteration of 45 degrees is statistically the most relevant manoeuvre to execute when parametric roll appears. Thus, a statistical study is conducted to assess the efficiency of each manoeuvre with regard to parametric roll. This statistical study is conducted on the C11-class container ship. The simulations are realised for a wide spectrum of environmental and loading conditions. The loading conditions consider a draught of 12 metres and covers 46 values of KG varying from 16 to 19 metres. The environmental conditions are described for wave heights varying from 5 to 12 metres with a step of 1 metre and wave periods varying from 7 to 16 seconds with a step of 1 second. The

environmental conditions are modelized with a Pierson-Moskowitz spectrum. Three spreading angles are considered (0, $\pm$ 30 degrees and $\pm$ 90 degrees). The ship's speed varies from 4 to 10 $m.s^{-1}$ with a step of 0.5 $m.s^{-1}$. All combinations are not assessed; the combinations are selected to obtain a relevant probability of appearance of parametric roll. This selection is conducted with regards to the encounter frequency calculated from the peak wave period (peak of the spectrum). Thus, 50000 simulations are realised, within which 1703 present a parametric roll detection in the first half of the simulation and are consequently identified as reference simulations. The 1703 reference simulations are re-run with the manoeuvres executed 20 seconds after the parametric roll alarm (t_{start}, see Section 5.1.3). The 4 course alterations and the 2 speed modifications presented respectively in Table 30 and Table 31 (page 125) are executed, representing 10218 additional simulations.

Statistical results are presented as the percentage of time spent above several roll amplitude thresholds after the beginning of the manoeuvres (t_{start}), Table 34. Each percentage is calculated by dividing the total time of the 1703 simulations where roll amplitude exceeds the selected threshold after t_{start} by the total time of the 1703 simulations after t_{start}. The first line in Table 34 presents the results for the reference simulations (without manoeuvre). Those results without manoeuvre are considered to assess the global efficiency of each manoeuvre.

As presented in Table 34, a course alteration of 22.5 degrees reduces the time spent above the roll amplitude threshold of 25 degrees by about 30 %. The efficiency of this manoeuvre reduces as the considered roll amplitude threshold decreases. A course alteration of 45 degrees reduces significantly the time spent above all roll amplitude thresholds. The time spent above 5 degrees remains above 15 %. A course alteration of 67.5 degrees provides the best statistical results, reducing significantly the time spent above each roll amplitude threshold. A course alteration of 90 degrees provides statical results equivalent to the ones observed for a course alteration of 45 degrees. t_{start} is also considered to calculate these percentage in the reference simulations even if no manoeuvre is engaged.

Speed modifications also lead to significant results. When the speed is reduced by 2.5 $m.s^{-1}$, the time spent above 25 degrees is multiplied by almost 8, and by more than 3 above 15 degrees. Reducing the speed statistically increases the parametric roll amplitude in head seas. When the speed is increased by 2.5 $m.s^{-1}$, the parametric roll is significantly reduced. The time spent above 25 degrees is divided by 30, and by almost 12 above 15 degrees. A speed modification of 2.5 $m.s^{-1}$ significantly modifies both the encounter period and the roll damping, and therefore the parametric roll response. It is observed that a speed reduction should be avoided since it statistically increases the roll amplitude. It is observed that a speed increase permits to significantly reduce statistically the roll amplitude. However, it should be noted that this study does not consider the engine loading sequence, which can last 10 to 30 minutes for such a large container ship. Therefore, the speed increase should be considered as a long-term option since it is expected that its statistical results considering the engine loading sequence would be closer to the one without manoeuvre due to the longer speed increase.

In addition to this first statistical study, ΦSim, ΦPR and Φ2ndPart defined in Section 5.1.3 are identified on the 1703 reference simulations in which parametric roll has been detected prior 1800 seconds. This permits to compute statistical results considering each simulation independently from each other. In 38 % of the reference simulations, the maximum roll angle observed during the roll episode where parametric roll is detected is the maximum roll amplitude observed in the whole simulation (ΦSimRef = ΦPRRef). In 43 % of the reference simulations, the maximum roll amplitude reached after the time of the manoeuvre is lower than the one observed when parametric roll is detected (Φ2ndPartRef < ΦPRRef). Thus, for those cases, the manoeuvres

cannot reduce the maximum roll amplitude of the whole simulations, however some may be counterproductive.

Table 35 presents statistical results based on ΦSim, ΦPR and Φ2ndPart observed for each manoeuvre. In the first column, Φ2ndPart observed in each manoeuvre is compared to the one of its reference simulation (Φ2ndPartRef). As in the first statistical study, it is observed that the most efficient course alteration to reduce the roll motions is the one of 67.5 degrees. As well, a course alteration of 45 and 90 degrees present results equivalent to the ones of the first statistical study. Thus, in the opinion of the author, the most relevant course alteration which can operationally be realised is 45 degrees since it presents interesting statistical results and it deviates the ship from her original course less than 67.5 degrees. Indeed, a course alteration of 67.5 degrees is not operationally acceptable most of the time. A speed reduction reduces the maximum roll angle observed after the manoeuvre in only 7.6 % of the cases, while a speed increase reduces this angle in 91.7 % of the cases. Thus, it is statistically undeniable that a speed increase is a more relevant option than a speed reduction to counter parametric roll.

In the second column of Table 35, Φ2ndPart observed for each manoeuvre is compared to the roll amplitude reached around t_{start} on the reference simulations (Φ2PRRef). This permits to observe the probability of not encountering roll motions larger than the ones observed during the detection of parametric roll. It is observed that a course alteration of 67.5 degrees permits to avoid to encounter larger roll motions than the one encountered at the time of the detection in 76 % of the cases. Course alterations of 45 and 90 degrees permit to avoid to encounter larger roll motions than the one encountered at the time of the detection in 59 % of the cases. Those statistical results have to be considered with regards to the 43 % of the reference simulations for which the maximum roll amplitude in the second half of the simulation were lower than the ones at the time of the detection. Thus, course alterations of 45 and 90 degrees permit to avoid roll amplitudes larger than the ones at the time of the detection in 16 % additional cases. As well, a course alteration of 67.5 degrees permits to avoid roll amplitudes larger than the ones at the time of the detection in 33 % additional cases. However, it has to be noticed that a course alteration of 22.5 degrees may be counterproductive since the roll amplitudes reached after the manoeuvre are lower than the ones observed at the time of the detection in only 40 % of the cases. In other words, in 3 % of the cases altering course of 22.5 degrees leads to roll episodes larger than the ones observed when no manoeuvre is engaged. This result is masked in the first statistical study where it is observed that this course alteration provides encouraging results. Speed modifications of +2.5 $m.s^{-1}$ and -2.5 $m.s^{-1}$ permit to avoid larger roll motions than the ones encountered at the time of the detection in 87.1 % and 13.8 % of the cases, respectively. Reducing speed leads to larger roll amplitudes than without manoeuvre in 29.2 % of the cases (43 % - 13.8 %). Thus, this manoeuvre should be avoided. Increasing speed permits to avoid roll amplitudes larger than the ones at the time of the detection in an additional 4.1 % of the cases (47.1 % - 43 %). Thus, statistically a speed increase is recommended to avoid large roll motions due to parametric roll.

Finally, in the last column of Table 35, Φ2ndPart is compared to the maximum roll amplitude observed during the whole simulation (ΦSim). The largest roll amplitude reached after course alterations of 45 and 90 degrees are lower than the one of whole simulation in 61 % of the cases. As well, the largest roll amplitude reached after a course alteration of 67.5 degrees is lower than the one of whole simulation in 80.1 % of the cases. Thus, those course alterations permit statistically to reduce the appearance of large roll episodes. Statistical results observed for the speed modifications confirm the conclusions previously formulated.

	%t > 25 deg	%t > 20 deg	%t > 15 deg	%t > 10 deg	%t > 5 deg
Reference simulation	0.30%	1.06%	3.09%	8.14%	21.78%
Course alteration of 22.5 deg	0.19%	0.67%	2.15%	6.74%	22.95%
Course alteration of 45 deg	0.07%	0.17%	0.52%	2.28%	15.59%
Course alteration of 67.5 deg	0.05%	0.12%	0.26%	0.91%	8.42%
Course alteration of 90 deg	0.05%	0.15%	0.45%	2.08%	15.75%
Speed reduction of 2.5 $m.s^{-1}$	2.35%	5.80%	12.51%	24.74%	47.20%
Speed increase of 2.5 $m.s^{-1}$	0.01%	0.05%	0.26%	1.13%	5.10%

Table 34 - Percentage of time spent above the threshold after manoeuvres

	Φ2ndPart < Φ2ndPartRef	Φ2ndPart < ΦPRRef	Φ2ndPart < ΦSim
Ref	-	43.0 %	45.7%
C+22.5	46.8%	40.0%	41.9%
C+45	62.7%	59.1%	61.4%
C+67.5	70.7%	76.0%	80.1%
C+90	61.0%	59.0%	61.2%
V-2.5	7.6%	13.8%	17.6%
V+2.5	91.7%	87.1%	85.9%

Table 35 - Percentage of simulations for which the manoeuvre provided an improvement

This study permits to state that the most relevant manoeuvre considering both statistical and operational aspect to realise when parametric roll is detected is to come to 45 degrees of the main wave direction and to increase simultaneously the engine load to reduce as much as possible the speed loss due to the course alteration. As well this study permits to state that no speed reduction should be executed when parametric roll occurs. Thus, the habit of prudent captains to reduce speed when encountering heavy weather, reported by DNV (2005), statistically leads to larger motions in case of parametric roll.

This study also comes as an additional validation of the parametric roll detection method presented in Chapter 4. In the 1703 reference simulations without manoeuvre, the maximum roll amplitude is observed during the roll episode where parametric roll is detected or later in 92 % of the cases (ΦPRRef = ΦSimRef or Φ2ndPartRef = ΦSimRef). This shows that parametric roll is identified by the method before or at the time of the worse roll episode, with an acceptable relevance in the opinion of the author. The maximum roll angle is observed prior the parametric roll detection in only 8 % of the reference simulations.

This work has led to the development of an operational reaction guide for the benefit of CMA CGM, to help the Officer Of the Watch to understand the physics of the phenomenon of parametric roll and to provide an effective advice on immediate actions which could be engaged when parametric roll is encountered (Annex 2, confidential). The content of this reaction guide is in accordance with the needs identified from the results obtained from a survey conducted within the scope of this PhD thesis. The survey dealt with the knowledge of the seafarers on the topic of parametric roll. This survey has been answered by 230 seafarers (89 masters, 48 chief officers and 93 OOW) from CMA CGM. The reaction guide and the detailed results of the survey are confidential to CMA CGM.

CONCLUSION

Parametric roll is a rare stability failure in waves. It is counterintuitive since it appears in head or following seas where roll motions are expected to be the least. Those unexpected roll motions are the consequences of a periodical variation of the transverse stability in longitudinal waves. This phenomenon has led to some rare but remarkable container losses, with possible tremendous impacts on the reputation of the ship owner. The aim of the work reported in this PhD thesis is to improve the operational avoidance of parametric roll throughout a physical, statistical and operational study of the phenomenon.

Avoiding parametric roll requires several complementary assessments. Global assessment of the ship's vulnerability permits to estimate risk of encountering such phenomenon during the entire life of the vessel. Specific operational roll polar plots, realised from the results of 6-degree-of-freedom time-domain simulations, permit to avoid dangerous combinations of course and speed. Real-time ship motions assessment permits to qualify the roll motions as due to parametric roll or not. Those three assessments are studied within this PhD thesis. However, those assessments provide a statistical view of the vulnerability of the vessel with regards to parametric roll. They do not replace the immediate response engaged by the Officer Of the Watch. Thus, an operational reaction guide has been written within the scope of this PhD thesis. This reaction guide is intended to be used onboard by the Officer Of the Watch to prevent the appearance of parametric roll. It provides a brief description of the phenomenon and an effective advice on the general immediate actions to undertake when parametric roll develops.

An innovative energy method to calculate the amplitude of parametric roll in regular longitudinal waves at any speed, considering non-linear transverse stability, is presented. The energy method considers that the exciting energy is equal to the damping energy when a parametric roll steady state is reached. Considering the evolution of the energies leads to an easily understandable explanation of the phenomenon. An estimation of both energies is realised for several possible roll amplitudes and the steady state roll amplitude is obtained when both energies are equal. The estimation of the exciting energy is realised by calculating the area of the lobe described by $GZ(\varphi; t)$ in a $[\varphi; GZ]$ coordinate system. An estimation of the shift angle within the lock-in field (speed range within parametric roll appears) is required to calculate the lobe accurately. Fits of the shift angle, as a function of two parameters defining the shape of the GZ curves up to a possible roll amplitude, are built for several dimensionless speeds in the lock-in field. The fits are built from on a large number of simulations performed by a 1-degree-of-freedom time-domain solver considering different type of vessels. The fits permit to obtain a relevant estimation of the shift angle without simulation, and thus, of the exciting energy. The damping energy is estimated from both the half phase diagram and the roll damping coefficient. The energy method provides accurate results within its limits of use, especially for a ship of one of the types considered when building the fits of shift angle. The method provides as well relevant results for a ship of a type other than the ones used to build the fits of shift angle. The accuracy of the method can be improved for a single type of ship if the fits of the shift angle are especially built for it. This energy method can be seen as an alternative to the averaging method (IMO, 2015). The energy method considers the real GZ in longitudinal waves while the averaging method considers both the polynomial fit of a the mean GZ curve in waves and the metacentric height variation in waves. The energy method could also be submitted as an alternative to 1-degree-of-freedom time-domain simulations for the 2nd check of level 2 of the parametric roll criterion in the second-generation intact stability criteria (IMO, 2020a).

The building of roll polar plots requires a large amount of 6-degree-of-freedom simulations performed by a time-domain solver. The input data of these simulations shall be carefully chosen. An iterative method to calculate the roll damping coefficients to be set in the solver to reproduce roll decay time series obtained from other sources (model test, full-scale data, other time-domain solver) is presented. This method starts from an initial rough estimation of the roll damping coefficients to be set in the solver. Any known method can be used to realise this initial estimation. The iterative method can easily be implemented in any 1-degree-of-freedom time-domain solver. It provides very accurate roll damping coefficients to be set specifically in the time-domain solver. The desired accuracy of the method is triggered by the user. The number of iterations, and thus the computational time required to obtain the roll damping coefficients depends on this desired accuracy. Another method which permits to realise such iterative process in 6-degree-of-freedom solvers has been developed by DGA TH and led to a joint paper (Luthy et al., 2021a). The definition of the sea state is another fundamental input of the simulation. Classically the sea state provided in the IACS standard wave scatter diagram (IACS, 2001), or derived from it, are considered in global parametric roll assessments. This standard wave scatter diagram is designed for North Atlantic. However, some vessels sail in other specific areas. Thus, a study on the relevance of the wave scatter diagram for a specific sailing area is realised. This study is based on the open-access data provided by the European Copernicus Marine Service. It concludes that a customised scatter diagram for a specific sailing area, and optionally a seasonal period, can be produced easily from these open-access data. The definition of the sea state also includes its spreading on both sides of the main propagation direction. A study of the ship motions in both monodirectional and spread sea states is conducted to identify the most conservative spreading angle. This study is firstly conducted on regular waves, and then on real sea state modelized by a Pierson-Moskowitz spectrum. The spread sea states are calculated to develop an overall energy equal to the one of the reference monodirectional sea state. Results show that an increase of the spreading angle tends to increase the width of combinations of course and speed where heavy roll motions appear. However, the maximum roll angles reached for those combinations of course and speed (where parametric or synchronous roll may appear) decreases with the increase of the spreading angle. This study leads to the conclusion that the most conservative spreading angle is statistically ± 90 degrees. The loading condition of the vessel is another fundamental input of the simulation. The global assessment methods propose a selection of loading conditions (defined by both the draught and the transverse metacentric height) to realise operational roll polar plots. The relevance of this selection is discussed. The comparison between full-scale loading conditions, obtained from the shipowner, and the theoretical selection proposed by the global assessment methods shows that the relevance of the selection can be improved. A simple method to calculate the most representative loading conditions from the shipowner data is proposed.

Real-time detection of parametric roll is required to warn the Officer Of the Watch of the immediate danger. An innovative method to evaluate the risk of parametric roll in real time, based on the vessel motions, is proposed. This method requires the data provided by the inertial unit in real time as input. It is based on physical conditions required for parametric roll to appear. The first physical condition considers the ratio of the up-crossing roll period over the up-crossing pitch period. This ratio permits to identify the synchronism condition required for parametric roll to develop. The second physical condition considers the ratio of the peak roll period over the up-crossing roll period. This ratio permits to reduce false alarm rate when the motions are not due to parametric roll, especially in beam waves. The third physical condition considers the shift phase between the roll motion and the pitch motion. This angle permits to refine the detection of the phenomenon. An alarm is associated to the detection to warn the Officer Of the Watch of the immediate danger. The identification of parametric roll can be realised even for low amplitude, since the method does not require large motions to detect parametric roll. The method is tested

in longitudinal and beam seas in regular waves. This test shows that no parametric roll is detected in beam regular waves. The method and the associated alarm are validated in irregular seas on a large number of simulations in 5 degrees of freedom, providing relevant results. A statistical analysis of the simulation results shows an alarm detection rate in head seas larger than 80 % and a false-alarm rate in beam seas lower than 4 %. Finally, the method and the alarm are assessed on a full-scale case where parametric roll developed on a large container ship. The method presents a relevant identification of the periods during which parametric roll appeared. Further study can be conducted to reduce the false alarm rate by adapting the thresholds to each type of ship and hull.

The detection of parametric roll in real time permits to warn the Officer Of the Watch, who shall undertake an immediate manoeuvre to stop the amplification of the roll motion. A 6-degree-of-freedom study is conducted on a container ship to assess the effect of several manoeuvres engaged after parametric roll is detected in head or following seas. The method used to evaluate the effect of each manoeuvre is presented. A statistical study is conducted on the C11-class container ship. Four course alterations and two speed modifications are assessed. Results permit to state that operationally the most relevant manoeuvre to realise when parametric roll develops is to come to 45 degrees of the main wave direction and to increase simultaneously the engine load to reduce as much as possible the speed loss due to the course alteration. As well, they permit to state that no speed reduction should be executed, since it reduces the roll damping and may lead to even larger roll motions. On the contrary, a speed increase, when it is possible, statistically reduces significantly the roll motions.

This PhD thesis covered a large spectrum of the possible means to avoid parametric roll. It has led to the development of new methods to estimate and detect the phenomenon. It has permit to provide a validation of the most relevant manoeuvre to execute when parametric roll is detected, which led to the development of an operational reaction guide for the Officer Of the Watch. In the opinion of the author all available assessments should be used to avoid parametric roll.

The innovative energy method to calculate the amplitude of parametric roll, presented in Chapter 2, demonstrated that the transverse stability variation describes a lobe in a [φ; GZ] coordinate system when parametric roll develops. Thus, parametric roll may be detected in real time based the shape of the variation of the transverse stability during half a period. This idea was not further investigated in this PhD since no method exists to calculate the transverse stability accurately onboard in real time. If such method is developed, it may be interesting to implement it in the parametric roll detection. However, at this time, several operational real-time detection methods exist, such as the one developed in this PhD thesis. The method should be further validated on full-scale measurements, especially on container vessel during winter season. As well, a validation on a larger diversity of vessels could be conducted using 5 or 6-degree-of-freedom simulations. The thresholds considered in the detection method proposed in this PhD thesis could be improved by fitting them on a large data set to obtain a more accurate detection rate. This could be of high interest if the method is intended to be improved for a single hull shape. Such improvement requires other data sets to validate the revised method.

RESUME ETENDU

Introduction

En 2011, 4849 porte-conteneurs naviguent dans le monde, représentant une capacité de transport totale de 14,277,000 conteneurs équivalent vingt pieds (EVP), (BRS, 2011). Le 31 décembre 2021, 5515 navires porte-conteneurs naviguent dans le monde, représentant une capacité totale de 24,970,022 EVP (BRS, 2022). La capacité de transport totale a presque doublé en 10 ans tandis que le nombre de porte-conteneurs n'a augmenté que d'environ 14 %. Cette augmentation montre que la tendance est à la construction de navires ayant des capacités de plus en plus importantes. L'augmentation du nombre de conteneurs transportés par voie maritime augmente en conséquence les risques associées et les incidents. Ces incidents peuvent être parmi d'autres consécutifs à des incendies, des problèmes techniques ou des défaillances de stabilité (AGCS, 2022). Les défaillances de stabilité peuvent être consécutives à une erreur sur le chargement du navire, à une erreur humaine, ou à des conditions environnementales défavorables (mauvaise prédiction météorologique). Les conséquences liées à une défaillance de stabilité sont multiples. La conséquence la plus médiatisée est la perte de conteneur en mer. La perte de conteneurs peut être accentuée si le matériel de saisissage est en mauvais état ou si l'évaluation du risque est sous-estimée. Les fausses déclarations du poids des conteneurs est également un facteur aggravant sur le point d'être résolu par un amendement à la SOLAS obligeant le chargeur à déclarer le poids total du conteneur (IMO, 2020b, Chapitre 6 Règle n°2). C'est en se basant sur ces informations que le plan de chargement du navire est établi et que la stabilité est calculée. Cela permet alors de s'assurer que le navire respecte les critères de stabilité en vigueur. Toutefois, la stabilité statique du navire évolue lors du voyage, entre autres dû aux transferts de ballast, à la consommation de carburant. La stabilité dynamique évolue également, en fonction des conditions environnementales rencontrées. C'est en se basant sur cette condition de chargement théorique que le routage du navire est réalisé afin d'optimiser la consommation de carburant et d'éviter les zones où les conditions météorologiques seraient jugées inacceptables. Malgré ce routage, le navire peut rencontrer des conditions environnementales imprévues, pouvant conduire à de larges mouvements. L'OMI a reconnu la perte de conteneurs en mer comme une source de pollution lors de sa 6ème assemblée en décembre 2017 (CEREMA, 2021). Les coûts liés à la perte d'un conteneur en mer directement imputables à la compagnie peuvent être très importants. En conséquence, l'OMI, les compagnies de porte-conteneurs et les propriétaires de navires souhaitent réduire ensemble autant que possible le nombre de conteneurs perdus en mer. Toutefois, des accidents continuent de se produire. Certains sont imputables au phénomène de roulis paramétrique, bien que les critères de stabilité en vigueur soient respectés (IMO, 2020b). Parmi ces accidents, le premier remarquable fut celui du porte-conteneur de classe C11 *APL China* en 1995 (France et al., 2003), puis celui du porte-conteneur de classe-G Panama *Maersk Carolina* en 2003 (Carmel, 2006) ; celui du porte-conteneur *CMA CGM G. Washington* en 2017 (MAIB, 2020), ou encore celui du porte-conteneur *Maresk Essen* en 2021 (DMAIB, 2022). Ces accidents se sont produits dans des zones de navigation différentes (figure 2, page 14) et sur des porte-conteneurs de toutes tailles. D'autres accidents fortement médiatisés, ayant mené à la perte de conteneurs en mer, sont en cours d'investigation. Parmi ces accidents, l'un des plus remarquables est celui du porte-conteneur *ONE Apus* qui a perdu 1816 conteneurs lors d'un unique accident en 2020. Cet accident induit par une défaillance de stabilité dans les vagues pourrait atteindre un coût de 200 millions de dollars (IIMS, 2020). A chaque accident, le propriétaire et la compagnie maritime font face à des coûts importants liés à la marchandise perdue, à la durée de détention du navire, à la durée d'investigation, aux possibles pollutions et à la perte de réputation liée à la médiatisation de l'accident. En moyenne sur les 14 dernières années, 1629 conteneurs sont perdus en mer chaque année (figure 3, page 15, IMO, 2022). Les

compagnies maritimes, les propriétaires de navires, l'Organisation Maritime Internationale et les assureurs ont donc l'objectif commun de réduire le nombre de conteneurs perdus en mer. Cet objectif nécessite de prévenir les défaillances de stabilité dans les vagues telle que le roulis paramétrique.

Le phénomène de roulis paramétrique se développe majoritairement lorsque le navire se trouve mer de face ou de l'arrière, alors que c'est dans ces situations que le commandant (ou l'officier chef de quart) se sent le plus en sécurité. Des méthodes permettant d'évaluer la vulnérabilité du navire vis-à-vis de ce phénomène et d'autres permettant d'aviser le commandant du risque sont nécessaires. Plusieurs types d'évaluation du risque de roulis paramétrique existent.

L'évaluation globale de la vulnérabilité du navire permet d'estimer statistiquement le risque de rencontre du roulis paramétrique durant la vie entière du navire. Cette évaluation peut être basée sur des relations empiriques considérant les caractéristiques du navire, ou sur des simulations du comportement du navire dans les vagues. Cette évaluation globale ne permet pas d'éviter le phénomène opérationnellement ; toutefois, elle permet de qualifier la vulnérabilité du navire vis-à-vis de celui-ci. Ce type d'évaluation est privilégié dans le cadre réglementaire (IMO, 2020a).

L'évaluation en temps réel des mouvements du navire permet de détecter l'apparition du roulis paramétrique. Les méthodes de détection associées ne sont généralement pas spécifiques à un navire. Elles peuvent donc être utilisées directement sur tous navires équipés d'une centrale inertielle. Ce type d'évaluation permet de qualifier les mouvements du navire et d'amorcer les manœuvres nécessaires. Toutefois, en fonction de la méthode utilisée, le phénomène peut être détecté alors que des mouvements de roulis importants sont déjà présents. Si aucun signe précurseur ne laisse présager de la survenue du phénomène ou si le phénomène se développe alors que les mouvements sont déjà importants, alors les manœuvres peuvent ne pas être engagées suffisamment tôt pour être efficaces.

Finalement, une évaluation des mouvements du navire dans les vagues peut être réalisée en utilisant un simulateur hydrodynamique considérant jusqu'à 6 degrés de liberté. Cette évaluation, permet de réaliser des polaires de roulis opérationnelles présentant l'angle de roulis maximum calculé pour des conditions environnementales et de chargement données. Les procédures associées à cette évaluation permettent de générer un catalogue de polaires de roulis, alors que le navire n'a pas encore pris la mer. Le maillage complet du navire est nécessaire à cette évaluation. Afin de générer les polaires de roulis, des conditions de chargement et des conditions environnementales représentatives doivent être sélectionnées. Une polaire de roulis est calculée pour chaque combinaison de condition de chargement et de condition environnementale, nécessitant une puissance de calcul importante. Cette évaluation ne prend pas en compte les conditions réellement rencontrées. En conséquence, les polaires sont utilisées pour éviter les combinaisons de cap et vitesse conduisant aux mouvements les plus importants.

L'objectif du travail effectué dans le cadre de cette thèse est d'améliorer la prévention opérationnelle du phénomène de roulis paramétrique au travers d'une étude physique, statistique et opérationnelle du phénomène. La prévention du risque de roulis paramétrique nécessite l'utilisation de plusieurs méthodes d'évaluations complémentaires. L'évaluation des mouvements du navire en temps réel permet de qualifier leur cause. Lorsque les mouvements du navire sont consécutifs au roulis paramétrique, la manœuvre la plus adéquate devrait immédiatement être entreprise. Dans cette optique, la stratégie est de développer une nouvelle méthode de détection du phénomène et d'identifier la manœuvre la plus adéquate. La prévention du risque peut également être réalisée en amont par la création de polaire de roulis qui seront utilisées opérationnellement afin d'éviter les combinaisons de cap et vitesse les plus dangereuses. L'étude de certains paramètres d'entrées des simulations temporelles nécessaires à la réalisation d'un

catalogue de polaire de roulis est réalisée. Enfin, opérationnellement, même si ces méthodes permettent de prévenir et d'alerter du risque d'apparition du phénomène, seul l'officier chef de quart en passerelle a la capacité de réagir lorsque le phénomène se développe. Dans cette optique, des recommandations opérationnelles sont formulées au travers d'un guide de réaction à destination des officiers chef de quart (annexe 2).

Dans le premier chapitre, le phénomène de roulis paramétrique ainsi que l'état de l'art des méthodes d'évaluation de la vulnérabilité du navire vis-à-vis de ce phénomène sont présentés. Dans le second chapitre, une méthode énergétique innovante permettant de calculer l'amplitude de roulis paramétrique atteinte en régime permanent sur mer longitudinale régulière quelle que soit la vitesse d'avance du navire en considérant les variations non-linéaires de la stabilité transversale, sans simulation, est présentée. Les résultats sont validés par comparaisons avec ceux obtenus dans un simulateur temporel 1 degré de liberté. Dans le troisième chapitre, des études portant sur la pertinence de certaines données d'entrées utilisées dans les simulateurs hydrodynamiques temporel en 6 degrés de libertés, est présenté. Dans le quatrième chapitre, une nouvelle méthode de détection du roulis paramétrique se basant sur les données issues de la centrale inertielle du navire est présentée. Dans le cinquième chapitre, une étude de l'efficacité de plusieurs manœuvres qui peuvent être réalisées par l'officier chef de quart lorsque le phénomène de roulis paramétrique est détecté est présentée. La manœuvre la plus pertinente est identifiée.

1. Etude de la vulnérabilité des navires face au roulis paramétrique

1.1. La physique du roulis paramétrique

Le phénomène de résonance paramétrique est étudié depuis longtemps en mécanique (Sanmartín Losada, 1984), en mathématiques (Mathieu, 1868), et en optique (Giordmaine, 1965). Froude (1861) démontre que ce phénomène peut théoriquement s'appliquer aux navires, conduisant à une augmentation rapide de l'amplitude de roulis. Lorsqu'un navire fait route dans les vagues, il subit une variation de sa stabilité transversale. Lorsque la fréquence de cette variation est le double de la fréquence de roulis naturelle du navire (équation 1 page 19, condition de synchronisme), alors le phénomène de roulis paramétrique peut se développer, à condition que l'amortissement soit suffisamment faible. Le phénomène de roulis paramétrique est principalement rencontré lorsque le navire se trouve mer de face ou mer de l'arrière, puisque c'est dans ces conditions que la variation de stabilité transversale est la plus importante. La vitesse d'avance théorique correspondant à la condition de synchronisme paramétrique peut être calculée pour une vague donnée (équation 2 page 19, notée V_{PR}). Toutefois, il est démontré analytiquement que le roulis paramétrique peut apparaître pour une plage de vitesse étendue (Grinnaert, 2017, annexe 3). Cette plage de vitesse est nommée domaine d'accrochage (figure 5, page 21).

1.2. Les simulations temporelles

L'équation différentielle de Mathieu (Mathieu, 1868) peut être utilisée pour modéliser le roulis. Lorsque le navire se trouve sur une mer longitudinale, il n'y pas d'excitation directe. L'équation linéarisée (équation 9, page 22) ou délinéarisée (équation 10, page 23) obtenue en 1 degré de liberté peut être résolue numériquement avec une précision acceptable par la méthode Runge-Kutta. Cette méthode a été implémentée dans un tableur (annexe 7), permettant de simuler le comportement du navire en roulis (1 degré de liberté). D'autres solveurs hydrodynamiques plus complexes prennent en compte les couplages entre les différents degrés

de libertés (figure 10, page 26) et permettent de reproduire numériquement avec une grande fidélité les mouvements du navire (équation 13, page 26). Le solveur hydrodynamique Fredyn (CRN, 2021) développé par le CRNav et MARIN est utilisé dans le cadre de cette thèse. Ce solveur considère les non-linéarités liées aux efforts de radiation et de diffraction. Ce solveur a été validé par comparaison avec d'autres solveurs hydrodynamiques (Kapsenberg et al., 2019 ; Kapsenberg et al., 2020).

1.3. Evaluation globale de la vulnérabilité du navire

Plusieurs évaluations globales de la vulnérabilité du navire vis-à-vis des défaillances de stabilité ont été développées. Les accidents liés aux défaillances de stabilité à l'état intact ont conduit à développer de nouveaux critères réglementaires prenant en compte la stabilité dynamique du navire. Les critères de seconde génération de stabilité à l'état intact (IMO, 2020a) ont été développés dans ce sens. Ils prennent en compte les défaillances de stabilité suivantes :

- Le navire privé d'énergie
- Les accélérations de roulis excessives
- La perte pure de stabilité
- Le roulis paramétrique
- La perte de manœuvrabilité en mer de l'arrière

Pour chaque défaillance de stabilité dynamique, ces critères présentent trois niveaux d'évaluation et des recommandations opérationnelles. Pour satisfaire aux critères de seconde génération, le navire doit satisfaire à un niveau pour chaque défaillance de stabilité (figure 11, page 29). La complexité de mise en œuvre et la précision augmente à chaque niveau d'évaluation. N'importe quel niveau peut être mis en œuvre en premier pour évaluer la vulnérabilité du navire. Le premier niveau se base sur une approche déterministe simplifiée procurant une grande marge de sécurité. Le second niveau se base sur une approche probabiliste considérant la physique du phénomène et réduisant la marge de sécurité. Le troisième niveau se base sur une approche probabiliste de l'apparition du phénomène. Il nécessite des simulations réalisées grâce à des solveurs hydrodynamiques ou des essais en bassin. Ce niveau nécessite l'expertise d'un laboratoire hydrodynamique. Si le navire est évalué comme sensible au phénomène étudié et que la forme de carène ne peut être modifiée, alors des mesures opérationnelles peuvent être imposées (limite de zone de navigation, de conditions environnementales rencontrés …). Le premier niveau de l'évaluation de la vulnérabilité du navire vis-à-vis du phénomène de roulis paramétrique considère la variation de la stabilité transversale sur une vague sinusoïdale et l'amortissement au roulis. Le second niveau est scindé en deux sous-niveaux. Le premier sous-niveau vérifie la probabilité de survenue du phénomène sur un ensemble de vagues sinusoïdales. La qualification de la vulnérabilité pour chaque vague consiste à vérifier que la variation de stabilité ne soit pas suffisante pour conduire au phénomène de roulis paramétrique ou que le navire ne peut pas atteindre la vitesse de synchronisme paramétrique (V_{PR}). Le second sous-niveau consiste à réaliser des simulations en un degré de liberté sur mer de l'avant et de l'arrière pour plusieurs vitesses en considérant un ensemble de vagues sinusoïdales équivalentes (Grim, 1961) pour chaque état de mer figurant dans l'atlas de vague de l'IACS (2001). La probabilité que le navire rencontre une vague conduisant au phénomène de roulis paramétrique est calculée et doit être inférieure au seuil réglementaire. Le troisième niveau consiste à réaliser un ensemble de simulations et\ou d'essais en bassin sur état de mer réel afin de calculer la probabilité d'apparition du phénomène de roulis paramétrique.

La procédure NR 667 du bureau Veritas (BV, 2019b) propose de réaliser un catalogue de polaires de roulis pouvant être utilisé opérationnellement et permettant d'éviter les combinaisons de cap

et vitesse menant à de grands angles de roulis. La réalisation de ces polaires nécessite l'utilisation d'un solveur hydrodynamique. Une sélection des conditions de chargement type est déduite des conditions de chargement du manuel de stabilité. La sélection des états de mer est réalisée en se basant sur l'atlas de vague de l'IACS (2001) et en calculant une enveloppe des états de mer pour une période de retour de 25 ans. L'amplitude de roulis maximum est comparée au maximum admissible par le matériel de saisissage, calculé conformément aux prescriptions de la NR 625 (BV, 2020a). Cette comparaison permet de fournir des polaires bichromes présentant les combinaisons de cap et vitesse pour lesquelles le navire risquerait de perdre des conteneurs en mer.

Le bureau Américain des transports (ABS) a également émis une procédure permettant de qualifier la vulnérabilité du navire vis-à-vis du phénomène de roulis paramétrique (ABS, 2019). Cette procédure est divisée en trois niveaux. Le premier niveau consiste en une étude statique, basée sur des formules empiriques et considérant une unique condition environnementale. La condition environnementale est modélisée par une vague sinusoïdale dont les caractéristiques correspondent à la plus forte probabilité de survenue du roulis paramétrique. Si le navire ne satisfait pas au premier niveau alors le second niveau doit être évalué. Le second niveau consiste en une étude des mouvements du navire en un degré de liberté. Plusieurs conditions de chargement sont considérés. L'état de mer est celui utilisé au niveau un. Si l'amplitude de roulis observé lors d'une simulation est supérieure à 15 degrés alors le niveau trois devra être évaluée. Le niveau trois consiste à réaliser des polaires de roulis. Ce niveau ne peut être conduit sans l'approbation préalable des conditions de chargement et ses conditions environnementales par ABS.

1.4. Evaluation en temps réel

À la suite de l'accident de l'APL China (France et al., 2003) et du Maersk Carolina (Carmel, 2006), tous les deux imputés au roulis paramétrique, les assureurs et les propriétaires de navires ont demandé de prendre des mesures afin d'éviter que ce type d'accident ne se reproduisent (Dølhie, 2006), avec pour objectif de développer des solutions opérationnelles permettant de réduire significativement la fréquence et la gravité de ces accidents. Trois solutions sont considérées. Le routage des navires permet d'éviter les zones les plus dangereuses. En se basant sur les prédictions météorologiques, les tempêtes, les cyclones et autres phénomènes rares peuvent être évités. Le routage peut être réalisé en se basant sur des éléments physiques représentant les conditions environnementales (hauteur des vagues, force du vent), sur la consommation de combustible ou sur la prédiction des mouvements du navire (figure 18, page 51). Une autre solution proposée par l'OMI est la formation et la sensibilisation des équipages aux phénomènes rares à travers la circulaire 1228 (IMO, 2007a). Cette circulaire permet une estimation du risque d'apparition de ces phénomènes rares par l'officier chef de quart en se basant sur les conditions qu'il\elle mesure en temps réel. Les recommandations présentes dans cette circulaire peuvent être intégrées dans des logiciels embarqués permettant de faciliter l'utilisation et l'interprétation de celles-ci. D'autres logiciels embarqués permettent d'évaluer le risque de roulis paramétrique en temps réel en se basant sur les mouvements du navire, tel que "SeaSense Monitoring" (Nielsen et al., 2006) et "OCTOPUS Resonance" (Acomi et al., 2016). Ces méthodes utilisent les données fournies par la centrale inertielle présente à bord pour évaluer le risque. Différentes approchent ont été envisagées afin de garantir une détection fiable avec un taux de fausse alarme le plus bas possible (Acanfora et al., 2018 ; Galeazzi, 2014; González at al., 2011; Holden et al. 2007; McCue and Bulian, 2007; Yu et al., 2018). Une fois implémentée à bord, ces méthodes temps réel permettent d'informer l'officier chef de quart du risque de roulis paramétrique. Cette évaluation du risque de roulis paramétrique en temps réel permet d'engager des contre-mesures lorsque le phénomène se développe.

2. Méthode énergétique

Ce chapitre présente une méthode innovante de calcul de l'amplitude de roulis paramétrique en régime permanent sur mer régulière longitudinale, en faisant l'hypothèse d'une variation non-linéaire de la stabilité transversale, sans simulation. Cette méthode a été présentée à travers deux articles publiés lors de la conférence STAB&S (Luthy et al., 2021b) et dans le journal Ocean Engineering (Luthy et al., 2022c).

2.1. Introduction

La méthode innovante de calcul de l'amplitude de roulis paramétrique en régime permanent se base sur les travaux de Kerwin (1955) et de Grinnaert et al. (2017). Kerwin a montré que cette amplitude est atteinte lorsque l'énergie d'excitation est égale à l'énergie d'amortissement (figure 20, page 55). Grinnaert et al. (2017) ont développés une méthode permettant de calculer cette amplitude en faisant l'hypothèse d'un GZ linéaire, au synchronisme paramétrique. Une première tentative d'extension de la méthode à l'ensemble du domaine d'accrochage est conduite par Grinnaert et al. (2017, équation 76 page 56).

2.2. Variation de la stabilité transversale

La variation de la stabilité transversale dans les vagues dépend à la fois des conditions extérieures et de la forme de la carène. Lorsque le navire se trouve à un angle de roulis maximum ($\varphi_{max.n}$), alors sa vitesse de roulis et son énergie cinétique sont nulles. L'énergie potentielle est égale à l'aire sous la courbe de GZ multipliée par le poids du navire (IMO, 1985). En faisant l'hypothèse d'un GZ linéaire, une absence d'amortissement et une variation instantanée de la stabilité transversale lorsque le navire se trouve à $\varphi_{max.n}$ et à gîte nulle (courbe de GZ_{min} de l'équilibre à φ_{max}, courbe de GZ_{max} de φ_{max} à l'équilibre), il est possible de calculer analytiquement l'angle de roulis jusqu'auquel le navire s'inclinera sur l'autre bord ($\varphi_{max.n+1}$, équation 79, page 57). Le même raisonnement est conduit en faisant l'hypothèse d'un GZ non-linéaire (figure 24, page 59). Lorsque l'hypothèse de la variation de la stabilité transversale instantanée est levée, le point GZ(φ,t) décrit un lobe sur une demi-période de roulis (figure 25, page 60). En faisant l'hypothèse d'un GZ linéaire, le ratio entre l'aire développée par le lobe (équation 84, page 60) et l'aire développée entre les courbes de GZ extrêmes est analytiquement défini et égal à $\pi/4$ (équation 85, figure 26, page 61).

2.3. Angle de décalage

L'hypothèse d'un roulis sinusoïdal est formulée lorsqu'un régime permanent de roulis paramétrique est atteint (équation 86, page 61). Il a été observé que la variation de stabilité peut ne pas être en phase avec les mouvements de roulis. Ce déphasage est appelé angle de décalage (α) et introduit dans l'équation de la variation de stabilité (équation 87, page 62). L'angle de décalage déforme le lobe décrit par GZ(φ; t) and le référentiel [φ; GZ] (figure 29 à figure 31, page 62). Il exerce donc une influence directe sur l'énergie fournie par les vagues au navire. Plus l'angle de décalage est éloigné de $\pi/2$, moins l'énergie apportée par les vagues au navire est importante.

L'analyse des résultats de simulation pour plusieurs navires au synchronisme paramétrique dans différentes conditions de chargement montre que l'angle de décalage est lié à la forme des courbes de GZ sur vagues. Deux coefficients ont été définis pour caractériser la forme des courbes de GZ jusqu'à une amplitude de roulis en régime permanent (Φ). Les deux coefficients sont

désignés par "MEAN" et "OPEN". Le coefficient MEAN, caractérise la linéarité de la courbe de GZ moyenne jusqu'à l'amplitude Φ (équation 89, figure 34, page 65). Le second coefficient OPEN, caractérise l'ouverture des courbes de GZ déphasé d'une demi-longueur d'onde et développant la plus grande aire (désigné par GZ_{UP} et GZ_{LOW}) (équation 90, figure 35, page 66).

L'angle de décalage peut être calculé à la fin de chaque simulation si un régime permanent est atteint (équation 91, page 67). L'évolution de l'angle de décalage en fonction de la vitesse du navire dans le domaine d'accrochage de roulis paramétrique est étudiée. Afin de pouvoir comparer les résultats obtenus pour plusieurs navires, conditions de chargement et conditions environnementales, la vitesse du navire est rendue adimensionnelle dans le domaine d'accrochage (désignée par γ, équation 92, page 67).

L'angle de décalage et les coefficients MEAN et OPEN sont calculés sur un grand nombre simulations réalisées pour un large spectre de navires dans des conditions de chargement et des conditions environnementales différentes, pour plusieurs vitesses adimensionnelles dans le domaine d'accrochage. Les points [α, MEAN, OPEN, γ] ainsi obtenu constituent une base de données de référence. Une surface est développée sur ces points de référence pour chaque vitesse adimensionnelle. Chaque surface est approximée par une équation polynomiale d'ordre trois en deux dimensions (équation 93, figure 38, page 68) dont les paramètres sont optimisés par la méthode des moindres carrées. Les paramètres de l'équation polynomiale sont fournis page 69 pour plusieurs vitesses adimensionnelles. Ces paramètres ont été optimisés sur un ensemble de points de référence obtenus pour six porte-conteneurs, un RoRo,un RoPax, et un tanker.

2.4. Méthode

Les hypothèses formulées lors de l'utilisation de la méthode énergétique sont les suivantes :

1. Le navire est symétrique et son centre de gravité est situé sur la ligne de foi
2. Les mouvements de roulis sont sinusoïdaux lorsqu'un régime permanent de roulis paramétrique est atteint
3. Le navire fait route à vitesse constante sur une mer régulière
4. Le navire roule à la moitié de la fréquence de rencontre dans l'ensemble du domaine d'accrochage (Grinnaert et al., 2017)
5. L'énergie d'excitation est égale à l'énergie d'amortissement lorsqu'un régime permanent de roulis paramétrique est atteint (Kerwin, 1955; Grinnaert et al., 2017)
6. L'amortissement au roulis est non-linéaire, il peut être estimé en utilisant une méthode simplifiée (Ikeda, 1978; Kawahara, 2009)

Le phénomène de roulis paramétrique peut conduire à de larges mouvements de roulis. En conséquence, l'OMI à travers les critères de seconde génération (IMO, 2020a) et Peters et al. (2015) recommandent de considérer les non-linéarités des courbes de GZ lors de l'évaluation de la vulnérabilité du navire en roulis paramétrique. De ce fait, la méthode énergétique développée dans le cadre de cette thèse prend en compte les non-linéarités des courbes de GZ, augmentant la précision de la méthode. Les hypothèses 1,3 et 6 sont également formulé lors de l'évaluation de vulnérabilité au roulis paramétrique de niveau 2 des critères de stabilité à l'état intact de seconde génération (IMO, 2020a).

L'énergie d'excitation à la vitesse adimensionnelle du navire est estimée pour toutes les amplitudes de roulis possible. Pour chaque amplitude, les coefficients MEAN et OPEN sont calculés à partir des courbes de GZ sur vagues. L'angle de décalage est estimé en utilisant ces coefficients (équation 91, page 67) et la surface polynomiale bâtie sur les points de référence. L'angle de décalage ainsi estimé permet de tracer le lobe. L'aire du lobe est calculée numériquement.

L'énergie d'excitation est obtenue en multipliant cette aire par le poids du navire (équation 96, page 71).

L'énergie d'amortissement à la vitesse d'avance adimensionnelle du navire est estimée pour les mêmes amplitudes de roulis possible que l'énergie d'excitation. L'hypothèse d'un roulis sinusoïdal permet de définir analytiquement le demi-diagramme de phase (vitesse de roulis en fonction de l'angle de roulis) sur une demi-période (figure 39, page 72). L'aire du demi-diagramme de phase est l'image de l'énergie d'amortissement. L'énergie d'amortissement peut donc être exprimée analytiquement (équation 99, page 71). Elle requière une estimation de l'amortissement en fonction de l'amplitude de roulis. Cette estimation peut être réalisée par n'importe que méthode (telle que la méthode d'Ikeda (Ikeda et al., 1978; Kawahara et al., 2009)).

Le régime permanent apparait lorsque l'énergie d'amortissement est égale à l'énergie d'excitation. L'amplitude de roulis correspondante (Φ) peut être obtenue graphiquement (figure 20, page 55) ou calculée numériquement. La méthode énergétique fournit une solution instable à 0 degré et une solution stable à Φ. Dans certains cas, il se peut qu'aucune intersection entre la courbe d'énergie d'excitation et la courbe d'énergie d'amortissement n'apparaisse. Dans ces cas, l'amplitude de roulis paramétrique en régime permanent est inférieure à l'amplitude la plus faible évaluée si l'énergie d'amortissement est supérieure à l'énergie d'excitation. Inversement, si l'énergie d'excitation est supérieure à l'énergie d'amortissement alors l'amplitude de roulis paramétrique en régime permanent est supérieure à l'angle maximum évalué.

2.5. Résultats

Les résultats obtenus avec la méthode énergétique sont comparés à ceux obtenus à l'issue de simulations conduites en 1 degré de liberté.

Il a été démontré analytiquement que l'aire du lobe est égale à $\pi/4$ fois l'aire entre les courbes de GZ jusqu'à Φ en faisant l'hypothèse d'un GZ linéaire. Les résultats montrent que ce ratio n'est pas exact lorsque l'on fait l'hypothèse d'un GZ non linéaire. Toutefois, les résultats montrent que la valeur de $\pi/4$ est conservative. Une méthode énergétique simplifiée considérant ce ratio conservatif pourrait donc être utilisée dans un cadre réglementaire comme premier niveau. La méthode énergétique simplifiée ne nécessite pas d'estimation de l'angle de décalage.

Les résultats obtenus avec la méthode énergétique considèrent les paramètres d'approximation de l'angle de décalage fournis page 69. La méthode énergétique fournit des résultats précis pour les navires utilisés comme référence pour calculer les paramètres de l'approximation de l'angle de décalage (figure 41 et figure 42, page 78). Les résultats obtenus avec méthode énergétique pour des navires qui n'ont pas été utilisés pour calculer les paramètres de l'approximation de l'angle de décalage présentent une précision acceptable (figure 43, page 79). La précision de la méthode décroît aux limites du domaine d'accrochage, en raison d'une plus faible qualité de l'approximation de l'angle de décalage pour ces vitesses. De plus, une légère différence peut apparaître entre les bornes du domaine d'accrochage calculées analytiquement (GZ linéaire) et celles observées lors des simulations (GZ non linéaire). Toutefois, dans certain cas, la méthode énergétique ne permet pas d'obtenir la précision attendue. Cela peut être dû à une estimation non pertinente de l'angle de décalage (figure 44, page 80). La méthode énergétique ne doit pas être utilisée si le GM minimum sur vague est inférieur à 0.2 mètre. La méthode énergétique pourrait être utilisée dans un cadre réglementaire pour évaluer la sensibilité des navires vis-à-vis au phénomène de roulis paramétrique.

3. Evaluation des données d'entrée des simulateurs temporels

3.1. Estimation des coefficients d'amortissement

L'estimation des coefficients d'amortissement avec précision est indispensable à toute étude quantitative des mouvements de roulis du navire. L'amortissement peut être estimé par des méthodes empiriques, par l'intermédiaire de modélisations numériques, par des essais en bassin ou des essais réels. Les coefficients d'amortissement peuvent être fournis sous la forme d'un terme linéaire B_{Lin} et d'un terme quadratique B_{Quad}. B_{Lin} à une influence prédominante lorsque les mouvements de roulis sont faibles et B_{Quad} à une influence prédominante lorsque les mouvements de roulis sont importants. Une nouvelle méthode itérative permettant de reproduire des essais d'extinction de roulis est présentée (Luthy et al., 2021a). Cette méthode a pour objectif d'estimer avec précision les coefficients d'amortissement B_{Lin} et B_{Quad} à utiliser dans un simulateur temporel. Une première estimation de ces coefficients est nécessaire, elle peut être réalisée à l'aide de n'importe quelle méthode connue. Le processus itératif est conduit en reproduisant l'extinction de roulis de référence. Le coefficient d'amortissement linéaire est modifié à chaque étape du processus itératif jusqu'à ce que l'amplitude finale de l'extinction de roulis simulée soit identique à celle de référence, puis le coefficient d'amortissement quadratique est modifié jusqu'à ce que l'amplitude des pics soit identique (figure 46, page 86). La précision de la méthode est définie par l'utilisateur en faisant varier la tolérance des valeurs cibles (amplitude de roulis finale et amplitude des pics). Cette méthode à l'avantage de fournir des résultats précis et de ne pas dépendre du modèle utilisé dans le simulateur. La qualité de l'estimation de l'amortissement dépend donc majoritairement de la source de l'extinction de roulis de référence.

3.2. Etats de mer

L'état de mer est un paramètre clef d'entrée des simulations temporelles. Les procédures d'évaluation globale de la vulnérabilité du navire considèrent en général les probabilités d'apparition des états de mer fournies dans l'atlas de vagues de l'IACS (2001) ou dans un atlas dérivé de celui-ci. Cet atlas a été bâti sur des observations réalisées dans l'Atlantique Nord. Toutefois, certains navires ne navigueront jamais dans cette zone. C'est pourquoi une étude de la pertinence des atlas de vagues réalisés à partir de données satellitaires libres d'accès fournies par le Service Européen Marin de Copernicus est réalisée. Les observations satellitaires ne couvrent pas l'entièreté du globe en permanence. Ces observations sont utilisées pour recalibrer un modèle global des Océans. La pertinence de la donnée fournie par ce modèle est validée par le Service Européen Marin de Copernicus par comparaison avec des données mesurées localement. L'étude montre que cette donnée permet de réaliser des atlas de vagues pour des zones données et optionnellement des saisons spécifiques. Un atlas de vagues pour la zone Atlantique Nord a été bâti (présentés page 93) dans le cadre d'un projet de fin d'étude (Gnalo et al., 2020 en utilisant ces données et comparé à celui fourni par l'IACS (2001), confirmant la pertinence de la méthode et de la base de données utilisée pour la génération d'atlas de vagues. Les atlas de vagues générés pour des zones précises ou des saisons particulières pourraient être utilisés pour l'évaluation de la vulnérabilité des navires dans le cadre des mesures opérationnelles des critères de seconde génération à l'état intact (IMO, 2020a).

3.3. Etalement directionnel

La définition de l'état de mer inclut également son étalement sur les deux côtés de la direction principale de propagation des vagues. Une étude des mouvements du navire est conduite à la fois sur un état de mer monodirectionnel et sur état de mer étalé afin d'identifier l'angle d'étalement

directionnel le plus conservatif pour la réalisation de polaires de roulis. Cette étude est conduite dans un premier temps sur mer régulière, puis sur des états de mer réels modélisés avec un spectre de Pierson-Moskowitz (équation 105, page 95 Les paramètres de l'état de mer étalé sont calculés pour que l'énergie totale développée soit égale à celle développée par l'état de mer monodirectionnel de référence. La première étude est conduite sur mer régulière sinusoïdale. L'énergie développée par la vague sinusoïdale monodirectionnelle est analytiquement définie (équation 104, page 94) et est proportionnelle au carré de la hauteur de la vague. Un état de mer étalé est défini par N vagues dont la direction et la hauteur sont calculées pour développer ensemble la même énergie que la vague monodirectionnelle de référence. Le calcul de la hauteur de chaque vague est réalisé en considérant l'aire sous la fonction d'étalement et la proportionnalité entre l'énergie et la hauteur de vague (Figure 52, équation 109, page 96). La modélisation des états de mer est validée dans le solveur hydrodynamique par comparaison avec leur description analytique (équation 111, page 97). Des polaires de roulis sont réalisées sur le navire porte-conteneur C11 (figure 56 à figure 58, page 102). Les résultats montrent que le nombre de combinaisons de cap et vitesse où le phénomène de roulis paramétrique peut apparaître augmente avec la valeur de l'étalement directionnel. Statistiquement l'angle d'étalement directionnel le plus conservatif est $\pm$ 90 degrés. Cette étude a été présentée lors de l'ISSW 2022 (Luthy et al., 2022a). Une étude similaire est conduite en considérant un état de mer réel modélisé avec un spectre de Pierson-Moskowitz comme référence (figure 59 à figure 61, page 105). Cette étude sera présentée lors des Journées de l'Hydrodynamiques en novembre 2022 (Luthy et al., 2022e). Les résultats montrent les angles maximums atteints en roulis paramétrique ou en roulis synchrone diminuent avec l'augmentation de l'étalement directionnel. Toutefois, cette étude complémentaire permet de conclure également que l'angle d'étalement directionnel le plus conservatif est statistiquement $\pm$ 90 degrés.

3.4. Conditions de chargement

La condition de chargement du navire est une autre donnée d'entrée fondamentale des simulations. Les méthodes d'évaluation globale de la vulnérabilité du navire proposent une sélection des conditions de chargement (définies par le tirant d'eau et la hauteur métacentrique transversale) afin de réaliser des polaires de roulis. La pertinence de cette sélection est discutée. La comparaison des conditions de chargement opérationnellement rencontrées fournies par le propriétaire ou l'exploitant du navire avec les conditions de chargement théoriques proposées lors de l'évaluation globale de la vulnérabilité du navire montre que la pertinence de cette sélection peut être améliorée. Il est proposé d'établir une sélection de conditions de chargement pertinente basée sur les données fournies par le propriétaire ou l'exploitant du navire. Cette sélection est réalisée en utilisant la courbe moyenne des cas de changement (figure 62, page 107). Si le nombre de conditions de chargement doit encore être réduit, la sélection est réalisée en calculant le barycentre des conditions présentes dans un intervalle de GM fixé (figure 63, page 107).

4. Amélioration de la détection du roulis paramétrique en temps réel

L'étude des mouvements du navire en temps réel permet de détecter l'apparition du phénomène de roulis paramétrique. Une nouvelle méthode de détection basée sur des conditions physiques nécessaire au développement du roulis paramétrique est présentée. Cette méthode a été soumise au Journal of Ship Research (Luthy et al., 2022d).

4.1. Méthode

La méthode de détection est basée sur trois conditions nécessaires à l'apparition du roulis paramétrique. Trois coefficients C1, C2 et C3 reflètent chacun l'une de ces conditions. Ces coefficients sont adimensionnés par les coefficients, respectivement nommées $\widehat{C1}$, $\widehat{C2}$ et $\widehat{C3}$, variant de 0 à 1. Chaque condition est nécessaire à l'apparition du phénomène. Les coefficients sont donc équipondérés. En conséquence, le coefficient global C utilisé pour la détection est la multiplication des trois coefficients $\widehat{C1}$, $\widehat{C2}$ et $\widehat{C3}$. Le coefficient C1 est basé sur le ratio de la période de roulis de passage à l'équilibre croissant ($T_{UP.\varphi}$) sur la période de tangage de passage à l'équilibre croissant ($T_{UP.\theta}$), figure 65 page 112. Ce ratio reflète la condition de synchronisme paramétrique (IMO, 2007a). Le coefficient C1 est calculé en utilisant une loi normale d'espérance 2 (ratio des périodes menant au synchronisme paramétrique) et d'écart-type 0.25 (équation 116, page 111), puis adimensionné (équation 117, page 111). Le coefficient C2 est basé sur le ratio de la période de pic de roulis sur la période de roulis de passage à l'équilibre croissant. Il a été observé que lorsque le phénomène de roulis paramétrique se développe, seuls un pic négatif et un pic positif apparaissent durant période de roulis de passage à l'équilibre croissant. Ce ratio permet donc de réduire la fréquence des fausses alarmes lorsque de larges mouvements de roulis ne sont pas causés par le roulis paramétrique, particulièrement lorsque le navire est mer de travers (le temporel de roulis présente plusieurs pics négatifs ou positifs durant une période, figure 66 page 113). Le coefficient C3 est basé sur l'angle de décalage entre les mouvements de roulis et de tangage (figure 67, page 114). Lorsque le phénomène de roulis paramétrique se développe, le décalage entre les signaux tends à être nul. Le coefficient C3 est calculé en utilisant une loi normale d'espérance nulle d'écart type variable égale à la période de roulis de passage à l'équilibre croissant ($T_{UP.\varphi}$) divisé par 8 (équation 124, page 114), puis adimensionné (équation 125, page 114). Une alarme est associée à la détection afin d'avertir l'officier chef de quart du danger immédiat. L'officier est alerté lorsque le coefficient C est supérieur à 0.4 durant au moins 15 secondes ou la moitié de la période de roulis (la plus grande des deux valeurs). Un seuil d'amplitude est associé à l'alarme. L'alarme ne sera effective que si l'amplitude de roulis est supérieure à trois degrés.

4.2. Tests et validations en mer régulière et irrégulière

La méthode de détection du roulis paramétrique est testée sur mer régulière de face (figure 68, page 116) et de travers (figure 69, page 117). La détection du roulis paramétrique est correctement réalisée en mer régulière de face et le coefficient C ne dépasse pas le seuil de 0.4 en mer régulière de travers. La méthode et l'alarme associée sont ensuite testées sur un état de mer réel de face (figure 70, page 118) et de travers (figure 71, page 118). Les épisodes de roulis paramétrique sont correctement identifiés en mer de face et aucune alarme de roulis paramétrique n'est émise lorsque des mouvements de roulis importants sont observés en mer de travers. La méthode et l'alarme associée sont validées par une étude statistique sur un grand nombre de résultats de simulations en 5 degrés de liberté sur le porte-conteneur C11. Une hystérésis sur l'amplitude de roulis est introduite, pour dénombrer les épisodes de roulis et éviter de compter un même épisode de roulis à plusieurs reprises (figure 72, page 119). Le taux d'alarme observé lorsque le navire est mer de face est supérieur à 80 %, validant quantitativement la détection du roulis paramétrique en mer de face. Le taux de fausse alarme observé lorsque le navire est mer de travers est inférieur à 4 %, validant qualitativement la discrimination entre les mouvements induits par le phénomène de roulis paramétrique de ceux induits par d'autres phénomènes (roulis synchrone ou autre).

4.3. Validation à échelle réel

La pertinence de la méthode et de l'alarme est évaluée en utilisant des données à échelle réelle obtenues sur un porte-conteneur. Au regard des conditions de navigation, le phénomène de roulis paramétrique est selon l'auteur la cause des larges mouvements de roulis observés. Le système embarqué qualifie également les mouvements du navire comme étant imputable au roulis paramétrique. La méthode proposée dans cette thèse permet une identification pertinente des épisodes de roulis paramétrique (figure 74, page 122).

5. Manœuvres d'évitement du roulis paramétrique

Le DNV à rapporter que en cas de mauvais temps conduisant à de forts mouvements de roulis un commandant prudent viendrait face à la mer et réduirait sa vitesse (DNV, 2005). Toutefois, c'est lorsque le navire est face à la mer que le phénomène de roulis paramétrique à la plus grande probabilité de se développer.

L'identification du phénomène de roulis paramétrique permet d'alerter l'officier chef de quart du danger immédiat. Il\Elle devrait immédiatement entreprendre une manœuvre permettant de stopper l'amplification paramétrique des mouvements de roulis. Une étude de l'efficacité des différentes manœuvres pouvant être engagées est réalisée.

5.1. Méthode d'évaluation des manœuvres

La méthode d'évaluation de l'efficacité des manœuvres ainsi que sa mise en œuvre sur un navire militaire pour un cas unique ont été présentées lors de l'ISSW 2022 (Luthy et al., 2022b).

Les officiers et commandant s'interrogent régulièrement naturellement sur l'efficacité qu'aurait eu une manœuvre si elle avait été engagée. Toutefois, évaluer l'efficacité d'une manœuvre face au phénomène de roulis paramétrique ne peut pas être réalisé à échelle réelle. Cette évaluation peut être réalisée grâce à des simulations. Une simulation sur état de mer réel peut être réalisée plusieurs fois de manière identique si les conditions initiales et la distribution des phases d'état de mer sont connues. Il est donc possible de reproduire à l'identique le début d'une simulation puis d'engager une manœuvre pour en constater l'effet. Les manœuvres étudiées sont un changement de cap de 25, 45, 67.5 et 90 degrés ainsi qu'une modification de la vitesse de plus ou moins 2.5 $m.s^{-1}$. Lorsqu'une simulation mer de l'avant est réalisée et que la méthode de détection présentée au chapitre 4 alerte sur le développement du phénomène du roulis paramétrique, alors la simulation est reconduite de manière identique et 20 secondes après l'alarme une manœuvre est engagée (temps de réaction de l'équipage). Les valeurs de l'amplitude de roulis au moment de la détection, sur le reste et sur l'ensemble de la simulation sont relevées et permettent d'évaluer l'efficacité des différentes manœuvres. Un exemple, réalisé sur le navire porte-conteneur de classe C11, sur un état de mer réel est présenté (figure 76, figure 77, figure 78, page 126). Dans cet exemple, un changement de cap d'au moins 45 degrés est nécessaire pour éviter l'apparition du roulis paramétrique. Une augmentation de la vitesse permet également de limiter l'apparition du phénomène tandis qu'une réduction de vitesse augmente significativement l'apparition et l'intensité du phénomène. Une étude statistique est nécessaire pour valider ces conclusions.

5.2. Etude probabiliste de l'efficacité des manœuvres

Une base de données composée de 50000 simulations d'une heure, conduites en 6 degrés de liberté sur le navire porte-conteneur de classe C11, en mer de face, pour différentes conditions de

chargement et conditions environnementales est réalisée. La méthode de détection du roulis paramétrique présentée au chapitre 4 est utilisée. Dans cette base de données, 1703 simulations présentent des mouvements de roulis ayant conduit à la détection du roulis paramétrique durant la première moitié de la simulation. Ces 1703 simulations sont reconduites de manière identique jusqu'à la détection du roulis paramétrique, puis 20 secondes après l'alarme une manœuvre est engagée. Les manœuvres évaluées sont celles présentés dans l'exemple ci-dessus (4 changements de cap, 2 modifications de vitesse), représentant 10218 simulations supplémentaires. Statistiquement un changement de cap de 45 degrés et de 90 degrés ont une efficacité équivalente. Toutefois, venir à 90 degrés de la direction principale de la houle peut conduire à l'apparition du phénomène de roulis synchrone. Statistiquement, venir à 67.5 degrés de la direction principale des vagues permet de réduire le plus significativement les mouvements de roulis. Statistiquement, réduire la vitesse augmente significativement l'amplitude des mouvements de roulis, tandis qu'une augmentation de la vitesse les réduit significativement. Opérationnellement, modifier le cap de 67.5 degrés peut ne pas être chose aisée. De même, une augmentation de la vitesse peut nécessiter un temps trop important. Au vu des résultats statistiques, lorsque le phénomène roulis paramétrique est détectée l'auteur recommande de modifier le cap pour venir à 45 degrés de la direction principale des vagues et d'augmenter simultanément la vitesse pour au minimum compenser la perte de vitesse liée à l'abattée.

Conclusion

L'objectif du travail effectué dans le cadre de cette thèse est d'améliorer la prévention opérationnelle du phénomène de roulis paramétrique au travers d'une étude physique, statistique et opérationnel du phénomène. La prévention du roulis paramétrique repose sur plusieurs évaluations complémentaires. L'évaluation globale de la vulnérabilité du navire permet d'estimer le risque de rencontre du phénomène durant la vie entière du navire. Des polaires de roulis, réalisées à partir de simulations temporelles conduites en 6 degrés de liberté, permettent d'éviter les combinaisons dangereuses de cap et de vitesse. L'évaluation en temps réel des mouvements du navire permet de qualifier si ceux-ci sont consécutifs au roulis paramétrique. Ces trois types d'évaluation sont étudiées dans cette thèse de doctorat. Toutefois, ces évaluations fournissent une représentation statistique de la vulnérabilité du navire. Elles ne remplacent pas la réponse immédiate qui peut être engagée par l'officier chef de quart. C'est pourquoi un guide de réaction opérationnelle a été écrit dans le cadre de cette thèse (annexe 2). Ce guide de réaction est destiné à être utilisé à bord par les officiers chef de quart afin de prévenir de l'apparition du roulis paramétrique et de réagir en conséquence lorsque celui-ci se développe. Il fournit une description rapide du phénomène et des conseils sur les contre-mesures à engager lorsque le phénomène se développe.

Une méthode énergétique innovante permettant de calculer l'amplitude de roulis paramétrique atteinte en régime permanent sur mer longitudinale régulière quelle que soit la vitesse d'avance du navire en considérant les variations non-linéaires de la stabilité transversale, sans simulation, est présentée. Cette méthode énergétique considère que l'énergie d'excitation est égale à l'énergie d'amortissement lorsque le régime permanent est atteint. Une estimation de l'énergie excitation et de l'énergie d'amortissement est réalisée pour toutes les amplitudes de roulis possibles, et l'amplitude en régime permanent est obtenue lorsque les deux énergies sont égales. L'estimation de l'énergie d'excitation est réalisée en calculant l'aire du lobe décrit par $GZ(\varphi; t)$ dans le référentiel $[\varphi; GZ]$. Une estimation de l'angle de décalage dans le domaine d'accrochage (plage de vitesse dans laquelle le phénomène de roulis paramétrique apparaît) pour calculer le

lobe avec précision est nécessaire. Cette estimation de l'angle de décalage est réalisée en se basant sur une approximation polynomiale de troisième ordre, fonction de deux paramètres définissant la forme des courbes de GZ jusqu'à l'amplitude de roulis considérée. L'approximation permet d'obtenir une estimation pertinente de l'angle de décalage sans simulation, et donc de l'énergie d'excitation. L'énergie d'amortissement est estimée à partir du demi-diagramme de phase et des coefficients d'amortissement. La méthode énergétique fournit des résultats pertinents dans ses limites d'utilisations. La précision de la méthode peut être améliorée pour un type de navire particulier si l'approximation polynomiale de l'angle de décalage est bâtie en utilisant des résultats de simulation obtenus pour ce type de navire. Cette méthode énergétique peut être vu comme une alternative à la méthode de résolution analytique nommée "averaging method" (IMO, 2015). La méthode énergétique considère le GZ réel sur houle longitudinale alors que la méthode de résolution analytique ("averaging method") considère une approximation polynomiale de la courbe de GZ moyenne sur vague et la valeur de la variation de la hauteur métacentrique dans les vagues. La méthode énergétique pourrait être soumise comme alternative aux simulations temporelles 1 degré de liberté mis en œuvre lors du 2ème contrôle du niveau 2 du critère de roulis paramétrique des critères de stabilité à l'état intact de seconde génération (IMO, 2020a).

La création de polaires de roulis requière un grand nombre de simulations en 6 degrés de libertés conduite avec un simulateur hydrodynamique temporel. Les données d'entrée de ces simulations doivent être choisies précautionneusement. Une méthode itérative permettant de calculer les coefficients d'amortissement à imposer dans un simulateur temporel afin de reproduire des extinctions de roulis obtenues à partir d'autres sources (essai en bassin, essai taille réelle, résultat provenant d'autres simulateurs temporels) est présentée. Cette méthode débute avec une première estimation grossière de l'amortissement au roulis à imposer dans le simulateur. Le processus itératif fournit une valeur des coefficients d'amortissement précise à imposer spécifiquement dans le simulateur temporel utilisé. La précision de la méthode est déterminée par l'utilisateur. Le nombre d'itérations et donc le temps de calcul nécessaire pour obtenir les coefficients d'amortissement dépendent de la précision désirée. Une autre méthode permettant de réaliser un procédé itératif dans un simulateur hydrodynamique 6 degrés de liberté a été développée par la Direction Générale de l'Armement (DGA TH) et a conduit à la rédaction d'un article commun (Luthy et al., 2021a). La définition de l'état de mer est une autre entrée fondamentale des simulateurs temporels hydrodynamiques. De manière classique, les états de mer présentés dans l'atlas de vagues fourni par l'Association Internationale des Société de Classes (IACS, 2001), ou dérivé de celui-ci, sont considérés lors de l'évaluation globale de la vulnérabilité du navire vis-à-vis du risque de roulis paramétrique. Cet atlas de vagues a été conçu à partir de données provenant d'observations en Atlantique Nord. Toutefois, certains navires naviguent dans d'autres régions. C'est pourquoi une étude de la pertinence des atlas de vagues construits pour des zones spécifiques est réalisée. Cette étude se base sur des données accessibles en libre accès, fournies par le Service Européen Marin de Copernicus. Cette étude conclut que des atlas de vagues réalisés pour des zones spécifiques, et optionnellement pour des saisons spécifiques, peuvent être construits à partir de cette donnée. La définition de l'état de mer inclut également son étalement des deux côtés de la direction principale de propagation des vagues. Une étude des mouvements du navire est conduite à la fois sur état de mer monodirectionnel et sur état de mer étalé afin d'identifier l'angle d'étalement directionnel le plus conservatif pour la réalisation de polaires de roulis. Cette étude est conduite dans un premier temps sur mer régulière, puis sur des états de mer réels modélisés par un spectre de Pierson-Moskowitz. Les paramètres de l'état de mer étalé sont calculés pour que l'énergie totale développée soit égale à celle développé par l'état de mer monodirectionnel de référence. Les résultats montrent que l'étalement directionnel tend à augmenter le nombre de combinaisons de cap et vitesse où de larges amplitudes de roulis peuvent

apparaître. Toutefois, les angles maximums de roulis atteints pour ces combinaisons de cap et vitesse (où du roulis paramétrique ou du roulis synchrone peut survenir) diminuent avec l'étalement directionnel. Cette étude permet de conclure que l'angle d'étalement directionnel le plus conservatif est statistiquement $\pm$ 90 degrés. La condition de chargement du navire est une autre donnée d'entrée fondamentale des simulations. Les méthodes d'évaluation globale de la vulnérabilité du navire proposent une sélection réduite de conditions de chargement (définies à la fois par le tirant d'eau et par la hauteur métacentrique transversale) afin de réaliser des polaires de roulis opérationnelles. La pertinence de cette sélection est discutée. La comparaison des conditions de chargement opérationnellement rencontrées, fournies par le propriétaire ou l'exploitant du navire, avec les conditions de chargement théoriques proposés lors de l'évaluation globale de la vulnérabilité du navire montre que la pertinence de cette sélection peut être améliorée. Une méthode de calcul simple permettant d'établir une sélection des conditions de chargement pertinente se basant sur les données fournies par le propriétaire ou l'exploitant du navire est proposée.

La détection du phénomène de roulis paramétrique en temps réel est nécessaire afin d'avertir l'officier chef de quart du danger immédiat. Une méthode innovante de détection du roulis paramétrique en temps réel, se basant sur les mouvements du navire, est proposée. Cette méthode utilise comme entrée les données provenant de la centrale inertielle. La méthode est basée sur trois conditions physiques nécessaire à l'apparition du phénomène de roulis paramétrique. Une alarme est associée à la détection afin d'avertir l'officier chef de quart du danger immédiat. Le roulis paramétrique peut être détecté même pour de faibles amplitudes de roulis. La méthode est testée sur mer régulière de face et de travers. Puis, la méthode et l'alarme sont validées sur état de mer réel sur un grand nombre de résultats de simulations en 5 degrés de libertés, fournissant des résultats pertinents. Une analyse statistique des résultats de simulations montre que le taux de détection en mer de face est supérieur à 80 % et que le taux de fausse-alarme est inférieur à 4 %. Finalement, la pertinence de la méthode et de l'alarme est évaluée en utilisant des données réelles obtenues sur un porte-conteneur ayant subit un épisode de roulis paramétrique. La méthode permet une identification pertinente des épisodes de roulis paramétrique. Des études complémentaires peuvent être conduites pour réduire le taux de fausse-alarme en adaptant les seuils pour chaque type de navire et forme de carène.

La détection du roulis paramétrique en temps réel permet d'avertir l'officier chef de quart du danger, qui devrait alors engager immédiatement une manœuvre afin de stopper l'amplification des mouvements de roulis. Une étude en 6 degrés de liberté est conduite sur un navire porte-conteneur afin d'évaluer l'efficacité de plusieurs manœuvres qui peuvent être engagées lorsque le phénomène de roulis paramétrique est détecté en mer de face ou de l'arrière. La méthode utilisée pour évaluer l'efficacité des manœuvres est présentée. Une étude statistique est conduite sur le navire porte-conteneur de classe C11. Quatre modifications de cap et deux modifications de vitesse sont évaluées. Les résultats montrent que la manœuvre la plus pertinente à effectuer lorsque le phénomène de roulis paramétrique se développe est de venir à 45 degrés de la direction principale des vagues et de réduire simultanément autant que possible la perte de vitesse liée au changement de cap. De plus, cette étude montre qu'aucune réduction de vitesse ne devrait être entreprise, puisqu'une telle manœuvre réduit l'amortissement au roulis et pourrait alors conduire à des mouvements de roulis plus importants. Au contraire, une augmentation de la vitesse, lorsqu'elle est possible, réduit statistiquement de manière significative l'amplitude de roulis.

Cette thèse de doctorat couvre un large spectre des différents moyens permettant de prévenir l'apparition du roulis paramétrique. Cette thèse a mené au développement de nouvelles

méthodes permettant d'estimer la sévérité du roulis paramétrique et de détecter le phénomène. Cette thèse a permis d'identifier la manœuvre la plus pertinente à exécuter lorsque le phénomène de roulis paramétrique est détecté. Cela a mené au développement d'un guide de réaction à destination des officiers chefs de quart.

La méthode énergétique innovante permettant de calculer l'amplitude de roulis paramétrique, présenté au Chapitre 2 démontre que la variation de la stabilité transversale dans les vagues décrit un lobe dans le référentiel [φ; GZ] lorsque le roulis paramétrique se développe. L'apparition du phénomène de roulis peut donc être détectée en temps réel en se basant sur la forme de la variation de la stabilité transversale sur une demi-période. L'idée n'a pas été plus approfondie dans cette thèse puisqu'il n'existe pas de méthode fiable pour calculer avec précision la stabilité transversale en temps réel à bord. Si une telle méthode venait à être développée, il serait intéressant de l'implémenter dans une méthode de détection du roulis paramétrique. Cependant, à ce jour, plusieurs méthodes opérationnelles de détection du roulis paramétrique existent, telle que celle développée dans le cadre de cette thèse. La méthode proposée devrait être validée sur une plus grande plage de donnée provenant de mesures embarquées, particulièrement sur des données obtenues sur des porte-conteneurs durant l'hiver. En outre, une validation sur une grande diversité de navires pourrait être menée en utilisant des résultats de simulations en 5 ou 6 degrés de liberté. Les seuils considérés dans la méthode de détection du roulis paramétrique proposée dans le cadre de cette thèse pourraient être améliorés par le biais d'une identification des seuils sur un large jeu de donnée afin d'améliorer le taux de détection. Cela pourrait être d'un grand intérêt si la méthode venait à être optimisée pour une seule forme de carène. Une telle amélioration nécessite d'autres jeux de données permettant la validation de la méthode révisée.

ANNEX 1. HYDROSTATIC VALIDATION METHOD

This annex presents how the hydrostatics validations of models are conducted. The presented method was used to validate the models used within this PhD.

The models of the vessels are realised using the Hydrostatic solver Calcoque (Grinnaert at al., 2015) based on the hull geometry (hull geometry files or plans). This software permits to model the ship's hull, Its appendices, superstructures, and propulsion. The appendages are modelled based on their descriptions available in stability booklet, shell expansion plan, docking plans or any other detailed plan. This software permits to compute the hydrostatics in calm water as well as in regular longitudinal waves. Such hydrostatics software complies with the requirements formulated by the IMO to assess parametric roll level 2 of the SGISCs (IMO, 2020a).

The models are validated by comparison with the vessel's stability booklet, considered as reference.

Hydrostatics are calculated using this software for all draughts available in the stability booklet (same water density). At least displacement (Δ), ton per one centimetre immersion (TPC), longitudinal centre of buoyancy from aft perpendicular (LCB), vertical centre of buoyancy above base line (KB), transverse metacentric height above base line (KM), moment to change trim of one centimetre (MTC) and longitudinal centre of buoyancy from aft perpendicular (LCF) are compared to the ones provided in the stability booklet. Typical observed errors (ε) in percent are presented in Table 36.

	Δ	TPC	LCB	KB	KMT	MTC	LCF
ε	<1%	0.3%	0.15%	0.1%	0.1%	2.5%	0.1%

Table 36 - Typical observed error

These comparisons permit to verify if the hull forms and hull thickness are correctly modelled. An example is provided for a 5700 TEU container ship. The absolute and relative error are provided as a function of the draught. Figure 79 provides the comparison of the displacement, it shows an error is smaller than 0.6 %. Figure 80 provides the comparison of the longitudinal centre of buoyancy, it shows an error smaller than 0.2 %. In this example, the maximum error on the metacentric height is lower than 4 cm, with a mean error of 2 cm. Thus, considering the magnitude of the error of the displacement, metacentric height and longitudinal centre of buoyancy it is conclude that the submerged hull is correctly modelled.

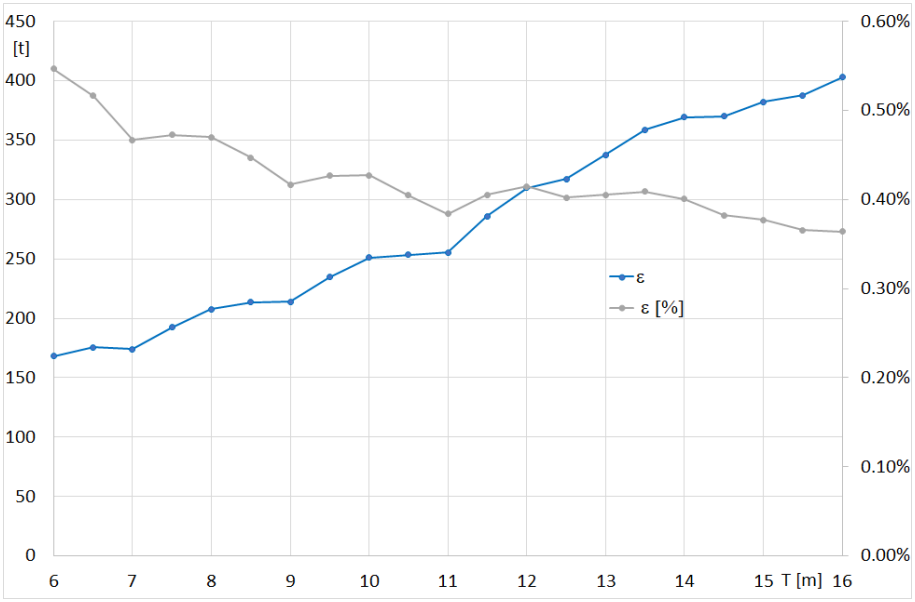

Figure 79 - 5700 TEU container ship displacement comparison

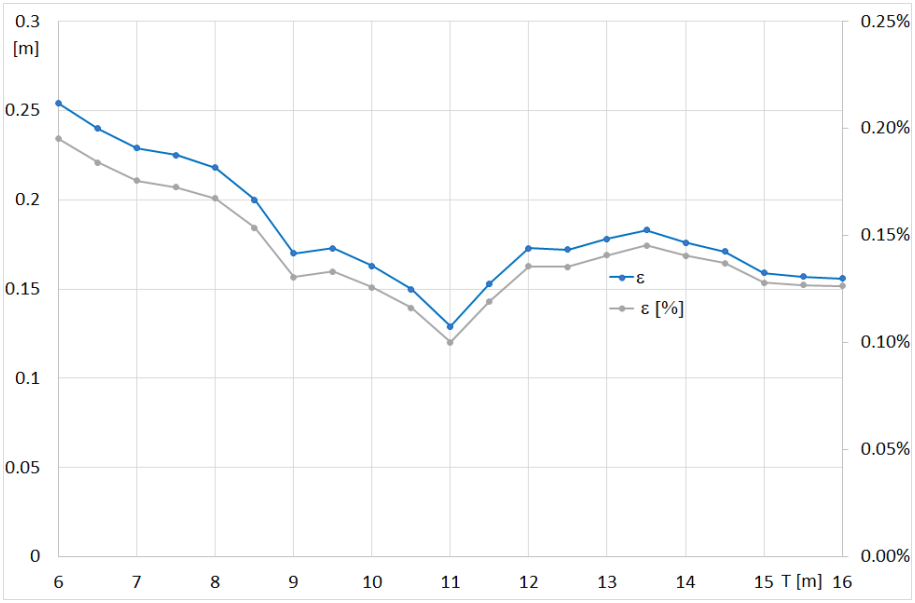

Figure 80 - 5700 TEU container ship LCB comparison

KN tables are available in the stability booklet and are calculated with the hydrostatic solver. The GZ curves are calculated for selected values of the draughts and height of the centre of gravity (KG) and compared. This comparison permits to validate the watertight volumes of the model, even above the still waterplane when considering large heel angles. An example is provided for the 5700 TEU container ship (Figure 81). It shows that the error is smaller than 2 % for heel angles smaller than 60 degrees (small absolute error after 60 degrees as well, less than 4 cm at 75 degrees of heel). Thus, in this example the watertight volume is correctly modelled.

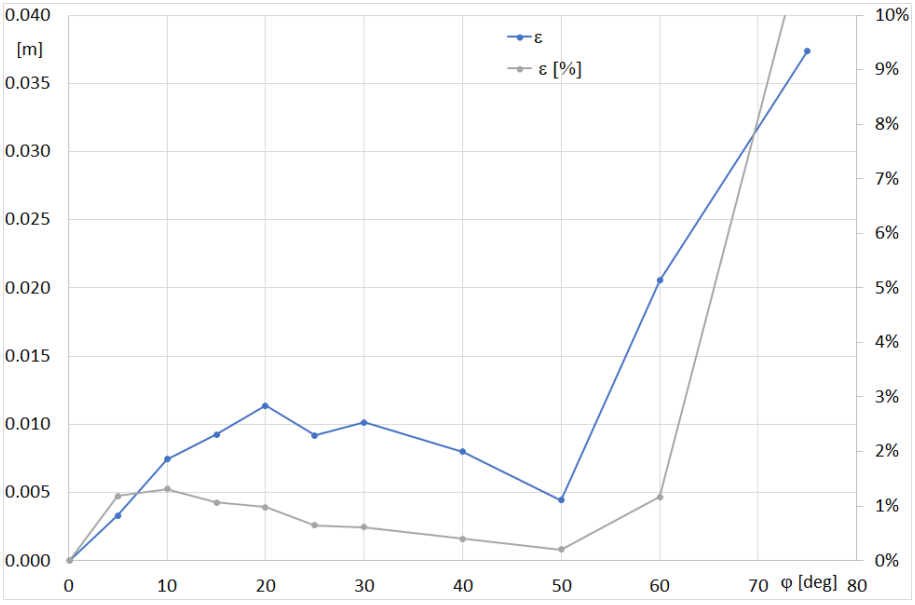

Figure 81 - 5700 TEU container ship GZ curve comparison

1-DoF Validation

1-Dof simulations, solving the parametric roll Equation 10 using Runge-Kutta method requires inputs that should be validated. The 1-DoF solver used throughout this PhD is presented in Section 1.2.1 page 22. This solver requires the GZ curves in waves obtained from hydrostatics calculation (the ship is balance in trim and sinkage). The GZ curves are calculated for a reference KG (denoted KG_{Ref} which permits to determine GM_{Ref}). An estimation of the roll inertia (denoted by J_{44}) is calculated based on the roll period table.

$$k_{moy} = \frac{1}{n}\sum_{i=1}^{n}\sqrt{GM} * T_{\varphi} \qquad 127$$

Thus, the roll period associated to GM_{Ref} can be calculated as:

$$T_{Ref} = \frac{k_{moy}}{\sqrt{GM_{Ref}}} \qquad 128$$

Finally, the roll inertia is calculated (as an average for any GM) as:

$$J_{44} = W * GM_{Ref} * \left(\frac{T_{Ref}}{2 * \pi}\right)^2 \qquad 129$$

Additionally, a roll decay simulation is conducted to verify that the observed roll period is identical to the one calculated at the corresponding loading condition.

Equation 130 is used to re-calculate the GZ curves to avoid computing once more the GZ curves with the hydrostatic solver when the height of the centre of gravity varies. Equation 130 is used for GZ curve in calm water and for GZ curves in waves.

$$GZ(\varphi)_{KG} = GZ(\varphi)_{KG_{Ref}} - \left(KG - KG_{Ref}\right)\sin(\varphi) \qquad 130$$

In conclusion this 1-DoF solver does not directly require the model of the ship. Thus, the estimated inputs must be provided with the greatest accuracy as possible. In this solver the roll damping is

estimated using Ikeda methods which only requires geometrical inputs provided to the solver, as well as the bilge keel definition.

6-DoF Validation

6-DoF simulation are realised using the time-domain solver Fredyn. Prior to realise simulations the software Shipmo is used to pre-compute the radiations and diffractions forces (both software are presented in Section 1.2.2 page 25).

Fredyn and Shipmo require a ship model. The model is validated using the output of both software. Shipmo realises the database of the radiation and diffraction forces. At high frequency the output can presents erroneous results sign of un insufficient discretisation of the description of the model. Then, Fredyn provides prior any simulation an output file containing the hull particulars calculated from the model for the specified loading condition. The main particulars and hydrostatics values are compared to the one of the stability booklets. This validation is equivalent to the one conducted in Calcoque. The validation is realised for each model.

Finally, additional validations can be conducted on the ship manoeuvring capacity if required (such as described in Chapter 5).

ANNEX 2. REACTION GUIDE FOR OFFICERS (CONFIDENTIAL)

This annex is confidential.

Bandwidth of the lock in field

Grinnaert (2017) states that the lock in field is symmetrical on each side of the lock-in speed calculated for which the roll period is twice the encounter period on regular waves. This statement is based on the work of Kerwin (1955) and demonstrated by Grinnaert (2017) for dimensionless speed ϒ. Here after, it is demonstrated that it can be provided that the half speed bandwidth of the lock-in field can be directly expressed.

Equation 61 page 91 in the PhD of Grinnaert (2017) states that

$$\gamma_0 = \frac{\omega_e}{\omega_0} \quad and \quad \gamma = \frac{\omega_e}{\omega} \tag{131}$$

The speed for which the first mode of parametric roll (V_{PR} in m.s^{-1}) is calculated as follows

$$V_{PR} = (2\omega_0 - \omega_w)\frac{g}{{\omega_w}^2} \tag{132}$$

Equation 65 page 97 in the PhD of Grinnaert (2017) provides Υ_0 as

$$\gamma_0 = \frac{\omega_e}{\omega_0} = \frac{\omega_w}{\omega_0}\left(1 + \frac{\omega_w V}{g}\right) \tag{133}$$

Grinnaert, 2017, demonstrated that the lock in field dis bounded by:

$$From \quad 2 - \frac{\delta GM}{2GM} \quad to \quad 2 + \frac{\delta GM}{2GM} \tag{134}$$

The dimensionless boundaries of the lock-in field Υ_{min} (Equation 135) and Υ_{max} (Equation 136) can be expressed as:

$$\gamma_{min} = 2 - \frac{\delta GM}{2GM} = \frac{\omega_e}{\omega_0} = \frac{\omega_w}{\omega_0}\left(1 + \frac{\omega_w V_{min}}{g}\right) \tag{135}$$

$$\gamma_{max} = 2 + \frac{\delta GM}{2GM} = \frac{\omega_e}{\omega_0} = \frac{\omega_w}{\omega_0}\left(1 + \frac{\omega_w V_{max}}{g}\right) \tag{136}$$

Thus, V_{min} (137) and V_{max} (138) are

$$V_{min} = \frac{g}{\omega_w}\left(\frac{2\omega_0}{\omega_w} - \frac{\delta GM\omega_0}{2GM\omega_w} - 1\right) \tag{137}$$

$$V_{max} = \frac{g}{\omega_w}\left(\frac{2\omega_0}{\omega_w} + \frac{\delta GM\omega_0}{2GM\omega_w} - 1\right) \tag{138}$$

The bandwidth of the lock-in field $2\delta V$ is expressed as $2\delta V = V_{max} - V_{min}$, using Equation 137 and 138, we have:

$$2\delta V = \frac{g}{\omega_w}\left(\frac{\delta GM\omega_0}{GM\omega_w}\right) \tag{139}$$

The validation is provided as $V_{PR} - V_{min} = V_{max} - V_{PR}$, such as $\delta V_1 = V_{PR} - V_{min}$ (Equation 140) and $\delta V_2 = V_{max} - V_{PR}$ (Equation 141)

$$\delta V_1 = (2\omega_0 - \omega_w)\frac{g}{{\omega_w}^2} - \frac{g}{\omega_w}\left(\frac{2\omega_0}{\omega_w} - \frac{\delta GM\omega_0}{2GM\omega_w} - 1\right)$$

$$\delta V_1 = \frac{g}{{\omega_w}^2}\left(2\omega_0 - \omega_w - \frac{2\omega_{0\omega_w}}{\omega_w} + \frac{\delta GM\omega_0\omega_w}{2GM\omega_w} + \omega_w\right) = \frac{g}{{\omega_w}^2}\frac{\delta GM\omega_0}{2GM} \quad 140$$

$$\Delta V_2 = \frac{g}{\omega_w}\left(\frac{2\omega_0}{\omega_w} + \frac{\delta GM\omega_0\omega_w}{2GM\omega_w} - 1\right) - (2\omega_0 - \omega_w)\frac{g}{{\omega_w}^2}$$

$$\Delta V_2 = \frac{g}{{\omega_w}^2}\left(-2\omega_0 + \omega_w + \frac{2\omega_0}{\omega_w} + \frac{\delta GM\omega_0}{2GM\omega_w} - 1\right) = \frac{g}{{\omega_w}^2}\frac{\delta GM\omega_0}{2GM} \quad 141$$

$\delta V_1 = \delta V_2$, thus the lock-in field dis symmetrical on each side of V_{PR}. The half bandwidth can be analytically expressed in speed.

QED

Analytical lobe area considering linear GZ

The objective is to demonstrate Equation 84 (page 60) providing the value of the area of the lobe described by GZ(φ; t) in a [φ; GZ] coordinate system when considering linear GZ in parametric synchronism condition and rewritten hereunder:

$$Area_{Lobe} = \frac{\Phi^2.\delta GM.\pi}{4} \qquad 84$$

Assuming a linear GZ and a sinusoidal roll motion, the variations of GM (Equation 82, page 59, rewritten hereunder) and GZ (Equation 142) are analytically described as:

$$GM(t) = GM_{mean} - \delta GM.sin(\omega_e.t) \qquad 82$$

$$GZ(\varphi;t) = (GM_{mean} - \delta GM.\sin(\omega_e.t))\varphi \qquad 142$$

GZ(φ; t) describes a lobe in a [φ; GZ] coordinate system. The area of this lobe is calculated using Equation 83 (page 60) and rewritten hereunder:

$$Area_{Lobe} = -\oint_{\frac{T_\varphi}{2}} GZ(\varphi;t)\, d\varphi \qquad 83$$

Minus sign in Equation 83 appears to obtain a positive lobe area, since the lobe is turning counterclockwise.

Introducing Equation 142 in Equation 83 leads to:

$$Area_{Lobe} = -\oint_{\frac{T_\varphi}{2}} (GM_{mean} - \delta GM.\sin(\omega_e.t))\varphi\, d\varphi \qquad 143$$

The equation of a sinusoidal roll motion is provided by Equation 86 (page 61), rewritten hereunder for the synchronism condition:

$$\varphi(t) = \Phi.\sin(\omega_0 t) \qquad 86$$

With:

$$\omega_e = 2\omega_0 \qquad 1$$

Thus, the derivate of Equation 86 provides the equation of the roll velocity, as follows:

$$\dot{\varphi}(t) = \omega_0.\Phi.\cos(\omega_0 t) \qquad 144$$

Hence, dφ becomes:

$$d\varphi = \dot{\varphi}dt = \omega_0.\Phi.\cos(\omega_0 t)\, dt \qquad 145$$

Introducing Equation 86 and 145 in Equation 143, we have:

$$Area_{Lobe} = -\int_{\frac{T_\varphi}{2}} \Phi^2.\omega_0.\cos(\omega_0 t).\sin(\omega_0 t)\,(GM_{mean} - \delta GM.\sin(\omega_e.t))\,\dot{\varphi}dt \qquad 146$$

Thus, it is possible to extract the constants from the integral and use the followings trigonometric identities to simplify Equation 146:

$$\sin(a)\,.\cos(a) = \frac{1}{2}\sin\,(2a) \tag{147}$$

$$sin^2(a) = \frac{1-\cos\,(2a)}{2} \tag{148}$$

Introducing Equations 147 and 148 in Equation 146 leads to:

$$Area_{Lobe} = \frac{-\Phi^2.\,\omega_0}{2}\int_{\frac{T_\varphi}{2}}\left(GM_{mean}.\sin(2\omega_0 t) - \,\delta GM\left(\frac{1-\cos(4\omega_0 t)}{2}\right)\right)dt \tag{149}$$

Since T_φ is equal to T_0 in synchronism condition, Equation 149 becomes:

$$Area_{Lobe} = \frac{-\Phi^2.\,\omega_0}{2}\left(\int_0^{\frac{T_0}{2}} GM_{mean}.\sin(2\omega_0 t)\,dt - \int_0^{\frac{T_0}{2}}\frac{\delta GM}{2}dt + \int_0^{\frac{T_0}{2}}\frac{\delta GM.\cos\,(4\omega_0 t)}{2}dt\right) \tag{150}$$

$$Area_{Lobe} = \frac{\Phi^2.\,\omega_0.\,\delta GM.\,T_0}{8} \tag{151}$$

$$Area_{Lobe} = \frac{\Phi^2.\,\delta GM.\,\pi}{4} \tag{152}$$

QED

The exciting energy is obtained by multiplying Equation 152 by the ship's weight. This equation is identical to the one obtained by Grinnaert (2017), directly calculated from the roll motion and the GM variation, assuming the worst case of shift angle and without notion of any lobe.

Vessel speed corresponding to the first mode of parametric roll, ABS

The objective is to demonstrate the equation proposed by the American Bureau of Shipping permitting to calculate the speed corresponding to the first mode of parametric roll (Equation 53, page 45, rewritten hereunder), under the corresponding assumptions.

$$V_{PR} = \frac{19.06|2\omega_{Mean} - \omega_W|}{{\omega_W}^2} \quad 53$$

Mathieu (1868) demonstrated that the first mode of parametric roll appears when the wave encounter frequency (denoted by ω_e) is twice the ship's roll frequency (denoted by ω), Equation 1, page 19, where ω replaces ω_0 since the ship's roll frequency may differ from the natural roll frequency.

$$\omega_e = 2\omega \quad 153$$

The encounter frequency is calculated according to the following equation:

$$\omega_e = \omega_w - \frac{{\omega_W}^2 V}{g}\cos\beta \quad 154$$

Thus, in head and following seas cos β takes respectively the value of -1 and +1. Thus, two values of ω_e are calculated in head and following seas ($\omega_{e.h}$ and $\omega_{e.f}$, respectively):

$$\omega_{e.h} = \omega_w + \frac{{\omega_W}^2 V}{g} \quad 155$$

$$\omega_{e.f} = \omega_w - \frac{{\omega_W}^2 V}{g} \quad 156$$

Mixing Equations 155 and 156 with the sign ± leads to:

$$\omega_e = \omega_w \pm \frac{{\omega_W}^2 V_{PR}}{g} \quad 157$$

The ship's roll frequency is the one associated to the mean GM in waves and locked to half the encounter frequency such as defined in Equation 153. Thus, introducing Equation 153 in Equation 157, leads to:

$$2\omega_{Mean} = \omega_w \pm \frac{{\omega_W}^2 V_{PR}}{g} \quad 158$$

$$V_{PR} = \frac{g|2\omega_{Mean} - \omega_w|}{{\omega_W}^2} \quad 159$$

V_{PR} in Equation 159 is expressed in $m.s^{-1}$. Replacing the gravity acceleration by its common value 9.81 $m.s^{-2}$, and expressing V_{PR} in knots leads to:

$$V_{PR} = \frac{19.06|2\omega_{Mean} - \omega_W|}{{\omega_W}^2} \quad 53$$

QED

ANNEX 4. SHIP'S PRESENTATION

15 merchants' ships and 9 naval vessels were considered in this thesis. Some of those models were realised by Grinnaert (2017) during his PhD. The other models were realised and validated using the method presented in Annex 1 (page 151). Those vessels were assessed through 1-DoF simulation for parametric roll. Within those models, 5 merchants' ships and 3 naval vessels were considered for 6-DoF simulations. Naval ships are known for their insensibility to parametric roll, they were used in this PhD to validate the simulation tools and enlarge the ship database (Chapter 2. Energy Method).

Merchant ships

15 merchant ships are modelized using the software Calcoque (Grinnaert et al., 2015) and used for 1-DoF parametric roll studies. Figure 82 to Figure 96 presents the watertight volumes of the merchant ships and the related incident if such exists. Within those vessels, 5 were selected for advance modelling, which permit to realise 6-DoF simulations. The vessels used in 6-DoF studies are identified in Table 37. Confidential Annex 5 presents the main characteristics of the merchant ships used throughout this PhD thesis.

Vessel Name	1-DoF	6-DoF	Comment
2100 TEU	x		merchant
C11 class (4832 TEU)	x	x	merchant
5700 TEU	x		merchant
5780 TEU	x	x	merchant
8500 TEU	x		merchant
8600 TEU	x		merchant
11000 TEU	x		merchant
14400 TEU	x	x	merchant
13800 TEU	x	x	merchant
18000 TEU	x		merchant
23000 TEU	x		merchant
Passenger vessel	x		merchant
KTH Roro	x		merchant
110-metre tanker	x		merchant
227.5-metre tanker	x	x	merchant

Table 37 - Merchant vessels' list

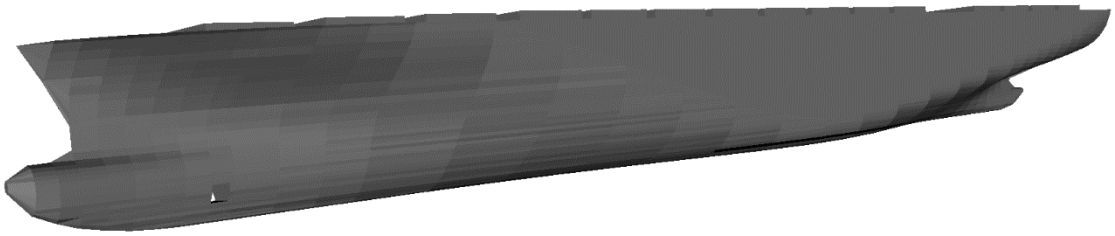

Figure 82 - Watertight volume of the 5780 TEU container ship

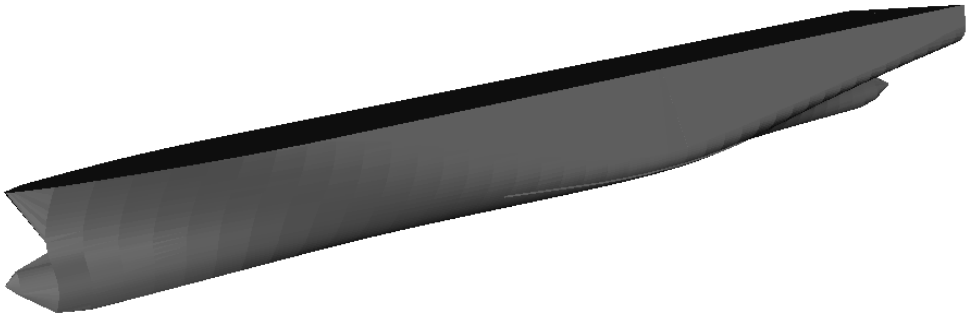

Figure 83 - Watertight volume of C11-class container ship (4832 TEU)

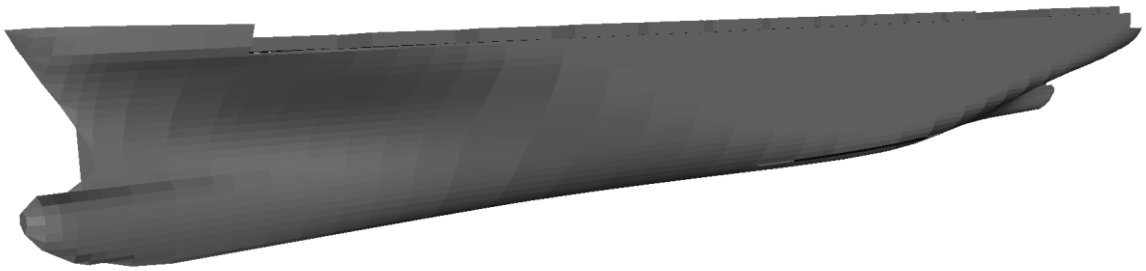

Figure 84 - Watertight volume of the 5700 TEU

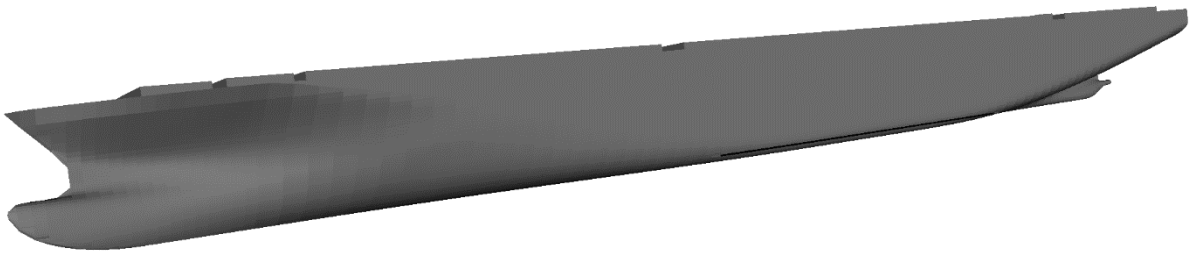

Figure 85 - Watertight volume of the 18000 TEU container ship

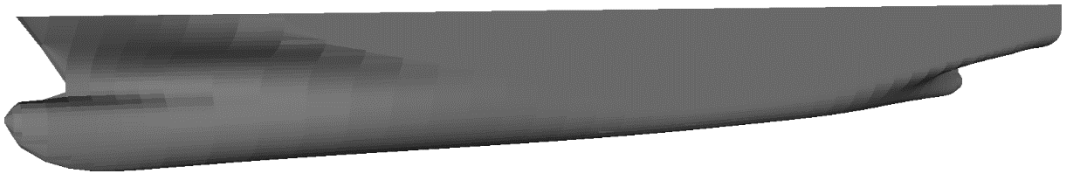

Figure 86 - Watertight volume of the 2100 TEU container ship

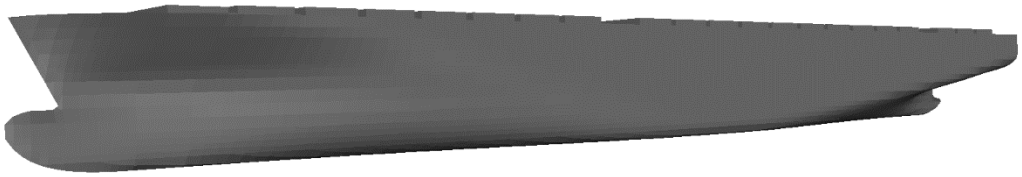

Figure 87 - Watertight volume of the 14400 TEU container ship

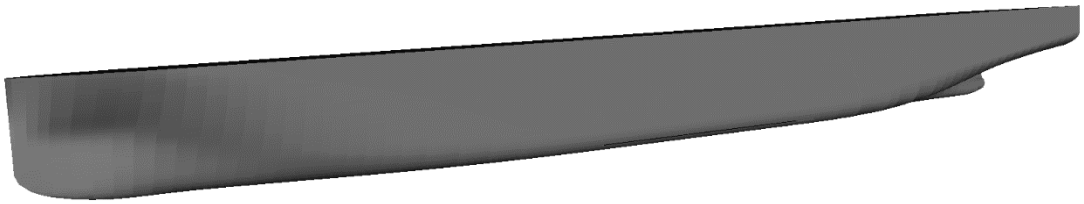

Figure 88 - Watertight volume of the 23000 TEU container ship

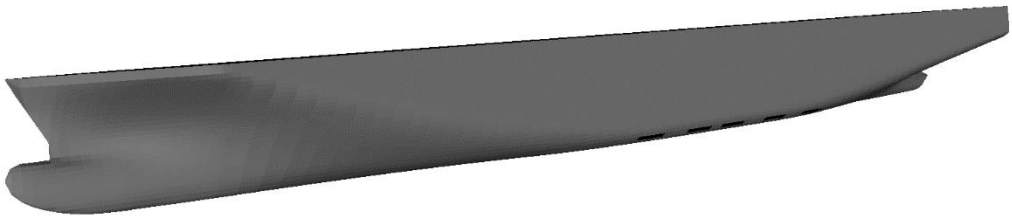

Figure 89 - Watertight volume of the 13800 TEU container ship

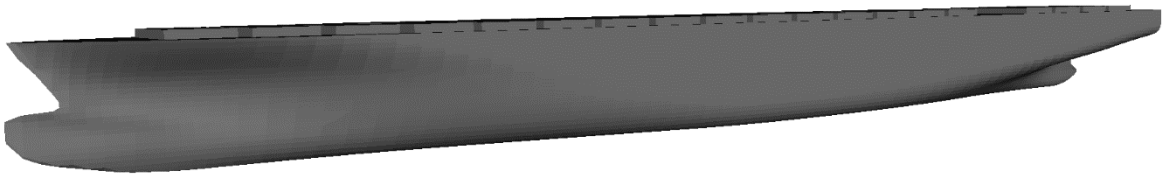

Figure 90 - Watertight volume of the 8500 TEU container ship

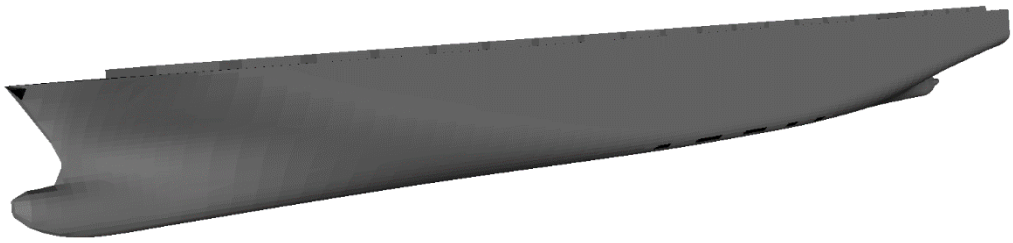

Figure 91 - Watertight volume of the 11000 TEU container ship

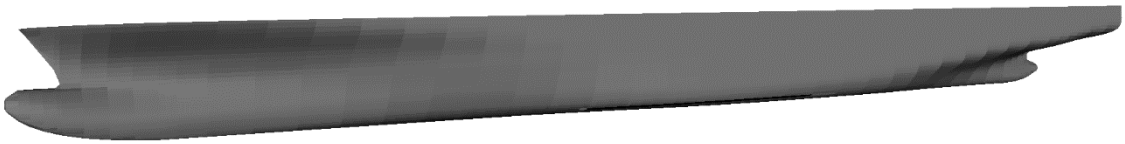

Figure 92 - Watertight volume of the 8600 TEU container ship

Figure 93 - Watertight volume of passenger vessel

Figure 94 - Watertight volume of KTH RoRo

Figure 95 - Watertight volume of the 110-metre tanker

Figure 96 - Watertight volume of the 227.5-metre tanker

Naval ships

9 naval ships are modelized using the software Calcoque (Grinnaert et al., 2015) and used for 1-DoF parametric roll studies. Figure 97 to Figure 105 present the watertight volumes of the naval ships. Within those vessels, 3 were selected for advance modelling, which permit to realise 6-DoF simulations. The vessels used in 6-DoF studies are identified in Table 38. Confidential Annex 5 presents the main characteristics of the merchant ships used throughout this PhD thesis.

Name	Vessel Type	1-DoF	6-DoF	Comment
OPV	Naval, small	x		naval
BPC	BPC	x	x	naval
DTMB-5415	Frigate	x	x	naval, open model
FASM	Frigate	x		naval
FLF	Frigate	x		naval
ONR-5613_Flare	Frigate	x		naval, open model
ONR-5613_Tumblehome	Frigate	x	x	naval, open model
ONR-5613_Wall	Frigate	x		naval, open model
Helicopter carrier	Naval, large	x		naval

Table 38 - Naval vessels' list

Figure 97 - Watertight volume of the OPV

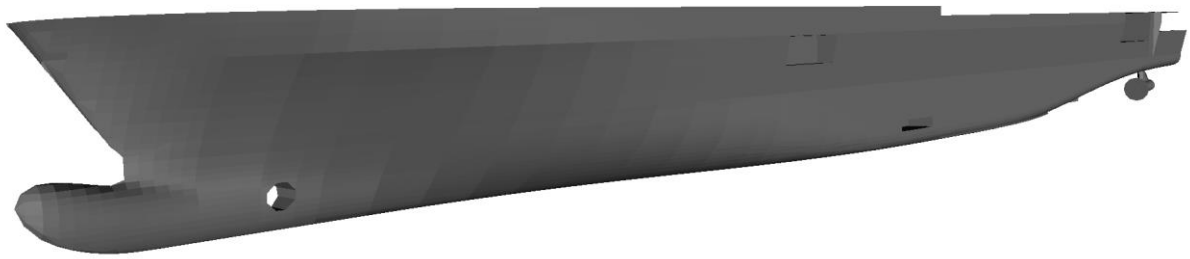

Figure 98 - Watertight volume of the BPC

The DTMB-5415 is an open form provided by the David Taylor Model Basin.

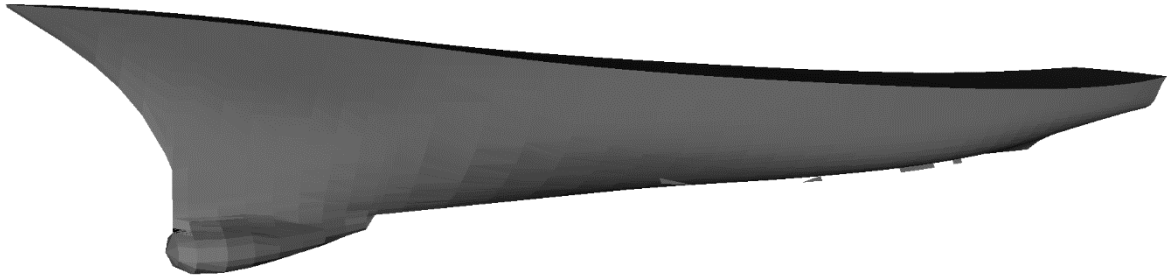

Figure 99 - Watertight volume of the open form DTMB-5415

Figure 100 - Watertight volume of the FASM

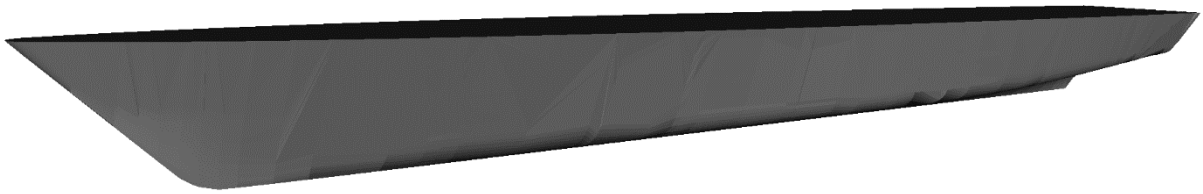

Figure 101 - Watertight volume of the FLF

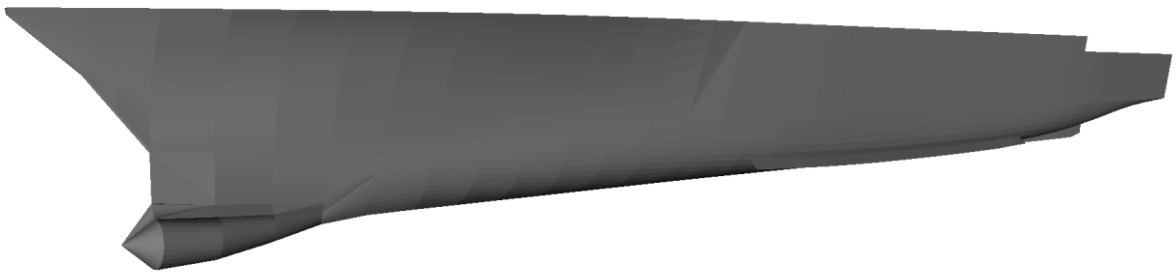

Figure 102 - Watertight volume of the open form ONR-5613_Flare

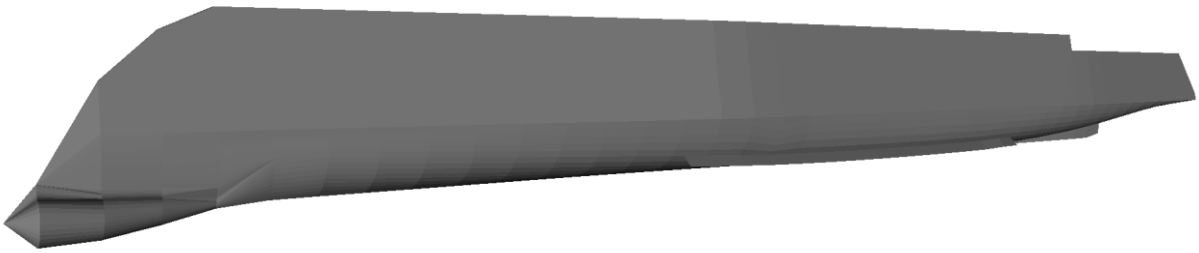

Figure 103 - Watertight volume of the open form ONR-5613_Thumblehome

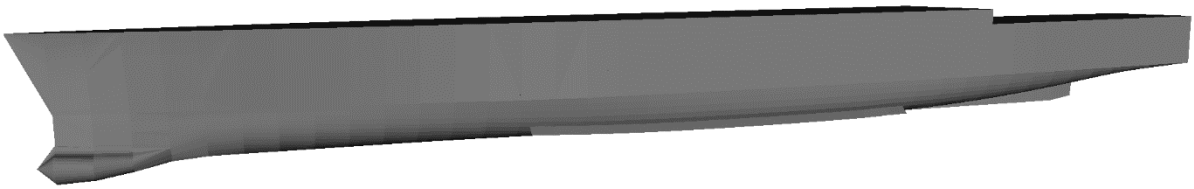

Figure 104 - Watertight volume of the open form ONR-5613_Wall

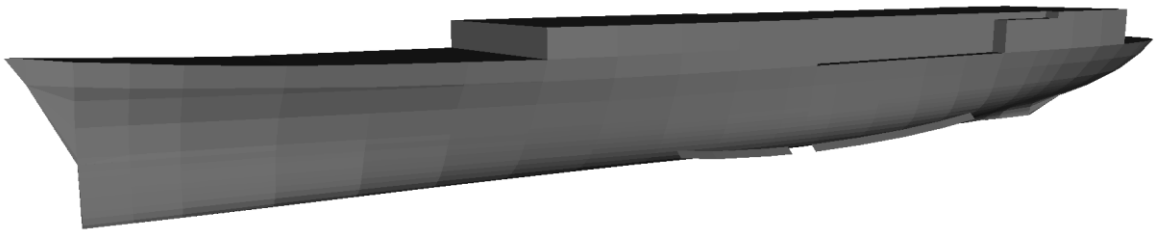

Figure 105 - Watertight volume of the helicopter carrier

ANNEX 5. SHIP'S MAIN PARTICULARS (CONFIDENTIAL)

This annex is confidential.

ENSM
ÉCOLE NATIONALE SUPÉRIEURE MARITIME

French Maritime Academy
www.supmaritime.fr

Probability of occurrence of parametric roll on a predefined sea state

PhD thesis 2020-2023
Vivien Luthy, vivien.luthy@supmaritime.fr
Supervision: Jean-Yves Billard and François Grinnaert

Introduction

Parametric roll (PR) is a rare phenomenon, which have led to several accidents in the last 20 years. Those accidents conducted the international maritime organization to revise the intact stability code [3] to consider possible stability failures in waves. This thesis aims to improve the assessment of the phenomenon, to predict the maximum roll motion of the vessel on predefined sea states conditions and to propose a reaction guide for the crew in case of doubt and/or heavy roll motion.
3 main axes are studied:
- Global assessment (vessel is subject or not subject to PR)
- Real time evaluation (onboard alarm, actions)
- Routing (pre-computed roll motions with forecast weather)

Parametric roll origins

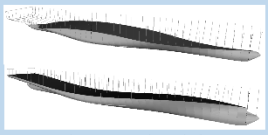
Fig 1. Waterplane variation on longitudinal wave

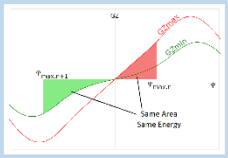

Fig 2. Amplification of roll the motion

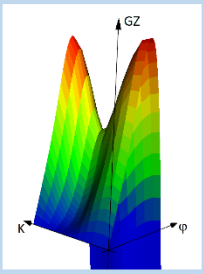

Fig 3. GZ variation on wave

The wave creates a variation of the waterplane area (Figure 1) inducing a variation of the transverse stability (Figure 3). In specific conditions the repetition of the variation of the transverse stability leads to an amplification of the roll motion (Figure 2).

Fundamental research

Fundamental researches have been conducted based on the work done by doctor François Grinnaert in 2017 on parametric roll [1]. His work permitted to predict the roll amplitude of any vessel on longitudinal sinusoidal waves based on energy considerations (Figure 4) within the lock-in field (Figure 5, speed limits for PR apparition). An Improvement of the method has been realised to better predict the reached steady state roll amplitude [2]. Energy consideration leads to an easy explanation of the amplification of the roll motion (Figure 2).

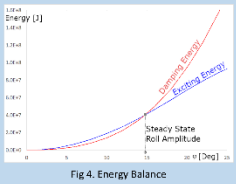

Fig 4. Energy Balance

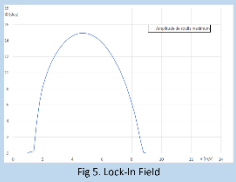
Fig 5. Lock-In Field

1. Grinnaert F., Billard J.-Y., Laurens J.-M. (2017). *An Energy Analysis of Parametric Roll for Application to the Second Generation Intact Stability Criteria*. Journal of Marine Science and Technology. DOI : 10.1007/s00773-017-0444-z.
2. Luthy V., Grinnaert F., Billard J.-Y. (2021). *Computation of parametric roll amplitude using energy method considering non-linear GZ in resonance condition*. 1st International Conference on the Stability and Safety of Ships and Ocean Vehicles, 7-11 June 2021.
3. International Maritime Organization (2020). SDC 7/WP.6. 7th session. *Finalization of Second Generation Intact Stability Criteria. Amendments to Part B of the 2008 IS Code on Towing, Lifting and Anchor Handling Operations*.

Operational research

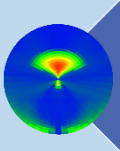
Roll polar plots: Permit to predict the maximum roll motion of the vessel in given conditions (loading condition, environmental condition).
It allow to route the vessel to avoid dangerous conditions.


Real time evaluation of the roll motion and appearance conditions: Permit to create an alarms of PR conditions, of appearance and of maximum allowable roll angle.
It allows to inform the officer of the watch.


Post accident studies: Permit to learn from known accidents and modify the procedures, and behaviours to avoid them.
It allows to determine the causes of the accidents.

Simulations on real sea states

Simulations on real sea states permit to study the phenomenon of PR without risking lives and cargo. The results allow to create operational roll polar plots. Since 2 simulations on a same real sea state do not provide the same roll motions, results are subject to a probabilistic approach. To create a roll polar plot such as presented in Figure 7 it requires 10500 simulations of 1 hour (Figure 6). Those simulations are also considered to test and improve real time evaluation of PR.

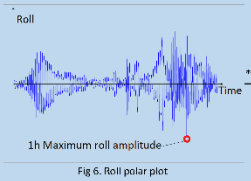

Fig 6. Roll polar plot

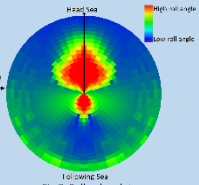

Fig 7. Roll polar plot

Conclusion

Parametric roll leads to significant roll angles that can have important economic and environmental issues. The use of operational solutions coupled with a global assessment seems to be the best way to avoid such accidents (ship deign, routing, real time evaluation). The work permitted to introduce an improved energy method to calculate roll polar plots and provide post accident study. Further work may provide an improved real time detection of parametric roll and a reaction guide.

CMA CGM
ARTS ET MÉTIERS ParisTech
IRENAV
CMA SHIPS

ANNEX 7. 1-DEGREE-OF-FREEDOM ROLL SIMULATOR: USER GUIDE

Simulateur de roulis

François Grinnaert, Vivien Luthy – 22 octobre 2020

1. PRESENTATION

1.1. Généralités

Le simulateur de roulis se présente sous la forme d'un fichier Excel avec macros. Les caractéristiques du navire simulé et ses courbes de GZ sont renseignées dans un fichier texte. Pour modifier le tirant d'eau du navire, il est nécessaire de recalculer les courbes de GZ et d'écrire un nouveau fichier texte.

1.2. Equation différentielle du roulis

Le simulateur de roulis effectue une simulation sur mer calme ou sur houle longitudinale en résolvant l'équation différentielle de second ordre du roulis en 1 degré de liberté :

$$J_{44}\ddot{\varphi} + B_{44}\dot{\varphi} + W.GZ(\varphi, t) = 0$$

J_{44} représente le moment d'inertie au roulis du navire (en kg.m^2).

B_{44} représente le coefficient d'amortissement au roulis (en N.m.s/rad).

W représente le poids du navire (en N).

GZ(φ,t) représente le bras de levier de redressement, fonction de l'angle de roulis φ, et éventuellement du temps t dans le cas d'une simulation sur houle longitudinale figée.

L'équation différentielle est résolue au moyen de la méthode de Runge-Kutta d'ordre 4 avec une intégration sur 1500 pas de temps (non modifiable par l'utilisateur). Le pas de temps est calculé comme une fraction de la période de roulis propre du navire T_0, calculée en préalable à la simulation comme suit :

$$T_0 = 2\pi\sqrt{\frac{J_{44}}{W.GM}}$$

Dans le cas d'une simulation sur houle longitudinale figée, la valeur de la hauteur métacentrique dans la relation ci-dessus est égale à la moyenne des N_k hauteur métacentriques correspondant aux N_k positions du navire par rapport à la crête de la houle.

1.2.1. Moment d'inertie

La valeur du moment d'inertie au roulis J_{44} est imposée dans le fichier texte. Elle est inchangée pendant la simulation. Elle inclut la masse ajoutée par les efforts de radiation.

1.2.2. Coefficient d'amortissement

Le coefficient d'amortissement au roulis B_{44} peut être :

- calculé pendant la simulation à l'aide de la méthode d'Ikeda; il dépend alors de la vitesse du navire (inchangée pendant la simulation) et de l'amplitude et de la période du roulis (calculées en temps réel pendant la simulation) ; voir [1] pour la composante liée à la vitesse du navire, [2] pour les autres composantes ;

- ou imposé par des coefficients constants, linéaire et quadratique (respectivement $B_{44.lin}$ et $B_{44.qua}$) ; cela revient à résoudre l'équation du roulis sous la forme suivante :

$$J_{44}\ddot{\varphi} + B_{44.lin}\dot{\varphi} + B_{44.qua}\dot{\varphi}|\dot{\varphi}| + W.GZ(\varphi,t) = 0$$

Nota : les coefficients d'amortissement linéaire et quadratique imposés par l'utilisateur doivent inclure la composante liée à la vitesse du navire.

1.2.3. Bras de levier de redressement

Le terme de rappel peut être linéaire ou non linéaire, sur mer calme et sur houle longitudinale figée. Quatre configurations sont possibles.

1.2.3.1. GZ linéaire sur mer calme

Le bras de levier de redressement est calculé à partir de la hauteur métacentrique transversale (GM), définie comme étant la pente de la tangente à l'origine de la courbe de GZ sur mer calme.

1.2.3.2. GZ non linéaire sur mer calme

Le bras de levier de redressement est interpolé sur la courbe de GZ sur mer calme en fonction de la gîte.

1.2.3.3. GZ linéaire sur houle longitudinale figée

En préalable à la simulation, les N_k hauteurs métacentriques transversales (GM) sont déterminées à partir des N_k courbes de GZ sur houle (pente de la tangente à l'origine). Les valeurs moyenne, minimale et maximale des hauteurs métacentriques sont déterminées (respectivement GM_{moy}, GM_{min} et GM_{max}).

La variation de GM est déterminée comme suit :

$$\delta GM = \frac{1}{2}(GM_{max} - GM_{min})$$

Pendant la simulation, le bras de levier de redressement est déterminé comme suit :

$$GZ(\varphi,t) = GM(t)\varphi = \left(GM_{moy} + \delta GM\cos\omega_e t\right)\varphi$$

ω_e représente la pulsation de rencontre de la houle longitudinale (en rad/s). Sa valeur est calculée comme suit :

$$\omega_e = \omega_w + \frac{V.{\omega_w}^2}{g}$$

V représente la vitesse du navire (m/s). Sa valeur est positive par mer de l'avant, négative par mer de l'arrière. g représente la pesanteur terrestre (m/s^2). ω_w représente la pulsation de la houle (rad/s). Elle est déduite de la longueur d'onde de la houle λ (égale à la longueur du navire entre perpendiculaires L_{PP}) en profondeur infinie :

$$\omega_w = \sqrt{\frac{2\pi g}{\lambda}} = \sqrt{\frac{2\pi g}{L_{PP}}}$$

1.2.3.4. GZ non linéaire sur houle longitudinale figée

Pendant la simulation, le bras de levier de redressement est interpolé en deux dimensions en fonction de la gîte et de la position du navire par rapport à la crête de la houle, à partir du réseau des courbes

de GZ sur houle. La position du navire sur la houle est modélisée par le coefficient k dont la valeur est comprise entre 0 et 1 et déterminée comme suit :

$$k(t) = \frac{\omega_e t}{2\pi}$$

Le coefficient k vaut 0 lorsque les crêtes de la houle sont centrées sur les perpendiculaires avant et arrière, et 0.5 lorsque la crête est centrée sur la perpendiculaire milieu.

1.2.1. Excitation

Il n'y a pas d'excitation directe du roulis, le terme d'excitation de l'équation différentielle est nul. Cependant, le roulis peut être excité indirectement par la variation de la stabilité transversale du navire en route sur la houle longitudinale (roulis paramétrique).

2. FICHIER DES DONNEES DU NAVIRE

Les données du navire simulé sont écrites dans un fichier texte dont le format est celui des fichiers transmis avec le simulateur. Chaque fichier est structuré en deux parties. Dans chaque partie, les mots clés et/ou les données sont séparés par une tabulation.

2.1. Première partie du fichier : caractéristiques du navire

La première partie comprend les caractéristiques du navire, matérialisées par les champs suivants qui peuvent être renseignés dans n'importe quel ordre :

NAME	Nom du navire
LPP	Longueur entre perpendiculaires et longueur d'onde des vagues, ces deux grandeurs étant obligatoirement égales (m)
BREADTH	Largeur du navire (m)
T	Tirant d'eau (m)
VOL	Volume de carène (m^3)
CM	Coefficient de remplissage du maître-couple (sans unité)
J44	Moment d'inertie en roulis, incluant la masse ajoutée ($kg.m^2$)
KGREF	Valeur de référence de KG (m) pour laquelle les courbes de GZ sont calculées
LBK	Longueur des quilles anti-roulis (m)
BBK	Largeur des quilles anti-roulis (m)

2.2. Seconde partie du fichier : courbes de GZ

La seconde partie contient les courbes de GZ, calculées sur mer calme et sur une houle longitudinale figée dont la longueur d'onde est égale à la longueur du navire et pour la valeur de référence de KG, notée KG_{ref} et spécifiée avec le mot clé KGREF dans la première partie (le simulateur recalcule les courbes de GZ pour la valeur de KG choisie par en préalable à la simulation).

Les courbes sur houle figée sont calculées pour un nombre pair (noté N_k) de positions du navire par rapport à la crête de houle, régulièrement réparties. Chaque position est identifiée par un nombre réel noté k et compris entre 0 (inclus, correspondant aux crêtes sur les perpendiculaires AV et AR) et 1 (exclus). Exemple : pour 10 positions différentes du navire par rapport à la crête de la houle, k prend les valeurs 0 à 0.9 avec un pas de 0.1.

Le début de la seconde partie est identifié par le mot clé GZ. Elle contient un tableau de $1+N_{phi}$ lignes et 2+Nk colonnes. N_{phi} représente le nombre de gîtes pour lesquelles les courbes de GZ sont calculées. N_k représente le nombre de positions du navire par rapport à la crête de la houle.

La première ligne contient les mots clés "phi" et "calm", suivis des N_k valeurs de k.

La première colonne contient les angles de gîte (degrés). La seconde colonne contient les GZ sur mer calme (m). Les N_k colonnes suivantes contiennent les GZ sur houle longitudinale figée.

3. SIMULATEUR

3.1. Simulation simple

Les données à modifier par l'utilisateur figurent en **bleu gras** dans la feuille « Data » du fichier Excel.

3.1.1. Constantes physiques

Spécifier les constantes physiques (gravité, masse volumique de l'eau et viscosité cinématique de l'eau) dans les cases B2, B3 et B4.

3.1.2. Données du navire

Spécifier le chemin du fichier texte dans la case E13.

Spécifier la valeur de KG dans la case E14.

Spécifier la vitesse du navire dans la case E15. Si la case est laissée vide, la vitesse est nulle dans le cas d'une simulation sur mer calme, ou égale à la vitesse du premier mode de synchronisme paramétrique dans le cas d'une simulation sur houle longitudinale figée.

Spécifier les coefficients d'amortissement linéaire et quadratique dans les cases E16 et E17, respectivement. Pour calculer le coefficient d'amortissement avec la méthode d'Ikeda, laisser ces deux cases vides.

Laisser les cases E18, E20, E21, E22 et E23 vides.

3.1.3. Conditions initiales et pas de temps

Spécifier l'angle de gîte initiale dans la case H3.

Spécifier la vitesse de roulis initiale dans la case H4.

Spécifier la division de la période de roulis propre définissant le pas de temps dans la case H5. Exemple : pour un pas de temps dt = $T_0/50$, spécifier 50 dans la case H5.

3.1.4. Options de simulation

Bras de levier de redressement linéaire : spécifier VRAI dans la case H6 pour imposer un bras de levier de redressement linéaire (voir 1.2.3.1 et 1.2.3.3) ou FAUX pour imposer un bras de levier de redressement non linéaire (voir 1.2.3.2 et 1.2.3.4).

Vagues : spécifier VRAI dans la case H7 pour simuler le roulis sur une houle longitudinale figée (voir 1.2.3.3 et 1.2.3.4) ou FAUX pour simuler une extinction de roulis sur mer calme (voir 1.2.3.1 et 1.2.3.2).

3.1.5. Lancement de la simulation

Cliquer sur le bouton « Roll Simul. ».

En préalable à la simulation, le fichier texte contenant les caractéristiques du navire et ses courbes de GZ est lu. Les courbes de GZ sont recalculées pour la hauteur du centre de gravité KG spécifiée par l'utilisateur et écrites dans les feuilles « GZ wave » et « GZ calm ».

Une fois la simulation terminée, les valeurs numériques du temporel de roulis simulé sont écrites dans la feuille « Sim ». Le temporel de roulis est tracé dans la feuille « Graph ». L'évolution du GZ en fonction de l'angle de roulis est écrite dans la feuille « GZ » et tracée dans la feuille « GZ graph » (superposée au réseau des courbes de GZ sur houle).

Un message d'information résume les principaux résultats de simulation. Dans le cas de la simulation d'une extinction de roulis, le message donne les valeurs des coefficients d'amortissement linéaire et quadratique mesurés sur le temporel de roulis issu de la simulation selon la méthode décrite en [3].

3.2. Simulations multiples

Il est possible d'ordonner une série de simulations avec des données du navire différentes à spécifier les unes à la suite des autres dans la feuille « Result ».

3.2.1. Constantes physiques, pas de temps et options de simulation

Les constantes physiques, conditions initiales, pas de temps et options de simulation sont celles spécifiées dans la feuille « Data ». Voir 3.1.1, 3.1.3 et 3.1.4.

3.2.2. Données du navire

Dans la feuille « Result », renseigner les colonnes suivantes à partir de la ligne 3 :

Laisser la colonne A vide.

Dans la colonne B, spécifier les valeurs de KG désirées.

Dans la colonne C, spécifier les valeurs de la vitesse du navire désirées, en regard des valeurs de KG. Si une case de vitesse est laissée vide, la vitesse est nulle dans le cas d'une simulation sur mer calme, ou égale à la vitesse du premier mode de synchronisme paramétrique dans le cas d'une simulation sur houle longitudinale figée.

Dans les colonnes D et E, spécifier les coefficients d'amortissement linéaire et quadratique, respectivement. Pour calculer le coefficient d'amortissement avec la méthode d'Ikeda, laisser les cases de ces deux colonnes vides.

3.2.1. Conditions initiales

Dans la colonne F, spécifier l'angle de roulis initial.

Dans la colonne G, spécifier la vitesse de roulis initiale.

Si les cases de ces colonnes sont laissées vides, les conditions initiales utilisées sont celles spécifiées dans la feuille « Data ».

3.2.2. Lancement des simulations

Cliquer sur le bouton « Sim x N » de la feuille « Result ».

En préalable à chaque simulation, la vitesse du navire et les conditions initiales sont écrites dans les colonnes C (vitesse), F et G (conditions initiales) si elles n'ont pas été spécifiées par l'utilisateur.

A la fin de chaque simulation, les résultats de simulations sont écrits dans les cases des colonnes H à O et V à AB. Dans le cas de la simulation d'une extinction de roulis, les valeurs des coefficients

d'amortissement linéaire et quadratique mesurés sur le temporel de roulis issu de la simulation selon la méthode décrite en [3] sont écrites dans les cases des colonnes D et E.

Un message d'information signale la fin de la série de simulations.

Nota : les lignes pour lesquelles les résultats de simulation sont déjà renseignés ne sont pas traitées.

4. REFERENCES

1. Ikeda Y., Himeno Y., Tanaka N. (1978). *Components of roll damping of ship at forward speed*. Department of Naval Architecture University of Osaka Prefecture, Report No 404.
2. Kawahara Y., Maekawa K., Ikeda Y. (2009). *A simple prediction formula of roll damping of conventional cargo ships on the basis of Ikeda's method and its limitation*. Proceedings of the 10th International Conference on Stability of Ships and Ocean Vehicles, St Petersburg.
3. Maritime Research Institute Netherlands (2011). *FREDYN - Version 10.3 User's Manual - Part I – Appendices*. Mai 2011.

GLOSSARY

Symbol	Unit	Definition
A		
A_i	-	Area associated to the direction i under the selected spreading function
A_K	m^2	Area of bilge keels
A_{tot}	-	Total area under the selected spreading function
A_W	m^2	Area of the water plane
ABS	-	American Bureau of Shipping
AGCS	-	Allianz Global Corporate & Specialty
Area	m.deg	Area between linear GZ_{min} and GZ_{max} curves up to Φ
AP	-	Aft perpendicular
$Area_{inst}$	m.deg	Area between GZ_{min} and GZ_{max} curves considering instantaneous variation of the transverse stability up to Φ
$Area_{lobe}$	m.deg	Area of the lobe described by GZ(φ,t) in a [φ,GZ] coordinate system on half a roll period
ART	-	Anti-Roll Tank
ATSB	-	Australian Transport Safety Bureau
B		
B	-	Centre of Buoyancy
B	m	Ship's Breadth
B_{44}	$N.m.s.rad^{-1}$	Linearised roll damping coefficient
B_{Lin}	$N.m.s.rad^{-1}$	Linear roll damping coefficient
$B_{Lin.INI}$	$N.m.s.rad^{-1}$	Initial linear roll damping coefficient considered in an iterative process
B_{Quad}	$N.m.s^2.rad^{-2}$	Quadratic roll damping coefficient
$B_{Quad.INI}$	$N.m.s^2.rad^{-2}$	Initial quadratic roll damping coefficient considered in an iterative process
BV	-	Bureau Veritas
C		
C	-	Ratio of $Area_{lobe}$ on $Area_{inst}$ (only encountered in Chapter 2 of this PhD Thesis)
C	-	Parametric roll coefficient (only encountered in Chapter 4 of this PhD Thesis)
C1	-	Ratio of the up-crossing roll period over the up-crossing pitch period
$\widehat{C1}$	-	Normalized coefficient C1

C2	-	Ratio of the peak roll period over the up-crossing roll period
$\widehat{C2}$	-	Boolean coefficient associated to C2
C3	-	Coefficient associated to the delay between the roll and the pitch motion
$\widehat{C3}$	-	Normalized coefficient C3
CEREMA	-	Centre d'études et d'expertise sur les risques, l'environnement, la mobilité et l'aménagement / Centre for Studies and Expertise on Risks, Environment, Mobility, and Urban and Country Planning
CFD	-	Computational Fluid Dynamics
CFOSAT	-	Chinese-French Oceanography SATellite
C_i	-	Boolean factor
CMEMS	-	Copernicus Marine Environment Monitoring Service
$C_{m.full}$	-	Midship section coefficient of the fully loaded departure condition in calm water

D

D	m	Moulded depth amidships as defined in IS Code 2008
d	m	Mean draught amidship
d_H	m	Highest draught calculated as function of a sinusoidal wave
d_L	m	Lowest draught calculated as function of a sinusoidal wave
D_m	m	Moulded depth amidships
DGA TH	-	Direction General de l'Armement Techniques Hydrodynamique
DMAIB	-	Danish Maritime Accident Investigation Board
DNV	-	Det Norske Veritas
DoF	-	Degree of Freedom
DSB	-	Dutch Safety Board

E

E_0	$J.m^{-2}$	Energy of the reference wave, sea state
E_D	J	Damping energy
E_E	J	Exciting energy
E_K	J	Kinetic energy
E_P	J	Potential energy

F

f_{BK}	-	BV Non-dimensional bilge keel coefficient

f_{fa}	-	BV Non-dimensional fatigue assessment coefficient
F_{ext}	N.m	External forces

G

g	$m.s^{-2}$	Acceleration of gravity (constant)
GLRT	-	Generalized Likelihood Ratio Test
GM	m	Metacentric height
GM_0	m	GM in calm water
GM_{ampl}	m	Half difference between GM_{max} and GM_{min}
GM_{max}	m	Maximum GM in waves
$GM_{max.book}$	m	Maximum GM appearing in the stability booklet
GM_{mean}	m	Mean GM in waves
GM_{min}	m	Minimum GM on waves
$GM_{min.book}$	m	Minimum GM appearing in the stability booklet
GZ	m	Righting arm
$GZ(\varphi,t)$	m	Righting arm as a function of the roll angle φ varying in time according to the encounter frequency
GZ_K	-	GZ curve associated to K (wave position)
GZ_{LOW}	-	Lower GZ curves of the pair of GZ curves presenting the greatest area
GZ_{max}	-	Maximum GZ curve in waves
GZ_{min}	-	Minimum GZ curve in waves
GZ_{UP}	-	Upper GZ curves of the pair of GZ curves presenting the greatest area
$G(\beta)$		Spreading function

H

H	m	Wave parameter calculated from LASHING (NR 625 section 3 (BV, 2020a))
H_0	m	Wave height of the reference sinusoidal wave
H_i	m	Wave height associated to the wave number i (regular wave)
H_{RA}	m	Wave parameter calculated from LASHING (specific area) (NR 625 section 3 and 14 (BV,2020a))
H_{ri}	m	Height of the equivalent wave of length equal to the one of the ships
H_S	m	Significant wave height
H_{Si}	m	Significant wave height associated to the wave number i (irregular wave)
H_{WW}	m	Wave parameter calculated from LASHING-WW (NR 625 section 3 and 14 (BV, 2020a)

I

I	m^4	Transverse moment of inertia
IACS	-	International Association of Class Societies
ICOAD	-	International Comprehensive Ocean-Atmosphere Dataset
IIMS	-	International Institute of Marine Surveying
IMO	-	International Maritime Organization
I_{TH}	m^4	Transverse moment of inertia of the waterplane at the draught d_H
I_{TL}	m^4	Transverse moment of inertia of the waterplane at the draught d_L
ITTC	-	International Towing Tank Conference

J

J	-	Advance ratio
J_{44}	$Kg.m^2$	Roll moment of inertia
$J_{44.INI}$	$Kg.m^2$	Initial roll moment of inertia considered in an iterative process

K

k	$rad.m^{-1}$	Wave number
K	-	Real number associated to position of the wave crest along the ship
KB	m	Vertical coordinate of the centre of buoyancy from base line
KG	m	Vertical coordinate of the centre of gravity from base line
KG_W	m	Vertical coordinate of the centre of gravity above the water surface
KMT	m	Vertical coordinate of the transverse metacentre from base line
k_{PR}	-	Weighting factor for parametric roll assessment
KT	-	Thrust coefficient
K_{UP}	-	Real number K associated to GZ_{UP}
k_{xx}	m	Roll radius of inertia

L

L	m	Ship's length
LCB	m	Longitudinal coordinate of the centre of buoyancy form aft perpendicular
LCF	m	Longitudinal centre of buoyancy from aft perpendicular
LCG	m	Longitudinal coordinate of the centre of buoyancy form aft perpendicular

L_{OA}	m	Ship's length over all
L_{PP}	m	Ship's length between perpendiculars

M

MAIB	-	Marine Accident Investigation Branch
MBARI	-	Monterey Bay Aquarium Research Institute
MEAN	-	Coefficient characterizing the linearity of the GZ_{mean} curve up to Φ
MFWAM	-	Météo France WAve Model
MTC	t.m	Moment to change trim of one centimetre

N

n	-	Exponent of the spreading function
n	-	BV Non dimensional coefficient depending on the area of navigation
N	-	Number of waves directions considered on the spreading function (only encountered in Section 3.3 of this PhD Thesis)
N	-	Number of points describing the lobe (only encountered in Chapter 2 of this PhD Thesis)

O

OOW	-	Officer Of the Watch
OPEN	-	Coefficient characterizing the "opening" of the pair of GZ curves developing the greatest area (GZ_{UP} and GZ_{LOW}) up to Φ

P

p	$(kg.m)^{-1}$	Parameter of the Mathieu differential equation of parametric roll
PaRoll1	-	BV additional class notation for container ship without any anti-rolling device or only using bilge keels as anti-rolling devices
PaRoll2	-	BV additional class notation for container ships using anti-roll devices such as anti-roll tank, stabilizer fins or other anti-rolling devices (other than bilge keels)
PR	-	Parametric roll
PIT	-	Parameter identification technique

Q

q	$(kg.m)^{-1}$	Parameter of the Mathieu differential equation of parametric roll

R

R_{PR}	-	Coefficient regarding the roll damping, used as the maximum allowed value of non-dimensional GM variation of parametric roll level-one and level-two criteria

S

$S(\omega)$	$m^2.rad^{-1}.s$	Wave energy density spectrum
$S_\eta(\omega,\beta)$	$m^2.rad^{-1}.s$	Wave energy density spectrum including directional spreading
SGISCs	-	Second-Generation Intact Stability Criteria
SOLAS	-	Safety Of Life At Sea
SPOS	-	Ship Performance Optimization System
STAB&S	-	International Conference on the Stability and Safety of Ships and Ocean Vehicles
S_w	-	Wave steepness

T

t	s	Time
$t_{\varphi.UpLast}$	s	Time of the last zero-up-crossing roll angle
t_{Alarm}	s	Time at which the parametric roll alarm rises
t_{Peak}	s	Time at which the local peak amplitude appears
t_{start}	s	Time of the beginning of the manoeuvre
t_{UP}	s	Up-crossing time
$t_{UP.\varphi}$	s	Up-crossing time of the roll motion
$t_{UP.\theta}$	s	Up-crossing time of the pitch motion
T	m	Ship's draught
T_E	s	Encounter period
TEU	-	Twenty-foot equivalent unit
T_{GMi}	m	Associated draught to GM_i
$T_{GMmax.book}$	m	Associated draught in the stability booklet to GM_{max}
$T_{GMmin.book}$	m	Associated draught in the stability booklet to GM_{min}
T_m	m	Moulded draught amidships
T_P	s	Peak wave period
T_R	s	Simulation duration
T_W	s	Wave period
T_Z	s	Zero-Up-crossing wave period
T_0	s	Natural roll period in calm water

T_θ	s	Pitch period (throughout this PhD Thesis, except in Sub-Section 1.3.2)
T_θ	s	Roll period (only encountered in Sub-Section 1.3.2 of this PhD Thesis in accordance with BV rules)
T_φ	s	Roll period
T_{UP}	s	Up-crossing period
$T_{UP.\varphi}$	s	Up-crossing roll period
$T_{UP.\theta}$	s	Up-crossing pitch period
$T_{P.\varphi}$	s	Peak roll period

V

V_i	kn	Vessel speed
V_{PR}	$m.s^{-1}$	Vessel speed for which the parametric synchronism condition is met (first mode of parametric roll)
V_s	$m.s^{-1}$	Ship service speed

W

W	N	Ship's Weight
W_i	-	Weighting factor
WRC	-	Nairobi International Convention on the Removal of Wrecks
WSC	-	World Shipping Council

X

X	m	Position of the wave from the aft perpendicular
x	m	x coordinates of the observer in the cartesian system
x	-	Current value

Y

y	m	y coordinates of the observer in the cartesian system

Greek Symbols

α	rad	Shift angle
α_p	rad	Possible shift angle
α_i	rad	Wave heading of the wave number i in the cartesian system
β	rad	Wave heading relative to the ship axis

∇	m^3	Ship's volume
∇_D	m^3	Ship's volume at a draught equal to D and at trim null
Δ	Kg	Ship's displacement
$\Delta\alpha$	deg	Spreading angle
Δf	s^{-1}	Step in BV NR 667 for calculation of the loading conditions
Δt	s	Time threshold
$\delta\alpha$	deg	Direction step between two wave trains
δGM	m	Half variation of transverse stability between minimum and maximum GM
δt	s	Duration between the up-crossing time of both roll and pitch time series
δV	$m.s^{-1}$	Half bandwidth of the parametric roll lock-in-field
$\delta\omega$	$rad.s_{-1}$	Frequency step
ε	-	Error
γ	-	Dimensionless speed (only encountered in Chapter 2 of this PhD Thesis)
γ	-	Phase angle (only encountered in section 3.3 of this PhD Thesis)
γ_{PR}	-	BV conversion factor permitting to pass from a long-term study to a short-term study
λ	m	Wavelength
μ	-	Expectation of the normal law (only encountered in Chapter 4 of this PhD Thesis)
μ	-	Critical damping coefficient (only encountered in Section 1.3 of this PhD Thesis)
φ	rad	Roll angle
φ_0	rad	Initial roll angle
φ_{max}	rad	Maximum roll angle reached during half a roll period
$\dot{\varphi}$	$rad.s^{-1}$	Roll velocity
$\ddot{\varphi}$	$rad.s^{-2}$	Roll acceleration
Φ	deg	Roll amplitude
$\Phi_{2ndPart}$	deg	Maximum roll amplitude reached once the manoeuvre is completed on the final part of the simulation
$\Phi_{2ndPartRef}$	deg	Maximum roll amplitude reached once the manoeuvre is completed on the final part of the reference simulation
Φ_P	deg	Possible steady state roll amplitude
Φ_{PR}	deg	Roll amplitude reached around t_{start}
Φ_{PRRef}	deg	Roll amplitude reached around t_{start} in the reference simulation
Φ_{Sim}	deg	Maximum roll amplitude reached during the simulation

Φ_{SimRef}	deg	Maximum roll amplitude reached during the reference simulation
Φ_{VPR}	deg	Roll amplitude calculated at VPR
ω	$rad.s^{-1}$	Actual ship's roll frequency
ω_e	$rad.s^{-1}$	Encounter wave frequency
ω_{ampl}	$rad.s^{-1}$	Frequency associated to GM_{ampl}
$\omega_{e.f}$	$rad.s^{-1}$	Encounter wave frequency associated to the vessel speed leading to the first mode of parametric roll in following seas
$\omega_{e.h}$	$rad.s^{-1}$	Encounter wave frequency associated to the vessel speed leading to the first mode of parametric roll in head seas
ω_{mean}	$rad.s^{-1}$	Frequency associated to GM_{mean}
ω_0	$rad.s^{-1}$	Natural roll frequency
ω_p	$rad.s^{-1}$	Peak frequency (sea spectrum)
ω_w	$rad.s^{-1}$	Wave frequency
ρ	$kg.m^{-3}$	Water density
σ	-	Standard deviation
θ_{lash}	deg	BV maximum permissible roll angle for lashing
θ_{PR}	deg	BV maximum parametric roll angle threshold
θ_{sh}	deg	one-hour maximum roll angle with a probability of exceedance of 0.5
θ_{ART}	deg	Extreme long-term roll angle (25 years return period for the North-Atlantic scatter diagram) from direct calculation including the effect of ART
$\theta_{wo\text{-}ART}$	deg	Extreme long-term roll angle (25 years return period for the North-Atlantic scatter diagram) from direct calculation without the effect of ART
θ	deg	Roll angle as defined in section 3 of Chapter 4 in NR 625 (BV, 2020a), calculated for unrestricted navigation (only encountered in Sub-Section 1.3.2 of this PhD thesis)
θ	deg	Pitch angle (throughout this PhD thesis, except in Sub-Section 1.3.2)
χ_i	-	Percentage of $Area_{tot}$ associated to the wave i

REFERENCES

ABB., 2012, “Theoretical Manual OCTOPUS”, J.M.J. Journée, Ship Hydromechanics Laboratory Delft University of Technology, L.J.M. Adegeest, Amarcon B.V.

ABS., 2019, “Assessment of parametric roll resonance in the design of container carriers”, USA, American Bureau of Shipping.

Acanfora, M., Krata, P., Montewka, J., Kujala, P., 2018, “Towards a method for detecting large roll motions suitable for oceangoing ships”, Applied Ocean Research, Volume 79, pp 49–61. https://doi.org/10.1016/j.apor.2018.07.005.

Acanfora, M., Balsamo, F., 2020, “The Smart Detection of Ship Severe Roll Motions and Decision-Making for Evasive Actions”, Journal of Marine Science and Engineering, Volume 8, pp 415. 10.3390/jmse8060415.

Acomi N., Ancuta C., Andrei C., Bostina A., 2016, “Avoiding the parametric roll”, 100102M. 10.1117/12.2243360.

Affaires Maritime., 2019, “Stabilité a l'état intact et après avarie”, France.

AGCS., 2022, “Safety and Shipping Review 2022”, AGCS annual report, Germany, Allianz Global Corporate & Specialty.

Aouf, L., 2020, “Quality information document for Global Ocean Waves Analysis and Forecasting Product GLOBAL_ANALYSIS_FORECAST_WAV_001_027”, Issue 2.1, Mercator Ocean International.

ATSB., 2009, “Independent investigation into the loss of containers from Pacific Adventurer off Cape Moreton, Queensland, 11 March 2009”, Australia, Australian Transport Safety Bureau.

ATSB., 2020a, “Loss of container overboard involving APL England”, Australia, Australian Transport Safety Bureau.

ATSB., 2020b, “Loss of containers overboard from YM Efficiency”, Australia, Australian Transport Safety Bureau.

Barry, J., 2011, “MBARI teams with Monterey Bay National Marine Sanctuary to study effects of shipping containers lost at sea”, Monterey Bay Aquarium Research Institute, March 7, 2011, available on www.mbari.org, visited on the 2022.07.25.

Bertram, V., 2000, “Practical Ship Hydrodynamics”, Butterworth-Heinemann, ISBN 0-7506-4851-1.

Bouguer, P., 1746, “Traité du Navire, de sa Construction et de ses Mouvements”, Jombert, Paris.

Breu, D., 2013, "Frequency Detuning of Parametric Roll Resonance", PhD thesis, Norwegian University of Science and Technology.

BRS., 2011, “Shipping and shipbuilding markets annual review 2011”, pp.83, France, Barry Rogliano Sales.

BRS., 2022, “Shipping and shipbuilding markets annual review 2022”, pp.122, France, Barry Rogliano Sales.

Bulian, G., 2003, “Estimation of nonlinear roll decay parameters using an analytical approximate solution of the decay time history”, International Shipbuilding Progress, 51(1), pp 5-32.

BV., 2019a, “NI 638 DT R00 E. Guidance for Long-term Hydro-structure Calculations”, France, Bureau Veritas.

BV., 2019b, “NR 667 DT R00 E. Parametric Roll Assessment”, France, Bureau Veritas.

BV., 2020a, “NR 625 DT R03 E. Structural Rules for Container Ships”, France, Bureau Veritas.

BV., 2020b, “NR 467.F1 DT R12 E. Rules for the Classification of Steel Ships, PART F – Additional Class Notations”, France, Bureau Veritas.

Carmel, S.M., 2006, “Study of parametric rolling event on a panamax container vessel”, Journal of the Transportation Research Board, Volume 1963, pp 56-63. DOI: 10.3141/1963-08.

CEREMA., 2021, “Technical solution for locating and tracking containers that have fallen into the sea”.

Committee on Large Container Ship Safety., 2013, “Interim Report of Committee on Large Container Ship Safety”, December 2013, Japan.

CRN., 2021, “FREDYN v16 Documentation”, Cooperative Research Navies.

Dalphinet, A., Aouf, L., Law-Chune S., Fernandez, E., 2022, “Product user manual for Global Ocean Waves Analysis and Forecasting Product GLOBAL_ANALYSIS_FORECAST_WAV_001_027”, Issue 1.2, Mercator Ocean International.

DMAIB., 2014, “Marine Accident Report, SVENDBORG MÆRSK, Heavy weather damage on 14 February 2014”, Danish Maritime Accident Investigation Board, Denmark.

DMAIB., 2022, “Marine Accident Report on Maersk Essen’s loss of cargo on 16 january 2021”, Danish Maritime Accident Investigation Board, Denmark.

DNV., 2005, “Parametric rolling - a concern for container ships?”, Paper series 2005-P011.

Dølhie, K.A., 2006, “Parametric rolling – a problem solved?”, DNV Container Ship Update, Volume 1, pp 12-15.

DSB., 2020, “Safe container transport north of the Wadden Islands, Lessons learned following the loss of containers from MSC ZOE”, The Hague, Dutch Safety Board.

European Commission., 2015, “Copernicus Europe’s eyes on Earth”, ISBN 978-92-79-45666-4.

European Commission., 2016, “Marine Environment Monitoring Service”, Mercator Ocean International.

Falzarano, J., Somayajula, Abhilash., and Seah, R., 2015, “An Overview of the Prediction Methods for Roll Damping of Ships”, Ocean Systems Engineering, Volume 5, pp 55-76.

Fernandes, A., Oliveira, A., 2009, “The roll damping assessment via decay model testing (new ideas about an old subject)”, Journal of Marine Science and Application, Volume 8, pp 144-150. 10.1007/s11804-009-8107-z.

France, W.N., Levadou, M., Treakle, T.W., Paulling, J.R., Michel, R.K., Moore, C., 2003, “An Investigation of Head Sea Parametric Rolling and its Influence on Container Lashing Systems”, Marine Technology¸ Volume 40, pp 1-19.

Francescutto, A., 2015, “Intact Stability Criteria of Ships – Past, Present and Future”, Proceedings of the 12th International Conference on the Stability of Ships and Ocean Vehicles, Glasgow, UK.

Froude, W., 1861, “On the rolling of ships”, Second Session of the Institution of Naval Architects.

Froude, W., 1872, “On the influence of resistance upon the rolling of ships[J]”, Naval Science, Volume i, pp 411-429.

Haddara, M. R., 2005, “Roll damping: a review”, Oceanic Engineering International, Volume 9, Number 1.

Hua, M., 2009, “Evaluation des coefficients d’amortissement en roulis”, Direction Générale de l'Armement, Report N°09-502056.

Galeazzi, R., Blanke, M., and Poulsen, N.K., 2009a, “Detection of parametric roll resonance on ships from indication of nonlinear energy flow”, Proceedings of the 7th IFAC Symposium on Fault Detection, Supervision and Safety of Technical Processes, SAFEPROCESS’2009.

Galeazzi, R., Blanke, M., and Poulsen, N.K., 2009b, “Parametric Roll Resonance Detection using Phase Correlation and Log-likelihood Testing Techniques”, Proceedings of the 8th IFAC International Conference on manoeuvring and Control of Marine Craft, September 16-18, 2009, Guarujá (SP), Brazil.

Galeazzi, R., Christian, H., Mogens, B., Fossen, T.I., 2009c, “Stabilisation of parametric roll resonance bycombined speed and fin stabiliser control”, Proceedings of the European Control Conference, 4895-4900, Budapest, Hungary.

Galeazzi, R., Blanke, M., & Poulsen, N. K., 2013, “Early Detection of Parametric Roll Resonance on Container Ships”, I E E Transactions on Control Systems Technology, Volume 21, pp 489-503.

Galeazzi, R., 2014, “Parametric Roll - Risk Reduction through Real-time Detection”, Container Ship Update, pp 20-22.

Galeazzi R., Blanke M., Falkenberg T., Poulsen N. K., Violaris N., Storhaug G., Huss M., 2015, “Parametric roll resonance monitoring using signal-based detection”, Ocean Engineering, Volume 109, pp 355-371.

Ginsberg S., 1998, “Lawsuit rock APL's boat”, San Francisco Business Times, November 22nd 1998.

Giordmaine, JA., Miller, RC., 1965 “Tunable coherent parametric oscillation in LiNb O 3 at optical frequencies”, Physical Review Letters, Volume 14, pp 973-976.

Gnalo, G., Gueye, M., Oliano, M., 2021, “Etude de l’état de la mer relevé par satellite”, Projet de fin d'étude, ENSM, Marine Nationale, Ecole Navale, IRENAV.

González, M., López Peña, F., Díaz Casás, V., Galeazzi, R., Blanke, M., 2011, “Prediction of Parametric Roll Resonance by Multilayer Perceptron Neural Network”, Proceedings of the 21st International Offshore and Polar Engineering Conference, pp. 522-529, Hawaii, USA.

Grim, O., 1961, “Beitrag zu dem Problem der Sicherheit des Schiffes im Seegang”, Schiff und Hafen, Volume 6, pp 490-497.

Grin, R., Ruano, S.F., Bradbeer, N., Koelman, H., 2016, “On the prediction of weight distribution and its effect on seakeeping”, Proceedings of PRADS 2016, 4–8 September, Copenhagen, Denmark, pp 227-235.

Grinnaert, F., Billard, J.Y., Laurens, J.M., 2015, “Calcoque: a fully 3D Ship Hydrostatic Solver”, Proceedings of the 12th International Conference on the Stability of Ships and Ocean Vehicles, Glasgow, UK.

Grinnaert, F., Billard, J.Y., Laurens, J.M., 2017, “An Energy Analysis of Parametric Roll for Application to the Second Generation Intact Stability Criteria”, Journal of Marine Science and Technology, DOI: 10.1007/s00773-017-0444-z.

Grinnaert, F., 2017, “Analysis and Implementation of Second Generation Criteria in a Stability Computer Code”, PhD Thesis, Ecole navale.

Hayashi, C., 1985, “Nonlinear oscillation in physical systems”, Princeton, New Jersey: Princeton University Press ISBN 0-691-08383-5.

Holden, C., Perez, T., Fossen, T.I., 2007, “Frequency-motivated observer design for the prediction of parametric roll resonance”, Proceedings of the 7th IFAC Conference on Control Applications in Marine Systems.

Holden, C., Breu, D.A., Fossen, T.I., 2012, “Frequency Detuning Control by Doppler Shift”, In: Fossen, T., Nijmeijer, H. (eds) “Parametric Resonance in Dynamical Systems”, Springer, New York, NY. ISBN 978-1-4614-1042-3.

Hyundai Heavy Industries., 2017, “Provisional trim and stability booklet 14 400 TEU container Carrier”, Drawing N° 7G-7000-004.

IACS., 2001, “Rec. No. 34. Standard Wave Data”, Rev.1, International Association of Classification Societies.

IACS., 2022, “Common Structural Rules for Bulk Carriers and Oil Tankers”, International Association of Classification Societies.

IIMS., 2020, “Cargo losses claim from ONE Apus incident may reach USD200 million”, iims.org.uk, Posted on December 18, 2020 by News Hound, website visited on the 2022.01.05, International Institute of Marine Surveying.

Ikeda, Y., Himeno, Y., Tanaka, N., 1978, “Components of roll damping of ship at forward speed”, Department of Naval Architecture University of Osaka Prefecture, Report No 404.

Ikeda, Y., Munif, A., Katayama, T. and Fujuwara, T., 2005, “Large parametric rolling of large passenger ship in beam seas and role of bilge keel in its restraint”, Proceeding of 8th International Workshop on Ship Stability, Istanbul Technical University, Istanbul.

IMO., 1985, “Recommendation on a Severe Wind and Rolling Criterion (Weather Criterion) for the Intact Stability of Passenger and Cargo Ships of 24 Metres in Length and Over”, Resolution A.562(14), London, UK, International Maritime Organization.

IMO., 1995, “MSC/Circ.707”, Guidance to the master for avoiding dangerous situations in following and quartering seas, London, International Maritime Organization.

IMO., 2006, “MSC.1/Circ.1200”, Interim guidelines for alternative assessment of the weather criterion, London, International Maritime Organisation.

IMO., 2007a, “MSC.1/Circ.1228”, Revised guidance to the master for avoiding dangerous situations in adverse weather and sea conditions, London, International Maritime Organization.

IMO., 2007b, “Nairobi International Convention on the Removal of Wrecks”, Kenya, International Maritime Organisation.

IMO., 2008, “International Code of Intact Stability, 2008”, MSC.267(85), London, International Maritime Organization.

IMO., 2014, “MSC.1/Circ.1475”, Guidelines regarding the verified gross mass of a container carrying cargo, London, International Maritime Organisation.

IMO., 2015, “SDC 2/WP.4”, 2nd session, Development of Second Generation Intact Stability Criteria, Development of Amendments to Part B of the 2008 IS Code on Towing and Anchor Handling Operations, International Maritime Organization.

IMO., 2016, “SDC 3/WP.5”, 3rd session, Finalization of Second Generation Intact Stability Criteria, Amendments to Part B of the 2008 IS Code on Towing, Lifting and Anchor Handling Operations, International Maritime Organization.

IMO., 2020a, “MSC.1/Circ.1627”, Interim Guidelines On The Second Generation Intact Stability Criteria, London, International Maritime Organization.

IMO., 2020b, “SOLAS consolidation edition 2020”, International Maritime Organization.

IMO., 2021a, “SDC 8/INF.2”, 8th session, Development of explanatory notes to the interim guidelines on Second Generation Intact Stability Criteria, Physical background and mathematical models for stability failures of the Second Generation Intact Stability Criteria. Submitted by ITTC, 9 November 2021, International Maritime Organization.

IMO., 2021b, “SDC 8/5/Add.2”, 8th session, Development of explanatory notes to the interim guidelines on Second Generation Intact Stability Criteria, Report of the Correspondence Group (part 3). Submitted by Japan, 4 October 2021, International Maritime Organization.

IMO., 2022, “SDC8/11”, Estimation du nombre de conteneurs perdus en mer, submitted by the World Shipping Council, Sub-Committee on Carriage of Cargoes and Containers, International Maritime Organisation.

International Chamber of Shipping., International group of P&I clubs., European community of shipowners’ association., Asian shipowners’ association., World shipping council., 2021, “Containers Lost at Sea - liability and insurance”, London.

Irkal, Mohsin A.R., Nallayarasu, S., Bhattacharyya, S.K., 2016, “CFD approach to roll damping of ship with bilge keel with experimental validation”, Applied Ocean Research, volume 55, pp 1-17, ISSN 0141-1187.

ITTC., 2011, “The Specialist Committee on Stability in Waves”, Final report and recommendations to the 26th ITTC, Rio de Janeiro, International Towing Tank Conference.

ITTC., 2017, “Numerical Simulation of Capsize Behaviour of Damages Ships in Irregular Seas”, Recommended Procedures and Guidelines 7.5-02-07-04.4, International Towing Tank Conference.

ITTC., 2021a, “Estimation of Roll Damping”, Recommended Procedures and Guidelines 7.5 02 07 04.5, Stability in wave committee of the 29th ITTC, International Towing Tank Conference.

ITTC., 2021b, “ITTC Symbols and Terminology List”, June 2021, International Towing Tank Conference.

ITTC., 2021c, “Predicting the Occurrence and Magnitude of Parametric Rolling”, Recommended Procedure 7.5-02-07-04.3, Revision 03, Effective Date 2021.

Kapsenberg, G., Abeil, B., Kim, S., Wandji, C., Ruth, E., Pages, A., 2019, “On parametric roll prediction”, 17th International Ship Stability Workshop, Helsinki, Finland.

Kapsenberg, G., Wandji, C., Duz, B., Kim, S., 2020, “A Comparison of Numerical Simulations and Model Experiments on Parametric Roll in Irregular Seas”, Journal of Marine Science and Engineering.

Kawahara, Y., Maekawa, K., Ikeda, Y., 2009, “A simple prediction formula of roll damping of conventional cargo ships on the basis of Ikeda’s method and its limitation”, Proceedings of the 10th International Conference on Stability of Ships and Ocean Vehicles, St Petersburg.

Kerwin, J.E., 1955, “Notes on rolling in longitudinal waves”, International Ship Building Progress, Volume 2(16), pp 597-614.

Komen, G., Cavaleri, L., Donelan, M., Hasselmann, K., Hasselmann, S., & Janssen, P., 1994, “Dynamics and Modelling of Ocean Waves”, Cambridge University Press. DOI:10.1017/CBO9780511628955.

Koning, J., Grin, R., Pauw, W., 2022, “TopTier, seakeeping and container cargo securing safety”, Proceedings of the 18th International Ship Stability Workshop, pp 259-264, Gdańsk, Poland.

Luthy, V., Grinnaert, F., Billard, J.Y., 2021a, “An iterative method to estimate damping coefficients from roll decay time series”, Proceedings of the first International Conference on the Stability and Safety of Ships and Ocean Vehicles, Glasgow.

Luthy, V., Grinnaert, F., Billard, J.Y., 2021b, “Computation of parametric roll amplitude using energy method considering non-linear GZ in resonance condition”, Proceedings of the first International Conference on the Stability and Safety of Ships and Ocean Vehicles, Glasgow.

Luthy, V., Grinnaert, F., Billard, J.Y., 2022a, “Identification of a conservative spreading angle to realize operational roll polar plots”, Proceedings of the 18th International Ship Stability Workshop, pp 103-108, Gdańsk, Poland.

Luthy, V., Grinnaert, F., Billard, J.Y., 2022b, “Mitigation manoeuvres to reduce parametric roll on a naval ship”, Proceedings of the 18th International Ship Stability Workshop, pp 195-200, Gdańsk, Poland.

Luthy, V., Grinnaert, F., Billard, J.Y., 2022c, “Computation of parametric roll amplitude using energy method considering non-linear transverse stability”, Ocean Engineering, Volume 263, ISSN 002-8018.

Luthy, V., Grinnaert, F., Billard, J.Y., Rapp, J., 2022d, “Real Time Identification of Parametric Roll”, Submitted to the Journal of Ship Research, SNAME.

Luthy, V., Grinnaert, F., Billard, J.Y., 2022e, “Identification of a conservative spreading angle to realize operational roll polar plots considering real sea states”, submitted to the 18èmes Journées de l'Hydrodynamique, Poitier, France.

MAIB., 2020, “Report on the investigation into the loss of 137 containers from the container ship, CMA CGM G. Washington, in the North Pacific Ocean on 20 January 2018”, MAIB Report 02.2020, Marine Accident Investigation Branch.

MARIN., 2009a, “Fredyn - A computer program for the simulation of a steered ship in wind and waves”, MARIN, Netherlands, Maritime Research Institute Netherlands.

MARIN., 2009b, “Fredyn - Users Manual”, MARIN, Netherlands, Maritime Research Institute Netherlands.

MARIN., 2012, “PANSHIP A time domain seakeeping panel method numerical modelling tool - User Manual”, Netherlands, Maritime Research Institute Netherlands.

MARIN., 2013, “SHIPMO - Theory Manual”, report n° 80052-2-RD, MARIN, Netherlands, Maritime Research Institute Netherlands.

Mathieu, E., 1868, “Mémoire sur le mouvement vibratoire d’une membrane de forme elliptique”, Journal de Mathématiques Pures et Appliquées, Volume 13, pp 137–203.

McCue, L. and Bulian, G., 2007, “A numerical feasibility study of parametric roll advance warning

system", Journal of Offshore Mechanics and Arctic Engineering, Volume 129, pp 165-175.

Molin, B., 2002, "Hydrodynamique des structures offshore", Edition Technip, ISBN 9782710808152.

Nayfeh, A.H., 1981, "Introduction to Perturbation Techniques", Wiley-Interscience, New York.

Nielsen, J.K., Pedersen, N.H., Michelsen, J., Nielsen, U.D., Baatrup, J., Jensen, J.J., and Petersen, E.S., 2006, "SeaSense - real-time onboard decision support", In World Maritime Technology Conference.

Panama Maritime Authority., Dutch Safety Board., Budesstelle für seeunfalluntersuchung., 2020, "Loss of containers overboard from MSC ZOE 1-2 January 2019", 25th of June 2020.

Petacco, N., Gualeni, P., 2020, "IMO Second Generation Intact Stability Criteria: General Overview and Focus on Operational Mesures", Journal of Marine Science and Engineering.

Petacco, N., Gualeni, P., 2021, "An overview about operational measures in the framework of Second Generation Intact Stability criteria", Proceedings of the first International Conference on the Stability and Safety of Ships and Ocean Vehicles, Glasgow.

Peters, W., Belenky, V., Chouliaras, S., Spyrou, K., 2015, "Requirements for Computational Methods to be Used for the IMO Second Generation Intact Stability Criteria", Proceedings of the 12th International Conference on the Stability of Ships and Ocean Vehicles, Glasgow, UK.

Quadvlieg, F., Rapuc, S., 2019, "A pragmatic method to simulate maneuvering in waves", SNAME Convention.

Sanmartín Losada, J.R., 1984, "O Botafumeiro: parametric pumping in the Middle Age", American Journal of Physics, Volume 52, pp 937-945.

Shin, Y. S., Belenky, V., Lin, Y. M., Weems, K., Engle A., 2003, "Nonlinear Time Domain Simulation Technology for Seakeeping and Wave Load Analysis for Modern Ship Design", SNAME Annual Meeting 2003, San-Francisco.

Shin, Y. S., Belenky, V., Paulling, J., Weems, K., Lin, W., 2004, "Criteria for parametric roll of large containerships in longitudinal seas", SNAME Annual Meeting, Washington, D.C., 29th September to the 1st October, 2004.

Söder, C., Rosén, A., Werner, S., Huss, M., Kuttenkeuler, J., 2012, "Assessment of Ship Roll Damping Through Full Scale and Model Scale Experiments and Semi-Empirical Methods", 11th International Conference on the stability of ships and oceans vehicles, Greece.

Spyrou, K. J., 2000, "On the parametric rolling of ships in a following sea under simultaneous nonlinear periodic surging", Philosophical Transactions of the Royal Society, Volume 358, pp 1813-1834.

Sun, J., Shao, M., 2019, "Estimation of Nonlinear Roll Damping by Analytical Approximation of Experimental Free-Decay Amplitudes", Journal of Ocean University of China, Volume 18, pp 812–822.

TATA AIG., 2021, “Marine Newslink February 2021”, India, TATA AIG Insurance.

TATA AIG., 2022, “Marine Newslink March 2022”, India, TATA AIG Insurance.

Theillard, T., 2020, “One : 1816 conteneurs perdues dans le pacifique. Le Marin”, 02 of December 2020, updated the 09 of December.

TOP TIER., 2022, “Notice to Mariners, Beware of parametric rolling in following seas”, V1.2 (28th July 2022).

TT club., WSC., ICHCA international., Global shipper forum., 2015, “Verified grossmass industry faqs, implementation of the SOLAS amendments effective from 1 July 2016”, United Kingdom.

Wassermann, S., FrederikFeder, D., Abdel-Maksoud, M., 2016, “Estimation of ship roll damping-A comparison of the decay and the harmonic excited roll motion technique for a post panamax container ship”, Ocean Engineering, Volume 120, pp 371–382.

W E Cox Claims Group., 2022, “Casualty Notices”, www wecoxclaimsgroup.com, visited on the 2022.08.01.

W K Webster., 2022, “Casualties & Major Incidents”, www.wkwebster.com, visited on the 2022.04.19.

WMN., 2020, “OOCL Rauma Loses Containers off Dutch Coast”, World Maritime News staff.

WSC., 2020, “Containers Lost At Sea – 2020 Update”, World Shipping Council.

Yu, L., Ma, N., Gu, X., 2016, “Early detection of parametric roll by application of the incremental real-time Hilbert-Huang Transform”, Ocean Engineering, Volume 113, pp 224-236. https://doi.org/10.1016/j.oceaneng.2015.12.050

Yu, L., Taguchi, K., Kenta, A., Ma, N., Hirakawa, Y., 2018, “Model experiments on the early detection and rudder stabilization of KCS parametric roll in head waves”, Journal of Marine Science and Technology, Volume 23, pp 141–163. https://doi.org/10.1007/s00773-017-0463-9

ABSTRACT

In 2021, 5515 container ships are sailing worldwide for a total instantaneous capacity of 24,970,022 TEU. During the last decades, impressive container loss due to stability failures in waves were observed. Each accident has been highly mediatized, tarnishing the reputation of the ship owner, which may be more financially damageable than the cargo loss itself. The phenomenon of parametric roll is one stabillity failure mode in waves which may lead to accidents. This phenomenon appears in head or following seas where no heavy roll motions are expected by the crew. It is now assessed by several procedures with the aim to either qualify the vessel sensibility, to predict the actual motions of the ship in waves, and to detect the appearance of parametric roll motions in real time. Thus, all assessments should be considered as complementary to avoid this dangerous phenomenon. An innovative energy method permitting to calculate the amplitude of parametric roll in regular longitudinal seas at any speed, considering non-linear transverse stability has been developed, increasing fundamental knowledge. Several inputs provided to time-domain hydrodynamic software toward a direct assessment of parametric roll were discussed and validated to increase their relevance. A new real-time detection method based on physical conditions required for parametric roll to appears and its associated parametric roll alarm was developed and validated. Considering this alarm, a statistical evaluation of the most relevant manoeuvre to undertake after the parametric roll detection to avoid the worse roll motions was conducted.

RESUME

En 2021, 5515 porte-conteneurs naviguaient à travers le monde, représentant une capacitée total instantanée de 24,970,022 EVP. Durant ces dernières décennies, de spectaculaires pertes de conteneurs à la mer dû à des défaillances de stabilité dans les vagues ont été observées. Chaque accident a été largement médiatisé, ternissant la réputation des armateurs, conduisant à des pertes financières plus importantes que la valeur de la marchandise elle-même. Le phénomène de roulis paramétrique est l'une de ces défaillances de stabilité dans les vagues pouvant mener à des accidents. Ce phénomène apparait lorsque le navire se trouve mer de face ou mer de l'arrière, dans ces conditions l'équipage ne s'attend pas à subir de larges mouvements de roulis. Ce phénomène est maintenant évalué par différentes procédures avec pour objectif soit de qualifier la sensibilité du navire, soit de prédire ces mouvements dans les vagues, soit de détecter l'apparition du roulis paramétrique en temps réel. Ces évaluations devraient être considérées comme complémentaires afin d'éviter ce phénomène dangereux. Une méthode énergétique innovante permettant de calculer l'amplitude de roulis paramétrique sur mer régulière longitudinal pour toute vitesse d'avance, considérant une variation non-linéaire de stabilité transversal dans les vagues a été développée, augmentant les connaissances fondamentales de ce phénomène. Plusieurs données d'entrées fournies au simulateurs temporels hydrodynamiques permettant de réaliser une évaluation directe du roulis paramétrique ont été discutés et validés afin d'accroitre leur pertinence. Une nouvelle méthode de détection en temps réel se basant sur des conditions physiques menant à l'apparition du roulis paramétrique et son alarme associée ont été développées et validées. En considérant cette alarme, une évaluation statistique de la manœuvre la plus pertinente à réaliser après la détection du roulis paramétrique afin d'éviter les mouvements de roulis les plus important a été menée.